

Mean Reaction Rate Closures for Nanoparticle Formation in Turbulent Reacting Flow

Jethro Akroyd

Churchill College

A dissertation submitted for the
degree of Doctor of Philosophy



UNIVERSITY OF
CAMBRIDGE

March 21, 2011

Mean Reaction Rate Closures for Nanoparticle Formation in Turbulent Reacting Flow

Jethro Akroyd

This thesis investigates mean reaction rate closures for turbulent reacting flow. The closures model the mean rate of reaction in the flow and are applied to simulations of nanoparticle formation. The simulations couple detailed chemical reaction, particle population dynamics and turbulent flow, and offer the potential to improve the understanding of a range of industrial processes.

The numerical behaviour of a mean reaction rate closure based on the direct quadrature method of moments using the interaction by exchange with the mean micromixing model (DQMoM-IEM) is studied in detail. An analytic expression is presented for the source terms and a filter function introduced to address issues of boundedness and singularity. Analytic integrals are presented for special cases of specific terms. The implementation of the method in the Star-CD computational fluid dynamics code is described in detail and validated against a test problem.

The numerical performance of DQMoM-IEM is systematically compared to the stochastic fields (SF) turbulent reaction model. The methods share many similarities and are presented in a common mathematical framework for the first time. They differ in their treatment of key terms that make DQMoM-IEM numerically challenging. A variance reduction technique using antithetic sampling is introduced to increase the efficiency of the SF method. However, DQMoM-IEM is shown to remain competitive for the test problem considered.

A new methodology is presented to couple a detailed particle model to simulations of turbulent reacting flow. A projected fields (PF) method based on DQMoM-IEM is used to combine detailed chemistry and the method of moments with interpolative closure (MoMIC) population balance model in Star-CD. The method is applied to the example of the chloride process for the industrial synthesis of titania nanoparticles and includes full coupling between the flow, chemistry and particles undergoing simultaneous inception, coagulation and surface growth.

Acknowledgements

There are many people and organisations without whom this thesis would not have been written, and I owe them all a debt of gratitude. Financial support was provided by reSolutions Ltd. and the EPSRC (EP/C537564/1).

I thank Professor Markus Kraft and Dr Amit Bhave for their supervision and for providing the opportunity to undertake this project. I also thank my co-workers. I specifically mention Laurence McGlashan, Alastair Smith and Raphael Shirley, and also Christopher Handscomb, Sebastian Mosbach, Robert Patterson, Alexander Vikhansky and Clive Wells, all of whom gave generous amounts of their time.

I acknowledge Dr Simon Lo of CD-adapco for licences and technical support, Dr Kyoung-Oh Kim of Toyota Motor Corporation and Dr Nigel Okey of Tioxide Europe Ltd. I thank Professors Epaminondas Mastorakos and Stewart Cant of the University of Cambridge, Dr Daniele Marchisio of Politecnico di Torino and Professor William Jones of Imperial College London for many discussions on turbulent reacting flow methods at various workshops and conferences.

There are many friends and family members to whom I am also very grateful. You should know who you are, and I will thank you all in person. Finally, I would like to mention Louise, and thank her for everything.

Preface

This dissertation is my own work and contains nothing which is the outcome of work done in collaboration, except as specified in the text and Acknowledgements. The work was performed at the University of Cambridge between July 2007 and December 2010. Chapter 2 and items relating to the method of moments include work previously submitted for a Certificate of Postgraduate Study in July 2008. No part of this thesis has been submitted for a degree to this or any other university. This dissertation contains approximately 45000 words and 103 figures and tables. Some of the work in this dissertation has been published:

1. J. Akroyd, A.J. Smith, L.R. McGlashan, M. Kraft (2010). Numerical investigation of DQMoM-IEM as a turbulent reaction closure. *Chemical Engineering Science*, doi:[10.1016/j.ces.2009.11.010](https://doi.org/10.1016/j.ces.2009.11.010).
2. J. Akroyd, A.J. Smith, L.R. McGlashan, M. Kraft (2010). Comparison of the Stochastic Fields method and DQMoM-IEM as turbulent reaction closures. *Chemical Engineering Science*, doi:[10.1016/j.ces.2010.06.039](https://doi.org/10.1016/j.ces.2010.06.039).
3. J. Akroyd, A.J. Smith, R. Shirley, L.R. McGlashan, M. Kraft (2010). A coupled CFD-population balance approach for nanoparticle synthesis in turbulent reacting flows. *Chemical Engineering Science*, doi:[10.1016/j.ces.2011.05.006](https://doi.org/10.1016/j.ces.2011.05.006).
4. R. Shirley, J. Akroyd, L.A. Miller, O. Inderwildi, U. Riedel, M. Kraft (2011). Theoretical insights into the surface growth of rutile TiO₂. *Combustion and Flame*, doi:[10.1016/j.combustflame.2011.06.007](https://doi.org/10.1016/j.combustflame.2011.06.007).

Jethro Akroyd

March 21, 2011 (approved corrections July 12, 2011)

Contents

List of figures	xi
List of tables	xiii
1 Introduction	1
1.1 Motivation	1
1.2 Novel elements of the thesis	3
1.3 Structure of the thesis	4
2 Background	5
2.1 Titania nanoparticles	6
2.1.1 Applications	7
2.1.2 Economic aspects	8
2.1.3 Manufacturing processes	9
2.1.4 Kinetic models for titania formation	11
2.2 Population balance models	12
2.2.1 Particle models	12
2.2.2 Numerical methods	13
2.2.3 Dilute and concentrated regimes	15
2.3 Turbulent flow models	15
2.3.1 Governing equations	16
2.3.2 Numerical methods	17
2.4 Turbulent reacting flow models	20
2.4.1 Mean reaction rate closures	20

CONTENTS

2.4.2	Probability density function methods	22
2.4.3	Tabulation methods	27
2.5	Nanoparticle formation in turbulent reacting flows	27
2.5.1	Existing modelling approaches	28
2.5.2	Points of compromise	30
2.6	Terminology	30
2.7	Scope of this thesis	32
3	The direct quadrature method of moments using the IEM micromixing model	33
3.1	Background	34
3.1.1	DQMoM-IEM equations	34
3.2	Numerical details	37
3.2.1	DQMoM-IEM coupling to Star-CD	37
3.2.2	Analytic expression for the source terms	38
3.2.3	General solver	42
3.2.4	Analytic solver	45
3.3	Numerical testing of DQMoM-IEM	46
3.3.1	Model problem	46
3.3.2	Application to scalar mixing	49
3.3.3	Application to reacting flow	51
3.3.4	Computational performance	57
3.3.5	Choice of boundary conditions	57
3.4	Chapter summary	59
4	The stochastic fields method	61
4.1	Background	62
4.1.1	Stochastic fields equations	62
4.1.2	Features shared with DQMoM-IEM	63
4.2	Numerical details	64
4.2.1	Stochastic fields coupling to Star-CD	64

4.2.2	Antithetic sampling	66
4.3	Comparison of DQMoM-IEM and SF	67
4.3.1	Model problem	68
4.3.2	Application to scalar mixing	69
4.3.3	Application to reacting flow	74
4.3.4	Computational performance	80
4.4	Chapter summary	82
5	Application of the projected fields method to nanoparticle modelling	85
5.1	Background	86
5.1.1	Kinetic model for titania formation	87
5.1.2	Population balance equations	88
5.1.3	Projected fields equations	93
5.2	Numerical details	96
5.2.1	Projected fields coupling to Star-CD	96
5.2.2	Treatment of the scalars	97
5.2.3	Pressure coupling	99
5.3	Titania production in a ‘slot’ reactor	100
5.3.1	Model problem	100
5.3.2	Ideal reactor studies	102
5.3.3	Scalar mixing simulations	107
5.3.4	Titania reactor simulations	112
5.4	Chapter summary	119
6	Conclusions	121
6.1	Conclusions of the thesis	121
6.2	Suggestions for future work	124
6.2.1	Further development of the method	124
6.2.2	Optimisation of the code	125
6.2.3	Application of the new model	125

CONTENTS

Appendices

A	Derivations	127
A.1	Joint composition PDF transport equation	128
A.1.1	Governing equations	128
A.1.2	Favre-averaged PDF transport equation	132
A.1.3	Constant density PDF transport equation	134
A.1.4	Dimensional consistency	134
A.2	The direct quadrature method of moments	136
A.2.1	Favre-averaged case	136
A.2.2	Constant density case	144
A.3	The stochastic fields method	145
A.3.1	Favre-averaged case	145
A.3.2	Constant density case	147
A.4	The method of moments	148
A.4.1	Favre-averaged case	148
A.4.2	Constant density case	150
B	Numerical treatment	151
B.1	More on filter functions	152
B.2	Estimation of the particle number distribution	154
B.3	Method of moments coupling to Star-CD	155
B.3.1	Favre-averaged case	156
B.3.2	Constant density case	157
B.4	Summary of numerical methods	158
	Nomenclature	161
	Bibliography	169
	Citation Index	189

List of figures

2.1	Transmission electron micrograph of titania nanoparticles.	6
2.2	Consumption of titania in the USA by product area.	7
2.3	World growth, demand and capacity for titania.	8
2.4	Chloride process for titania manufacture.	10
3.1	DQMoM-IEM micromixing and diffusion source terms, $N=2$ fields.	41
3.2	DQMoM-IEM diffusion source term, $N=3$ fields.	41
3.3	DQMoM-IEM filtered diffusion source term, $N=3$ fields.	43
3.4	Configuration of the axisymmetric single-jet tubular reactor.	47
3.5	Geometry of the jet reactor computational domain.	47
3.6	Jet reactor empirical moments of species A, inert $Re=3530$ high concentration case, analytic DQMoM-IEM solver, $N=2$ fields.	50
3.7	Jet reactor empirical means, reacting $Re=3530$ high concentration case, analytic DQMoM-IEM solver, $N=2$ fields.	52
3.8	Jet reactor empirical means, reacting $Re=3530$ high concentration case, general DQMoM-IEM solver, $N=3$ fields.	53
3.9	Jet reactor empirical standard deviations, reacting $Re=3530$ high concentration case, analytic DQMoM-IEM solver, $N=2$ fields.	54
3.10	Jet reactor empirical standard deviations, reacting $Re=3530$ high concentration case, general DQMoM-IEM solver, $N=3$ fields.	55
4.1	Jet reactor empirical moments of species A, inert $Re=3530$ high concentration case, standard SF solver, $N=64$ fields.	69
4.2	SF fluctuations of the jet reactor empirical mean of species B, inert $Re=3530$ high concentration case.	72
4.3	SF jet reactor convergence vs. the method of moments, inert $Re=3530$ high concentration case.	73
4.4	Jet reactor empirical means, reacting $Re=3530$ high concentration case, antithetic SF solver, $N=64$ fields.	76
4.5	Jet reactor empirical standard deviations, reacting $Re=3530$ high concentration case, antithetic SF solver, $N=64$ fields.	77

LIST OF FIGURES

4.6	SF fluctuations of the jet reactor yield, reacting $Re = 3530$ high concentration case.	78
4.7	SF jet reactor yield, reacting $Re = 3530$ high concentration case.	79
4.8	SF jet reactor CPU times, $Re = 3530$ high concentration case.	81
5.1	Configuration of the axisymmetric titania reactor.	100
5.2	Titania batch reactor concentration and number moments.	103
5.3	Titania batch reactor particle number distributions.	104
5.4	Titania batch reactor non-isothermal temperature profiles.	105
5.5	Arrhenius plot of the oxidation rate of $TiCl_4$	106
5.6	Titania reactor ‘cold’ velocity field.	107
5.7	Titania reactor moments of enthalpy, inert case.	110
5.8	Titania reactor moments of temperature, inert case.	111
5.9	Titania reactor mean temperature, reacting case.	113
5.10	Titania reactor mean particle number moments, reacting case (1).	114
5.10	Titania reactor mean particle number moments, reacting case (2).	115
5.11	Titania reactor mean concentrations, reacting case.	117
5.12	Titania reactor moments of the particle size, reacting case.	118
B.1	DQMoM-IEM filtered diffusion source terms, $N = 3$ fields.	153
B.2	Operator splittings used to implement DQMoM-IEM / PF and SF.	159

List of tables

3.1 Inlet boundary conditions for the jet reactor. 49

3.2 DQMoM-IEM jet reactor convergence vs. MoM. 51

3.3 DQMoM-IEM jet reactor yields on the base grid. 56

3.4 DQMoM-IEM jet reactor yields on the refined grid. 56

3.5 DQMoM-IEM jet reactor CPU times. 57

3.6 DQMoM-IEM jet reactor initial and inlet boundary conditions. . . 58

4.1 SF jet reactor initial and inlet boundary conditions. 68

4.2 DQMoM-IEM jet reactor convergence vs. MoM on the SF grids. . 71

4.3 DQMoM-IEM jet reactor yields on the SF grids. 74

4.4 DQMoM-IEM jet reactor CPU times on the SF grids. 80

5.1 Titania reactor initial and inlet boundary conditions. 101

5.2 PF titania reactor convergence vs. MoM. 109

A.1 Units and dimensions of key equations and quantities. 135

B.1 Filter functions considered for the general DQMoM-IEM solver. . 152

B.2 Summary of numerical methods. 160

Chapter 1

Introduction

1.1 Motivation

Nanoparticles are big business and their synthesis in turbulent reacting flows is a key field of current engineering research. For example, titania nanoparticles represent a three-quarters share of the global white pigment market (1996) ([Grant et al., 2004](#)) worth annual sales of £7 billion (2009) ([Hill, 2009](#)). The titania is increasingly produced via the *chloride process*, which exhibits strong coupling between turbulent reacting flow and the quality of the pigment defined by the size, shape and crystal phase of the nanoparticles. The chloride process is typical of many industrial processes in that although it is widely used, it is not well understood and optimisation is often empirical.

Detailed models of nanoparticle formation in turbulent reacting flow offer a possible means to gain insight into a range of industrial processes. Such models must describe the gas-phase chemistry, the inception and coagulation of the nanoparticles, the interaction between the gas and particulate phases via reactions on the surface of the particles, and must resolve the coupling between the heat release from all these processes and the turbulent flow. The problem considered in this thesis is how to model the turbulent reacting flow and couple it to detailed models for the gas-phase chemistry and particle formation.

Turbulent flows are inherently unsteady and irregular. The main difficulty from a modelling perspective is how to deal with the fluctuation of the flow.

1 INTRODUCTION

Several established turbulent flow methods exist. Direct numerical simulation (DNS) resolves the full motion of the flow without the need for any models. The disadvantage is that DNS is prohibitively expensive and quickly becomes computationally intractable for practical problems. Other methods separate the velocity and scalar quantities (like species concentration) into resolved and unresolved components. However, the equations for the resolved velocity and scalars contain terms that require unresolved quantities. These are known as *unclosed* terms and they must be modelled. For example, large eddy simulation (LES) resolves the large scale unsteady motion of the flow, but models all unclosed processes that occur below this scale. Similarly Favre- and Reynolds-averaged methods resolve the mean flow, but model all processes that depend on unresolved fluctuations about the mean. LES is significantly cheaper than DNS and is increasingly popular, but is still too expensive for many applications. Favre- and Reynolds-averaged methods are cheaper again and are among the most popular and widely commercialised methods due to their computational efficiency.

The principal difficulty with applying LES, Favre- and Reynolds-averaged methods to turbulent *reacting* flow is that the chemical source term in the resolved material balance equation is unclosed for non-linear chemistry. For example, the mean reaction rate for Favre- and Reynolds-averaged turbulent reaction methods cannot be calculated without knowledge of the fluctuations about the scalar means. A number of turbulent reaction closures exist to overcome this problem. Some rely on explicit assumptions, for example fast or slow chemistry. Others solve for additional information that they use to calculate a rate of reaction. For example, probability density function (PDF) methods solve for a joint composition PDF that describes the statistics of the scalar composition of the flow. They require some additional modelling of the scalar mixing, but provide an exact treatment of the chemical source term.

The direct quadrature method of moments using the interaction by exchange with the mean micromixing model (DQMoM-IEM) and the stochastic fields (SF) method are two promising PDF-based turbulent reaction methods from the recent literature. The literature shows that both methods can be coupled to standard computational fluid dynamics (CFD) software and have been used to model a range of turbulent reaction problems, including unsteady flames. However, DQMoM-IEM presents a number of numerical difficulties. No previous studies have systematically compared the two methods, nor applied them to detailed models of nanoparticle formation in turbulent reacting flow.

The **objective of this thesis** is to investigate the application of DQMoM-IEM and SF as mean reaction rate closures for Favre- and Reynolds-averaged turbulent flow methods. The closures model the mean chemical source term in turbulent reacting flow and we are interested in methods that can be coupled to detailed chemistry and particle formation models in order to study nanoparticle formation. In practice, we interpret this as computationally efficient methods that have sufficient accuracy for engineering studies, that make no assumptions about the chemistry and that can be implemented within off-the-shelf CFD software.

1.2 Novel elements of the thesis

This thesis presents the following **novel developments**:

- The numerical behaviour and implementation of a mean reaction rate closure based on DQMoM-IEM is investigated in detail. A new analytic expression is presented for the source terms and a filter function introduced to address issues of boundedness and singularity. Analytic integrals are presented for special cases of specific terms. The implementation of the method in the Star-CD CFD code is described in detail.
- The numerical performance of DQMoM-IEM is systematically compared to the SF method. The methods share many similarities and are presented in a common mathematical framework for the first time. They differ in their treatment of key terms that make DQMoM-IEM numerically challenging. A variance reduction technique using antithetic sampling is introduced to increase the efficiency of the SF method.
- A new methodology is presented for the detailed modelling of nanoparticle formation in turbulent reacting flows. A projected fields (PF) method based on DQMoM-IEM is used to combine detailed chemistry and the method of moments with interpolative closure (MoMIC) population balance model in Star-CD. The method includes *full coupling* between the flow, chemistry and particles undergoing inception, coagulation and surface growth.

1.3 Structure of the thesis

The remainder of this thesis is structured as follows. Chapter 2 introduces relevant background material. It starts with a discussion of titania nanoparticles and introduces relevant aspects of population balance and turbulent flow models. It explains the origin of the mean reaction rate closure problem and describes common models for turbulent reacting flow. It reviews previous models for nanoparticle formation in turbulent reacting flow and concludes with a discussion of the scope and terminology of the investigations in this thesis.

Chapters 3 and 4 are concerned with turbulent reacting flow models. Chapter 3 investigates the application of DQMoM-IEM as a mean reaction rate closure. Two new solvers are introduced and validated against a constant density turbulent reaction test problem from the literature. Chapter 4 compares the performance of DQMoM-IEM to the SF method. DQMoM-IEM is shown to remain competitive for the test problem considered in chapter 3.

Chapter 5 is concerned with coupling a population balance method that describes nanoparticle formation to a turbulent reacting flow model. It extends the developments in chapter 3 to introduce a PF method that couples variable density turbulent flow to detailed chemistry and a MoMIC population balance model. The method is applied to the example of the chloride process for the synthesis of titania nanoparticles in a representative ‘slot’ reactor geometry.

Chapter 6 summarises the conclusions of the thesis and suggests areas for future work. A nomenclature and bibliography can be found at the back, along with appendices that provide supplementary information regarding the derivation and numerical treatment of methods relevant to this thesis.

Chapter 2

Background

This thesis investigates the application of mean reaction rate closures for simulations of nanoparticle formation in turbulent reacting flow. Detailed models offer a possible means to gain insight into a range of industrial processes. The overall method must couple models for detailed chemistry and turbulent flow to a population balance that describes the evolution of the nanoparticles. The thesis considers the example of the chloride process for the production of titania nanoparticles and this chapter starts with a discussion of the titania industry to provide some context for the work. The remainder of this chapter reviews current population balance, turbulent flow and turbulent reacting flow methods and examines the suitability of possible models from each area. It critically assesses previous models of nanoparticle formation in turbulent reacting flow and concludes with a discussion of the scope and terminology of the investigations in this thesis.

2 BACKGROUND

2.1 Titania nanoparticles

Titania (titanium dioxide, TiO_2) nanoparticles are a white pigment. The titania itself is colourless (Boulos et al., 2002) and the white appearance of the product is controlled by the size, shape and crystal phase of the particles. **Figure 2.1** shows an image of typical TiO_2 nanoparticles composed of small agglomerates.

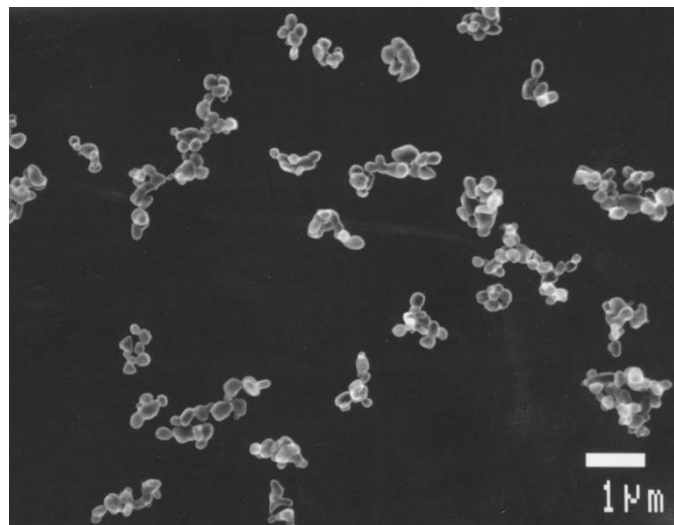


Figure 2.1: *Transmission electron micrograph of titania nanoparticles, courtesy of and with permission from Tioxide Europe Ltd.*

The nanoparticles scatter light by a combination of reflection, refraction and diffraction (DuPont Titanium Technologies, 2002). Diffraction occurs when light passes near a particle and is most effective when the particle diameter is slightly less than half the wavelength of the incident light. The particle diameter affects the quality of the product and must be tightly controlled. For example, pigments with smaller particles give products that tend to have a bluish tint; pigments with larger particles cause a more yellowish tint (Allen and Gergely, 1998).

Reflection and refraction occur due to a difference in refractive index between the pigment and the material in which it is dispersed. The greater the refractive index of the pigment, the greater the reflection and refraction. Titania pigments are commercially available in two crystal phases: anatase and rutile. Both phases have high refractive indices, making them effective pigments.

2.1.1 Applications

Titania pigments are used in paints, paper, plastics and textiles. **Figure 2.2** shows the consumption of titania across different product areas in the USA, historically the largest consumer of titania in the world. The preferred phase depends on the application. Rutile is preferred for paints and plastics. It scatters light more efficiently and is less likely to result in degradation of the product when exposed to sunlight (DuPont Titanium Technologies, 2007).

Anatase is photocatalytic and less abrasive than rutile. It is used to pigment paper to avoid unnecessary wear of the cutting blades in the paper-mill. Likewise, it is used to brighten man-made fibres such as polyester, rayon and viscose (Boulos et al., 2002). It reduces wear during the manufacturing process, but the fibres are subject to photocatalytic degradation when exposed to sunlight. A few applications exploit the photocatalysis. For example, anti-fogging glass, self-cleaning and anti-microbial coatings (Fujishima et al., 1999). Applications in solar water purification are being developed (Morgan, 2008; Williams and Duffy, 2009).

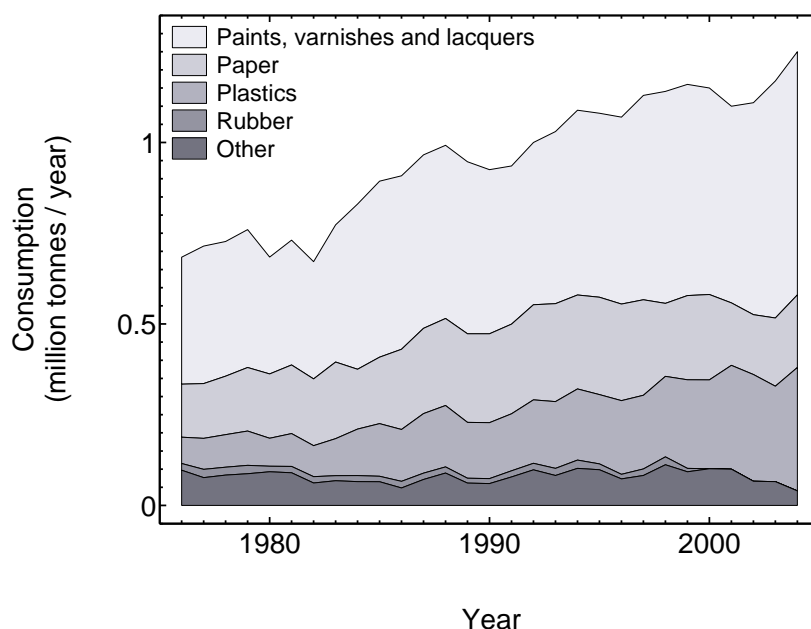


Figure 2.2: Consumption of titania in the USA by product area, (data from the U.S. Geological Survey, Buckingham and Gambogi, 2006).

2 BACKGROUND

2.1.2 Economic aspects

Titania nanoparticles represent a three-quarters share of the global white pigment market (1996) (Grant et al., 2004) and are produced at a rate of 5 million tonnes per year, worth sales of £7 billion in over 170 countries (2009) (Hill, 2009).

Figure 2.3 illustrates a few economic aspects of the titania industry. It shows that the growth in the world gross domestic product (GDP), a measure of global living standards, broadly correlates with world demand for titania between 1989–1996. The increase in demand for titania since 1980 has been met by an increase in capacity via the chloride process.

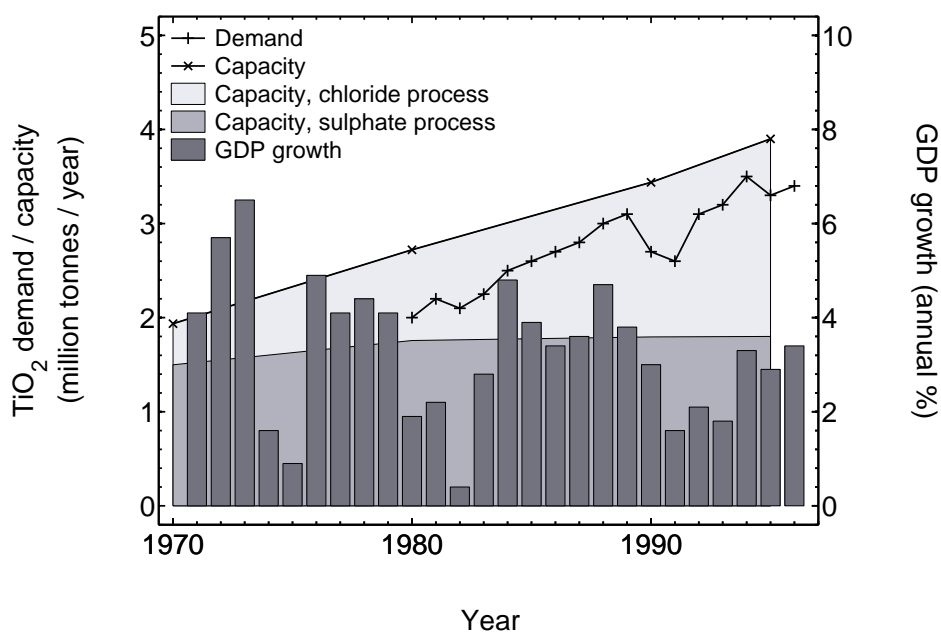


Figure 2.3: World GDP growth, demand and capacity for titania. The capacity is broken down into contributions from the chloride and sulphate processes. Adapted from Grant et al. (2004) with permission from The Royal Society of Chemistry and the University of Hull. GDP data: World Bank (2011), demand data: Grant et al. (2004), capacity data: Büchel et al. (2000).

2.1.3 Manufacturing processes

Titania pigments are manufactured via either the chloride or sulphate processes. The sulphate process was commercialised in 1931 and can produce either anatase or rutile (post 1941). The chloride process was introduced by DuPont in 1948 (Schaumann, 1949; Krchma and Schaumann, 1951) and can only produce rutile (DuPont Titanium Technologies, 2007). The chloride process requires higher grade ores, but generally has lower capital and operating costs (ICIS, 2011). The remainder of this section (2.1.3) is mainly summarised from Büchel et al. (2000).

The chloride process

The chloride process typically uses a rutile ore. The overall economics depend on the purity of the available material. The ore is chlorinated to form titanium tetrachloride (TiCl_4). This is mixed with reducing agents to treat impurities and purified by distillation. The purified TiCl_4 is oxidised in either a flame (Pratsinis et al., 1997) or by stage-wise addition to an oxygen plasma (Morris and Coe, 1989; Deberry et al., 2002) at elevated pressure (Haddow, 1997) to produce TiO_2 particles and chlorine. The chlorine can be recycled. **Figure 2.4** illustrates the process.

Various additives and in particular water and aluminium trichloride are used to modify the oxidation and control the product quality (for example see Schaumann, 1949; Krchma and Schaumann, 1951; Santos, 1970; Hartmann, 1996).

Post treatments

TiO_2 pigments are often milled to break up agglomerated particles. Excessive agglomeration reduces the product quality and leads to products with lower gloss (Allen and Gergely, 1998). Figure 2.1 shows pre-milled material, whereas the ideal product would show a monodisperse distribution with a prescribed mean size. The milling is typically performed using either fluid-energy (Slepetys, 1970) or media mills (Niedenzu et al., 1996) and adds significant cost to the pigment. The more control that can be used to minimise agglomeration and reduce the need for milling, the lower the overall production cost.

2 BACKGROUND

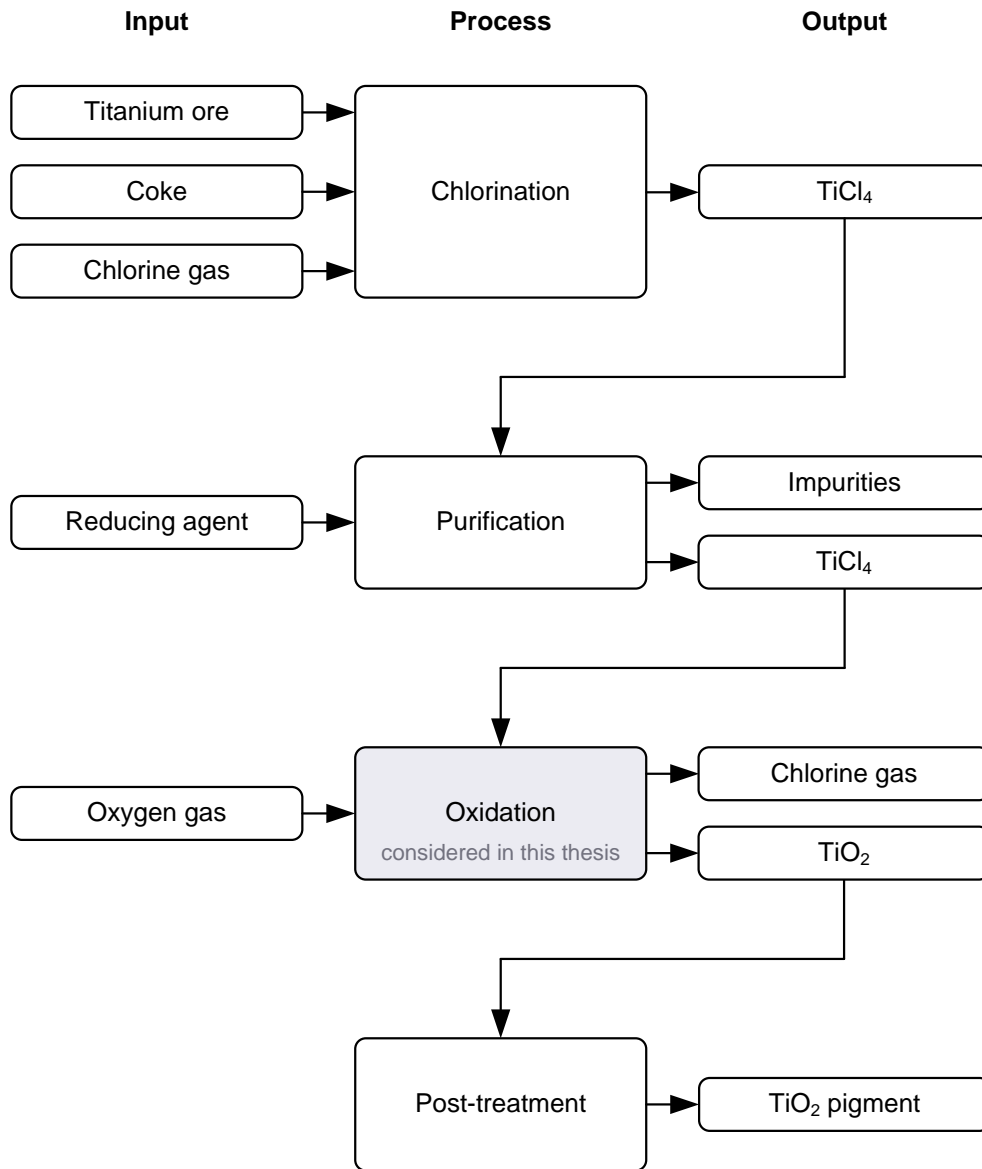


Figure 2.4: Chloride process for titania manufacture, adapted from Büchel et al. (2000) with permission from Wiley-VCH. Original copyright held by Wiley-VCH Verlag GmbH & Co. KGaA. Chapter 5 of this thesis considers how to model the oxidation process.

2.1.4 Kinetic models for titania formation

Typical industrial conditions for the oxidation step of the chloride process are a stoichiometric mixture of TiCl_4 and O_2 plus additives reacting at 1500–2000 K. The process is difficult to investigate experimentally under these conditions. It has been widely studied at milder conditions, but understanding remains incomplete.

[Ghoshtagore \(1970\)](#) investigated the surface addition of TiCl_4 to a TiO_2 film. The reaction was suggested to display an Eley-Rideal dependence on TiCl_4 and O_2 at 673–1120 K. [Pratsinis et al. \(1990\)](#) studied the global oxidation kinetics of TiCl_4 vapour at 973–1273 K. The reaction was first-order in TiCl_4 and approximately zero-order in O_2 up to ten-fold excess O_2 . [Pratsinis and Spicer \(1998\)](#) compare the overall kinetics with a gas-phase rate inferred from the difference between the overall rate ([Pratsinis et al., 1990](#)) and a surface growth rate ([Ghoshtagore, 1970](#)) assuming monodisperse spherical particles. They show that surface reaction has a significant effect on the particle diameter. Later studies using more detailed population balance models draw similar conclusions ([Tsantilis and Pratsinis, 2004](#); [Morgan et al., 2005, 2006](#); [Heine and Pratsinis, 2007a](#)).

[West et al. \(2007a,b\)](#) argue that more detailed understanding of the chemical mechanism may yield deeper insight. They present a detailed mechanism for the high temperature oxidation of TiCl_4 . The reaction is suggested to proceed via titanium oxychloride species. Unknown thermochemical data are estimated by density functional theory based quantum calculations. Subsequent investigations present an updated mechanism ([West et al., 2009](#)) and consider the role of aluminium trichloride additives ([Shirley et al., 2009](#)).

[Mehta et al. \(2010\)](#) compare the inception behaviour of the mechanisms from [Pratsinis and Spicer \(1998\)](#) and [West et al. \(2009\)](#). They show that the choice of mechanism causes particle inception to occur at different locations in simulations of a turbulent flame and would be expected to significantly influence the behaviour of the model. This is consistent with recent observations ([Shirley et al., 2011](#)) where the choice of inception mechanism is noted to strongly affect simulations of Pratsinis' original experiment ([Pratsinis et al., 1990](#)).

2.2 Population balance models

Population balance models are often used to describe nanoparticle formation and are discussed in detail by [Ramkrishna \(2000\)](#). The basic population balance equation (PBE) is the [Smoluchowski \(1917\)](#) equation. In discrete form

$$\frac{dn_i}{dt} = \frac{1}{2} \sum_{j=1}^{i-1} \beta_{j,i-j} n_j n_{i-j} - \sum_{j=1}^{\infty} \beta_{i,j} n_i n_j, \quad (2.1)$$

where n_i is the number density of particles of size i and $\beta_{i,j}$ describes the rate of successful collisions between particles of size i and j . The first term on the right-hand side describes the creation of particles due to collisions between all combinations of particles with sizes that sum to i . The second term describes the destruction of particles due to collisions between particles of size i and any other size j . The main approaches that have been applied to nanoparticles are summarised below.

2.2.1 Particle models

The particle model is the numerical description of the particles. The choice of model is often constrained by the numerical method.

Spherical particle models consider a univariate particle description, for example particle size ([Spicer et al., 2002](#); [Tsantilis and Pratsinis, 2004](#)), and assume a fixed geometric relationship between particle diameter, surface area and volume. Coagulation conserves volume, but not surface area. Such models can describe particle formation, growth and coalescence, but preclude the sintering of aggregates.

Surface-volume models consider a bivariate particle description, for example surface area and volume ([Xiong and Pratsinis, 1993](#)). Coagulation is aggregative and conserves surface area and volume. Sintering can be modelled as a relaxation of the surface area back to that of an equivalent spherical particle of equal mass.

Multi-variate models offer the most complete particle description of the models considered. For example, they enable a description of aggregates where sintering and growth depend on the connectivity and chemical composition of primary particles within each aggregate ([Sander et al., 2009, 2011](#); [Shekar et al., 2011](#)).

2.2.2 Numerical methods

The numerical method is how a PBE is solved for the chosen particle model.

Moment methods

The method of moments (MoM) solves low-order moments of the PBE. It was developed to model particles in inhomogeneous flows (Hulbert and Katz, 1964). The distribution itself remains unknown and the moment equations are generally unclosed. Early studies often assumed a log-normal distribution (for example Pratsinis, 1988). More recent closures have relaxed this assumption.

The method of moments with interpolative closure (MoMIC) uses interpolation among known whole-order moments to close fractional-order moments that arise due to coagulation and surface growth processes. It was introduced by Frenklach and Harris (1987) and has been reviewed in detail by Frenklach (2002). It is efficient and widely favoured for problems involving populations and flow. For example, a modified version (Revzan et al., 1999) of PREMIX (Kee et al., 1985) has been used for a number of fully coupled 1D laminar flame simulations (Appel et al., 2000; Zhao et al., 2003; Singh et al., 2005). Good accuracy is reported in the first moment for organic (Balthasar and Kraft, 2003) and inorganic (Grosschmidt et al., 2002) systems. Most implementations are univariate and assume spherical particles, but MoMIC has also been extended to bivariate studies of aggregate particle growth (Balthasar and Frenklach, 2005; Mueller et al., 2009).

The quadrature method of moments (QMoM) (McGraw, 1997) uses a quadrature approximation to close the MoM equations. It solves for moments of the population and calculates the quadrature approximation as required. The method was developed for univariate distributions, but has been extended to bivariate (Wright Jr et al., 2001) and trivariate (Fox, 2008) cases, and several alternative quadrature algorithms have been studied (see Grosch et al., 2007). QMoM has been shown to give reliable results compared to other MoM (Terry et al., 2001) and sectional (Marchisio et al., 2006) methods. It is easily coupled to computational fluid dynamics (CFD) codes and has been used to model barium sulphate nanoparticle formation in a confined impinging jet reactor (Gavi et al., 2007b).

2 BACKGROUND

The direct quadrature method of moments (DQMoM) (Marchisio and Fox, 2005) uses a projection method and quadrature approximation of the PBE to derive equations that force the statistics of the quadrature approximation to obey specified moments of the approximated PBE. The method solves for the parameters of the quadrature approximation, rather than moments of the population. It has been rigorously compared to QMoM (Fox, 2006a) and its application to PBEs and CFD is well established. It has been used to study fluidised beds (Fan et al., 2004; Fan and Fox, 2008), spray coalescence (Fox et al., 2008; Desjardins et al., 2008) and soot formation (Zucca et al., 2006, 2007). DQMoM is easily extended to multi-variate models, but can be numerically challenging (Zucca et al., 2007).

Moment inversion methods are often used to estimate a distribution from a finite set of moments (for example see Souza et al., 2010). In general, such problems are poorly conditioned and the methods are limited to low dimensional cases. Independent advection of the moments may sometimes give ‘invalid moment sets’ for which no underlying distribution exists. This is the *moment advection problem*. It occurs in algorithms that are greater than first order in space and is considered in detail by Wright Jr (2006).

Sectional methods

Sectional methods approximate the distribution by discretising the particle state space. Moving sectional methods were introduced to control numerical diffusion and have been applied to several studies of titania nanoparticle formation (Spicer et al., 2002; Tsantilis and Pratsinis, 2004). Bivariate formulations are possible and have been used to investigate the sintering of silica and titania (Seto et al., 1997; Heine and Pratsinis, 2007a). Sectional methods resolve the full distribution, but are significantly more expensive than moment methods.

Monte Carlo methods

Monte Carlo methods simulate the evolution of the particle distribution as a series of discrete events acting on an ensemble of stochastic particles. They efficiently

extend to multi-variate particle models and have been proved to converge to the solution of the governing population balance (Eibeck and Wagner, 2003; Wells, 2006). A number of stochastic algorithms have been developed (Eibeck and Wagner, 2000, 2001) and refined (Goodson and Kraft, 2002; Wells and Kraft, 2005; Wells et al., 2006; Patterson et al., 2006a,b) for nanoparticle applications. They can be used to post process existing chemistry data (Zhao et al., 2003; Singh et al., 2005; Morgan et al., 2007) or coupled directly to homogeneous chemistry solvers (Celnik et al., 2007, 2009). Stochastic methods allow detailed multi-variate particle models and are an attractive option for post processing existing data, but are often expensive and not easily coupled to CFD simulations.

2.2.3 Dilute and concentrated regimes

Heine and Pratsinis (2007a,b) use a surface-volume model to assess the validity of equation (2.1) at high volume fractions. They note a transition from dilute to concentrated aerosol dynamics at *effective* volume fractions (which include the volume of voids within the aggregate structures) greater than 1%. They suggest that “at these conditions, classic Smoluchowski theory may no longer describe agglomerate coagulation and particles may affect fluid flow”.

Heine and Pratsinis (2007c) follow this with a first principles investigation using Langevin Dynamics simulations of particle collisions at volume fractions between 0.01–35%. The Smoluchowski equation is shown to be accurate for dilute systems with volume fraction less than 0.1%. Buesser et al. (2009) extend this work to propose a modified coagulation rate expression for volume fractions up to 20%.

2.3 Turbulent flow models

Turbulent flows are unsteady and irregular. The velocity varies significantly and irregularly in both position and time. The main approaches to modelling turbulent flows are discussed below. The discussion is largely summarised from the books by Tennekes and Lumley (1972), Acheson (1990) and Pope (2000).

2 BACKGROUND

2.3.1 Governing equations

The fundamental equations governing turbulent reacting flow are conservation of mass, momentum, chemical species and enthalpy (Pope, 1985, 2000)

$$\frac{\partial \rho}{\partial t} + \frac{\partial}{\partial x_i} (\rho U_i) = 0, \quad (2.2)$$

$$\rho \frac{\partial U_j}{\partial t} + \rho U_i \frac{\partial U_j}{\partial x_i} = \frac{\partial \tau_{ij}}{\partial x_i} - \frac{\partial p}{\partial x_j} + \rho g_j, \quad (2.3)$$

$$\rho \frac{\partial \phi_\alpha}{\partial t} + \rho U_i \frac{\partial \phi_\alpha}{\partial x_i} = - \frac{\partial J_i^\alpha}{\partial x_i} + \rho S_\alpha. \quad (2.4)$$

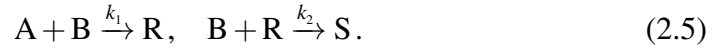
The species and enthalpy equations are written in common form in terms of the scalar *composition* vector ϕ . The velocity U and composition ϕ are Eulerian fields referenced by the position x in an inertial frame, where ρ and p are the fluid density and pressure, and g_j is the body force per unit mass in the j -direction. τ_{ij} is a stress tensor and describes viscous surface forces, J_i^α is a diffusive flux vector and describes molecular transport of scalar α . At low Mach numbers, the coupling between equations (2.3) and (2.4) is mainly through the density. The equations are in cartesian tensor notation and the summation convention applies.

The solution to equation (2.3) is *turbulent* at high Reynolds numbers. The turbulence results from instabilities to small perturbations in the flow. The instabilities cause unsteady and irregular eddies that are themselves unstable and are broken down. There is a cascade of energy and loss of directionality down the length scale of the eddies. The largest eddies are influenced by the geometry of the flow and are characterised by the *turbulence integral scale*. The smallest eddies are characterised by the *Kolmogorov scale*, defined by the eddy size at which the Reynolds number is of order unity, where the instabilities are overcome by viscosity. Their behaviour is dictated by the rate of energy transfer from the larger scales.

The largest structures in the solution to equation (2.4) are characterised by the *scalar integral scale* and are affected by the flow and the initial conditions. The smallest structures are characterised by the *Batchelor scale*, where molecular diffusion overcomes turbulent mixing. The rate of molecular diffusion is negligible at large scales and non-premixed scalars will remain segregated above the Batche-

lor scale. The Batchelor and Kolmogorov scales are of the same order in gas-phase flows. In liquid-phase flows, the Batchelor scale is smaller than the Kolmogorov scale, and the scalar field contains more fine-scale structure than the velocity field.

The term in S_α in equation (2.4) is a *source term*. It describes the source of species due to chemical reaction and the source of enthalpy due to compressibility, viscous dissipation and radiation. Equation (2.4) is harder to solve for reacting than non-reacting flow. The chemical source term is often non-linear and strongly coupled to the turbulent mixing of the scalars ϕ . For example, consider the reaction



The chemical source term is given (in terms of the molar concentrations C_α)

$$\begin{aligned} S_A(C) &= -k_1 C_A C_B, \\ S_B(C) &= -k_1 C_A C_B - k_2 C_B C_R, \\ S_R(C) &= +k_1 C_A C_B - k_2 C_B C_R, \\ S_S(C) &= +k_2 C_B C_R. \end{aligned} \quad (2.6)$$

In the case $k_1 \gg k_2$, the selectivity of species R is sensitive to mixing (see [Bourne and Rys, 1981](#)) and this reaction is used as a test case on this basis later on.

2.3.2 Numerical methods

Direct numerical simulation

Turbulent flows may be fully described by direct numerical simulation (DNS). The conservation equations are discretised and solved numerically over a spatial grid to *resolve* the whole range of spatial and temporal turbulence scales. The main difficulty is that the method requires such high resolution grids that it quickly becomes intractable. The use of DNS is limited by computational expense.

Many practical applications require turbulent flows to be *modelled* rather than resolved. Turbulent flow models typically separate the velocity and scalar fields into resolved and unresolved components. Two common approaches are Large-eddy simulation (LES) and Reynolds-averaged Navier-Stokes (RANS) methods.

2 BACKGROUND

Large-eddy simulation

Large-eddy simulation (LES) uses a filter to separate the velocity and scalar fields into filtered (resolved) and residual (unresolved) fields. The filtered fields are simulated directly and LES resolves three-dimensional time dependent solutions of the large energy-containing scales in the flow. However, the information in the residual fields is lost. The equations for the filtered fields contain unclosed terms that depend on the residual fields. Models are required to close any processes that occur at the unresolved scales, including chemical reaction. The computational cost of LES is much less than DNS, but significantly more than RANS.

Reynolds-averaged methods

Reynolds-averaged methods use a *Reynolds decomposition* to separate the velocity and scalar fields into a mean (resolved) and fluctuating (unresolved) component

$$U = \langle U \rangle + u', \quad (2.7)$$

$$\phi = \langle \phi \rangle + \phi'. \quad (2.8)$$

Reynolds-averaged Navier-Stokes (RANS) equations can be derived from equations (2.3) and (2.4) for constant-property Newtonian fluids (see Pope, 2000, ch. 4)

$$\frac{\partial \langle U_j \rangle}{\partial t} + \langle U_i \rangle \frac{\partial \langle U_j \rangle}{\partial x_i} + \frac{\partial \langle u'_i u'_j \rangle}{\partial x_i} = \nu \nabla^2 \langle U_j \rangle - \frac{1}{\rho} \frac{\partial \langle p \rangle}{\partial x_j}, \quad (2.9)$$

$$\frac{\partial \langle \phi_\alpha \rangle}{\partial t} + \langle U_i \rangle \frac{\partial \langle \phi_\alpha \rangle}{\partial x_i} + \frac{\partial \langle u'_i \phi'_\alpha \rangle}{\partial x_i} = \Gamma_\alpha \nabla^2 \langle \phi_\alpha \rangle + \langle S_\alpha \rangle, \quad (2.10)$$

where ν is the kinematic viscosity, Γ_α is the diffusivity of scalar α and the pressure field p includes gravitational body forces. The diffusive mass fluxes are assumed to obey Fick's law. Unity Lewis numbers are assumed for all species.

RANS methods solve equations (2.9) and (2.10) for the mean velocity and scalar fields. The fluctuating fields are unresolved and several terms must be closed. The *Reynolds stress* $\langle u'_i u'_j \rangle$ describes momentum transfer by the velocity fluctuations.

The *scalar flux* $\langle u'_i \phi'_\alpha \rangle$ describes scalar transport due to the velocity fluctuations.¹ The most common models provide direct closures for the Reynolds stress and scalar flux terms using the *gradient-diffusion* and *turbulent-viscosity* hypotheses

$$\langle u'_i \phi \rangle = -\Gamma_T \frac{\partial \langle \phi \rangle}{\partial x_i}, \quad (2.11)$$

$$\langle u'_i u'_j \rangle = \frac{2}{3} k \delta_{ij} - \nu_T \left(\frac{\partial \langle U_i \rangle}{\partial x_j} + \frac{\partial \langle U_j \rangle}{\partial x_i} \right), \quad (2.12)$$

where k is the turbulent kinetic energy, ν_T is the turbulent viscosity and Γ_T is the turbulent diffusivity. The most common example is the k - ε model. This solves additional transport equations for the turbulent kinetic energy k and the turbulent dissipation rate ε , and models ν_T and Γ_T as a function of k and ε .

RANS methods are computationally efficient and for this reason are the workhorse of most commercial CFD codes. At high Reynolds numbers, the efficiency of RANS simulations is often further increased by using wall functions to model rather than resolve the flow next to solid boundaries. The RANS velocity equation (2.9), the k - ε model and standard wall functions are the basis of the flow simulations in this thesis. Pope (2000) discusses the benefits and limitations of the k - ε model and alternative approaches in more detail.

Favre-averaged methods

Density fluctuations occur in many turbulent reactions, for example combustion. It is convenient to modify the RANS method to avoid fluctuating density terms by decomposing the fields in terms of fluctuations about a *density-weighted* mean

$$U = \tilde{U} + u'', \quad \text{where } \langle \rho \rangle \tilde{U} = \langle \rho U \rangle, \quad (2.13)$$

$$\phi = \tilde{\phi} + \phi'', \quad \text{where } \langle \rho \rangle \tilde{\phi} = \langle \rho \phi \rangle. \quad (2.14)$$

Density-weighted (known as *Favre-averaged*) transport equations can be derived from equations (2.3) and (2.4). The equations share the form of their RANS counterparts and can be closed using the same turbulence models (see Jones, 1994).

¹ Note that some authors write the scalar flux as $\langle u'_i \phi_\alpha \rangle = \langle u'_i \phi'_\alpha \rangle + \langle u'_i \overset{0}{\phi_\alpha} \rangle = \langle u'_i \phi'_\alpha \rangle$.

2.4 Turbulent reacting flow models

The principal difficulty in the application of turbulent flow models to reacting flows is that the *chemical source term is unclosed for non-linear reactions* if the scalar fields are not fully resolved. This is manifested as the *mean reaction rate closure problem* in RANS and Favre-averaged methods

$$\langle S_\alpha(\phi) \rangle \neq S_\alpha(\langle \phi \rangle), \quad (2.15)$$

and an analogous problem exists for LES. The problem can often be addressed using the same turbulent reaction models for all three methods.

Comprehensive reviews of turbulent reaction models are given in the books by Libby and Williams (1980, 1994), Peters (2000), Fox (2003), Cant and Mastorakos (2008) and the articles by Klimenko and Bilger (1999), Veynante and Vervisch (2002) and Haworth (2010). In general, knowledge of the joint composition probability density function (PDF) f_ϕ is required to close the source term

$$\langle S_\alpha(\phi) \rangle = \int_{-\infty}^{+\infty} S_\alpha(\psi) f_\phi(\psi) d\psi, \quad (2.16)$$

where the integration is over the full composition vector space. It has been shown that “all commonly employed models for turbulent reacting flows can be formulated in terms of the joint PDF of the chemical species and enthalpy” (Fox, 2003). The following section (2.4.1) summarises the basis of salient reaction rate closures. PDF-based methods are discussed in more detail in section 2.4.2.

2.4.1 Mean reaction rate closures

Moment methods

The chemical source term can be closed by judicious assumptions in a few cases. In the *slow chemistry* limit, mixing is assumed to finish before reaction starts, such that the scalars react at their mean concentrations. This is equivalent to the ideal reactor models used in chemical reaction engineering (*cf.* Levenspiel, 1999).

2.4 Turbulent reacting flow models

In the *fast chemistry* limit, the rate of premixed reactions is often assumed to be equal to the rate of mixing with hot products. This is the basis of the eddy break up model (Spalding, 1971). A number of related models assume a rate equal to the minimum of the eddy dissipation and chemical (based on mean concentration) rates, for example the eddy dissipation model (Magnussen and Hjertager, 1977).

Equilibrium chemistry

In the equilibrium chemistry limit, non-premixed reactions can be parameterised by a mixture fraction (see Fox, 2003). The mixture fraction is a conserved scalar and the problem is reduced to modelling the scalar mixing and variance of the mixture fraction. The equilibrium limit is known to be inaccurate for *finite-rate* chemistry, where the chemical and mixing time scales are of the same order.

Conditional moment closures

Conditional moment closures solve equations for the moments of non-premixed scalars conditioned on a mixture fraction (see Klimenko and Bilger, 1999). The chemical source term is calculated using the conditional moments, and often just the conditional means. The approach is motivated by experimental and DNS data that show little fluctuation about the conditional mean, even for finite-rate chemistry. However, inhomogeneous flows are problematic due to significant fluctuations arising from back-mixing, ignition and extinction effects (Fox, 2003).

Flamelet methods

Flamelet methods model non-premixed reactions as occurring in thin sheets (see Peters, 2000). The problem is reformulated in terms of a mixture fraction and a one-dimensional reaction-diffusion equation describing the direction normal to the flame surface. The reaction equation is independent of spatial location and can be solved separately from the flow. Flamelet methods can describe extinction and are typically valid for fast combustion-like reactions. They work less well for slower reactions or cases with back-mixing (Fox, 2003).

2 BACKGROUND

2.4.2 Probability density function methods

PDF methods are applicable to all flows and chemistry. The most common methods transport either a joint composition or joint velocity-composition PDF. In this thesis, it will be sufficient to consider a one-point one-time Favre-averaged joint composition PDF \tilde{f}_ϕ subject to the transport equation (Pope, 1985)

$$\begin{aligned} \frac{\partial}{\partial t} \left(\langle \rho \rangle \tilde{f}_\phi \right) + \frac{\partial}{\partial x_i} \left(\tilde{U}_i \langle \rho \rangle \tilde{f}_\phi \right) + \frac{\partial}{\partial \psi_\alpha} \left(S_\alpha(\psi) \langle \rho \rangle \tilde{f}_\phi \right) = \\ \frac{\partial}{\partial \psi_\alpha} \left(\left\langle \frac{1}{\rho} \frac{\partial J_i^\alpha}{\partial x_i} \middle| \psi \right\rangle \langle \rho \rangle \tilde{f}_\phi \right) - \frac{\partial}{\partial x_i} \left(\langle u_i'' | \psi \rangle \langle \rho \rangle \tilde{f}_\phi \right), \end{aligned} \quad (2.17)$$

where the scalars ϕ obey equation (2.4). The critical advantage is that all terms on the left hand side of equation (2.17) are closed, *including the chemical source term*. The terms on the right hand side describe the diffusive and turbulent convective fluxes. They are unclosed and must be modelled. The turbulent convective flux is often closed using a gradient diffusion model (*cf.* equation 2.11)

$$\langle u_i'' | \psi \rangle \langle \rho \rangle \tilde{f}_\phi = -\Gamma_T \frac{\partial \tilde{f}_\phi}{\partial x_i}. \quad (2.18)$$

Assuming equal molecular diffusivities, unity Lewis number for all species and that the diffusive mass flux obeys Fick's law, the diffusive flux can be written

$$\left\langle \frac{1}{\rho} \frac{\partial J_i^\alpha}{\partial x_i} \middle| \psi \right\rangle = -\langle \Gamma \nabla^2 \phi_\alpha | \psi \rangle, \quad (2.19)$$

and needs to be closed using a *micromixing* model. The simplest mixing model is the interaction by exchange with the mean (IEM) model (Villermaux and Devillon, 1972) (also introduced by Dopazo and O'Brien (1974) as the LMSE model)

$$\langle \Gamma \nabla^2 \phi_\alpha | \psi \rangle = \frac{C_\phi}{2\tau_\phi} (\langle \phi_\alpha \rangle - \psi_\alpha), \quad (2.20)$$

where C_ϕ is an empirical constant and τ_ϕ is a scalar mixing time. Other mixing models exist (for example Curl, 1963; Pope, 1982) and are reviewed by Dopazo (1994), although none are totally satisfactory. Further details are beyond the scope of this work, but Pope (2000, ch. 12) and Haworth (2010) are good places to start.

PDF methods fall into two categories, *presumed* and *transported* PDF methods. Presumed methods assume a form for the PDF *a priori* and transport the parameters of this assumption, for example a mean and variance. An assumed beta PDF works well for the binary mixing of conserved scalars such as a mixture fraction, where a unimodal PDF is expected to evolve from a u-shaped distribution. However, complex systems are problematic and presumed PDF methods have not been successful for non-premixed turbulent combustion (Cant and Mastorakos, 2008).

Transported PDF methods solve a transport equation for the joint PDF of a set of variables that describe the hydrodynamic and/or thermochemical state of a flow. However, the numerical solution of such systems is formidable using the conventional finite-difference methods (Cant and Mastorakos, 2008) found in commercial CFD codes. The standard approach is to use the Monte Carlo methods introduced by Pope (1985). The transport equation is solved by discretising the PDF using an ensemble of stochastic particles and transporting the particles in physical and composition space. We denote these *full* or *Lagrangian* transported PDF methods. They scale efficiently to multiple scalars and, unlike presumed methods, can approximate any PDF. In practice, they are computationally expensive because large numbers of particles are required to reduce statistical error.

The development of transported PDF methods since Pope's 1985 paper has been reviewed by Pope (1991), Kollmann (1990), Dopazo (1994) and Haworth (2010). Two recent and related methods amenable to existing CFD codes are the stochastic fields (SF) method and the direct quadrature method of moments using the interaction by exchange with the mean micromixing model (DQMoM-IEM). Despite the attention, no studies have directly compared the methods.

The stochastic fields method

The SF method uses a set of Eulerian fields to discretise a joint composition PDF transport equation. The fields are defined over the entire spatial domain and evolve according to a stochastic partial differential equation (SPDE) such that they remain statistically equivalent to the joint composition PDF. The method was investigated in detail by Valiño (1998) and Sabel'nikov and Soular (2005a). Valiño derives an Itô SPDE for fields defined as twice differentiable in space,

2 BACKGROUND

whereas [Sabel'nikov and Soulard](#) derive a Stratonovich SPDE without this stipulation and show equivalence to [Valiño's](#) result. The method extends to multiple scalars ([Hauke and Valiño, 2004](#)) and is also known as the Field Monte Carlo and Eulerian Monte Carlo method.

The SF method is a Monte Carlo method and a significant number of fields may be required to control statistical error. The implementation and application of the Itô and Stratonovich SPDEs are studied by [Garmory \(2007\)](#). The stochastic terms arise from the turbulent convective flux in the PDF transport equation. They are proportional to the spatial scalar gradient and [Valiño \(1998\)](#) argues that the model preserves boundedness because the scalar derivatives tend to zero at extremal values. However, [Garmory \(2007\)](#) shows that the numerical implementation must still enforce boundedness because of the spatial discretisation of the scalars. To date, all implementations have used the IEM model.

A number of investigations have applied the SF method to turbulent reacting flow problems. [Sabel'nikov and Soulard \(2005b, 2006\)](#) provide more information about the derivation and numerical implementation of the method and test its application to a premixed methane flame over a backward facing step. [Soulard and Sabel'nikov \(2006\)](#) extend the method to a joint velocity-mass fraction PDF. [Garmory et al. \(2006, 2008, 2009\)](#) investigate the dispersion of reactive pollutants in RANS simulations of a test plume, aircraft exhaust and street canyon.

Jones and co-workers present a systematic study of extinction and re-ignition in LES simulations of increasingly complex flames. The work starts with a piloted methane flame described by a global mechanism ([Mustata et al., 2006](#)), before considering the auto-ignition of hydrogen ([Jones et al., 2007](#); [Jones and Navarro-Martinez, 2007](#)) and n-heptane ([Jones and Navarro-Martinez, 2009](#)). [Jones and Prasad \(2010, 2011\)](#) consider the local extinction and spark ignition of methane flames. Most recently, [Jones and Tyliszczak \(2010\)](#) use a two-phase model to study ignition in an aircraft engine. The studies show that the SF method is capable of simulating local extinction and re-ignition in LES. The n-heptane study is one of the first attempts to do this for realistic fuels.

All the above studies use an Itô formulation, apart from [Jones and Navarro-Martinez \(2009\)](#) and the work by [Sabel'nikov and Soulard](#).

The direct quadrature method of moments using the interaction by exchange with the mean micromixing model

DQMoM-IEM uses a weighted field approximation to discretise a joint composition PDF transport equation that includes the IEM mixing model. A projection method is used to derive transport equations that force the statistics of the fields to obey specified moments of the discretised PDF transport equation. The method was suggested by [Fox \(2003\)](#) and is analogous to the DQMoM population balance method (see page 14). The IEM suffix denotes a modified projection used to enforce boundedness in inhomogeneous scalar mixing problems and we talk about *fields* because the approximation is continuous in physical space.

DQMoM-IEM is deterministic and offers a potential advantage over Monte Carlo methods in that, theoretically at least, the number of fields can be chosen based on the requirements of the problem, suggesting a computationally efficient method. The model equations are derived in an appendix to [Fox \(2003\)](#) as a specific case of a multi-environment presumed PDF method (see [Fox, 2003](#), section 5.10). The source terms are calculated by inverting a linear system. [Fox](#) notes that accurate numerical inversion is difficult because the linear system is often poorly conditioned and is singular if any fields are degenerate at a given physical location. A local perturbation in composition space is suggested to overcome this. It is also noted ([Fox, 2003](#), pp. 232–233) that multi-environment methods with few environments (and implicitly DQMoM-IEM with few fields) may struggle in cases that are sensitive to the shape of the PDF, for example non-isothermal reactions.

Several investigations have applied DQMoM-IEM to turbulent reacting flows. The principal reference is [Wang and Fox \(2004\)](#), who show good agreement between DQMoM-IEM, multi-environment and full transported PDF simulations of the reactive precipitation of barium sulphate. They note that DQMoM-IEM may lose boundedness due to terms arising from the turbulent convective flux, and they neglect these terms where variables are close to theoretical bounds. They describe the perturbation used to help invert the linear system and suggest an alternative approach using average information from neighbouring grid points. Prior to this, elements of DQMoM-IEM can be found in studies of finite-mode PDF multi-environment methods, for example [Tsai et al. \(2002\)](#) and [Fissore et al. \(2002\)](#).

2 BACKGROUND

Later studies apply DQMoM-IEM to investigate the scale-up (Lui and Fox, 2006; Gavi et al., 2007a) and precipitation of barium sulphate (Gavi et al., 2007b) in confined impinging jet reactors. In each case, the problem is solved for a mixture fraction and two progress variables. Tang et al. (2007) benchmark the use of RANS simulations using DQMoM-IEM (labelled MEPDF) with two fields to model turbulent bluff-body methane flames. They solve the system for the species mass fractions and enthalpy and address the numerical difficulties by limiting the maximum value of the source terms. They show reasonable agreement with experimental data. Denison et al. (2010) show subsequent applications to industrial furnaces and gasifiers. Other studies use DQMoM-IEM to model fluctuations about the conditional mean in a conditional moment closure (Fox and Raman, 2004; Smith and Fox, 2007; Ali et al., 2011) and apply DQMoM-IEM in LES (Raman et al., 2006; Marchisio, 2009; Zhao et al., 2011). Raman et al. (2006) address the conditioning by setting the responsible terms to zero where any fields are separated by less than a threshold value. Zhao et al. (2011) re-implement some of the methane flame simulations of Tang et al. (2007) and show that DQMoM-IEM is capable of simulating local extinction in LES.

Further insight into the numerical behaviour of DQMoM-IEM can be inferred from some DQMoM population balance studies. Fan et al. (2004) use a condition number to determine when to perturb the scalars. In singular cases, they either set the source terms to zero or take an average value from neighbouring grid points. Zucca et al. (2007) report better accuracy at the expense of increased numerical difficulties as the order of the quadrature approximation (equivalent to the number of fields) is increased. The choice of moments used to specify the projection affects accuracy and numerical stability, with low-order moments favouring better conditioning. Upadhyay and Ezekoye (2006) report similar findings regarding the moments. They suggest revising the choice of moments mid-calculation.

Whilst it has been shown that DQMoM-IEM offers a crude, but possibly efficient transported PDF method, several issues persist. The inversion of the linear system to evaluate the source terms remains numerically challenging. There is no study of the form of the source terms, no systematic analysis of the numerical issues and only high-level discussion of how to couple the method to a CFD code. At this point, it is not clear how to best address the numerical issues, nor how such choices would impact the performance and implementation of the method.

2.4.3 Tabulation methods

Much of the cost of turbulent reacting flow models arises from the chemistry. Methods that parameterise the chemistry in terms of a few variables, for example flamelet and equilibrium methods, offer the advantage that the chemistry can be solved off-line and read into the model from lookup tables. This makes such models very efficient, but is not practical in full transported PDF methods where the chemistry is parameterised by all the composition variables. However, PDF methods may still benefit from tabulating the chemistry *during* the calculation. Pope (1997) introduced *in-situ* adaptive tabulation (ISAT) to do just this.

The premise of ISAT is that the chemistry is an initial value problem where the same problem is solved with similar initial conditions many times during a calculation. ISAT initially solves and tabulates solutions to the chemistry when queried for new initial conditions, but otherwise interpolates solutions from the tabulation. The method prescribes an algorithm to control the interpolation error by deciding when to grow the table versus when to look up the solution. Since its introduction, ISAT has attracted a lot of interest and has been further refined by Pope and co-workers (Singer et al., 2006a,b; Liu and Pope, 2005; Lu and Pope, 2009). There is precedent for its application to DQMoM-IEM, where Tang et al. (2007) estimate that it gave a 150–250× speed-up for simulations using a 19 species mechanism.

2.5 Nanoparticle formation in turbulent reacting flows

Nanoparticle formation in turbulent reacting flows is a key field of research. Flame aerosol technology is used for the large-scale synthesis of many nanoparticle products, of which titania formed via the chloride process is the second largest product by value and volume (after carbon black) (Wegner and Pratsinis, 2003).

Pratsinis (1998) presents an overview of the history of flame aerosol technology. Rosner (2005) and Roth (2007) explain the rationale for combustion synthesis and review recent developments. Rosner (2009) reviews the contributions of various

2 BACKGROUND

submodels to an overall description of spray combustors and highlights the advent of *interacting population balance* methods, where the model considers both a reactive flow and its interaction with a discrete phase.

2.5.1 Existing modelling approaches

A number of studies have modelled nanoparticle formation in reacting flows in the manner of Rosner's (2009) interacting population balances. The studies typically assume small Stokes numbers such that the particles experience the same velocity and turbulent diffusivity as the fluid (Fox, 2006b; Gavi et al., 2007b), and the model can neglect the momentum equation for the solid phase. Current methods for modelling population balances within reactive flows are discussed in detail and formulated in a PDF transport equation framework by Rigopoulos (2007, 2010).

Soot formation in flames has been widely studied. The availability of experimental data mean that soot cases are often used for method development. A few studies use a two-stage methodology to model soot formation in premixed 1D laminar flames (Zhao et al., 2003; Singh et al., 2005; Morgan et al., 2007). The first stage solves the chemistry and a coupled MoMIC population balance. The second stage post processes the gas-phase data with a multi-variate population balance. The approach combines an efficient description of the coupling with a detailed particle model. Studies in turbulent flows have taken different approaches. Lindstedt and Louloudi (2005) use MoMIC and reduced soot chemistry in a full transported PDF method. Other studies have used commercial CFD codes to solve Favre-averaged equations. Zucca et al. (2006, 2007) use a presumed PDF and reduced soot chemistry during their development of the DQMoM population balance method. More recently, Chittipotula et al. (2011) use an equilibrium chemistry assumption and DQMoM population balance in an optimisation study of a soot model.

Several studies have used RANS CFD models to consider other systems. Gavi et al. (2007b) simulate barium sulphate precipitation in a confined impinging jet reactor using DQMoM-IEM for the chemistry and a QMoM population balance. Garmory and Mastorakos (2008) compare experimental data for the nucleation

2.5 Nanoparticle formation in turbulent reacting flows

and growth of dibutyl phthalate in a hot turbulent jet to SF simulations using an assumed log-normal size distribution. They show that the log-normal distribution is insufficient and that turbulent mixing affects the spatial particle size distribution across the jet. Veroli and Rigopoulos (2010) present a technique to couple CFD simulations to a joint composition-population PDF using a sectional population balance (see also Rigopoulos, 2007). The flow field is solved using CFD. The joint composition-population PDF is approximated using an ensemble of stochastic particles and solved using a Lagrangian Monte Carlo method. The study shows excellent agreement with experimental data for barium sulphate precipitation in a turbulent pipe. The decoupling of the flow field is acceptable because the precipitation has negligible effect on the overall mass and energy balance.

Some work has considered titania. Johannessen et al. (2001) model a turbulent diffusion flame doped with titanium tetrachloride. The flame is simulated using a commercial CFD code and the eddy dissipation model to solve Favre-averaged transport equations. The titania is modelled in post processing by integrating gas-phase data along characteristic trajectories in the flame. The integration assumes instantaneous titania formation above a threshold temperature and solves a monodisperse population balance. The decoupling of the CFD calculation is acceptable because the flow is dominated by the flame. Moody and Collins (2003) use MoMIC in a DNS study of the effect of mixing on titania particle size. The study considers one-step chemistry, inception and coagulation, and shows that mixing reduces polydispersity and mean particle size. Wang and Garrick (2005) apply the same titania chemistry with a sectional population balance and instantaneous inception model to a DNS study of titania formation in methane flames. The study shows mixing limited particle formation and growth, with the mean particle size and width of the particle size distribution increasing as the initial concentration of the reactants increases. Mehta et al. (2010) study titania inception in an LES model of a turbulent diffusion flame. The combustion reactions are closed using a flamelet model. The titania is modelled using one-step chemistry and QMoM to describe inception and coagulation. No closure is described for the titania chemistry. All of these studies neglect surface growth.

2 BACKGROUND

2.5.2 Points of compromise

The above studies use a range of methods to model nanoparticle formation in turbulent reacting flows. Each method entails some compromise, whether this be simplification of the flow, chemistry, population balance or the coupling. The greater the acceptable computational cost, the less compromise is required.

The studies make various compromises in the choice of chemistry and flow methods based on both what is possible and what is appropriate for each study. In order to be generally applicable, a method should not make any assumptions about the chemistry. The choice of whether it is appropriate to simplify the chemistry should be left to the user. For example, some or all of the chemistry could be solved using a flamelet method or a reduced mechanism. Likewise, the method should be applicable to a range of turbulent flow models and the choice left to the user.

The coupling of the population balance to the flow largely depends on the mass of material entering and leaving the population (where the mass of the population is proportional to the first moment of the number distribution). MoMIC is reasonably accurate for the first moment ([Grosschmidt et al., 2002](#); [Balthasar and Kraft, 2003](#)) and is a popular choice. A more detailed model can be applied in post processing, for example a multi-variate Monte Carlo method. DQMoM enables multi-variate distributions to be solved directly in the CFD, but is numerically challenging and cannot match the detail of Monte Carlo methods. Likewise, the method of [Veroli and Rigopoulos \(2010\)](#) cannot match Monte Carlo methods and does not yet account for the coupling from the particle processes back to the flow.

2.6 Terminology

There is a lack of consistency regarding the terminology applied to DQMoM-IEM in the turbulent reacting flow literature. The name QMoM originates from the use of a quadrature approximation to close integral terms in a population balance moment equation ([McGraw, 1997](#)). The *direct* prefix denotes the case where the method transports the parameters of the approximation, rather than the moments of the population ([Marchisio and Fox, 2005](#)). It uses a projection method

to derive model equations that force the statistics of the quadrature approximation to obey specified moments of the PBE. In the case of turbulent reacting flows, the method is applied to a PDF transport equation that includes the IEM mixing model. The IEM suffix was added when the projection was simplified to improve the numerical behaviour of the method (Fox, 2003) and we talk about a weighted *field* approximation because the approximation is continuous in physical space.

The quadrature terminology is not appropriate for turbulent reacting flows because the PDF transport equation does not contain integral terms. However, the DQMoM-IEM label is often still used. An alternative name, the multi-environment probability density function (MEPDF) method is sometimes applied (Tang et al., 2007; Denison et al., 2010). This reflects a physical interpretation of the method as a multi-environment reaction model (Fox, 2003; Wang and Fox, 2004), but provides no description of the numerical method. For example, the stochastic fields (SF) method invokes an analogous field approximation (see chapter 4) without the projection and could equally be described as an MEPDF method.

We want to emphasise the distinction between the *model* and the *numerical method*. We consider the PDF transport equation to be the model and the field approximation and projection to be the numerical method. For this reason, we refer to a ***projected fields (PF) method***. This highlights the projection that distinguishes it from a wider class of mathematically related field methods and is consistent with the existing SF terminology.

This thesis uses both the DQMoM-IEM and PF terminologies, reflecting a change in understanding during the course of the work. The terminology in each section is chosen to maintain consistency with the existing literature, including publications from this work. For example, chapters 3 and 4 refer to DQMoM-IEM, whereas chapter 5 refers to the PF method. The conclusions use both terminologies, drawing the choice of words from the chapter under discussion. Likewise, much of chapter 3 was developed by considering the numerical behaviour of DQMoM-IEM at a fixed point in space and the published version of the work refers to weighted particles rather than fields (Akroyd et al., 2010). In hindsight, this was confusing and the terminology is modified to refer to fields throughout this thesis. Some exceptions occur in the nomenclature, where we retain the original notation and note the anomaly in the text.

2.7 Scope of this thesis

The **scope of this thesis** is to investigate the application of DQMoM-IEM and SF as mean reaction rate closures for simulations of nanoparticle formation in turbulent reacting flow. The overall method is required to be computationally efficient and capable of providing sufficient accuracy for engineering studies using existing CFD software. The emphasis at this stage is on proof of concept.

This thesis makes the following assumptions:

- Off-the-shelf CFD software is the method of choice for studies of turbulent flow in industry. This thesis is restricted to Eulerian methods implemented within the Star-CD CFD code and all simulations use Reynolds/Favre-averaged methods with upwind differencing for the scalars. The methods developed in this thesis could be applied to LES with little extra difficulty.
- The flow, chemistry and population balance are strongly coupled. The method must resolve this coupling and should not make any assumptions about the chemistry. Simplified chemistry may be acceptable in some cases.
- The coupling to the population balance primarily depends on the mass of material entering and leaving the population and can be adequately resolved using a simplified particle model. Further information about the population can be recovered by applying a detailed particle model in post processing.
- The nanoparticles move with the same velocity and turbulent diffusivity as the fluid, and the momentum equation for the solid phase can be neglected. The particle dynamics are governed by the Smoluchowski equation (2.1). An assessment of the validity of this assumption is not attempted.
- The computational time is likely to be limited by the chemistry and may be improved in the future by using tabulation methods such as ISAT.

Chapter 3

The direct quadrature method of moments using the IEM micromixing model

This chapter investigates the numerical implementation of a mean reaction rate closure based on DQMoM-IEM. The method was introduced for reacting flows by Fox (2003). We present a systematic study that addresses several important aspects of the method. In particular, we introduce a new analytic expression for the DQMoM-IEM source terms. We present a rigorous numerical investigation and discuss problems of boundedness and singularity in detail. We use a filter function to overcome these issues in the general case and present analytic integrals for special cases of specific terms. We extend the methodology to take advantage of these developments and show details of the implementation in the Star-CD CFD code. We present an extensive set of numerical experiments and validation. The method is proven for a problem known from the literature. Experimental and full transported PDF data compare very well. The method is discussed critically and areas for further research are suggested.

3.1 Background

The direct quadrature method of moments using the interaction by exchange with the mean micromixing model (DQMoM-IEM) was suggested as a mean reaction rate closure by Fox (2003). The method uses a weighted field approximation to discretise a joint composition PDF transport equation. A projection method is used to derive transport equations that force the statistics of the fields to obey specified moments of the discretised PDF transport equation.

DQMoM-IEM is potentially attractive compared to Monte Carlo methods because it is deterministic. This suggests a computationally efficient method where the number of fields can be chosen based on the priority given to speed versus accuracy for any given simulation, with more fields refining the approximation of the underlying PDF at the expense of a longer computation. In practice, the literature considered in chapter 2 reports that the method is numerically challenging.

The **purpose of this chapter** is to investigate the numerical behaviour of DQMoM-IEM as a turbulent reaction closure. The rest of this section introduces the model equations and the main assumptions in the method. Section 3.2 presents a new analytic expression for the DQMoM-IEM source terms. This prescribes the moment set that defines the projection and avoids the previous numerical difficulties associated with evaluating the source terms. Issues regarding boundedness and singularities are discussed and resolved using a filter function. Two new DQMoM-IEM solvers and the coupling to the Star-CD CFD code are described in detail. Section 3.3 validates the new solvers against the method of moments and a turbulent reaction test case known from the literature. Constraints imposed on the choice of boundary conditions are identified and discussed. Areas for further investigation are suggested to make the method more practical.

3.1.1 DQMoM-IEM equations

The derivation of DQMoM-IEM is well documented by Fox (2003, appendix B). The key features of the method are summarised below. Appendix A presents a formal derivation and discusses the origin of the equations presented here.

A closed joint composition PDF transport equation

$$\begin{aligned} \frac{\partial f_\phi}{\partial t} + \langle U_i \rangle \frac{\partial f_\phi}{\partial x_i} - \frac{\partial}{\partial x_i} \left(\Gamma_T \frac{\partial f_\phi}{\partial x_i} \right) = \\ - \frac{\partial}{\partial \psi_\alpha} \left(\left[\frac{C_\phi}{2\tau_\phi} (\langle \phi_\alpha \rangle - \psi_\alpha) + S_\alpha(\psi) \right] f_\phi \right), \end{aligned} \quad (3.1)$$

is discretised using a weighted field approximation

$$\begin{aligned} f_\phi(\psi(x,t)) \, d\psi &= f_\phi(\psi_1, \psi_2, \dots, \psi_K(x,t)) \, d\psi_1 \cdots d\psi_K \\ &\approx \sum_{n=1}^N w^{(n)}(x,t) \prod_{\alpha=1}^K \delta_{\psi_\alpha^{(n)}(x,t)}(d\psi_\alpha), \end{aligned} \quad (3.2)$$

where

$$\delta_{\psi_\alpha^{(n)}(x,t)}(d\psi_\alpha) \equiv \delta(\psi_\alpha - \psi_\alpha^{(n)}(x,t)) \, d\psi_\alpha, \quad (3.3)$$

$$\sum_{n=1}^N w^{(n)}(x,t) = 1. \quad (3.4)$$

The turbulent convective flux in equation (3.1) is closed using a gradient diffusion model. The diffusive flux is closed using the IEM mixing model and implicitly assumes equal molecular diffusivities for all species. (See the background on PDF methods in section 2.4.2 and section A.1 in appendix A).

The field approximation introduces N weights $w^{(n)}(x,t)$ and NK composition variables $\psi_\alpha^{(n)}(x,t)$, where $\alpha = 1, \dots, K$. Transport equations that share the form of standard scalar transport equations are derived

$$\frac{\partial w^{(n)}}{\partial t} + \langle U_i \rangle \frac{\partial w^{(n)}}{\partial x_i} - \frac{\partial}{\partial x_i} \left(\Gamma_T \frac{\partial w^{(n)}}{\partial x_i} \right) = a^{(n)}, \quad (3.5)$$

$$\frac{\partial s_\alpha^{(n)}}{\partial t} + \langle U_i \rangle \frac{\partial s_\alpha^{(n)}}{\partial x_i} - \frac{\partial}{\partial x_i} \left(\Gamma_T \frac{\partial s_\alpha^{(n)}}{\partial x_i} \right) = b_\alpha^{(n)}, \quad (3.6)$$

where

$$s_\alpha^{(n)} \equiv w^{(n)} \psi_\alpha^{(n)}. \quad (3.7)$$

3 THE DIRECT QUADRATURE METHOD OF MOMENTS

Note that the x - t dependencies of the terms in equations (3.5–3.7) onwards are suppressed for clarity of presentation. DQMoM-IEM constrains the source terms

$$a^{(n)} = 0, \quad (3.8)$$

and the weights evolve as conserved scalars subject to transport as per the left hand side of equation (3.5). A set of $M = NK$ unmixed empirical moments

$$\langle \phi_\alpha^{m_{\lambda\alpha}} \rangle_N = \sum_{n=1}^N w^{(n)} \psi_\alpha^{(n)m_{\lambda\alpha}} \quad \text{for } \lambda = 1, \dots, M, \quad (3.9)$$

are used to derive a linear system of NK equations for the source terms $b_\alpha^{(n)}(x, t)$

$$\begin{aligned} \sum_{n=1}^N \psi_\alpha^{(n)m_{\lambda\alpha}-1} (b_\alpha^{(n)} - w^{(n)} r_\alpha^{(n)}) = \\ \sum_{n=1}^N (m_{\lambda\alpha} - 1) \psi_\alpha^{(n)m_{\lambda\alpha}-2} w^{(n)} c_{\alpha\alpha}^{(n)} \quad \text{for } \lambda = 1, \dots, M, \end{aligned} \quad (3.10)$$

where

$$r_\alpha^{(n)} \equiv \frac{C_\phi}{2\tau_\phi} \left(\langle \phi_\alpha \rangle_N - \psi_\alpha^{(n)} \right) + S_\alpha \left(\psi^{(n)} \right), \quad (3.11)$$

and

$$c_{\alpha\beta}^{(n)} \equiv \Gamma_T \frac{\partial \psi_\alpha^{(n)}}{\partial x_i} \frac{\partial \psi_\beta^{(n)}}{\partial x_i}. \quad (3.12)$$

The use of equations (3.8–3.12) to evaluate the source terms of equations (3.5) and (3.6) imposes the projection. It constrains the statistics of the fields to obey the discretised PDF transport equation for each of the empirical moments specified by equation (3.9). The term ‘empirical’ denotes that the moments are estimators calculated from the field approximation as opposed to moments of the true PDF.

The questions of how to specify suitable boundary conditions and solve equation (3.10) for $b_\alpha^{(n)}$ remain open and are the focus of the rest of this chapter.

3.2 Numerical details

This section describes the method used to couple DQMoM-IEM to CFD. It presents a new analytic expression for the source terms $b_\alpha^{(n)}$ and considers their numerical behaviour in detail. The problems of boundedness and singularity are discussed and two DQMoM-IEM solvers are suggested to resolve these issues.

3.2.1 DQMoM-IEM coupling to Star-CD

DQMoM-IEM is coupled to the Star-CD CFD code (CD-adapco, 2008) as a transient problem in order to solve equations (3.5) and (3.6). Equation (3.6) is implemented using a second-order operator splitting technique, commonly known as a Strang (1968) splitting

$$s_\alpha^{(n)\dagger_1} = s_\alpha^{(n)}(t) + \int_0^{\frac{1}{2}\Delta t} b_\alpha^{(n)} d\tau, \quad (3.13)$$

where $s_\alpha^{(n)} = s_\alpha^{(n)}(t)$ at $\tau = 0$,

$$s_\alpha^{(n)\dagger_2} = s_\alpha^{(n)\dagger_1} + \int_0^{\Delta t} \left(-\langle U_i \rangle \frac{\partial s_\alpha^{(n)}}{\partial x_i} + \frac{\partial}{\partial x_i} \left(\Gamma_T \frac{\partial s_\alpha^{(n)}}{\partial x_i} \right) \right) d\tau, \quad (3.14)$$

where $s_\alpha^{(n)} = s_\alpha^{(n)\dagger_1}$ at $\tau = 0$,

$$s_\alpha^{(n)}(t + \Delta t) = s_\alpha^{(n)\dagger_2} + \int_0^{\frac{1}{2}\Delta t} b_\alpha^{(n)} d\tau, \quad (3.15)$$

where $s_\alpha^{(n)} = s_\alpha^{(n)\dagger_2}$ at $\tau = 0$.

Equations (3.5) and (3.14) are solved using Star-CD with upwind differencing to transport $w^{(n)}$ and $s_\alpha^{(n)}$ as passive scalars with time step Δt . Equations (3.13) and (3.15) are solved using user-defined subroutines called at the beginning and end of each Star-CD iteration. At intermediate iterations, they are combined and solved as a single step with time step Δt . This improves the efficiency of the implementation whilst preserving the convergence of the splitting, and is a well-known advantage of this technique.

3 THE DIRECT QUADRATURE METHOD OF MOMENTS

The gradients of $\psi_\alpha^{(n)}$ are required to evaluate the $c_{\alpha\alpha}^{(n)}$ terms that appear in equation (3.10) when calculating $b_\alpha^{(n)}$ during the solution of equations (3.13) and (3.15). The gradients of the transported scalars $w^{(n)}$ and $s_\alpha^{(n)}$ are evaluated using Star-CD and the gradients of $\psi_\alpha^{(n)}$ calculated

$$\frac{\partial \psi_\alpha^{(n)}}{\partial x_i} = \begin{cases} \frac{1}{w^{(n)}} \left(\frac{\partial s_\alpha^{(n)}}{\partial x_i} - \frac{s_\alpha^{(n)}}{w^{(n)}} \frac{\partial w^{(n)}}{\partial x_i} \right) & \text{if } w^{(n)} \neq 0 \\ 0 & \text{otherwise.} \end{cases} \quad (3.16)$$

In the case $w^{(n)} = 0$, the gradient is arbitrarily set to zero. It is convenient to calculate the gradients over the whole domain at the start of each step. The values of the gradient terms $c_{\alpha\alpha}^{(n)}$ and likewise the weights $w^{(n)}$ and micromixing parameters C_ϕ and τ_ϕ are treated as constants for the remainder of the step.

3.2.2 Analytic expression for the source terms

The following sections consider the numerical behaviour of DQMoM-IEM. The objective is to identify and resolve the problems that occur when integrating the set of NK ordinary differential equations (ODEs) as per equations (3.13) and (3.15)

$$\frac{\partial s_\alpha^{(n)}}{\partial t} = b_\alpha^{(n)} \quad \text{for } n = 1, \dots, N \quad \text{and} \quad \alpha = 1, \dots, K. \quad (3.17)$$

The source terms $b_\alpha^{(n)}$ are described by equation (3.10). If the unmixed empirical moments are specified

$$m_{\lambda\alpha} = \begin{cases} n & \text{where } n = \lambda - (\alpha - 1)N \quad \text{if } n \geq 1 \text{ and } n \leq N \\ 0 & \text{otherwise} \end{cases} \quad (3.18)$$

$$\text{for } \lambda = 1, \dots, M \quad \text{and} \quad \alpha = 1, \dots, K,$$

equation (3.10) represents a set of N equations for each scalar $\alpha = 1, \dots, K$ and

can be solved analytically such that equation (3.17) can be written

$$\frac{\partial s_\alpha^{(n)}}{\partial t} = b_{\text{rx}_\alpha}^{(n)} + b_{\text{mx}_\alpha}^{(n)} + b_{\text{dx}_\alpha}^{(n)}, \quad (3.19)$$

where the source terms are given

$$b_{\text{rx}_\alpha}^{(n)} = w^{(n)} S_\alpha \left(\psi^{(n)} \right), \quad (3.20)$$

$$b_{\text{mx}_\alpha}^{(n)} = w^{(n)} \frac{C_\phi}{2\tau_\phi} \left(\langle \phi_\alpha \rangle_N - \psi_\alpha^{(n)} \right), \quad (3.21)$$

$$b_{\text{dx}_\alpha}^{(n)} = w^{(n)} c_{\alpha\alpha}^{(n)} \sum_{\substack{i=1 \\ i \neq n}}^N \frac{1}{\psi_\alpha^{(n)} - \psi_\alpha^{(i)}} + \sum_{\substack{i=1 \\ i \neq n}}^N \frac{1}{\psi_\alpha^{(n)} - \psi_\alpha^{(i)}} \sum_{\substack{j=1 \\ j \neq n}}^N w^{(j)} c_{\alpha\alpha}^{(j)} \prod_{\substack{k=1 \\ k \neq j, n}}^N \left(\psi_\alpha^{(j)} - \psi_\alpha^{(k)} \right). \quad (3.22)$$

Equations (3.20) and (3.21) describe chemical reaction and micromixing. The $b_{\text{rx}_\alpha}^{(n)}$ and $b_{\text{mx}_\alpha}^{(n)}$ terms are referred to as the *reaction* and *micromixing* terms. The reaction term will likely require an implicit ODE solver. The numerical treatment of such systems has been widely studied (Hairer and Wanner, 1996). The presence of these terms does not pose a new challenge.

Equation (3.22) is a new result and was derived for the first time as part of the work in this thesis. It describes the effect of turbulent diffusion in the presence of spatial gradients of scalar α . The $b_{\text{dx}_\alpha}^{(n)}$ term is denoted the *diffusion* term. The equation is constrained to the moment set in equation (3.18), but is general in the sense that it *applies to any number of fields and scalars*. The diffusion term conserves the scalar means. For example, in the $N=2$ case, equation (3.22) simplifies to give two equal and opposite terms

$$b_{\text{dx}_\alpha}^{(1)} = \frac{w^{(1)} c_{\alpha\alpha}^{(1)} + w^{(2)} c_{\alpha\alpha}^{(2)}}{\psi_\alpha^{(1)} - \psi_\alpha^{(2)}}, \quad b_{\text{dx}_\alpha}^{(2)} = \frac{w^{(1)} c_{\alpha\alpha}^{(1)} + w^{(2)} c_{\alpha\alpha}^{(2)}}{\psi_\alpha^{(2)} - \psi_\alpha^{(1)}}. \quad (3.23)$$

3 THE DIRECT QUADRATURE METHOD OF MOMENTS

The functional form of the diffusion term presents several challenges to the DQMoM-IEM implementation. However, the availability of equation (3.22) presents two significant advantages. Firstly, it allows the diffusion source terms $b_{dx_\alpha}^{(n)}$ to be evaluated without the need to solve equation (3.10) numerically. Secondly, it gives several valuable insights into how the diffusion term affects the numerical behaviour of the system.

Figure 3.1(a) shows the form of the micromixing and diffusion terms given by equations (3.21) and (3.22) for an $N=2$ system. The diffusion term produces variance by causing the scalars $\psi_\alpha^{(1)}$ and $\psi_\alpha^{(2)}$ to diverge. It is discontinuous and singular where $\psi_\alpha^{(1)} = \psi_\alpha^{(2)}$. The micromixing term is responsible for decay of the variance and causes the scalars to converge. **Figure 3.1(b)** shows the net source term and illustrates a problem. If $\psi_\alpha^{(n)}$ is defined on a bounded domain $[0, 1]$, a scalar $0.8 < \psi_\alpha^{(2)} \leq 1$ has a net positive source term and will move out of bounds.

Figure 3.2 shows two possible forms of the diffusion term in an $N=3$ system. The diffusion term is discontinuous and singular where any scalar $\psi_\alpha^{(n)} = \psi_\alpha^{(i)}$ for $i \neq n$. The difference between figure 3.2(a) and 3.2(b) is due to the relative magnitude of the $c_{\alpha\alpha}^{(n)}$ terms. Figure 3.2(a) shows two unstable discontinuities. Figure 3.2(b) shows a stable and an unstable discontinuity. $\psi_\alpha^{(1)}$ and $\psi_\alpha^{(3)}$ will converge where $\psi_\alpha^{(3)} \approx 0.2$, $\psi_\alpha^{(2)}$ and $\psi_\alpha^{(3)}$ will diverge where $\psi_\alpha^{(3)} \approx 0.6$. Both figures show potential boundedness problems. For example, the positive source terms for $\psi_\alpha^{(3)} > 0.6$ and the negative source term for $\psi_\alpha^{(3)} < 0.2$ in figure 3.2(a). The diffusion terms for $N > 3$ show more instances of the behaviour illustrated in figure 3.2, up to a maximum of $N-1$ discontinuities.

The numerical integration of the diffusion term presents several challenges. At a stable discontinuity, the scalars will converge and the discontinuity will persist. The risk is that the solution may ‘overshoot’ and oscillate about the discontinuity. At an unstable discontinuity, the scalars will diverge. The sign of the diffusion term will determine the direction of divergence. However, the sign is undefined at the discontinuity and cannot be arbitrarily assigned. The diffusion term may lead to violations of boundedness. This is most likely in regions of high turbulence and large scalar gradients. The following sections present two methodologies which address both the issues of stability and boundedness.

3.2 Numerical details

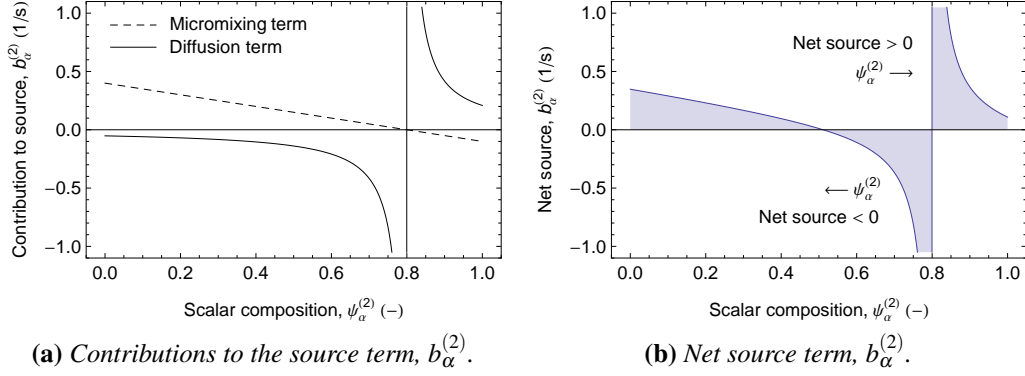


Figure 3.1: Functional form of the DQMoM-IEM micromixing and diffusion source terms for $N=2$ fields. The source terms are shown as a function of the scalar $\psi_\alpha^{(2)}$, where $\psi_\alpha^{(1)}=0.8$ and $w^{(n)}=1/2$; $c_{\alpha\alpha}^{(1)}=10^{-1}$ 1/s, $c_{\alpha\alpha}^{(2)}=10^{-4}$ 1/s and $C_\phi=2$, $\tau_\phi=1/2$ s.

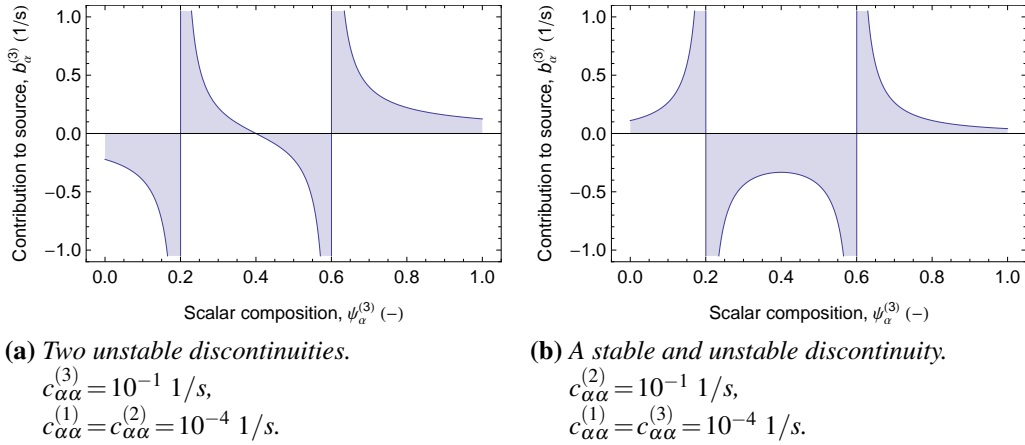


Figure 3.2: Functional form of the DQMoM-IEM diffusion source term for $N=3$ fields. The source term is shown as a function of the scalar $\psi_\alpha^{(3)}$, where $\psi_\alpha^{(1)}=0.2$, $\psi_\alpha^{(2)}=0.6$ and $w^{(n)}=1/3$.

3 THE DIRECT QUADRATURE METHOD OF MOMENTS

3.2.3 General solver

A general DQMoM-IEM solver was developed to numerically integrate equation (3.19). The diffusion term is modified to address the issues highlighted in figures 3.1 and 3.2 and the source terms are supplied by *functional evaluation*. The modified forms of equations (3.19) and (3.22) are written

$$\frac{\partial s_\alpha^{(n)}}{\partial t} = b_{\text{mx}_\alpha}^{(n)} + b_{\text{rx}_\alpha}^{(n)} + f_b\left(\psi_\alpha^{(n)}, b_{\text{dx}_\alpha}^{(n)}\right), \quad (3.24)$$

and

$$\begin{aligned} b_{\text{dx}_\alpha}^{(n)} = & w^{(n)} c_{\alpha\alpha}^{(n)} \sum_{\substack{i=1 \\ i \neq n}}^N f_p\left(\psi_\alpha^{(n)} - \psi_\alpha^{(i)}\right) \\ & + \prod_{\substack{i=1 \\ i \neq n}}^N f_p\left(\psi_\alpha^{(n)} - \psi_\alpha^{(i)}\right) \sum_{\substack{j=1 \\ j \neq n}}^N w^{(j)} c_{\alpha\alpha}^{(j)} \prod_{\substack{k=1 \\ k \neq j, n}}^N \left(\psi_\alpha^{(j)} - \psi_\alpha^{(k)}\right), \end{aligned} \quad (3.25)$$

where

$$f_b(\psi, b_{\text{dx}}) = \begin{cases} b_{\text{dx}} f\left(\frac{\psi_{\text{ub}} - \psi}{\varepsilon_b}\right) & \text{if } b_{\text{dx}} > 0 \text{ and } \psi_{\text{ub}} - \psi > 0 \\ b_{\text{dx}} f\left(\frac{\psi - \psi_{\text{lb}}}{\varepsilon_b}\right) & \text{if } b_{\text{dx}} < 0 \text{ and } \psi - \psi_{\text{lb}} > 0 \\ 0 & \text{otherwise,} \end{cases} \quad (3.26)$$

and

$$f_p(\Delta\psi) = \begin{cases} \frac{1}{\Delta\psi} f\left(\frac{\Delta\psi}{\varepsilon_p}\right) & \text{if } \Delta\psi \neq 0 \\ 0 & \text{otherwise.} \end{cases} \quad (3.27)$$

3.2 Numerical details

A bounding function $f_b(\psi, b_{dx})$ is used to clip the diffusion term to enforce bound-
edness. The lower bound ψ_{lb} and upper bound ψ_{ub} are defined for each $\psi_\alpha^{(n)}$

$$\psi_{\alpha lb}^{(n)} = \max\left(\phi_{\alpha glb}, \min\left[\left\{\psi_\alpha^{(n)}\right\}_{nb}\right]\right), \quad (3.28)$$

$$\psi_{\alpha ub}^{(n)} = \min\left(\phi_{\alpha gub}, \max\left[\left\{\psi_\alpha^{(n)}\right\}_{nb}\right]\right), \quad (3.29)$$

where $\{\cdot\}_{nb}$ denotes the set of neighbour cells and $[\phi_{\alpha glb}, \phi_{\alpha gub}]$ is a global interval
imposed over the entire domain. In the case of mass fractions $[Y_{glb}, Y_{gub}] = [0, 1]$.

A *particle function* $f_p(\Delta\psi)$ is used to control the discontinuities and singularities.²
Several approaches were considered. The most obvious is to impose a minimum
separation between the scalars $\psi_\alpha^{(n)}$ (cf. Raman et al., 2006). This avoids singu-
larities, but not discontinuities. It risks limiting the effect of the diffusion term
and would not necessarily prevent oscillation of the numerical solution about a
stable discontinuity. The same reasoning may be applied to approaches that limit
the maximum value of the diffusion term (cf. Tang et al., 2007) or set it to zero
near a discontinuity. A less arbitrary approach is to replace the discontinuity and
singularity with a smooth transition.

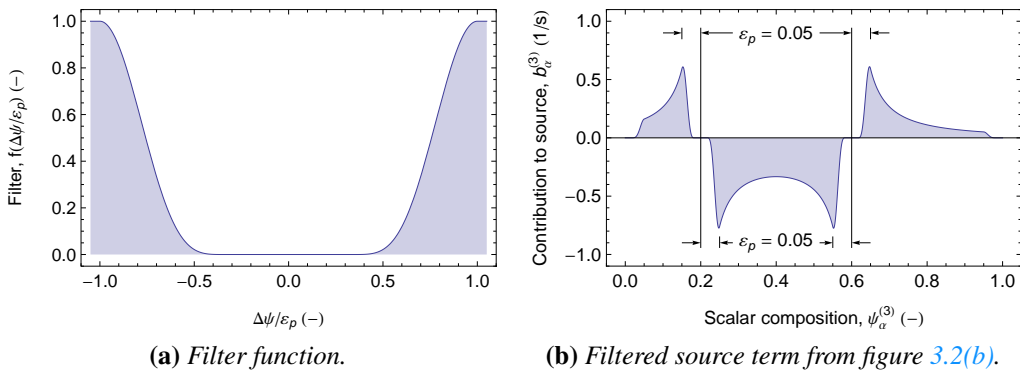


Figure 3.3: Filtered diffusion source term for $N = 3$ fields.

² The ‘particle function’ terminology is retained from Akroyd et al. (2010).

3 THE DIRECT QUADRATURE METHOD OF MOMENTS

The particle function uses a symmetrical *filter function* $f(\Delta\psi/\varepsilon_p)$ to remove the discontinuities in the diffusion source term. The effect of the filter function is illustrated in **figure 3.3**. An exaggerated value of ε_p is used for clarity. The diffusion term is set to zero at and slightly to either side of each discontinuity. The zero-valued region negates the requirement to assign an arbitrary sign to the diffusion term. The width of the region can be used to prevent oscillation of the numerical solution without changing the integration tolerances. The same filter is used by the bounding function to ensure smooth clipping at the bounds. ε_p and ε_b are small positive numbers and in this thesis $\varepsilon_b = \varepsilon_p = 10^{-7}$. Further details about the filter function in **figure 3.3(a)** and a discussion of the effects of other filters considered during this work are given in **appendix B.1**.

The filter function preserves as much of the diffusion term as possible. However, a side-effect is that the diffusion terms only sum to zero for an $N = 2$ system with a symmetric filter. This also occurs where a maximum value is imposed instead of using a filter. A similar problem is presented where the diffusion term is clipped to enforce boundedness. In general, the diffusion term cannot be modified for one scalar on a given field without disturbing the scalar mean and mass balance over the set of fields. The diffusion term $f_b(\psi, b_{dx})$ in **equation (3.24)** is normalised to enforce mass balance and conservation of the scalar mean.

Equation (3.24) is integrated numerically using RADAU5 (**Hairer and Wanner, 1996**), an implicit 5th order Runge-Kutta ODE solver with low start-up cost. The micromixing parameters C_ϕ and τ_ϕ , weights $w^{(n)}$ and scalar gradient terms $c_{\alpha\alpha}^{(n)}$ are treated as constant during the integration as per **section 3.2.1**. In the original investigation (**Akroyd et al., 2010**), **equation (3.24)** was solved as a single step. In this thesis, **equation (3.24)** is solved using a further Strang splitting, using RADAU5 to integrate each step separately

$$S_{\Delta t}^{b_{\alpha}^{(n)}} \left(s_{\alpha}^{(n)} \right) \approx \left[S_{\frac{1}{2}\Delta t}^{b_{mx+dx_{\alpha}}^{(n)}} \circ S_{\Delta t}^{b_{rx_{\alpha}}^{(n)}} \circ S_{\frac{1}{2}\Delta t}^{b_{mx+dx_{\alpha}}^{(n)}} \right] \left(s_{\alpha}^{(n)} \right), \quad (3.30)$$

where the combined micromixing and filtered diffusion term is defined

$$b_{mx+dx_{\alpha}}^{(n)} = b_{mx_{\alpha}}^{(n)} + f_b \left(\psi_{\alpha}^{(n)}, b_{dx_{\alpha}}^{(n)} \right), \quad (3.31)$$

and the solution operator $S_{\Delta t}^{b_\alpha^{(n)}}(s_\alpha^{(n)})$ denotes the evolution of $s_\alpha^{(n)}$ subject to $b_\alpha^{(n)}$

$$S_{\Delta t}^{b_\alpha^{(n)}}(s_\alpha^{(n)}) : s_\alpha^{(n)}(t) \mapsto s_\alpha^{(n)}(t + \Delta t). \quad (3.32)$$

The operator splitting enables the reaction term to be solved in terms of the molar concentrations $C_\alpha^{(n)}$, independent of the choice of variables used elsewhere and transported by Star-CD. The reasons for doing this relate to numerical convenience and are discussed in more detail in appendix B.4.

3.2.4 Analytic solver

A solver was developed to analytically integrate the micromixing and diffusion terms in the $N=2$ case. Equation (3.19) is solved using a further operator splitting

$$S_{\Delta t}^{b_\alpha^{(n)}}(s_\alpha^{(n)}) \approx \left[S_{\frac{1}{2}\Delta t}^{b_{\text{mx}\alpha}^{(n)}} \circ S_{\frac{1}{2}\Delta t}^{b_{\text{dx}\alpha}^{(n)}} \circ S_{\Delta t}^{b_{\text{rx}\alpha}^{(n)}} \circ S_{\frac{1}{2}\Delta t}^{b_{\text{dx}\alpha}^{(n)}} \circ S_{\frac{1}{2}\Delta t}^{b_{\text{mx}\alpha}^{(n)}} \right] (s_\alpha^{(n)}), \quad (3.33)$$

where $S_{\Delta t}$ denotes the solution operator as per equation (3.32). The integrals of the micromixing and diffusion terms are given

$$\int_{t_1}^{t_2} b_{\text{mx}\alpha}^{(n)} d\tau = \Delta\psi_\alpha^{(n)} \prod_n w^{(n)} \left[1 - \exp\left(-\frac{C_\phi}{2\tau_\phi} \Delta t\right) \right], \quad n \in \{1, 2\} \quad (3.34)$$

and

$$\begin{aligned} \int_{t_1}^{t_2} b_{\text{dx}\alpha}^{(n)} d\tau &= \Delta\psi_\alpha^{(n)} \prod_n w^{(n)} \\ &\pm \sqrt{2\Delta t \left(\sum_n w^{(n)} c_{\alpha\alpha}^{(n)} \right) \prod_n w^{(n)} + \left(\Delta\psi_\alpha^{(n)} \prod_n w^{(n)} \right)^2}, \quad n \in \{1, 2\} \end{aligned} \quad (3.35)$$

where

$$\Delta t = t_2 - t_1,$$

$$\Delta\psi_\alpha^{(n)} = \psi_\alpha^{(i)}(t_1) - \psi_\alpha^{(n)}(t_1), \quad i, n \in \{1, 2\}, i \neq n.$$

3 THE DIRECT QUADRATURE METHOD OF MOMENTS

The root in equation (3.35) is chosen so that the scalars diverge as per figure 3.1. If $\Delta\psi_\alpha^{(n)} < 0$, the positive root is chosen. If $\Delta\psi_\alpha^{(n)} > 0$, the negative root is chosen. If $\Delta\psi_\alpha^{(n)} = 0$, the right hand side of equation (3.35) is set to zero. The current implementation clips the magnitude of the root to enforce the bounds defined by equations (3.28) and (3.29). The micromixing parameters C_ϕ and τ_ϕ , weights $w^{(n)}$ and scalar gradient terms $c_{\alpha\alpha}^{(n)}$ are treated as constant during the integration.

The reaction term is integrated using RADAU5 as per the general solver. The advantage of the analytic solver is that the diffusion term is treated very efficiently. The method is general in the sense that it can be applied to any number of scalars.

3.3 Numerical testing of DQMoM-IEM

This section validates the DQMoM-IEM solvers described in section 3.2 against a test case known from the literature.

Section 3.3.1 presents salient details of the test case. Section 3.3.2 compares the solvers against the method of moments. This validates the treatment of the diffusion term described in section 3.2. Section 3.3.3 demonstrates the application of the general solver to a reacting system. Sections 3.3.4 and 3.3.5 discuss the solver CPU times and constraints on the choice of boundary conditions.

3.3.1 Model problem

The system considered is the *constant density* isothermal liquid-phase reaction, previously introduced by equation (2.5)



$k_1 = 5.0 \times 10^6 \text{ m}^3/\text{kmol s}$, $k_2 = 1.8 \times 10^3 \text{ m}^3/\text{kmol s}$. In regions where mixing is slow relative to the second reaction, a significant proportion of B and R react to form S before B can be quenched by further mixing with A. The yield of R

$$Y = \frac{C_R}{C_R + 2C_S}, \quad (3.36)$$

3.3 Numerical testing of DQMoM-IEM

is sensitive to the rate of mixing. The reaction offers a simple approximation to stiff chemistry and was selected because it has been well studied numerically (Tsai and Fox, 1994; Tsai et al., 2002) and experimentally (Li and Toor, 1986).

The reactor configuration is shown in **figure 3.4**. It is the single-jet system studied by Tsai and Fox (1994). This thesis considers the case where a turbulent jet of species B is injected into a laminar annular co-flow of species A. Cases are considered for high and low reactant concentrations at jet Reynolds numbers $Re = 3530$ and $Re = 7552$.

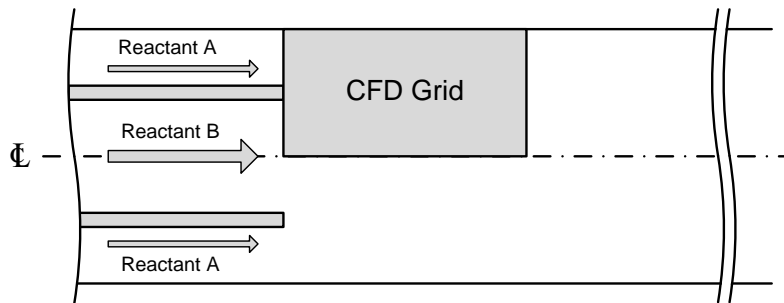


Figure 3.4: Configuration of the axisymmetric single-jet tubular reactor.

The reactor is modelled using a triangular prism-shaped domain and boundary conditions to exploit axial symmetry. The geometry of the computational domain is illustrated in **figure 3.5**. The flow was solved as a steady problem using Star-CD (CD-adapco, 2008) as per the approach detailed by Tsai and Fox (1994). The RANS equations were solved using a $k-\epsilon$ High Reynolds Number turbulence model and standard wall functions. The default model constants were used with unit Prandtl numbers. The inlet boundary conditions are summarised in **table 3.1**.

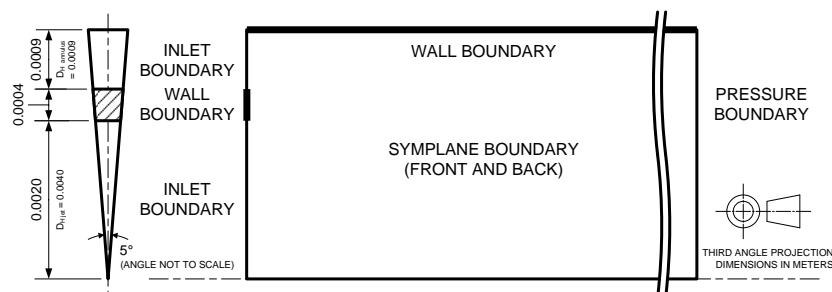


Figure 3.5: Geometry of the jet reactor computational domain.

3 THE DIRECT QUADRATURE METHOD OF MOMENTS

A *base* grid was defined for each Reynolds number as per Tsai and Fox (1994, tables 1 and 2). A *refined* grid was defined for each case by dividing the base grid cells by a factor of two in the axial direction, and each cell except those adjacent to the outer wall by a factor of two in the radial direction. The exception was imposed by the wall function, which required the coarse radial resolution to be retained at the wall. The grids were all one cell deep in the azimuthal direction.

The flow fields were consistent with Tsai and Fox (1994). The data in this investigation are considered to be grid-independent based on the grid causing a variation of less than 0.5% in the yield of the cases considered in section 3.3.3. The base grid cases were run with time step $\Delta t = 10^{-4}$ s for $t = 2$ s physical time. The refined grid cases were run with $\Delta t = 4 \times 10^{-5}$ s for $t = 2$ s.

The DQMoM-IEM scalar transport equations are solved as unsteady problems (see section 3.2.1) without re-solving the flow. This one-way coupling is acceptable for the constant density case. The flow affects the scalars, but the scalars are *passive* and do not affect the flow. The data are presented in terms of the empirical mean and standard deviation of each species. The composition space is defined in terms of the mass fractions

$$\phi^T = [Y_A, Y_B, Y_R, Y_S, Y_{\text{solvent}}]. \quad (3.37)$$

The reaction term is solved in terms of molar concentrations

$$C_\alpha = \frac{\rho Y_\alpha}{W_\alpha}, \quad (3.38)$$

where ρ is the fluid density, W_α are the species molecular weights

$$\begin{aligned} W_A &= 143.1 \text{ kg/kmol}, \\ W_R &= 183.2 \text{ kg/kmol}, \\ W_B &= 326.3 \text{ kg/kmol}, \\ W_S &= 509.5 \text{ kg/kmol}, \end{aligned} \quad (3.39)$$

and the chemical source terms are given by equation (2.6).

3.3 Numerical testing of DQMoM-IEM

Table 3.1: Inlet boundary conditions for the jet reactor.

	Units	Re = 3530 case		Re = 7552 case	
		Jet	Annulus	Jet	Annulus
Volumetric flow	m ³ /s	0.988 × 10 ⁻⁵		2.11 × 10 ⁻⁵	
Average velocity	m/s	0.786	0.613	1.68	1.13
Mixing length	m	28 × 10 ⁻⁵	6.3 × 10 ⁻⁵	28 × 10 ⁻⁵	6.3 × 10 ⁻⁵
Turbulence intensity	%	5.76	4.00	5.24	4.00
Density	kg/m ³	998		998	
Molecular viscosity	kg/m s	0.889		0.889	

Mass balance was not used to reduce the number of transport equations. This was a deliberate decision made to keep the test case general. Likewise, the option to use a mixture fraction and progress variable approach (*cf.* [Lui and Fox, 2006](#)) is acknowledged, but was not pursued.

The micromixing parameters are given as $C_\phi = 1.65$ and $\tau_\phi = d/\sqrt{k}$ ([Tsai and Fox, 1994](#)), where $d = 0.0066$ m is the reactor diameter and k is the turbulent kinetic energy. The turbulent diffusivity Γ_T is calculated $\Gamma_T = \nu_T/\rho\sigma_T$, where the turbulent Schmidt number is given $\sigma_T = 0.7$ for all scalars ([Tsai et al., 2002](#)). The turbulent kinetic energy k and turbulent viscosity ν_T are supplied by Star-CD.

3.3.2 Application to scalar mixing

The treatment of the micromixing and diffusion terms in the DQMoM-IEM solvers presented in section 3.2 is validated against a scalar mixing case. A reference solution is provided using the method of moments (MoM). The application of the method of moments to such problems is well established and provides an exact solution to equation (3.1) where the chemical source term is zero, $S_\alpha = 0$. This validation is particularly important because it tests the treatment of the diffusion term that is responsible for the numerical difficulties associated with DQMoM-IEM. More information about the method of moments equations and their treatment is given in sections A.4 and B.3 of the appendices.

3 THE DIRECT QUADRATURE METHOD OF MOMENTS

The scalar mixing of species A and B was investigated for the *high concentration case* at $Re = 3530$. The empirical mean and standard deviation are presented for species A in **figure 3.6**. The scalar boundary conditions are given in table 3.6.

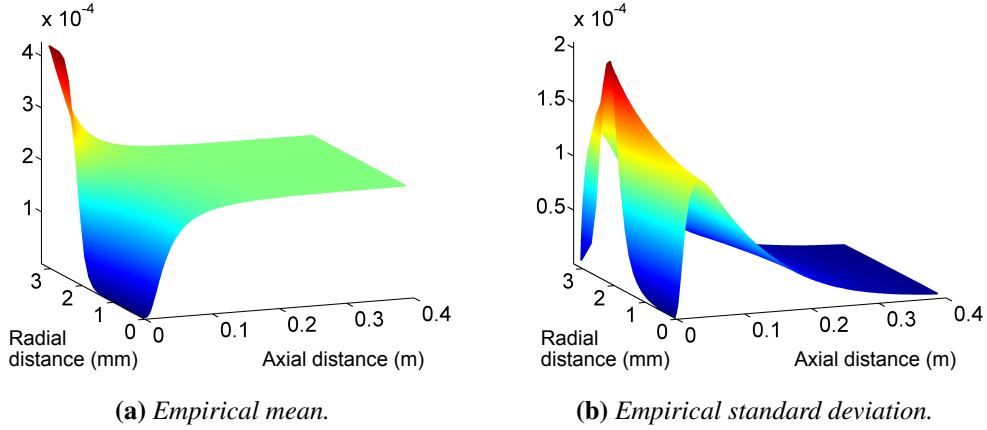


Figure 3.6: Jet reactor empirical moments of species A for the inert (micromixing and diffusion only) $Re = 3530$ high concentration case on the base grid, analytic DQMoM-IEM solver with $N = 2$ fields.

Table 3.2 shows excellent agreement between DQMoM-IEM and the method of moments. The level of agreement was assessed for the first four empirical integer moments and the empirical standard deviation

$$\varepsilon_{m_\alpha} = \frac{1}{\sqrt{N_{\text{cells}}}} \sum_{\alpha=1}^K \left\| \langle \phi_\alpha^{m_\alpha} \rangle_N - \langle \phi_\alpha^{m_\alpha} \rangle_{\text{MoM}} \right\|, \quad m_\alpha \in \{1, 2, 3, 4\}, \quad (3.40)$$

$$\varepsilon_{\text{sd}} = \frac{1}{\sqrt{N_{\text{cells}}}} \sum_{\alpha=1}^K \left\| \sqrt{\langle \phi_\alpha^2 \rangle_N - \langle \phi_\alpha \rangle_N^2} - \sqrt{\langle \phi_\alpha^2 \rangle_{\text{MoM}} - \langle \phi_\alpha \rangle_{\text{MoM}}^2} \right\|, \quad (3.41)$$

where $\varepsilon_{m_\alpha=1} = \varepsilon_{\text{mean}}$ and $\|\cdot\|$ denotes an L^2 -norm over space. The differences between the MoM and DQMoM-IEM data occur at the turbulent jet inlet, where a small perturbation is applied to the scalars to ensure that the diffusion source terms are not filtered at the inlet boundary (see table 3.6). The agreement between MoM and the $N = 3$ general solver is improved over that reported by Akroyd et al. (2010) due to the use of a tighter filter width, where $\varepsilon_p = 10^{-7}$ in this example as opposed to $\varepsilon_p = 10^{-3}$ in Akroyd et al. (2010).

3.3 Numerical testing of DQMoM-IEM

Table 3.2: Convergence of DQMoM-IEM versus the method of moments for the inert $Re=3530$ high concentration jet reactor case on the base grid.

	ϵ_{mean}	$\epsilon_{m_a=2}$	$\epsilon_{m_a=3}$	$\epsilon_{m_a=4}$	ϵ_{sd}
$N=2^a$	$6.9 \times 10^{-7}{}^c$	3.7×10^{-7}	5.6×10^{-7}	7.4×10^{-7}	$4.7 \times 10^{-6}{}^d$
$N=2^b$	6.9×10^{-7}	3.7×10^{-7}	5.6×10^{-7}	7.4×10^{-7}	4.7×10^{-6}
$N=3^b$	4.4×10^{-7}	2.4×10^{-7}	3.6×10^{-7}	4.8×10^{-7}	4.8×10^{-6}

^a Analytic solver, ^b General solver, ^c See figure 3.6(a), ^d See figure 3.6(b).

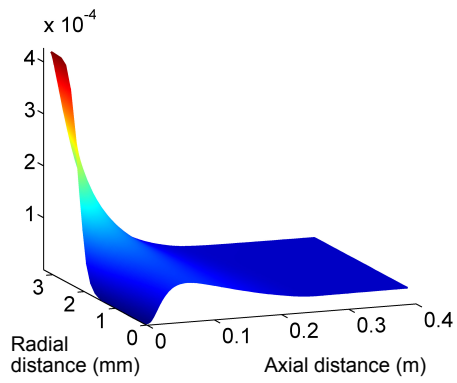
3.3.3 Application to reacting flow

This section describes the application of the DQMoM-IEM solvers presented in section 3.2 to a real turbulent reaction problem. The results are validated against previous studies of the same system (Li and Toor, 1986; Tsai and Fox, 1994). The scalar boundary conditions are given in table 3.6 (see section 3.3.5).

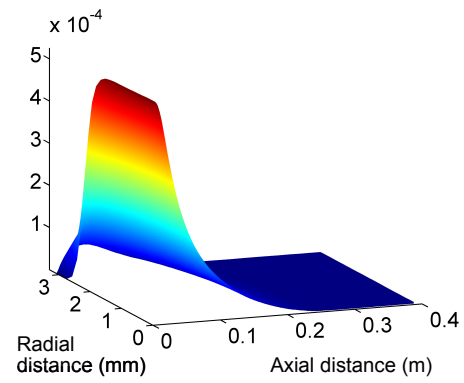
Figures 3.7 and 3.8 show the empirical mean of species A, B, R and S for the high concentration case at $Re = 3530$ calculated by the analytic solver with $N = 2$ fields (figure 3.7) and the general solver with $N = 3$ fields (figure 3.8). Figures 3.7 and 3.8 are visually indistinguishable and are consistent with the full transported PDF data of Tsai and Fox (1994, fig. 7, although note that the data in this thesis are given as mass fractions as opposed to molar concentrations). Figures 3.7 and 3.8 show rapid reaction between species A and B, with a small region of coexistence near the inlets. The product R forms rapidly in the reaction zone. The side-product S forms more slowly, with most forming in the zone of high concentration of B and R at the centre of the reactor near the jet inlet.

Figures 3.9 and 3.10 show the empirical standard deviation of species A, B, R and S for the high concentration case at $Re = 3530$ calculated by the analytic solver with $N = 2$ (figure 3.9) and the general solver with $N = 3$ fields (figure 3.10). The figures are visually indistinguishable for species A, B and S, and the data are consistent with the full transported PDF data of Tsai and Fox (1994, fig. 8). Note that Tsai and Fox (1994) only show the standard deviations for species A and B and that their data look less ‘peaky’ than figures 3.9 and 3.10 because they are plotted as molar concentrations versus cell number rather than physical distance.

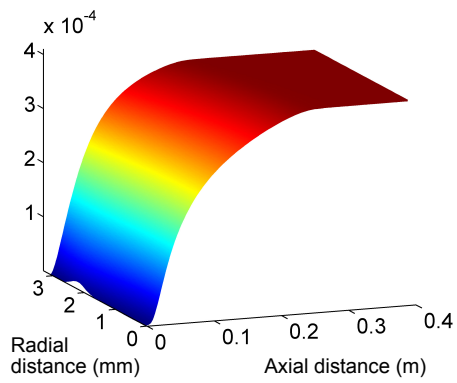
3 THE DIRECT QUADRATURE METHOD OF MOMENTS



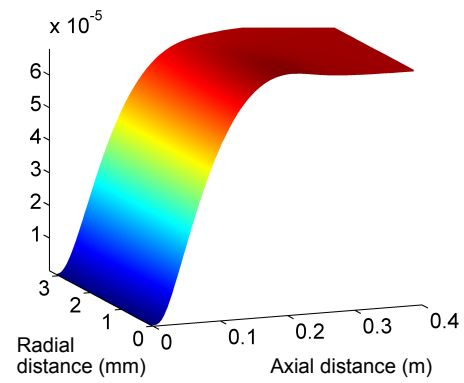
(a) Species A.



(b) Species B.



(c) Species R.



(d) Species S.

Figure 3.7: Jet reactor empirical means for the reacting $Re = 3530$ high concentration case on the base grid, analytic DQMoM-IEM solver with $N = 2$ fields.

3.3 Numerical testing of DQMoM-IEM

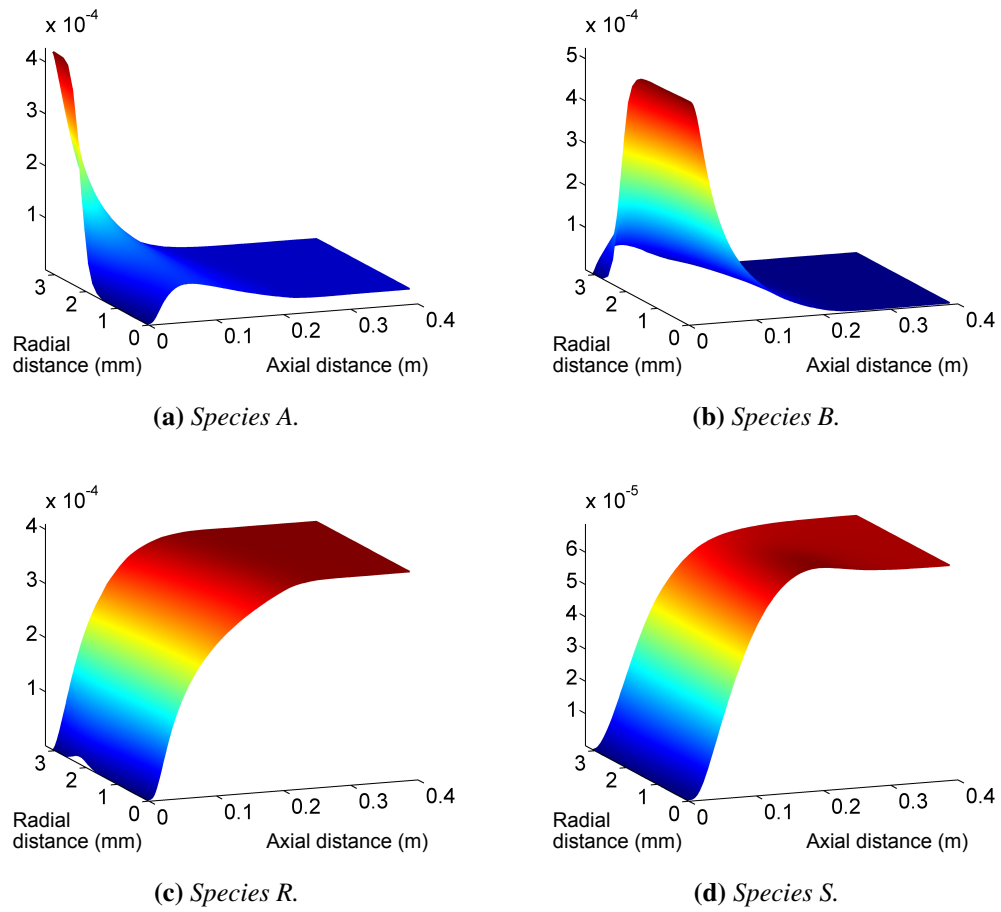
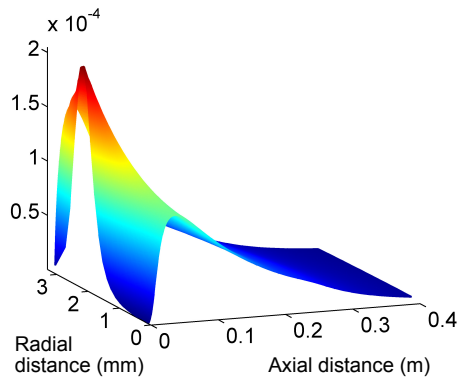
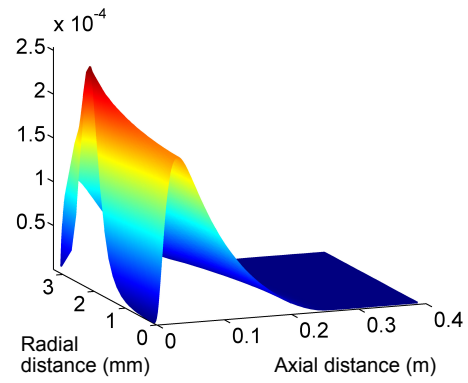


Figure 3.8: Jet reactor empirical means for the reacting $Re = 3530$ high concentration case on the base grid, general DQMoM-IEM solver with $N = 3$ fields.

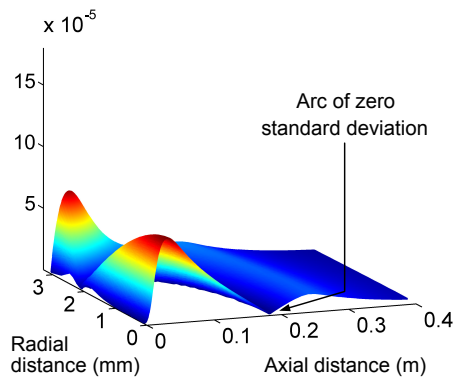
3 THE DIRECT QUADRATURE METHOD OF MOMENTS



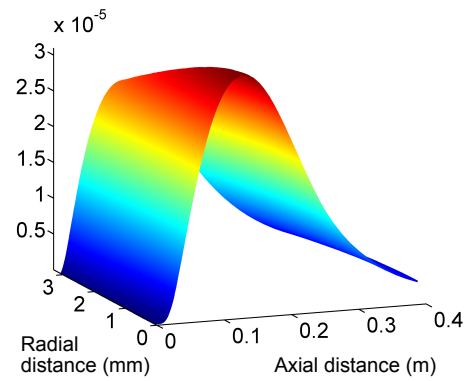
(a) Species A.



(b) Species B.



(c) Species R.



(d) Species S.

Figure 3.9: Jet reactor empirical standard deviations for the reacting $Re = 3530$ high concentration case on the base grid, analytic DQMoM-IEM solver with $N=2$ fields.

3.3 Numerical testing of DQMoM-IEM

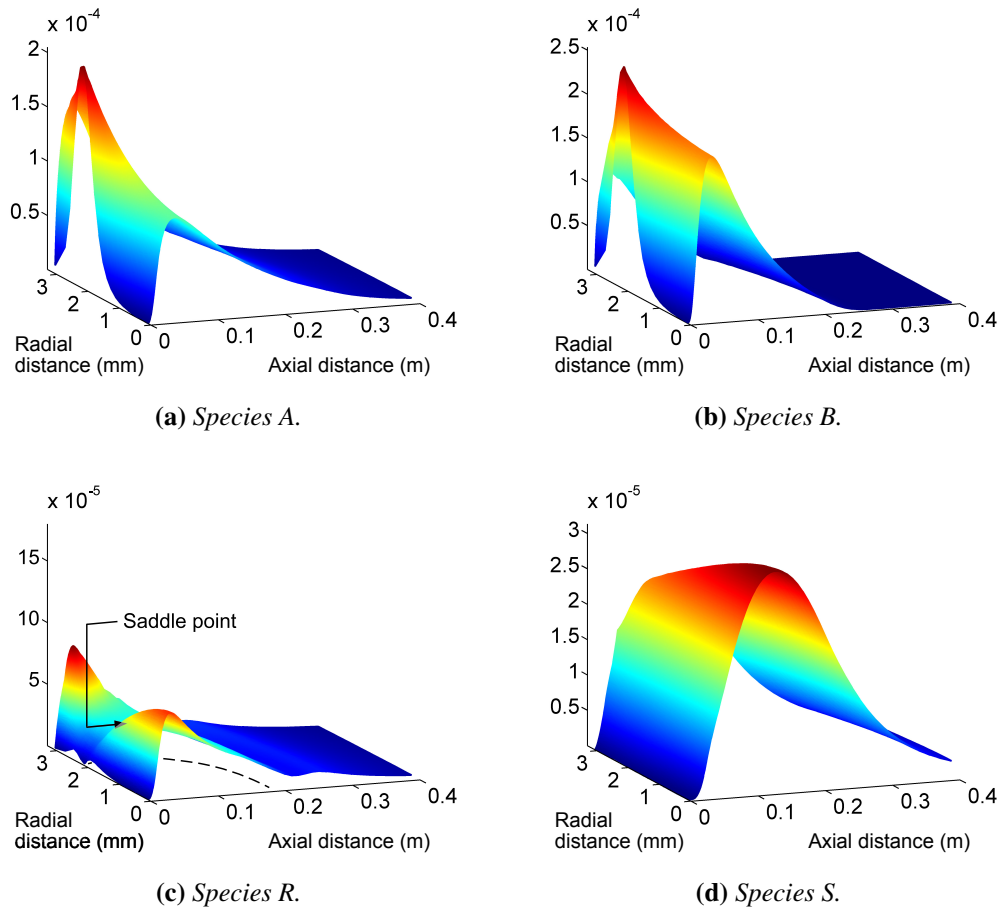


Figure 3.10: Jet reactor empirical standard deviations for the reacting $Re = 3530$ high concentration case on the base grid, general DQMoM-IEM solver with $N = 3$ fields.

3 THE DIRECT QUADRATURE METHOD OF MOMENTS

Figure 3.9(c) shows an arc of zero standard deviation running from between the inlets to the centre of the reactor. This is an artefact of the $N=2$ case. It marks the locus $\psi_R^{(1)} = \psi_R^{(2)}$ and is caused by a transition from $\psi_R^{(1)} > \psi_R^{(2)}$ near the jet inlet to $\psi_R^{(1)} < \psi_R^{(2)}$ in the bulk of the reactor. Figure 3.10(c) shows that it does not occur in the $N=3$ case, where the dashed line marks the previous location of the arc. Rather, there is a saddle point in the standard deviation near the inlets.

Tables 3.3 and 3.4 summarise the predicted yields. The data correctly show the effect of reactant concentration and Reynolds number and show good agreement with Li and Toor (1986) and Tsai and Fox (1994). The use of $N=3$ fields offers better resolution of the standard deviation near the inlets and is responsible for a small improvement in the agreement with the experimental yield. In particular, the agreement is improved over the original implementation (Akroyd et al., 2010) due to the inclusion of the solvent in the composition space, see equation (3.37).

Table 3.3: DQMoM-IEM jet reactor yields on the base grid.

Case		DQMoM-IEM yield (%)			Literature yield (%)	
Conc.	Re	$N=2^a$	$N=2^b$	$N=3^b$	Full PDF ^c	Expt. ^d
High	3530	80.4 ^e	80.7	81.9 ^f	81.0	82.1
High	7552	87.8	—	—	88.3	88.3
Low	3530	91.1	—	—	91.8	89.0
Low	7552	95.0	—	—	95.4	93.5

^a Analytic solver, ^b General solver, ^c Full transported PDF data, Tsai and Fox (1994, table 3), ^d Experimental data, Li and Toor (1986, table 1, experimental repeatability ± 0.5 %), ^e See figure 3.7, ^f See figure 3.8.

Table 3.4: DQMoM-IEM jet reactor yields on the refined grid.

Case		DQMoM-IEM yield (%)			Literature yield (%)	
Conc.	Re	$N=2^a$	$N=2^b$	$N=3^b$	Full PDF	Expt.
High	3530	80.3	80.7	81.5	—	82.1
High	7552	87.6	—	—	—	88.3
Low	3530	91.1	—	—	—	89.0
Low	7552	94.9	—	—	—	93.5

^a Analytic solver, ^b General solver.

3.3.4 Computational performance

Table 3.5 shows the computational times for the high concentration cases at $Re = 3530$ on the base grid. All cases were run on identical hardware. The analytic solver is significantly faster than the general solver for the $N = 2$ case.

Table 3.5: *DQMoM-IEM jet reactor CPU times for the high concentration case at $Re = 3530$ on the base grid.*

	CPU time (h)		
	$N = 2^a$	$N = 2^b$	$N = 3^b$
Inert case	0.14 ^c	3.26	4.96
Reacting case	0.45 ^d	3.56	6.05 ^e

^a Analytic solver, ^b General solver, ^c See figure 3.6, ^d See figure 3.7, ^e See figure 3.8.

The performance of the general solver is strongly influenced by the numerical integration of the diffusion term. The efficient treatment of this term represents an important area of research required to make the general solver more practical.

The observation of [Akroyd et al. \(2010\)](#) that the computational time for the $N = 3$ reacting case is less than that for the $N = 3$ inert case is not repeated here. This is attributed to the use of the tighter filter width, where $\epsilon_p = 10^{-7}$ in this example as opposed to $\epsilon_p = 10^{-3}$ in [Akroyd et al. \(2010\)](#).

3.3.5 Choice of boundary conditions

The choice of boundary conditions to represent a given system is not arbitrary. Different representations of the *same physical condition* can give different results.

The DQMoM-IEM code was developed using the inert case and equi-weighted fields such that the observed central moments were due to the diffusion term only. However, equal weights are a poor choice. For example, $N = 2$ equi-weighted fields cannot reproduce figure 3.6(b): the maximum standard deviation is restricted by the physical bounds on the mass fractions of the scalars. The correct scalar mixing was only given when the boundary conditions were specified to be consistent with each field being assigned to a specific inlet.

3 THE DIRECT QUADRATURE METHOD OF MOMENTS

Table 3.6 summarises the initial and inlet boundary conditions for the cases in this chapter. The $N=2$ case is specified such that field 1 represents the annular inlet and field 2 the jet inlet. The $N=3$ case is specified such that field 1 represents the annulus and fields 2 and 3 the jet inlet. The rationale for assigning the extra field to the jet is that it gave slightly better agreement with the method of moments.

The restrictions on the boundary conditions are perhaps intuitive given the interpretation of DQMoM-IEM as a multi-environment presumed PDF method (Fox, 2003). The number of inlets should dictate the *minimum* number of fields. The benefit of extra fields is illustrated by the difference between Figures 3.9 and 3.10.

In order to benefit from extra fields, the diffusion term must not see degenerate scalars at the inlets. This was previously achieved using the initial conditions (Akroyd et al., 2010). In this thesis, it is achieved by perturbing the inlet mass fractions such that the diffusion terms are not filtered and remain non-zero at the inlet boundaries. It is also convenient to avoid fields with zero weight. For example, this negates the need to assume a value for $\psi_\alpha^{(n)}$ in the event that $w^{(n)}=0$. Section 3.3.2 shows that this approach has negligible impact on the results.

Table 3.6: DQMoM-IEM jet reactor initial and inlet boundary conditions.

	Initial condition	Inlet boundary			
		Jet	Annulus		
$w^{(n)}$	$1/N$	0^a	$1/\lfloor \frac{N}{2} \rfloor$	for $n \leq \lfloor \frac{N}{2} \rfloor$	
	$1/N$	$1/\lceil \frac{N}{2} \rceil$	0^a	for $n > \lfloor \frac{N}{2} \rfloor$	
$Y_A^{(n)}$	0	0	$4.27 \times 10^{-4}{}^b$ $1.44 \times 10^{-4}{}^b$	high low	conc. case
$Y_B^{(n)}$	0	$5.25 \times 10^{-4}{}^b$ $1.77 \times 10^{-4}{}^b$	0	high low	conc. case
$Y_{R,S}^{(n)}$	0	0	0		
$Y_{\text{solvent}}^{(n)}$	1	$1 - Y_B^{(n)}$	$1 - Y_A^{(n)}$		

Note that the table specifies the scalars in terms of $Y_\alpha^{(n)}$, but that DQMoM-IEM transports $w^{(n)}$ and $s_\alpha^{(n)} = w^{(n)} \psi_\alpha^{(n)}$, where the composition space is defined by equation (3.37). ^a A perturbation was applied to avoid specifying exactly $w^{(n)}=0$, subject to $\sum_n w^{(n)}=1$. ^b A perturbation was applied to avoid specifying $\psi_\alpha^{(n)} = \psi_\alpha^{(i)}$ for $i \neq n$.

3.4 Chapter summary

The numerical behaviour of DQMoM-IEM has been investigated as a turbulent reaction closure. DQMoM-IEM uses weighted fields to discretise a joint composition PDF transport equation that includes the IEM mixing model. A projection is used to derive transport equations that force the statistics of the fields to obey specified moments of the discretised PDF transport equation. The method is potentially suitable for engineering calculations using standard CFD software. It is attractive because it could offer efficient calculations where the number of fields can be chosen based on the priority assigned to speed versus accuracy, with more fields refining the discretisation at the expense of a longer computation.

An *analytic expression* has been introduced for the DQMoM-IEM source terms. It prescribes the choice of the moments in the projection and is valid for any number of fields and scalars. Explicit *reaction*, *micromixing* and turbulent *diffusion* terms can be identified. The diffusion term can cause loss of boundedness. It is discontinuous and singular where any given scalar is equal on two or more fields at a given location in physical space.

Two new DQMoM-IEM solvers have been coupled to the Star-CD CFD code using an operator splitting technique. They have been validated against the method of moments and a reacting flow case. The choice of boundary conditions to represent a given physical condition is not arbitrary. The correct scalar mixing was only reproduced when the boundary conditions were specified to be consistent with each field being assigned to a specific inlet.

The first (general) solver can be applied to cases with any number of fields and scalars. The diffusion terms are calculated by *functional evaluation* and a filter function is introduced to eliminate discontinuities and enforce boundedness. The approach is similar to methods that limit the size of the diffusion term or set it to zero near a discontinuity. It differs in that it preserves more information and eliminates the discontinuity, which the other methods would not. The source terms are integrated numerically using RADAU5. The second (analytic) solver is specific to $N=2$ fields. It uses *analytic solutions* of the DQMoM-IEM terms arising due to turbulent diffusion and micromixing and can be applied to any number of scalars.

3 THE DIRECT QUADRATURE METHOD OF MOMENTS

The key challenge is the diffusion term. The analytic solver provides an elegant method for $N=2$ fields. The numerical treatment of the diffusion term by the general solver was considered in detail and demonstrated for $N=2$ and $N=3$ fields, and remains an important area of research to make the method more practical.

Chapter 4

The stochastic fields method

This chapter compares mean reaction rate closures based on DQMoM-IEM and the SF method. The methods have many common features and have received much attention in recent literature, yet have not been systematically compared. We present both methods in the same mathematical framework and compare their numerical performance. We introduce antithetic sampling as a variance reduction technique to increase the efficiency of the SF algorithm. We extend the SF methodology to take advantage of this development and show details of the implementation in the Star-CD CFD code. We present a systematic investigation and consider both axisymmetric and 3D formulations of a problem known from the literature. DQMoM-IEM showed excellent agreement with experimental and transported PDF data. SF gave reasonable agreement, but retained a minor grid-dependence not seen with DQMoM-IEM and did not fully resolve the sub-grid segregation of the species. The antithetic sampling was demonstrated to significantly increase the efficiency of the axisymmetric SF cases.

4.1 Background

The stochastic fields (SF) method uses a set of Eulerian fields to discretise a joint composition PDF transport equation. The fields are defined over the entire spatial domain and evolve according to a stochastic partial differential equation (SPDE) such that they remain statistically equivalent to the joint composition PDF.

The SF discretisation is analogous to that in DQMoM-IEM, except that the SF method can be freely scaled to any number of fields to refine the approximation of the underlying PDF, subject to hardware constraints. This is potentially attractive compared to DQMoM-IEM, where the previous chapter shows that the maximum number of fields is likely to be constrained by numerical difficulties. The price of this freedom is that SF is a Monte Carlo method, such that a *minimum* number of fields will now be required to control statistical error.

The **purpose of this chapter** is to systematically compare the performance of DQMoM-IEM and SF as turbulent reaction closures. We follow the majority of the literature considered in chapter 2 and investigate the Itô SPDE derived by Valiño (1998). The rest of this section reiterates the model equations and discusses the features shared by the methods. Section 4.2 summarises the SF implementation and explains the use of antithetic sampling to increase the statistical efficiency of the simulations. Section 4.3 investigates the performance of DQMoM-IEM and SF against the method of moments and a turbulent reaction test case known from the literature. Both axisymmetric and 3D cases are considered. The benefits of antithetic sampling are discussed and areas for further research suggested.

4.1.1 Stochastic fields equations

The SF method was derived independently by Valiño (1998) and Sabel'nikov and Soulard (2005a). Valiño derives an Itô SPDE for fields defined as twice differentiable in space, whereas Sabel'nikov and Soulard present a general derivation of a Stratonovich SPDE and show equivalence to Valiño's result. The key features of the method are summarised below in the framework developed for DQMoM-IEM. Appendix A presents a formal derivation.

The closed joint composition PDF transport equation, previously given on page 35 as equation (3.1)

$$\begin{aligned} \frac{\partial f_\phi}{\partial t} + \langle U_i \rangle \frac{\partial f_\phi}{\partial x_i} - \frac{\partial}{\partial x_i} \left(\Gamma_T \frac{\partial f_\phi}{\partial x_i} \right) = \\ - \frac{\partial}{\partial \psi_\alpha} \left(\left[\frac{C_\phi}{2\tau_\phi} (\langle \phi_\alpha \rangle - \psi_\alpha) + S_\alpha(\psi) \right] f_\phi \right), \end{aligned}$$

is discretised using an ensemble of N fields

$$\begin{aligned} f_\phi(\psi(x,t)) \, d\psi &= f_\phi(\psi_1, \psi_2, \dots, \psi_K(x,t)) \, d\psi_1 \cdots d\psi_K \\ &\approx \frac{1}{N} \sum_{n=1}^N \prod_{\alpha=1}^K \delta_{\psi_\alpha^{(n)}(x,t)}(d\psi_\alpha), \end{aligned} \quad (4.1)$$

where $\delta_{\psi_\alpha^{(n)}(x,t)}(d\psi_\alpha)$ is defined as per equation (3.3). Hauke and Valiño (2004) state the equivalent Itô SPDE describing the transport of each field $\psi_\alpha^{(n)}(x,t)$

$$\begin{aligned} d\psi_\alpha^{(n)} = - \langle U_i \rangle \frac{\partial \psi_\alpha^{(n)}}{\partial x_i} dt + \frac{\partial}{\partial x_i} \left(\Gamma_T \frac{\partial \psi_\alpha^{(n)}}{\partial x_i} \right) dt + (2\Gamma_T)^{1/2} \frac{\partial \psi_\alpha^{(n)}}{\partial x_i} dW_i^{(n)} \\ + \frac{C_\phi}{2\tau_\phi} (\langle \phi_\alpha \rangle_N - \psi_\alpha^{(n)}) dt + S_\alpha(\psi^{(n)}) dt, \end{aligned} \quad (4.2)$$

where W is a Wiener process (see Gardiner, 2004) and the fields $\psi_\alpha^{(n)}$ evolve such that they remain statistically equivalent to the joint composition PDF f_ϕ . The final three terms describe the effect of turbulent diffusion, micromixing and chemical reaction. We refer to them as the SF *diffusion*, *micromixing* and *reaction* terms. Note also that the x - t dependencies of the terms in equation (4.2) onwards are suppressed for clarity of presentation.

4.1.2 Features shared with DQMoM-IEM

The SF method invokes an analogous discretisation to DQMoM-IEM. Both methods derive a joint composition PDF transport equation that is discrete in composition space, but continuous in time and physical space. In this particular example, the methods are also applied to the same equation (3.1).

4 THE STOCHASTIC FIELDS METHOD

The SF discretisation in equation (4.1) is an equi-weighted form of the field system introduced by DQMoM-IEM in equation (3.2). In the case that equation (3.2) is constrained $w^{(n)} = 1/N$, the DQMoM-IEM transport equation (3.6) can be rewritten in terms of $\psi_\alpha^{(n)}$ in an analogous form to the SF transport equation (4.2), where the methods differ only in the treatment of the diffusion terms.

DQMoM-IEM is deterministic and typically only a few fields are required. In particular, it is the use of weighted fields and the boundary conditions on the weights that allows specified moments of the underlying PDF to be modelled with only a few fields (see section 3.3.5). In the case of SF, the benefit of the variable weights is lost and the moments of the modelled PDF are governed entirely by the stochastic action of equation (4.2). The treatment of the diffusion term is simplified at the cost of requiring a larger number of fields both to compensate for the loss of weighted fields and to control statistical error.

4.2 Numerical details

This section presents details of the SF implementation. It describes the method used to couple SF to CFD and introduces the use of antithetic sampling to improve the statistical efficiency of the method.

4.2.1 Stochastic fields coupling to Star-CD

SF is coupled to the Star-CD CFD code (CD-adapco, 2008) using the same operator splitting technique as DQMoM-IEM (see section 3.2.1). Equation (4.2) is solved as a transient problem using a Strang (1968) splitting

$$d\psi_\alpha^{(n)} = -\langle U_i \rangle \frac{\partial \psi_\alpha^{(n)}}{\partial x_i} dt + \frac{\partial}{\partial x_i} \left(\Gamma_T \frac{\partial \psi_\alpha^{(n)}}{\partial x_i} \right) dt, \quad (4.3)$$

$$d\psi_\alpha^{(n)} = \frac{C_\phi}{2\tau_\phi} \left(\langle \phi_\alpha \rangle_N - \psi_\alpha^{(n)} \right) dt + S_\alpha \left(\psi^{(n)} \right) dt + \left(2\Gamma_T \right)^{1/2} \frac{\partial \psi_\alpha^{(n)}}{\partial x_i} dW_i^{(n)}. \quad (4.4)$$

Equation (4.3) is solved using Star-CD with upwind differencing to transport $\psi_\alpha^{(n)}$ as passive scalars with time step Δt . Equation (4.4) is solved using user-defined subroutines with time step $\frac{1}{2}\Delta t$ before the first and after the last iteration, and time step Δt otherwise. It is further split (for time step Δt)

$$\psi_\alpha^{(n)\dagger_1} = \psi_\alpha^{(n)}(t) + \int_0^{\frac{1}{2}\Delta t} \frac{C_\phi}{2\tau_\phi} \left(\langle \phi_\alpha \rangle_N - \psi_\alpha^{(n)} \right) d\tau, \quad (4.5)$$

$$\text{where } \psi_\alpha^{(n)} = \psi_\alpha^{(n)}(t) \text{ at } \tau = 0,$$

$$\psi_\alpha^{(n)\dagger_2} = \psi_\alpha^{(n)\dagger_1} + \int_0^{\Delta t} \left(2\Gamma_T \right)^{1/2} \frac{\partial \psi_\alpha^{(n)}}{\partial x_i} dW_i^{(n)}, \quad (4.6)$$

$$\text{where } \frac{\partial \psi_\alpha^{(n)}}{\partial x_i} \leftarrow \frac{\partial \psi_\alpha^{(n)}(t)}{\partial x_i} \text{ at } \tau = 0,$$

$$\psi_\alpha^{(n)\dagger_3} = \psi_\alpha^{(n)\dagger_2} + \int_0^{\Delta t} S_\alpha \left(\psi^{(n)} \right) d\tau, \quad (4.7)$$

$$\text{where } \psi_\alpha^{(n)} = \psi_\alpha^{(n)\dagger_2} \text{ at } \tau = 0,$$

$$\psi_\alpha^{(n)}(t + \Delta t) = \psi_\alpha^{(n)\dagger_3} + \int_0^{\frac{1}{2}\Delta t} \frac{C_\phi}{2\tau_\phi} \left(\langle \phi_\alpha \rangle_N - \psi_\alpha^{(n)} \right) d\tau, \quad (4.8)$$

$$\text{where } \psi_\alpha^{(n)} = \psi_\alpha^{(n)\dagger_3} \text{ at } \tau = 0,$$

where Star-CD is used to evaluate the gradients $\partial \psi_\alpha^{(n)}(t) / \partial x_i$ at the start of each step, resulting in the approximation shown in equation (4.6) (*cf.* section 3.2).

The reaction term in equation (4.7) is integrated using RADAU5. The micromixing terms are solved analytically, where the solutions are given for equation (4.5)

$$\psi_\alpha^{(n)\dagger_1} = \langle \phi_\alpha \rangle_N - \left(\langle \phi_\alpha \rangle_N - \psi_\alpha^{(n)}(t) \right) \exp \left[-\frac{C_\phi}{2\tau_\phi} \frac{\Delta t}{2} \right], \quad (4.9)$$

and equation (4.8)

$$\psi_\alpha^{(n)}(t + \Delta t) = \langle \phi_\alpha \rangle_N - \left(\langle \phi_\alpha \rangle_N - \psi_\alpha^{(n)\dagger_3} \right) \exp \left[-\frac{C_\phi}{2\tau_\phi} \frac{\Delta t}{2} \right]. \quad (4.10)$$

4 THE STOCHASTIC FIELDS METHOD

The diffusion term in equation (4.6) is solved over the whole time step Δt in order to maintain the required independence between the integrand and $dW_i^{(n)}$ (Gardiner, 2004). It is solved as per Garmory (2007), using the Euler-Maruyama approximation of an Itô process (Kloeden and Platen, 1995)

$$\psi_\alpha^{(n)\dagger_2} = \psi_\alpha^{(n)\dagger_1} + \left(2\Gamma_T\right)^{1/2} \frac{\partial \psi_\alpha^{(n)}}{\partial x_i} \Delta W_i^{(n)}, \quad (4.11)$$

where

$$\Delta W_i^{(n)} = \xi_i^{(n)} (\Delta t)^{1/2}, \quad (4.12)$$

$$\xi_i^{(n)} \sim \mathcal{N}(0, 1). \quad (4.13)$$

The variates $\xi_i^{(n)}$ are independent for each spatial dimension and field, but common for all scalars. They are generated using the method of Ahrens and Dieter (1973), with uniform variates supplied by the Mersenne Twister MT19937 algorithm (Matsumoto and Nishimura, 1998) with a fixed seed. This implementation may lead to loss of boundedness at large time steps. A stable and accurate method that avoids bias away from the bounds can be achieved by limiting the maximum size of the Wiener step to prevent unbounded scalars (Garmory, 2007). We apply an analogous method to bound the SF implementation in this chapter.

4.2.2 Antithetic sampling

Antithetic sampling is a variance reduction technique. It was first introduced by Hammersley and Morton (1956) to increase the efficiency of Monte Carlo simulations, where the efficiency is defined in terms of the effort required to achieve a given reduction in statistical error. The premise of the method is that the variance between repetitions of a Monte Carlo simulation is reduced by introducing pair-wise negative correlation between replicates.

The mathematical basis for antithetic sampling is defined in work led by Hammersley and co-workers (Hammersley and Morton, 1956; Hammersley and Mauldon, 1956; Hammersley and Handscomb, 1958) and Wilson (1979, 1983), and sum-

4.3 Comparison of DQMoM-IEM and SF

marised by Fishman (1996). The method has mostly been applied within quantitative economics (Geweke, 1988) and finance (Paskov and Traub, 1995; Boyle et al., 1997). Its application within computer simulations has been investigated by Cheng (1982) and Fishman and Huang (1983).

We apply antithetic sampling to the SF method, treating each field as a replicate. The idea is to increase the efficiency, such that a given result can be achieved with fewer fields and without requiring repetition of the entire simulation. The variates are sampled for odd-numbered fields, but prescribed for even-numbered fields

$$\xi_i^{(n)} \sim \mathcal{N}(0, 1) \text{ if } n \in 2\mathbb{N}-1, \quad \xi_i^{(n)} = -\xi_i^{(n-1)} \text{ if } n \in 2\mathbb{N}. \quad (4.14)$$

This is the *reflection sampling* method described by Fishman and Huang (1983) and the ‘standard’ method used as the basis for the investigation by Cheng (1982). Cheng suggests several possible refinements, but we restrict our attention to the method defined by equation (4.14) for the purposes of this investigation.

The rest of this chapter compares the performance of DQMoM-IEM and SF, and considers the impact of antithetic sampling. SF cases with sampling as per equation (4.13) are denoted as *standard cases*, and those with sampling as per equation (4.14) as *antithetic cases*. Note that for a given number of iterations, a standard case with N fields uses the same sequence of variates as the first half of a standard case or a full antithetic case with $2N$ fields.

4.3 Comparison of DQMoM-IEM and SF

This section compares the performance of the SF method described in section 4.2 against the DQMoM-IEM solvers and test cases considered in chapter 3.

Section 4.3.1 describes additional details of the test case. Section 4.3.2 compares the performance of the SF method against the method of moments. This enables the effect of the numerical implementation of the diffusion terms (see sections 4.1 and 4.2) to be investigated in isolation. Section 4.3.3 investigates the application of the SF method to a reacting system. Section 4.3.4 summarises the CPU times.

4 THE STOCHASTIC FIELDS METHOD

4.3.1 Model problem

The case considered is the single-jet reactor system described in section 3.3 for the *constant density* isothermal liquid-phase reaction



This chapter considers the high concentration case where a turbulent jet of species B with Reynolds number $Re=3530$ is injected into a laminar co-flow of species A. The system was solved using Star-CD (CD-adapco, 2008) as per section 3.3. The initial and inlet boundary conditions are summarised in **table 4.1**. The conditions are identical to those used previously for DQMoM-IEM (tables 3.1 and table 3.6), only without the perturbations required by DQMoM-IEM (see section 3.3.5).

Table 4.1: SF jet reactor initial and inlet boundary conditions.

	Initial condition	Inlet boundary	
		Jet	Annulus
$Y_A^{(n)}$	0	0	4.27×10^{-4}
$Y_B^{(n)}$	0	5.25×10^{-4}	0
$Y_{R,S}^{(n)}$	0	0	0
$Y_{\text{solvent}}^{(n)}$	1	$1 - Y_B^{(n)}$	$1 - Y_A^{(n)}$

The DQMoM-IEM and SF methods are investigated using three grids. The first is the *base* grid from section 3.3. This uses a wedge-shaped domain of 68×23 (axial \times radial) fully structured hexahedral cells. The second is a *coarse* grid, which is a simplified version of the base grid and uses a 34×14 (axial \times radial) domain. The third is a *coarse 3D* grid, which models the full reactor geometry using a cylindrical domain of $34 \times 14 \times 18$ (axial \times radial \times azimuthal) fully structured hexahedral cells defined in a cartesian coordinate system. All cases were solved with time step 10^{-4} s on the base grid and 10^{-3} s on the coarse grids.

4.3 Comparison of DQMoM-IEM and SF

The SF method has so far inhibited the use of symmetric boundary conditions, since it is not clear how they should be applied to the stochastic fields (Sabel'nikov and Soulard, 2005a; Garmory, 2007). However, the test case flow field is axisymmetric and the DQMoM-IEM solutions are dominated by radial gradients. We use this to justify imposing an azimuthal zero-gradient condition to enforce an axisymmetric solution on the base and coarse grids. The difference between the grids causes small differences between the solutions near the inlets. However, the data are considered to be sufficiently grid-independent based on the grid causing a variation of less than 0.5% in the yield of the DQMoM-IEM cases solved in section 4.3.3 (see table 4.3). The effect of the grid on the SF cases is considered in more detail in the following sections.

4.3.2 Application to scalar mixing

This section compares the performance of the DQMoM-IEM and SF methods for a scalar mixing case. A reference solution is provided using the method of moments (MoM, see also section 3.3.2). This approach allows the effect of the numerical implementation of the diffusion terms described in sections 4.1 and 4.2 to be examined in isolation from the effects of reaction.

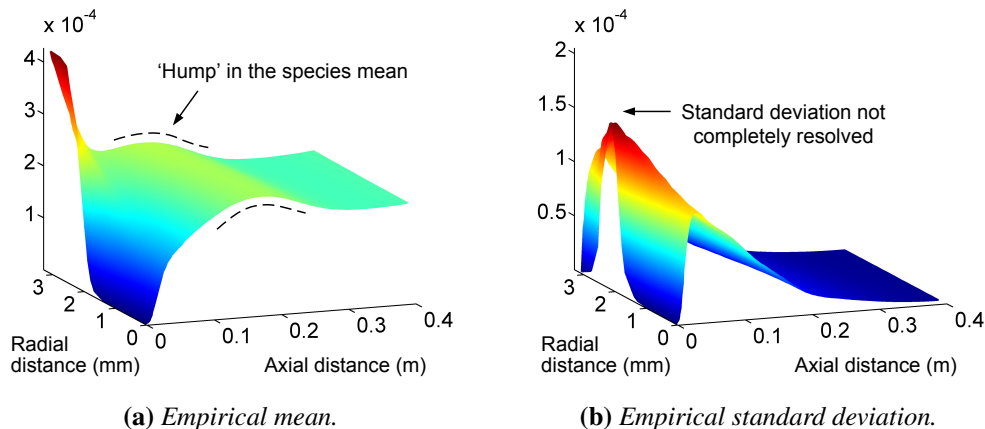


Figure 4.1: Jet reactor empirical mean and standard deviation of species A for the inert $Re = 3530$ high concentration case at $t = 5$ s on the base grid, SF solver with standard sampling and $N = 64$ fields.

4 THE STOCHASTIC FIELDS METHOD

Figure 4.1 presents the empirical mean and standard deviation of species A for a typical SF simulation of the scalar mixing of species A and B. Corresponding DQMoM-IEM data are shown in figure 3.6. The figure highlights some important issues. Figure 4.1(a) shows a ‘hump’ in the mean of species A. It is caused by the diffusion term where the SF implementation applies a set of variates $\xi_i^{(n)}$ that do not have exactly zero mean. This is most apparent in the radial direction because the effect of the diffusion term is dominated by the relative magnitude of the radial gradients. Such ‘humps’ are convected by the flow and can be observed as *fluctuations* in the values of the species means at the reactor outlet. This effect should decrease as the number of fields is increased, since the mean of the set of variates will converge in probability at a rate proportional to $N^{-1/2}$

$$\lim_{N \rightarrow \infty} \mathbb{P} \left(\left| \frac{1}{N} \sum_{n=1}^N \xi_i^{(n)} \right| \geq \varepsilon_i \right) = 0, \quad \forall \varepsilon_i > 0. \quad (4.15)$$

Comparison of figures 4.1(b) and 3.6(b) shows that the SF solution does not completely resolve the standard deviation near the reactor inlets. A similar observation is made using DQMoM-IEM with equal weights (see section 3.3.5). In this instance, DQMoM-IEM can reproduce figure 4.1(b) with $N=2$ and boundary conditions on the weights $w_{\text{jet}}^{(1)} \approx 0.4$, $w_{\text{jet}}^{(2)} \approx 0.6$ and $w_{\text{annulus}}^{(n)} = 1 - w_{\text{jet}}^{(n)}$.

Figure 4.2 plots the fluctuation of the mean species B mass fraction at the reactor outlet for SF cases with $N = 4, 8, 16, 32, 64$ fields. The fluctuation is calculated

$$\max_{\substack{\text{reactor outlet} \\ t \in [1, 5] \text{ s}}} \left(\langle Y_B \rangle_N \right) - \min_{\substack{\text{reactor outlet} \\ t \in [1, 5] \text{ s}}} \left(\langle Y_B \rangle_N \right), \quad (4.16)$$

where the calculation is defined from $t = 1$ s since this is the time at which DQMoM-IEM is observed to reach steady state. Figure 4.2 confirms that the fluctuations converge at a rate proportional to $N^{-1/2}$ for both the standard and antithetic cases. The antithetic cases show significantly reduced fluctuation on the base and coarse grids due to the antithetic sampling enforcing a zero mean condition on the set of variates $\xi_i^{(n)}$ in each direction i . However, the fluctuations remain finite because the antithetic case does not enforce equal spatial gradients within each antithetic pair of fields.

4.3 Comparison of DQMoM-IEM and SF

The coarse 3D grid shows little difference between the standard and antithetic cases, with fluctuations approximately two-thirds the size of those for the standard case on the coarse grid. This is less than the $\sqrt{\frac{2}{3}}$ size that might be expected by considering that the coarse grid cases use only two-thirds of the variates (the rest are multiplied by the zero azimuthal gradient). The data are not spatially averaged, so this is not a symmetry effect. It is suggested that this is a consequence of solving the case in cartesian coordinates. The cartesian contributions to the SF diffusion term act at different angles to the radial and azimuthal directions at different points in the radial-azimuthal plane. This gives a non-axisymmetric solution and reduces the magnitude of the fluctuations in the standard case, but undoes most of the effect of the antithetic sampling causing an increase in the magnitude of the fluctuations in the antithetic case. This explanation suggests that a 3D case solved in cylindrical polar coordinates, where the radial and azimuthal contributions to the diffusion term would remain in fixed alignment with the radial and azimuthal directions, should preserve the symmetry of the solution and reproduce the results from the coarse rather than coarse 3D grid.

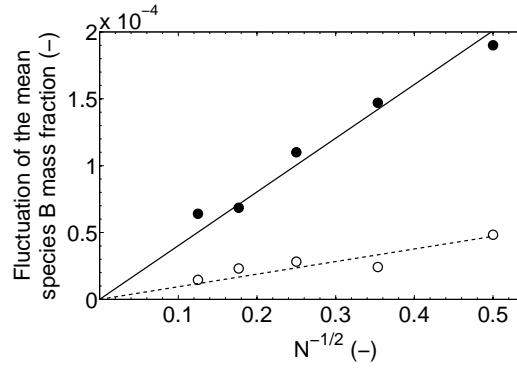
Figure 4.3 plots the convergence between the SF simulations and the method of moments. **Table 4.2** shows equivalent data for DQMoM-IEM. The convergence was assessed for the empirical mean and standard deviation using the metrics ϵ_{mean} and ϵ_{sd} defined as per equations (3.40) and (3.41). Note that figure 4.3 represents a ‘snapshot’ of the SF data at $t = 5$ s, so should be expected to show more noise than figure 4.2, where the data were collected over the interval $t \in [1, 5]$ s.

Table 4.2: Convergence of the DQMoM-IEM empirical mean and standard deviation versus the method of moments for the inert $Re = 3530$ high concentration jet reactor case at $t = 2$ s.

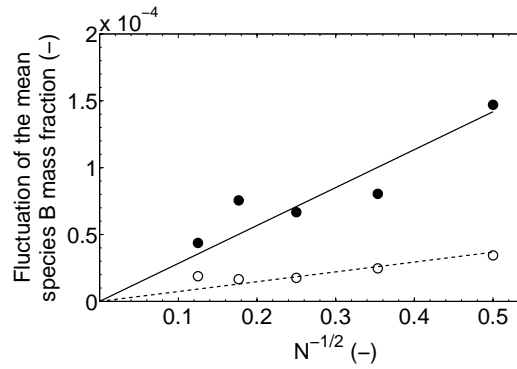
Grid	ϵ_{mean}			ϵ_{sd}		
	$N = 2^a$	$N = 2^b$	$N = 3^b$	$N = 2^a$	$N = 2^b$	$N = 3^b$
Base	6.9×10^{-7}	6.9×10^{-7}	4.4×10^{-7}	4.7×10^{-6}	4.7×10^{-6}	4.8×10^{-6}
Coarse	6.5×10^{-7}	—	—	2.9×10^{-6}	—	—
3D coarse	6.5×10^{-7}	—	—	4.5×10^{-6}	—	—

^a Analytic solver (see section 3.2 and figure 3.6), ^b General solver (see section 3.2).

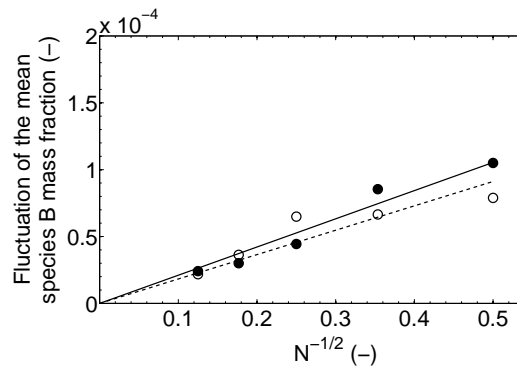
4 THE STOCHASTIC FIELDS METHOD



(a) Base grid.



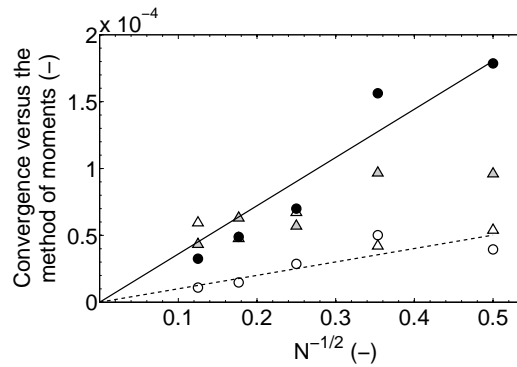
(b) Coarse grid.



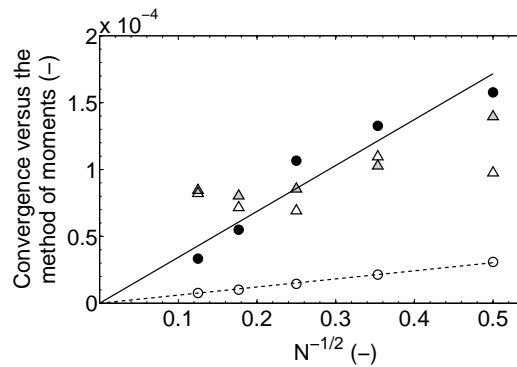
(c) Coarse 3D grid.

Figure 4.2: Fluctuation of the SF empirical mean of species B at the jet reactor outlet for the inert $Re = 3530$ high concentration case in the interval $t \in [1, 5]$ s. Solid symbols: standard case; Solid line: standard case guide line; Hollow symbols: antithetic case; Dashed line: antithetic case guide line.

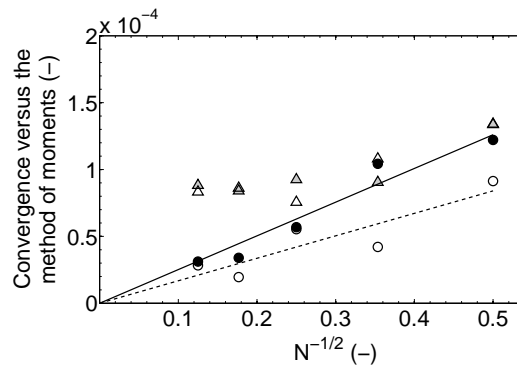
4.3 Comparison of DQMoM-IEM and SF



(a) Base grid.



(b) Coarse grid.



(c) Coarse 3D grid.

Figure 4.3: Convergence of the SF jet reactor empirical mean and standard deviation versus the method of moments for the inert $Re = 3530$ high concentration case at $t = 5$ s. Solid symbols: standard case; Solid line: standard case guide line; Hollow symbols: antithetic case; Dashed line: antithetic case guide line. Circles (\circ): mean metric, ϵ_{mean} ; Triangles (Δ): standard deviation metric, ϵ_{sd} .

4 THE STOCHASTIC FIELDS METHOD

Figure 4.3 shows that ϵ_{mean} converges at a rate proportional to $N^{-1/2}$. A clear improvement is shown for the antithetic versus standard case for the base and coarse grids. Again, the coarse 3D grid shows a similar effect to that in figure 4.2. The convergence is between that observed for the standard and antithetic cases on the coarse grid, with a small benefit from the antithetic case in this instance. Similar convergence is shown for ϵ_{sd} up to $N = 16$ fields, possibly with some benefit and certainly no harm from the antithetic case. At $N > 16$ fields, ϵ_{sd} is observed to reach a steady value. The coarse grids reach $\epsilon_{\text{sd}} \approx 0.8 \times 10^{-4}$, whereas the base grid does slightly better at $\epsilon_{\text{sd}} \approx 0.6 \times 10^{-4}$. This is indicative of at least some grid dependence in the SF solution. Similar observations have been reported for DQMoM-IEM by Gavi et al. (2007b). In all cases, comparison of figure 4.3 with table 4.2 shows that DQMoM-IEM achieves better convergence than SF.

4.3.3 Application to reacting flow

This section investigates the application of the DQMoM-IEM and SF methods to the turbulent jet reactor discussed in section 4.3.1. Table 4.3 summarises the yields for the DQMoM-IEM cases. The data agree with that in chapter 3 and show that a good estimate of the yield can be obtained on each grid.

Figures 4.4 and 4.5 present the empirical means and standard deviations for a typical SF case with antithetic sampling. Corresponding DQMoM-IEM data are given in figures 3.7 to 3.10 for the $N = 2$ and $N = 3$ cases.

Table 4.3: DQMoM-IEM jet reactor yields for the reacting $Re = 3530$ high concentration case on the SF grids.

Grid	DQMoM-IEM yield (%)			Literature yield data (%)	
	$N = 2^a$	$N = 2^b$	$N = 3^b$	Full transported PDF ^c	Expt. ^d
Base	80.4	80.7	81.9	81.0	82.1
Coarse	80.1	—	—	—	—
3D coarse	80.3	—	—	—	—

^a Analytic solver (see section 3.2 and figures 3.7 and 3.9), ^b General solver (see section 3.2 and figures 3.8 and 3.10), ^c Tsai and Fox (1994, table 3), ^d Li and Toor (1986, table 1, experimental repeatability ± 0.5 %)

4.3 Comparison of DQMoM-IEM and SF

Figures 4.4 and 4.5 still show some artifacts due to fluctuations, particularly in the mean of species R and S shown in figures 4.4(c) and (d). The sub-grid segregation of the species is not fully resolved in the region between the inlets. This results in a significant concentration of the product R adjacent to the wall between the inlets in figure 4.4(c). It is also evident in the lower values of the SF standard deviations reported for species A, B and S in figures 4.5(a), (b) and (d), and the over-prediction of the standard deviation of species R in figure 4.5(c), compared to the DQMoM-IEM standard deviations in figure 3.10.

Figure 4.6 shows the fluctuation of the yield at the reactor outlet for SF cases with $N = 4, 8, 16, 32, 64$ fields. The yield Y is calculated using equation (3.36) where

$$Y = \frac{\langle C_R \rangle}{\langle C_R \rangle + 2\langle C_S \rangle}, \quad \langle C_\alpha \rangle = \frac{\rho \langle Y_\alpha \rangle_N}{W_\alpha} \Big|_{\text{reactor outlet}}.$$

The fluctuation is calculated as the difference between the maximum and minimum yields at the reactor outlet

$$\max_{t \in [1, 5]_s} (Y) - \min_{t \in [1, 5]_s} (Y), \quad (4.17)$$

and shows analogous behaviour to figure 4.2, with convergence proportional to $N^{-1/2}$ and reduced fluctuations for the antithetic case on the base and coarse grids.

Figure 4.7 plots the SF time-averaged yield and the loci of the maximum and minimum yields at the reactor outlet, as defined by equation (4.17). The yields converge to values slightly higher than for DQMoM-IEM and are estimated as 84–86% for the base grid and 86–88% for the coarse grids. The difference from DQMoM-IEM is due to the failure to fully resolve the sub-grid segregation near the reactor inlets. It can be shown that DQMoM-IEM reproduces an 85% yield when using the boundary conditions shown to reproduce the SF behaviour in section 4.3.2. The differences between the SF cases on the base and coarse grids are due to how far each resolves the sub-grid segregation, as per the minor grid dependence identified in relation to figure 4.3. In this example, DQMoM-IEM achieves a grid-independent solution more easily than SF. What defines an acceptable level of grid-independence will of course be application specific.

4 THE STOCHASTIC FIELDS METHOD

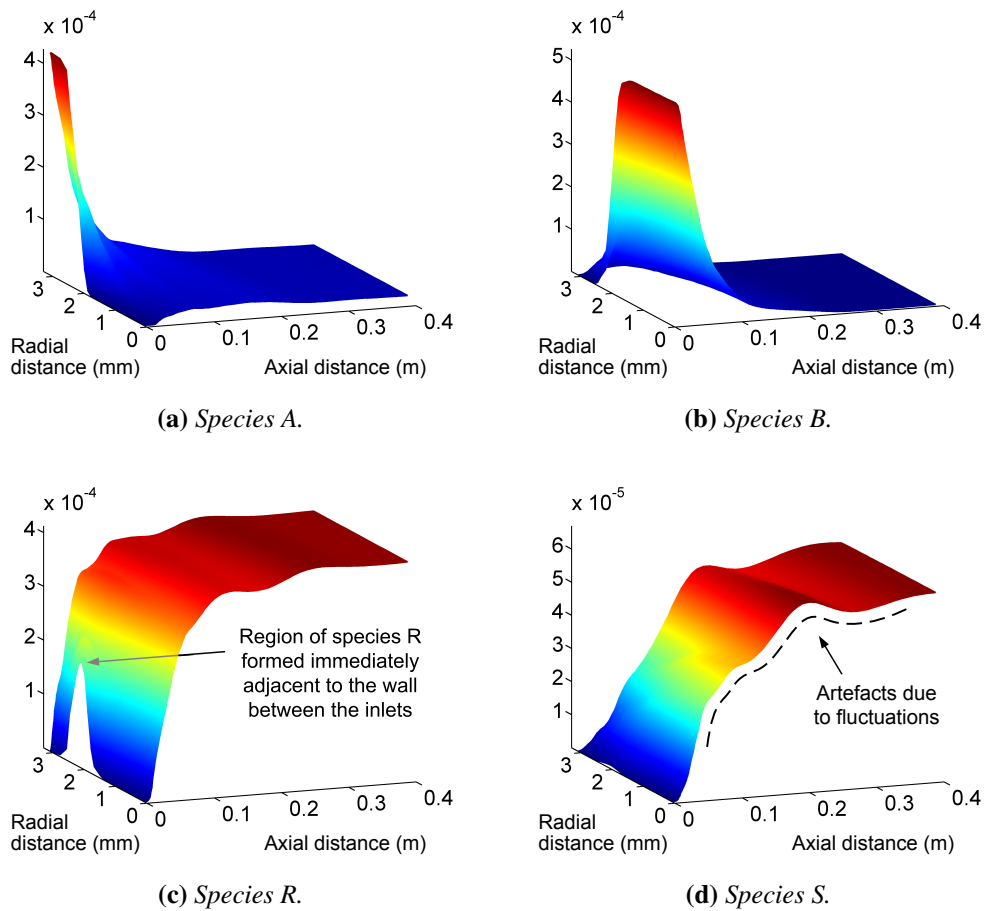


Figure 4.4: Jet reactor empirical means for the reacting $Re = 3530$ high concentration case at $t = 5$ s on the base grid, SF solver with antithetic sampling and $N = 64$ fields.

4.3 Comparison of DQMoM-IEM and SF

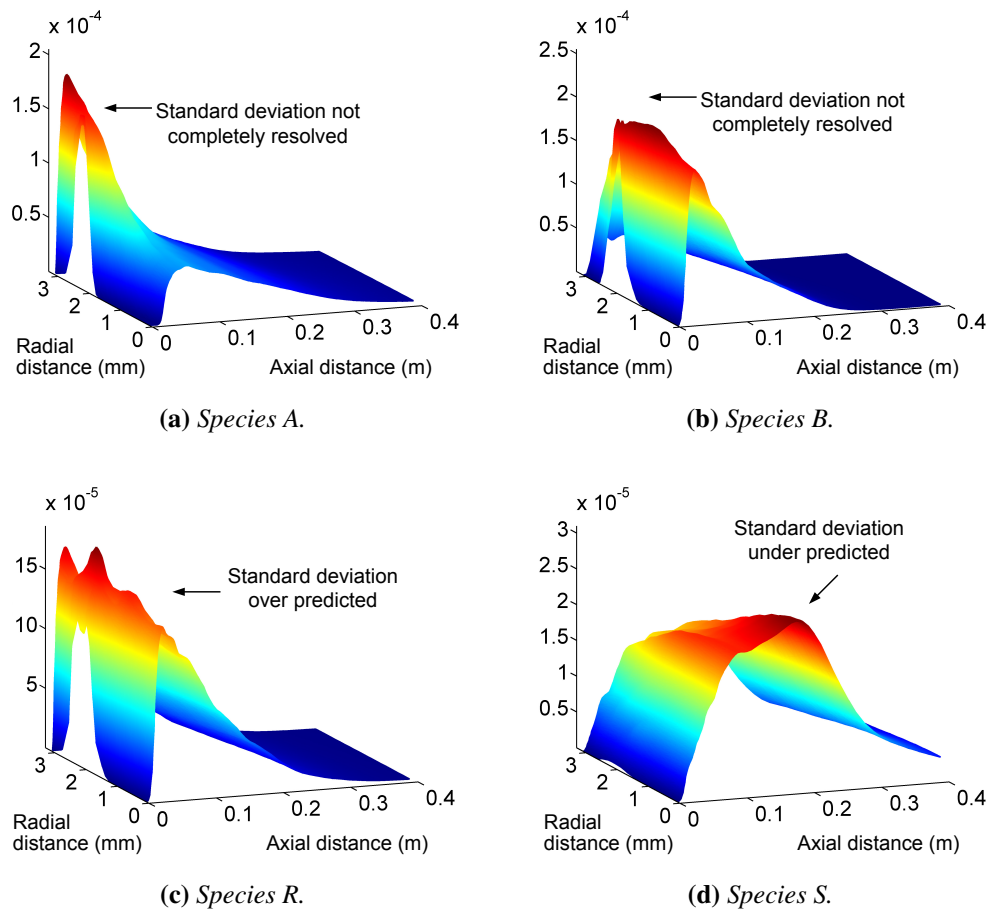
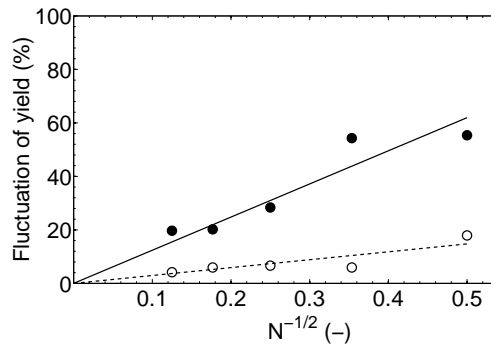
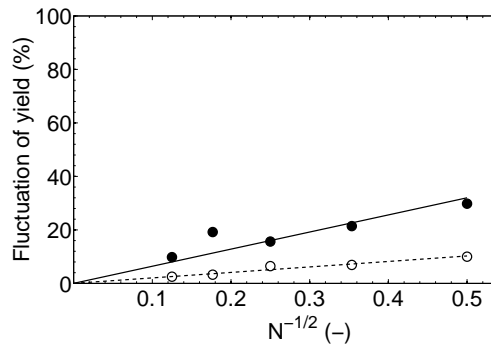


Figure 4.5: Jet reactor empirical standard deviations for the reacting $Re=3530$ high concentration case at $t = 5$ s on the base grid, SF solver with antithetic sampling and $N = 64$ fields.

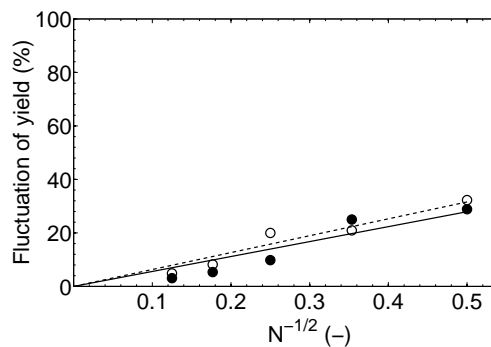
4 THE STOCHASTIC FIELDS METHOD



(a) Base grid.



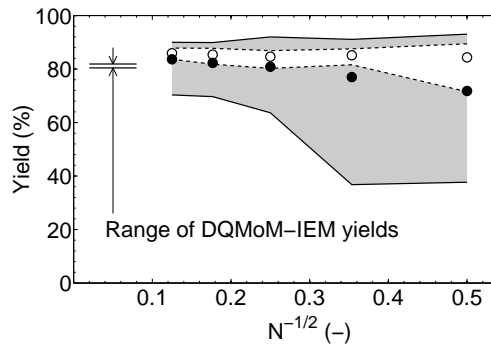
(b) Coarse grid.



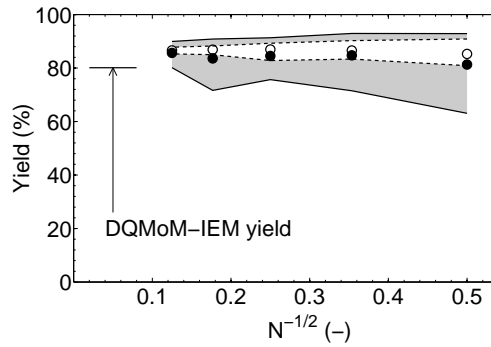
(c) Coarse 3D grid.

Figure 4.6: Fluctuation of the SF yield at the jet reactor outlet for the reacting $Re = 3530$ high concentration case in the interval $t \in [1, 5]$ s. Solid symbols: standard case; Solid line: standard case guide line; Hollow symbols: antithetic case; Dashed line: antithetic case guide line.

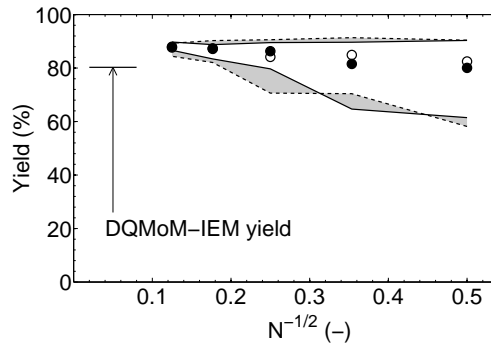
4.3 Comparison of DQMoM-IEM and SF



(a) Base grid.



(b) Coarse grid.



(c) Coarse 3D grid.

Figure 4.7: SF yield at the jet reactor outlet for the reacting $Re=3530$ high concentration case in the interval $t \in [1, 5]$ s. Solid symbols: standard case time-averaged yield; Solid line: standard case loci of maximum and minimum yields; Hollow symbols: antithetic case time-averaged yield; Dashed line: antithetic case loci of maximum and minimum yields. Shaded area: difference between standard and antithetic case loci of maximum and minimum yields. The marked DQMoM-IEM yields are those given in table 4.3.

4 THE STOCHASTIC FIELDS METHOD

The difference between the standard and antithetic case loci of the maximum and minimum yields (marked by the gray areas on figure 4.7) illustrate a clear benefit from the application of antithetic sampling to the base and coarse grids: a better estimate of the yield can be achieved with fewer fields. The data for the coarse 3D grid are consistent with, but no better than the standard case on the coarse grid.

4.3.4 Computational performance

This section summarises the computational times for the DQMoM-IEM and SF cases considered. All cases were run on identical hardware.

Table 4.4 presents the DQMoM-IEM computational times. The analytic solver shows a significant speed advantage over the general solver (see section 3.3.4).

Table 4.4: *DQMoM-IEM jet reactor CPU times for the $Re = 3530$ high concentration case on the SF grids at $t = 2$ s.*

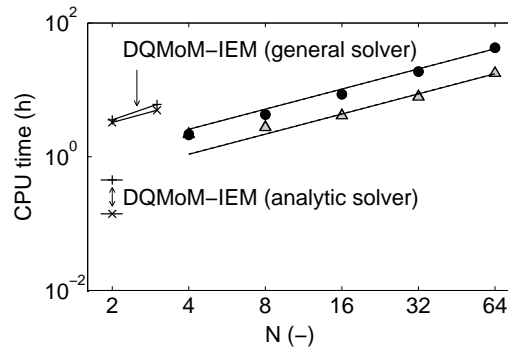
Grid	CPU times (h)					
	Scalar mixing cases			Reacting cases		
	$N = 2^a$	$N = 2^b$	$N = 3^b$	$N = 2^a$	$N = 2^b$	$N = 3^b$
Base	0.14 ^c	3.26	4.96	0.45 ^d	3.56	6.05 ^e
Coarse	0.01	—	—	0.03	—	—
3D coarse	0.30	—	—	0.53	—	—

^a Analytic solver, ^b General solver, ^c See figure 3.6, ^d See figure 3.7, ^e See figure 3.8.

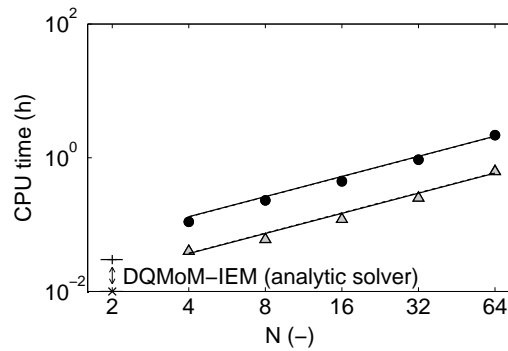
Figure 4.8 plots the SF computational times. The standard and antithetic cases are in close agreement and the data overlay each other in the figure. The computational times are proportional to the number of fields N , where the reacting cases take longer than the equivalent scalar mixing cases due to the chemistry.

The computational times are broadly equivalent between the general DQMoM-IEM solver and the SF method with $N = 8$ –16 fields for the cases considered here. As more complex chemistry is considered, it is anticipated the computational time will increase more quickly for the SF method than the general DQMoM-IEM solver because the SF method requires the greater number of fields.

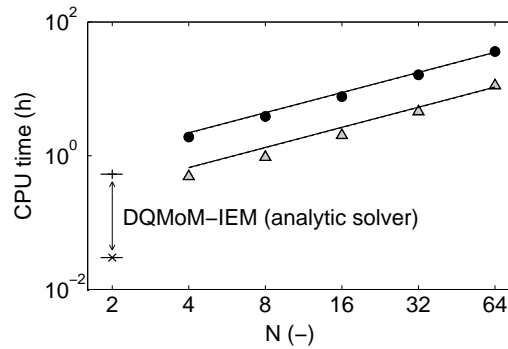
4.3 Comparison of DQMoM-IEM and SF



(a) Base grid.



(b) Coarse grid.



(c) Coarse 3D grid.

Figure 4.8: SF jet reactor CPU times for the $Re=3530$ high concentration case at $t = 5$ s. Solid symbols: standard case; Solid line: standard case guide line; Hollow symbols: antithetic case; Dashed line: antithetic case guide line. Circles (\circ): reacting case; Triangles (Δ): scalar mixing case.

The marked DQMoM-IEM CPU times are those given in table 4.4 for the scalar mixing (\times) and reacting ($+$) cases.

4.4 Chapter summary

SF uses a set of Eulerian fields to discretise a closed joint composition PDF transport equation. This is an equi-weighted form of the method used by DQMoM-IEM. Explicit *reaction*, *micromixing* and turbulent *diffusion* terms can again be identified. The difference from DQMoM-IEM is that SF invokes a stochastic process to approximate the diffusion term. The implementation is simplified at the cost of requiring a larger number of fields to compensate for the use of equi-weighted fields and to control statistical error. The application of antithetic sampling is introduced to improve the statistical efficiency of the SF algorithm.

The performance of DQMoM-IEM and SF has been compared for the turbulent reaction problem described in chapter 3. SF is coupled to the Star-CD CFD code using an operator splitting technique analogous to that applied to DQMoM-IEM. Cases have been considered on two grids that enforce an axisymmetric solution and on a 3D grid that resolves the full domain in a cartesian coordinate system. DQMoM-IEM showed good agreement with experimental and transported PDF data and equivalent results were demonstrated between the axisymmetric and 3D cases. SF gave similar results, but retained a minor grid-dependence not seen with DQMoM-IEM. It did not fully resolve the sub-grid segregation of the species, resulting in a systematic over-prediction of the yield. The prediction improved as the grid was refined, but remained less good than for DQMoM-IEM.

The SF results showed significant variance. The expected convergence was demonstrated in the non-reacting case for fluctuations of the species mass fractions at the reactor outlet and for convergence of the full domain versus the method of moments. In the reacting case, convergence was demonstrated for fluctuations of the yield. Antithetic sampling was shown to enable better convergence to be achieved with fewer fields on the axisymmetric grids. The situation for the 3D grid was less clear. The extra dimension gave improved statistical efficiency at greater computational cost for the standard case, but eliminated much of the benefit from the antithetic case. It is believed that this is a consequence of solving the case in cartesian coordinates, such that an equivalent case solved in cylindrical polar coordinates would reproduce the observations from the axisymmetric grids.

4.4 Chapter summary

The example in this chapter demonstrates an axisymmetric SF formulation that combines the benefits of antithetic sampling and reduced dimensionality. It also highlights where DQMoM-IEM offers some advantages. DQMoM-IEM was more easily able to achieve a grid-independent solution and gave a deterministic, accurate and computationally efficient prediction of the yield with as few as $N=2$ fields. The questions of whether these advantages translate to applications with more complicated chemistry and whether antithetic sampling offers benefits to SF simulations in other geometries remain important areas of research.

Chapter 5

Application of the projected fields method to nanoparticle modelling

This chapter investigates the first part of a two-stage methodology for the detailed modelling of nanoparticle formation in turbulent reacting flows. We use a projected fields (PF) method to approximate the joint composition PDF transport equation that describes the evolution of the nanoparticles. The method combines detailed chemistry and a MoMIC population balance model in the Star-CD CFD code. We show details of the implementation and present an extensive set of numerical experiments and validation. We consider the example of the chloride process for the industrial synthesis of titania. We show good agreement with experimental data and present fully coupled simulations of a representative ‘slot’ reactor. The simulations show that inception occurs in a mixing zone near the reactor inlets. Most of the nanoparticle mass is due to surface growth downstream of the mixing zone. The implications for the second part of the methodology, where it is proposed to post process the data using a more detailed particle model, are discussed critically.

5.1 Background

The previous chapters have investigated turbulent reacting flow models using DQMoM-IEM and the SF method as mean reaction rate closures. Both methods solve a discretised joint composition PDF transport equation. Both have been coupled to the Star-CD CFD code and applied to a constant density test case, where the analytic DQMoM-IEM solver showed good agreement with experimental data for the least computational effort.

The **purpose of this chapter** is to extend the work to consider nanoparticle formation. We investigate the first part of a two-stage methodology:

- The first-stage extends the developments in chapter 3 to introduce a projected fields (PF) method that combines detailed chemistry and a population balance for CFD simulations involving *full coupling* between turbulent flow, chemistry and particles undergoing simultaneous inception, coagulation and surface growth. The objective is to achieve a reasonable description of the flow and gas-phase composition PDF for minimum computational effort.
- The second-stage models the evolution of the nanoparticles using a *detailed* population balance model to post process the gas-phase composition data. There is free choice of the population balance model because the gas-phase data already include the coupling to the population, negating the need to re-solve the chemistry or flow.

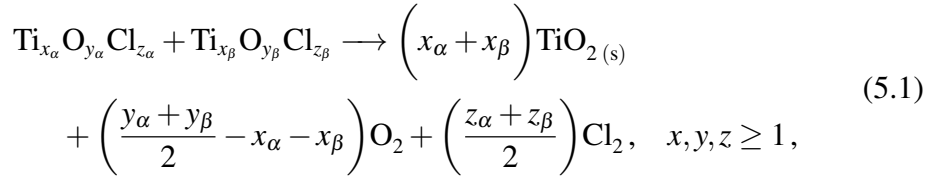
This approach is well established for soot simulations of premixed 1D laminar flames (Zhao et al., 2003; Singh et al., 2005; Morgan et al., 2007) and has been applied to titania formation in turbulent diffusion flames (Johannessen et al., 2001) (where the coupling is ignored). We follow the approach for soot and use the method of moments with interpolative closure (MoMIC) (Frenklach and Harris, 1987) to describe the population balance. The investigation considers the example of the chloride process for the industrial production of titania nanoparticles, and uses the analytic solver from chapter 3 in order to minimise the computational cost whilst the method is in development.

The remainder of this section introduces key aspects of the titania chemistry, the population balance and PF equations. Section 5.2 summarises the implementation of the method and the coupling to the CFD code. Section 5.3 investigates the performance of the model against test case and experimental data, and demonstrates its application to a representative industrial ‘slot’ reactor.

5.1.1 Kinetic model for titania formation

The titania mechanism is based on the chemistry of [West et al. \(2009\)](#). The mechanism comprises 66 reactions involving 28 gas-phase species plus TiO_2 product.

Inception and surface reaction are treated slightly differently from [West et al. \(2009\)](#). This choice is based on theoretical investigations of TiO_2 growth and fits to experimental data discussed by [Shirley et al. \(2011\)](#). All bimolecular collisions between titanium oxychloride species are treated as inception steps



where the molecular collision diameter is taken as 0.65 nm ([West et al., 2009](#)). Surface growth is treated as a second-order reaction



subject to the rate expression

$$\begin{aligned} \frac{d[\text{TiO}_2]}{dt} &= k_s A [\text{TiCl}_4] [\text{O}_2], \\ k_s &= 200 \exp\left(\frac{-50\text{kJ/mol}}{RT}\right) \frac{\text{m}}{\text{s}} \cdot \frac{\text{m}^3}{\text{mol}}, \end{aligned} \quad (5.3)$$

where A is the surface area of the population per unit volume. Equation (5.3) assumes fixed reaction orders with respect to TiCl_4 and O_2 , but is sufficient for this work. Alternative approaches are discussed by [Shirley et al. \(2011\)](#). The full model has 29 species and 172 (66 gas-phase, 105 inception, 1 surface) reactions.

5.1.2 Population balance equations

The population balance is solved using the method of moments with interpolative closure (MoMIC). The method describes the evolution of a truncated set of whole-order moments of a distribution of spherical particles undergoing simultaneous inception, coagulation and surface growth. The coupling to the flow primarily depends on the mass of material entering and leaving the population, where the total particulate mass is proportional to the first moment of the particle number distribution. MoMIC is reasonably accurate for the first moment ([Grosschmidt et al., 2002](#); [Balthasar and Kraft, 2003](#)) and is computationally efficient.

[Balthasar et al. \(2002\)](#) show that the enhancement of the collision frequency due to turbulence ([Saffman and Turner, 1956](#)) is small compared to Brownian coagulation under a wide range of conditions. They neglect the turbulent enhancement and we invoke the same approximation here. They show that the moments of a particle distribution can be included in a consistent PDF formulation. In conjunction with the numerical treatment described in section 5.2, MoMIC can be implemented directly within the PF method without further changes.

MoMIC is described in detail by [Frenklach \(2002\)](#) and is summarised below. The population is described by the number density moments of the size distribution

$$M_r = \sum_{i=1}^{\infty} i^r n_i, \quad r = 0, \dots, U - 1, \quad (5.4)$$

where n_i is the number density of particles of size i and mass $m_i = i m_1$, m_1 is the mass of the smallest unit in the population and U is the number of moments in the truncated set. The low-order moments have simple physical interpretations

$$M_0 = \sum_{i=1}^{\infty} n_i = n, \quad (5.5)$$

$$M_1 = \sum_{i=1}^{\infty} i \cdot n_i = f_v \frac{\rho_s}{m_1}, \quad (5.6)$$

where n is the total number density, f_v is the volume fraction occupied by the population and ρ_s is the particle density.

The population dynamics are governed by a population balance equation describing the effect of collisions between particles of the same type

$$\frac{dn_i}{dt} = \frac{1}{2} \sum_{j=1}^{i-1} \beta_{j,i-j} n_j n_{i-j} - \sum_{j=1}^{\infty} \beta_{i,j} n_i n_j, \quad (5.7)$$

where $\beta_{i,j}$ is a frequency factor describing the rate of successful collisions between particles of size i and j . The first term on the right-hand side describes the creation of particles due to collisions between all combinations of particles with sizes that sum to i . It is multiplied by a factor of 1/2 to avoid double counting. The second term describes the destruction of particles due to collisions between particles of size i and any other size j . Equation (5.7) can be used to write an analogous expression to describe the evolution of the *moments* of the distribution

$$\frac{dM_r}{dt} = \frac{1}{2} \sum_{i=1}^{\infty} \sum_{j=1}^{\infty} (i+j)^r \beta_{i,j} n_i n_j - \sum_{i=1}^{\infty} \sum_{j=1}^{\infty} i^r \beta_{i,j} n_i n_j. \quad (5.8)$$

The form of the frequency factor $\beta_{i,j}$ depends on the Knudsen number, defined in terms of the mean free path of the gas λ and a representative length scale L

$$\text{Kn} = \frac{2\lambda}{L}. \quad (5.9)$$

The *continuum regime* is characterised by $\text{Kn} \ll 1$, where $\beta_{i,j}$ is given

$$\beta_{i,j}^c = K_c \left(\frac{C_i}{r_i} + \frac{C_j}{r_j} \right) (r_i + r_j), \quad (5.10)$$

and C is the Cunningham slip correction factor

$$C = 1 + 1.257 \text{Kn}. \quad (5.11)$$

The *free-molecular regime* is characterised by $\text{Kn} \gg 1$, where $\beta_{i,j}$ is given

$$\beta_{i,j}^f = \varepsilon_{ij} \sqrt{\frac{8\pi k_B T}{\mu_{i,j}}} (r_i + r_j)^2, \quad (5.12)$$

and ε_{ij} is a size-dependent coagulation enhancement factor due to attractive or repulsive inter-particle forces, k_B is the Boltzmann constant, T is the temperature, $\mu_{i,j}$ is the reduced mass and r_i is the radius of particles of size i .

5 APPLICATION TO NANOPARTICLE MODELLING

In the case of *spherical particles*, equations (5.10) and (5.12) can be rewritten

$$\beta_{i,j}^c = K_c \left(\frac{1}{i^{1/3}} + \frac{1}{j^{1/3}} + K_c' \left[\frac{1}{i^{2/3}} + \frac{1}{j^{2/3}} \right] \right) \left(i^{1/3} + j^{1/3} \right), \quad (5.13)$$

$$\beta_{i,j}^f = K_f \left(\frac{1}{i} + \frac{1}{j} \right)^{1/2} \left(i^{1/3} + j^{1/3} \right)^2, \quad (5.14)$$

with

$$K_c = \frac{2k_B T}{3\mu}, \quad K_c' = 2.514\lambda \left(\frac{\pi\rho_s}{6m_1} \right)^{1/3}, \quad K_f = \varepsilon_{ij} \left(\frac{3m_1}{4\pi\rho_s} \right)^{1/6} \left(\frac{6k_B T}{\rho_s} \right)^{1/2}, \quad (5.15)$$

where μ is the absolute viscosity of the gas, and the length scale required by the Knudsen number in equation (5.11) is specified as the particle diameter d_i . We follow Balthasar (2000) and set $\varepsilon_{ij} = 2.2$ for collisions of uncharged particles.

The following sections use the population balance equation (5.8) to derive rate equations for particle inception, surface growth and coagulation. The resulting surface growth (5.22) and coagulation equations (5.26) and (5.27) require unknown fractional-order moments. The equations are closed by estimating the fractional-order moments using logarithmic Lagrange interpolation between known whole-order reduced moments $\mu_r = M_r/M_0$. This is equivalent to assuming a monodisperse distribution in the two-moment case, $r = 0, 1$.³

Inception rate

Inception is assumed to occur in the free molecular regime. Equation (5.8) can be formulated for particle inception by omitting the second term and substituting $\beta_{i,j}^f$ defined in equation (5.12). In terms of the reaction scheme given by equation (5.1)

$$\dot{M}_r^{\text{in}} = \frac{1}{2} \sqrt{8\pi k_B T N_A^2} \sum_{\substack{\text{inception} \\ \text{reactions}}} \frac{\varepsilon_{\alpha\beta}}{\sqrt{\mu_{\alpha,\beta}}} (x_\alpha + x_\beta)^r (r_\alpha + r_\beta)^2 C_\alpha C_\beta, \quad (5.16)$$

³ Robert Patterson.

where each inception reaction uniquely defines

$$C_\alpha = C_{\text{Ti}_{x_\alpha}\text{O}_{y_\alpha}\text{Cl}_{z_\alpha}}, \quad C_\beta = C_{\text{Ti}_{x_\beta}\text{O}_{y_\beta}\text{Cl}_{z_\beta}}, \quad (5.17)$$

$$r_\alpha = r_\beta = 0.65 \times 10^{-9} \text{ m}, \quad (5.18)$$

with

$$\varepsilon_{\alpha\beta} = 2.2, \quad (5.19)$$

$$\frac{1}{\mu_{\alpha,\beta}} = \frac{N_A}{W_{C_{\text{Ti}_{x_\alpha}\text{O}_{y_\alpha}\text{Cl}_{z_\alpha}}}} + \frac{N_A}{W_{C_{\text{Ti}_{x_\beta}\text{O}_{y_\beta}\text{Cl}_{z_\beta}}}}. \quad (5.20)$$

The smallest unit in the population is defined as a single TiO_2 molecule, such that the smallest particle size is $(x_\alpha + x_\beta) = 2$ and M_1/N_A is the number of moles of TiO_2 in the population.

Surface growth rate

The surface growth rate can be written in terms of the mechanism defined by equation (5.3) and the population balance equation (5.8) using

$$\beta_{i,j}^{\text{sg}} = k_s A_i C_{\text{O}_2}. \quad (5.21)$$

Assuming spherical particles

$$\dot{M}_r^{\text{sg}} = \begin{cases} 0, & r = 0 \\ k_s A_1 C_{\text{O}_2} C_{\text{TiCl}_4} N_A \sum_{k=0}^{r-1} \binom{r}{k} v_{\text{TiO}_2}^{r-k} \mu_{k+\frac{2}{3}} M_0, & r \geq 1, \end{cases} \quad (5.22)$$

where

$$A_i = A_1 i^{2/3}, \quad A_1 = 4.787 \times 10^{-19} \text{ m}^2, \quad (5.23)$$

$$v_{\text{TiO}_2} = 1. \quad (5.24)$$

The factor of $v_{\text{TiO}_2}^{r-k}$ arises from the reaction stoichiometry, where each TiCl_4 reacting as per equation (5.2) contributes one TiO_2 unit to the population.

5 APPLICATION TO NANOPARTICLE MODELLING

Coagulation rate

The coagulation rate is calculated as described by [Frenklach \(2002\)](#)

$$\dot{M}_r^{\text{cg}} = \frac{\dot{M}_r^{\text{c}} \dot{M}_r^{\text{f}}}{\dot{M}_r^{\text{c}} + \dot{M}_r^{\text{f}}}, \quad r = 0, 2, 3, \dots \quad (5.25)$$

The *continuum* coagulation rate described by equations (5.8) and (5.13) is given

$$\dot{M}_r^{\text{c}} = \begin{cases} -K_{\text{c}} \left(1 + \mu_{\frac{1}{3}} \mu_{-\frac{1}{3}} + K_{\text{c}}' \left[\mu_{-\frac{1}{3}} + \mu_{\frac{1}{3}} \mu_{-\frac{2}{3}} \right] \right) M_0^2, & r = 0 \\ 0, & r = 1 \\ \frac{K_{\text{c}}}{2} \sum_{k=1}^{r-1} \binom{r}{k} \left(\mu_{k+\frac{1}{3}} \mu_{r-k-\frac{1}{3}} \right. \\ \quad + 2\mu_k \mu_{r-k} + \mu_{k-\frac{1}{3}} \mu_{r-k+\frac{1}{3}} \\ \quad + K_{\text{c}}' \left[\mu_{k+\frac{1}{3}} \mu_{r-k-\frac{2}{3}} + \mu_k \mu_{r-k-\frac{1}{3}} \right. \\ \quad \left. \left. + \mu_{k-\frac{1}{3}} \mu_{r-k} + \mu_{k-\frac{2}{3}} \mu_{r-k+\frac{1}{3}} \right] \right) M_0^2, & r \geq 2. \end{cases} \quad (5.26)$$

The *free molecular* coagulation rate described by equations (5.8) and (5.14) is

$$\dot{M}_r^{\text{f}} = \begin{cases} -\frac{1}{2} K_{\text{f}} (\frac{1}{2} f_{0,0}) M_0^2, & r = 0 \\ 0, & r = 1 \\ \frac{1}{2} K_{\text{f}} \sum_{k=1}^{r-1} \binom{r}{k} ({}^l f_{k,r-k}) M_0^2, & r \geq 2 \end{cases} \quad (5.27)$$

where

$${}^l f_{x,y} = \sum_{i=1}^{\infty} \sum_{j=1}^{\infty} \frac{i^x j^y}{\sqrt{ij}} (i+j)^l (i^{1/3} + j^{1/3})^2 \frac{n_i n_j}{M_0^2}, \quad l = \frac{1}{2}. \quad (5.28)$$

Equation (5.28) is only closed for integer values of the parameter l . The function $\frac{1}{2}f_{x,y}$ is estimated by logarithmic Lagrange interpolation between evaluations of a grid function

$${}^m f_{x,y} = \sum_{k=0}^m \binom{m}{k} \left(\mu_{k+x+\frac{1}{6}} \mu_{m+y-k-\frac{1}{2}} + 2\mu_{k+x-\frac{1}{6}} \mu_{m+y-k-\frac{1}{6}} + \mu_{k+x-\frac{1}{2}} \mu_{m+y-k+\frac{1}{6}} \right), \quad m \in \mathbb{N}_0, \quad (5.29)$$

using the parameterisation

$$\begin{aligned} m &= 0, \dots, n-1, \\ n &= \min(4, U - \max(x, y)), \quad U \in \{3, \dots, 6\}, \end{aligned} \quad (5.30)$$

where U is the number of moments such that $r = 0, \dots, U-1$. This is a generalisation of the method recommended by [Frenklach \(2002\)](#) for the case $r = 0, \dots, 5$.

The following physical properties are assumed

$$m_1 = 1.327 \times 10^{-25} \text{ kg}, \quad \rho_s = 4260 \text{ kg/m}^3, \quad (5.31)$$

and the mean free path and viscosity are approximated as those of air

$$\lambda = 2.370 \times 10^{-5} \frac{T}{p} \text{ m}, \quad (5.32)$$

$$\mu = 1.458 \times 10^{-6} \frac{T\sqrt{T}}{T+100.4} \text{ kg/ms}, \quad (5.33)$$

where the temperature T and pressure p are in K and Pa respectively.

5.1.3 Projected fields equations

The PF method uses a weighted field approximation and projection to derive transport equations that force the statistics of the fields to obey specified moments of a discretised PDF transport equation. The approach was introduced by [Fox \(2003\)](#) under the name DQMoM-IEM. Its implementation and performance as a turbulent reaction model have been investigated in chapters 3 and 4.

5 APPLICATION TO NANOPARTICLE MODELLING

This chapter considers the case when a closed Favre-averaged joint composition PDF transport equation

$$\begin{aligned} \langle \rho \rangle \frac{\partial \tilde{f}_\phi}{\partial t} + \langle \rho \rangle \tilde{U}_i \frac{\partial \tilde{f}_\phi}{\partial x_i} - \frac{\partial}{\partial x_i} \left(\Gamma_T \frac{\partial \tilde{f}_\phi}{\partial x_i} \right) = \\ - \frac{\partial}{\partial \psi_\alpha} \left(\left[\frac{C_\phi}{2\tau_\phi} (\langle \phi_\alpha \rangle - \psi_\alpha) + S_\alpha(\psi) \right] \langle \rho \rangle \tilde{f}_\phi \right), \end{aligned} \quad (5.34)$$

is discretised using a weighted field approximation

$$\begin{aligned} \tilde{f}_\phi(\psi(x,t)) \, d\psi &= \tilde{f}_\phi(\psi_1, \dots, \psi_K(x,t)) \, d\psi_1 \cdots d\psi_K \\ &\approx \sum_{n=1}^N w^{(n)}(x,t) \prod_{\alpha=1}^K \delta_{\psi_\alpha^{(n)}(x,t)}(d\psi_\alpha). \end{aligned} \quad (5.35)$$

The field approximation introduces N weights $w^{(n)}(x,t)$ and NK composition variables $\psi_\alpha^{(n)}(x,t)$, where $\alpha = 1, \dots, K$ scalars. The fields are defined by $\delta_{\psi_\alpha^{(n)}(x,t)}(d\psi_\alpha)$ as per equation (3.3) and the weights constrained to sum to unity as per equation (3.4). The turbulent convective flux in equation (5.34) is closed using a gradient diffusion model. The diffusive flux is closed using the IEM mixing model and implicitly assumes equal molecular diffusivities and unity Lewis numbers for all species. (See section 2.4.2 and section A.1 in appendix A).

Transport equations are derived

$$\frac{\partial w^{(n)}}{\partial t} + \tilde{U}_i \frac{\partial w^{(n)}}{\partial x_i} - \frac{1}{\langle \rho \rangle} \frac{\partial}{\partial x_i} \left(\Gamma_T \frac{\partial w^{(n)}}{\partial x_i} \right) = a^{(n)}, \quad (5.36)$$

$$\frac{\partial s_\alpha^{(n)}}{\partial t} + \tilde{U}_i \frac{\partial s_\alpha^{(n)}}{\partial x_i} - \frac{1}{\langle \rho \rangle} \frac{\partial}{\partial x_i} \left(\Gamma_T \frac{\partial s_\alpha^{(n)}}{\partial x_i} \right) = b_\alpha^{(n)}, \quad (5.37)$$

where

$$s_\alpha^{(n)} \equiv w^{(n)} \psi_\alpha^{(n)}. \quad (5.38)$$

Note that the x - t dependencies of the terms in equations (5.36–5.38) onwards are suppressed for clarity of presentation.

The source terms $a^{(n)}$ are set to zero and a set of $M = NK$ unmixed empirical moments of the form

$$\langle \phi_\alpha^{m_{\lambda\alpha}} \rangle_N = \sum_{n=1}^N w^{(n)} \psi_\alpha^{(n)m_{\lambda\alpha}}, \quad \text{for } \lambda = 1, \dots, M, \quad (5.39)$$

are used to derive a linear system of NK equations for the source terms $b_\alpha^{(n)}$. In the case that the moments in equation (5.39) are specified

$$m_{\lambda\alpha} = \begin{cases} n & \text{where } n = \lambda - (\alpha - 1)N \quad \text{if } n \geq 1 \text{ and } n \leq N \\ 0 & \text{otherwise} \end{cases} \quad (5.40)$$

$$\text{for } \lambda = 1, \dots, M \quad \text{and} \quad \alpha = 1, \dots, K,$$

the linear system can be solved to give a set of N equations for each scalar $\alpha = 1, \dots, K$ (see chapter 3)

$$b_\alpha^{(n)} = b_{\text{rx}_\alpha}^{(n)} + b_{\text{mx}_\alpha}^{(n)} + b_{\text{dx}_\alpha}^{(n)}, \quad (5.41)$$

where

$$b_{\text{rx}_\alpha}^{(n)} = w^{(n)} \mathcal{S}_\alpha(\psi^{(n)}), \quad (5.42)$$

$$b_{\text{mx}_\alpha}^{(n)} = w^{(n)} \frac{C_\phi}{2\tau_\phi} \left(\langle \phi_\alpha \rangle_N - \psi_\alpha^{(n)} \right), \quad (5.43)$$

$$\begin{aligned} b_{\text{dx}_\alpha}^{(n)} = & w^{(n)} c_{\alpha\alpha}^{(n)} \sum_{\substack{i=1 \\ i \neq n}}^N \frac{1}{\psi_\alpha^{(n)} - \psi_\alpha^{(i)}} \\ & + \prod_{\substack{i=1 \\ i \neq n}}^N \frac{1}{\psi_\alpha^{(n)} - \psi_\alpha^{(i)}} \sum_{\substack{j=1 \\ j \neq n}}^N w^{(j)} c_{\alpha\alpha}^{(j)} \prod_{\substack{k=1 \\ k \neq j, n}}^N \left(\psi_\alpha^{(j)} - \psi_\alpha^{(k)} \right), \end{aligned} \quad (5.44)$$

and

$$c_{\alpha\beta}^{(n)} \equiv \frac{\Gamma_T}{\langle \rho \rangle} \frac{\partial \psi_\alpha^{(n)}}{\partial x_i} \frac{\partial \psi_\beta^{(n)}}{\partial x_i}. \quad (5.45)$$

5 APPLICATION TO NANOPARTICLE MODELLING

The projection is imposed by equations (5.36–5.45). It constrains the statistics of the fields to obey the discretised PDF transport equation for each of the empirical moments specified by equations (5.39) and (5.40). The $b_{rx_\alpha}^{(n)}$ and $b_{mx_\alpha}^{(n)}$ terms describe chemical reaction and micromixing, $b_{dx_\alpha}^{(n)}$ describes the effect of turbulent diffusion. Equation (5.44) is poorly conditioned and is singular if $\psi_\alpha^{(n)} = \psi_\alpha^{(i)}$ for $i \neq n$. Its numerical behaviour and treatment has been investigated in chapter 3.

5.2 Numerical details

This section summarises the PF implementation and the coupling to the CFD code.

5.2.1 Projected fields coupling to Star-CD

The Star-CD CFD code (CD-adapco, 2009) is used to solve Favre-averaged conservation equations as a transient problem with a k - ε High Reynolds Number turbulence model and standard wall functions. The default model constants are used with unit Prandtl and Schmidt numbers. The PF model is coupled to Star-CD using an operator splitting technique analogous to that in section 3.2.1. The method is summarised below for the case considered in this chapter.

Equation (5.37) is solved using a Strang (1968) splitting

$$\frac{\partial s_\alpha^{(n)}}{\partial t} = -\tilde{U}_i \frac{\partial s_\alpha^{(n)}}{\partial x_i} + \frac{1}{\langle \rho \rangle} \frac{\partial}{\partial x_i} \left(\Gamma_T \frac{\partial s_\alpha^{(n)}}{\partial x_i} \right), \quad (5.46)$$

$$\frac{\partial s_\alpha^{(n)}}{\partial t} = b_\alpha^{(n)}. \quad (5.47)$$

Equations (5.36) and (5.46) are solved using Star-CD with upwind differencing to transport $w^{(n)}$ and $s_\alpha^{(n)}$ as passive scalars with time step Δt , and equation (5.47) is solved with time step $\frac{1}{2}\Delta t$ before the first and after the last iteration, and time step Δt otherwise. The numerical treatment of equation (5.47) requires special care. It is solved using the *analytic solver* and operator splitting described in section 3.2.4 such that the current study is limited to $N=2$ fields.

5.2.2 Treatment of the scalars

The composition space of the joint composition PDF is defined

$$\phi_\alpha = \begin{cases} Y_\alpha, & \alpha = 1, \dots, s, \\ M_r / \langle \rho \rangle, & \alpha = 1 + s + r, \quad r = 0, \dots, U - 1, \\ h, & \alpha = 1 + s + U = K, \end{cases} \quad (5.48)$$

where Y_α are the species mass fractions, $M_r / \langle \rho \rangle$ are the number moments per unit mass and h is the specific enthalpy. The global bounds required by the method described in section 3.2.4 are specified

$$[Y_{\text{glb}}, Y_{\text{gub}}] = [0, 1], \quad (5.49)$$

$$[M_{\text{glb}}, M_{\text{gub}}] = [0, \infty], \quad (5.50)$$

$$[h_{\text{glb}}, h_{\text{gub}}] = [h(T_{\text{glb}}, Y^{(n)}(x, t)), h(T_{\text{gub}}, Y^{(n)}(x, t))]. \quad (5.51)$$

The enthalpy bounds are calculated at the prevailing composition using global temperature bounds. The temperature bounds are defined using the bounds on the thermodynamic data that accompany the gas-phase mechanism.

The micromixing parameters C_ϕ , τ_ϕ and turbulent diffusivity Γ_T required by the micromixing and diffusion terms in equations (5.43) and (5.44) are calculated

$$C_\phi = 2.0, \quad \tau_\phi = k/\varepsilon, \quad (5.52)$$

$$\Gamma_T = \nu_T/\sigma_T, \quad (5.53)$$

where k , ε and ν_T are the turbulent kinetic energy, turbulent dissipation and turbulent viscosity prescribed by Star-CD and $\sigma_T = 0.7$.

The reaction term in equation (5.42) is integrated numerically using RADAU5 in terms of the molar concentrations $C_\alpha^{(n)}$, the number moments per unit volume $M_r^{(n)}$ and the temperature $T^{(n)}$ of each field. The total moment source terms are given

$$\dot{M}_r^{(n)} = \dot{M}_r^{(n)\text{in}} + \dot{M}_r^{(n)\text{sg}} + \dot{M}_r^{(n)\text{cg}}, \quad (5.54)$$

where the process rates are defined as per equations (5.16), (5.22) and (5.25).

5 APPLICATION TO NANOPARTICLE MODELLING

The concentration source terms due to gas-phase reaction are calculated using the mechanism of [West et al. \(2009\)](#). The additional contributions due to particle processes are calculated

$$\dot{C}_\alpha^{(n)} = \sum_i \frac{\nu_{\alpha i}}{\nu_{\text{TiO}_2 i}} \frac{\dot{M}_{1i}^{(n)}}{N_A}, \quad (5.55)$$

where the sum is over the set of inception and surface reactions, $\nu_{\alpha i}$ is the stoichiometric coefficient of species α in reaction i , and $\dot{M}_{1i}^{(n)}$ is the contribution to $\dot{M}_1^{(n)}$ due to reaction i . Under the assumptions of a constant pressure system at low Mach number and in the absence of radiative heat transfer, the specific enthalpy source term is null (see appendix section [A.1](#)). The gas-phase and particles are assumed to have the same temperature T , and the temperature source term due to all reactions (gas-phase, inception and surface growth) is given

$$\dot{T}^{(n)} = - \frac{\sum_{\alpha=1}^s h_\alpha^{(n)} \dot{C}_\alpha^{(n)} W_\alpha}{\sum_{\alpha=1}^s c_{p\alpha} C_\alpha^{(n)} W_\alpha}. \quad (5.56)$$

The total source terms are adjusted to account for gas-phase expansion

$$\dot{C}_\alpha^{(n)} \leftarrow \dot{C}_\alpha^{(n)} - \gamma^{(n)} C_\alpha^{(n)}, \quad (5.57)$$

$$\dot{M}_r^{(n)} \leftarrow \dot{M}_r^{(n)} - \gamma^{(n)} M_r^{(n)}, \quad (5.58)$$

where the rate of gas-phase expansion $\gamma^{(n)}$ is calculated using the ideal gas law at constant pressure

$$pV(1 - f_v) = nRT, \quad (5.59)$$

$$\gamma = \frac{\dot{V}}{V}, \quad \gamma^{(n)} = \frac{\dot{f}_v^{(n)}}{1 - f_v^{(n)}} + \frac{\dot{T}^{(n)}}{T^{(n)}} + \frac{\sum_{\alpha=1}^s \dot{C}_\alpha^{(n)}}{\sum_{\alpha=1}^s C_\alpha^{(n)}}, \quad (5.60)$$

where $V(1 - f_v)$ is gas-phase volume and $f_v^{(n)}$ is calculated as per equation [\(5.6\)](#)

$$f_v^{(n)} = \frac{m_1 M_1^{(n)}}{\rho_s}, \quad \dot{f}_v^{(n)} = \frac{m_1 \dot{M}_1^{(n)}}{\rho_s}. \quad (5.61)$$

5.2.3 Pressure coupling

Changes in the composition and temperature are coupled to the flow field via the density and viscosity. An updated density and viscosity are passed to Star-CD after the solution of equation (5.47) at each time step

$$\langle \rho \rangle = \langle \rho_g \rangle + \langle \rho_s \rangle, \quad (5.62)$$

where ρ_g is a gas-phase density estimated using the ideal gas law in equation (5.59)

$$\langle \rho_g \rangle = \frac{p(1 - \langle f_v \rangle_N)}{R \langle T \rangle_N \sum_{\alpha=1}^s \frac{\langle Y_{g\alpha} \rangle_N}{W_\alpha}}, \quad (5.63)$$

Y_g are the gas-phase mass fractions and ρ_s is the solid-phase density

$$\langle \rho_s \rangle = m_1 \langle M_1 \rangle_N. \quad (5.64)$$

The viscosity is calculated using equation (5.33)

$$\langle \mu \rangle = 1.458 \times 10^{-6} \frac{\langle T \rangle_N \sqrt{\langle T \rangle_N} \text{ kg}}{\langle T \rangle_N + 100.4 \text{ m s}}. \quad (5.65)$$

A *strong pressure coupling* can be implemented by using the Star-CD pressure field in the calculation of the density in equation (5.63). A *weak pressure coupling* is more robust and can be implemented by using a constant pressure in equation (5.63). This is often acceptable because the density is only a weak function of pressure. The calculations in this chapter use a weak pressure coupling.

An updated density is also calculated after each operator splitting step during the solution of equation (5.47). It is calculated directly from the concentrations $C_\alpha^{(n)}$ after each reaction step. The micromixing and diffusion steps conserve the mean mass fraction and enthalpy, but not necessarily the mean temperature or density. An updated density is estimated using equation (5.62) at the end of each micromixing and diffusion step.

5.3 Titania production in a ‘slot’ reactor

This section investigates the performance of the PF method for a model problem involving full coupling between the flow, chemistry and titania nanoparticles undergoing inception, coagulation and surface growth in a ‘slot’ reactor.

Section 5.3.1 introduces details of the model problem. Section 5.3.2 considers some ideal reactor cases. It checks the MoMIC implementation and compares results to experimental data. Section 5.3.3 validates the PF implementation in a scalar mixing case. Section 5.3.4 demonstrates the application of the method to the full reacting case.

5.3.1 Model problem

This chapter considers the production of titania nanoparticles in a lab scale ‘slot’ reactor. The geometry and input conditions are representative of industrial conditions for the chloride process. The reactor configuration is illustrated in **figure 5.1**.

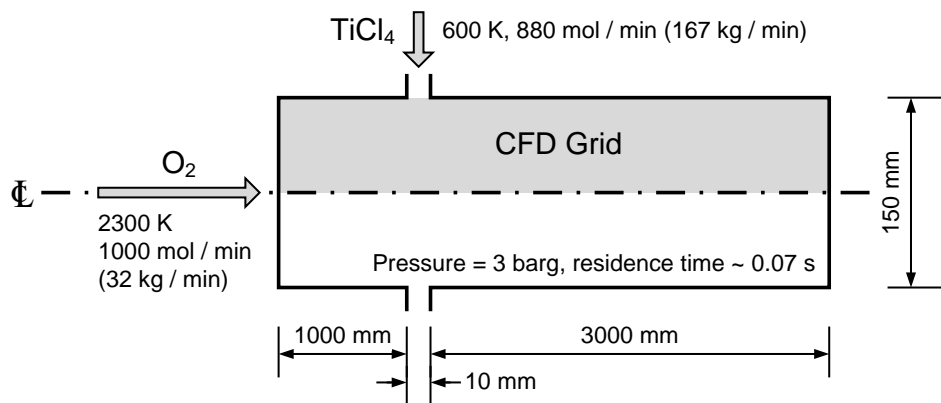


Figure 5.1: Configuration of the axisymmetric titania reactor.

The reactor is modelled using a wedge-shaped domain with boundary conditions to exploit axial symmetry. Two grids were considered. The first is a *base* grid. It uses a 238×15 (axial×radial) domain of fully structured hexahedral cells. The axial spacing is shrunk into and stretched out of the reaction zone by a factor of

5.3 Titania production in a ‘slot’ reactor

1.05 subject to the size bounds [5, 50] mm. The second is a *refined* version of the base grid. It uses a 588×30 (axial \times radial) domain subject to the same axial stretching and size bounds [2.5, 25] mm. All cases were solved with time step 2×10^{-5} s on the base grid and 6×10^{-6} s on the refined grid.

Star-CD (CD-adapco, 2009) was used to solve the flow and PF equations as per section 5.2. The initial and inlet boundary conditions are given in **table 5.1**. The turbulence boundary conditions were estimated using the empirical correlations

$$l = 0.07L, \quad \text{TI} = 0.16\text{Re}_{D_H}^{(-1/8)}, \quad (5.66)$$

where l is the mixing length and TI is the turbulence intensity. L is a length scale and Re_{D_H} a Reynolds number, both based on the relevant hydraulic diameter.

Table 5.1: Titania reactor initial and inlet boundary conditions.

	Initial condition	Inlet boundary		
		Axial inlet	Radial inlet	
$w^{(n)}$	$1/N$	0	1	for $n = 1$
	$1/N$	1	0	for $n = 2$
$Y_{\text{TiCl}_4}^{(n)}$	1	0	1	
$Y_{\text{O}_2}^{(n)}$	0	1	0	
$Y_\alpha^{(n)}$	0	0	0	for $\alpha \neq \text{TiCl}_4, \text{O}_2$
$M_r^{(n)} / \langle \rho \rangle$	0	0	$4^r \times 10^{10}$	for section 5.3.3
	0	0	0	for section 5.3.4
$T^{(n)}$	600	2300	600	
$\langle \rho \rangle$	—	0.669	15.2	kg/m ³
$\langle \mu \rangle$	—	6.7×10^{-5}	3.1×10^{-5}	kg/ms
Volumetric flow	—	0.797	0.183	m ³ /s
Mixing length	—	0.011	0.001	m
Turbulence intensity	—	0.038	0.034	-

Note that the table specifies the scalars in terms of Y_α , M_r and T , but that the PF method transports $w^{(n)}$ and $s_\alpha^{(n)} = w^{(n)} \psi_\alpha^{(n)}$, where the composition space is defined by equation (5.48) and $h^{(n)}$ is calculated $h^{(n)} = h(T^{(n)}, Y^{(n)})$.

5.3.2 Ideal reactor studies

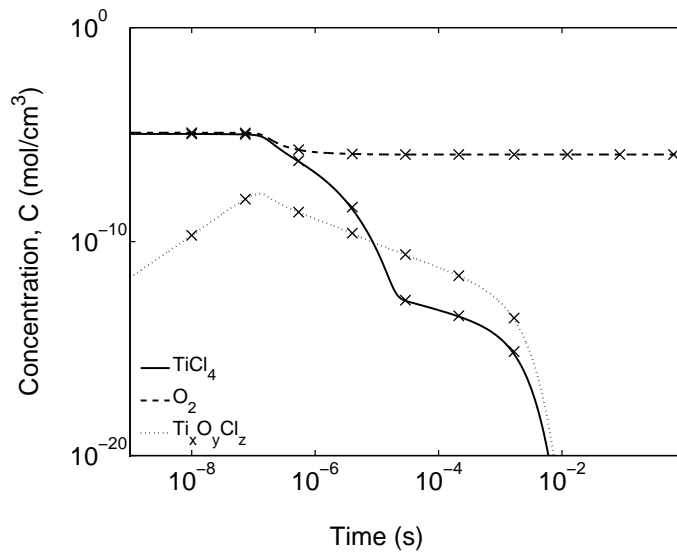
This section considers some ideal reactor cases. It checks that MoMIC has been correctly implemented and reproduces experimental data. The simulations are performed by solving equation (5.47) for the $N = 1$ case. This is equivalent to assuming perfect mixing. It gives insight into the behaviour of the reaction without spatial transport and in isolation from the micromixing and diffusion terms described in section 5.1.3.

Figure 5.2 validates the MoMIC implementation against test data from an established stochastic population balance model (Goodson and Kraft, 2002; Wells and Kraft, 2005; Patterson et al., 2006a,b). The initial conditions were defined as a binary mixture of 1000:880 (mol/mol) $O_2 : TiCl_4$ at 3 barg based on figure 5.3.1. Both methods were solved under isothermal conditions at 2100 K and 1500 K (not shown) using the chemical mechanism described in section 5.1.1 and a spherical particle model. The test data were generated using both a predictor-corrector coupling to the gas-phase chemistry (Celnik et al., 2009) and by post processing the gas-phase data from the MoMIC simulations.

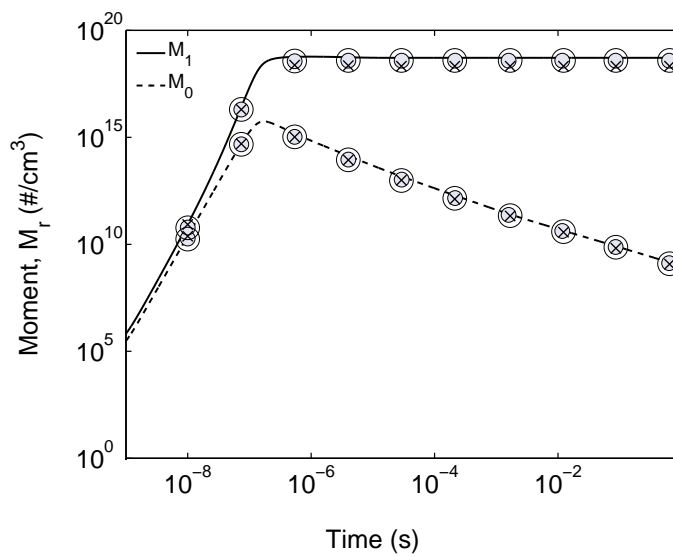
MoMIC shows excellent agreement with the test data for the concentrations of key gas-phase species and the zeroth and first moments of the particle number distribution. The oxygen is in slight excess and is not completely consumed. The rapid consumption of the titanium species is dominated by surface reaction. This is consistent with industrial experience of the chloride process. The test data show that the particle number moments can be accurately reproduced by post processing the gas-phase composition with as few as 256 stochastic particles. The MoMIC data show little sensitivity to an increase from $U = 3$ to $U = 6$ moments (not shown). All remaining MoMIC simulations in this chapter set $U = 3$.

Figure 5.3 shows particle number distributions calculated using the stochastic population balance model to post process the gas-phase data in figure 5.2(a). The data show the emergence of a bimodal distribution due to coagulation, with mean particle size approximately 200 μm after 0.01 s. There is reasonable agreement between the 256 and 4096 stochastic particle cases, but with more pronounced differences than are apparent in figure 5.2(b).

5.3 Titania production in a 'slot' reactor



(a) Gas-phase concentrations.



(b) Particle number moments.

Figure 5.2: Titania batch reactor concentration and particle number moments at $T = 2100$ K. Lines: MoMIC, $U = 3$; Crosses: test data, predictor-corrector splitting with 256 (\times) stochastic particles; Circles: test data, gas-phase data post processed with 256 (\circ) and 4096 (\odot) stochastic particles.

5 APPLICATION TO NANOPARTICLE MODELLING

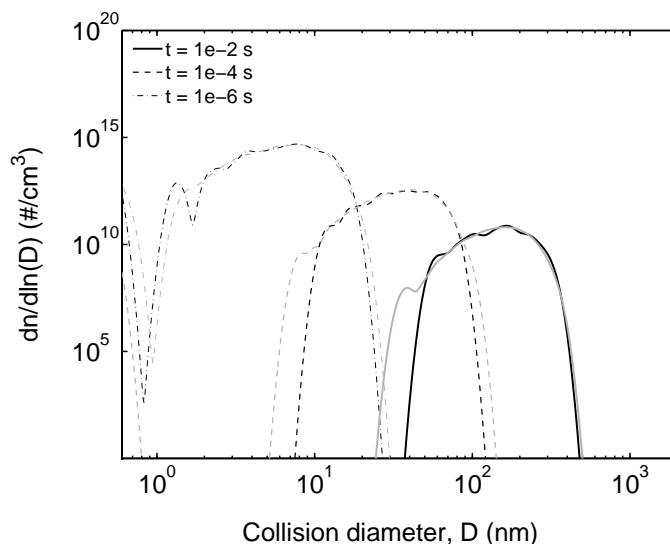
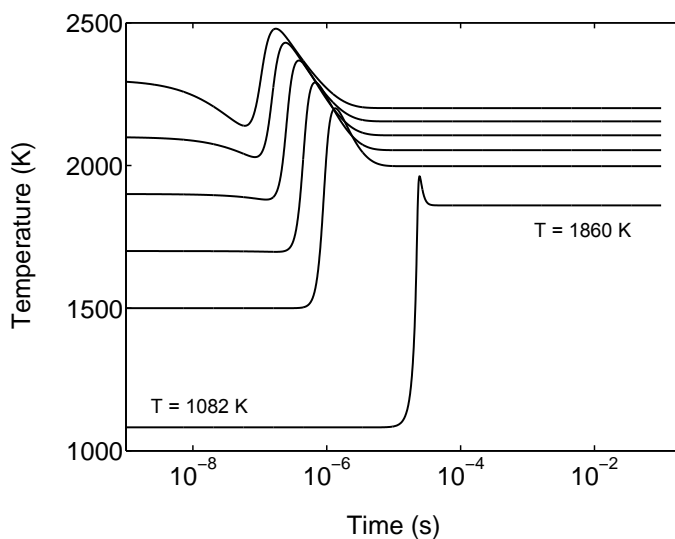


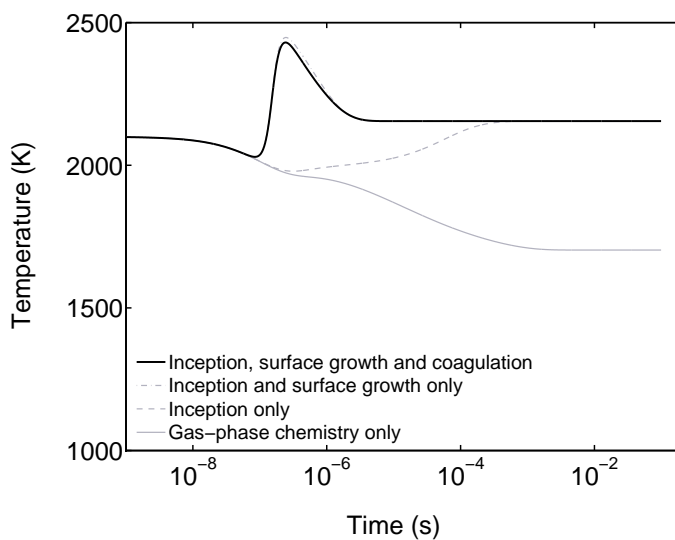
Figure 5.3: *Titania batch reactor particle number distributions calculated from figure 5.2(b) at three different times. Black lines: 256 stochastic particles; Gray lines: 4096 stochastic particles.*

Figure 5.4 shows non-isothermal MoMIC simulations with different initial temperatures. Figure 5.4(a) shows an initial endothermic induction period due to decomposition of TiCl_4 , followed by a rapid exotherm as the reaction ‘takes off’. Higher initial temperatures give shorter induction times. The final temperatures are in the range 1850–2200 K and are determined by the initial temperature and gas-phase equilibria. The initial temperature of 1082 K is that given by the inlet streams in figure 5.1 if they are allowed to mix without reacting and corresponds to a final temperature of 1860 K. Figure 5.4(b) shows temperature profiles in the absence of the MoMIC inception, surface growth and coagulation processes for an initial temperature of 2100 K. The exotherm is mainly caused by surface growth and is slightly moderated by the reduction in surface area due to coagulation.

5.3 Titania production in a 'slot' reactor



(a) Effect of initial temperature.



(b) Effect of the particle processes.

Figure 5.4: Titania batch reactor non-isothermal temperature profiles.

5 APPLICATION TO NANOPARTICLE MODELLING

Figure 5.5 shows good agreement between MoMIC and experimental data from [Pratsinis et al. \(1990\)](#) compared with the mechanism presented by [West et al. \(2009\)](#), which showed up to eight orders of magnitude disagreement in k_{eff} (see [Shirley et al., 2011](#), figure 9). The experimental investigation measured the reaction of 5:1 (mol/mol) O_2 : TiCl_4 in argon (99% by volume) in a 1/8-in-I.D. tube heated to 973–1273 K. [Pratsinis et al. \(1990\)](#) estimate an effective rate constant by assuming that the reaction is first-order in TiCl_4 vapour with Arrhenius kinetics

$$k_{\text{eff}} = -\frac{\ln(C_o/C_i)}{t}, \quad (5.67)$$

where C_i and C_o are the measured inlet and outlet TiCl_4 concentrations and t is residence time in the isothermal zone of the reactor held at temperature T . The experiment was modelled using an imposed temperature profile taken from [Pratsinis et al. \(1990, fig. 3\)](#). The data are presented in the form used by [Pratsinis et al. \(1990, fig. 4\)](#) for easy comparison.

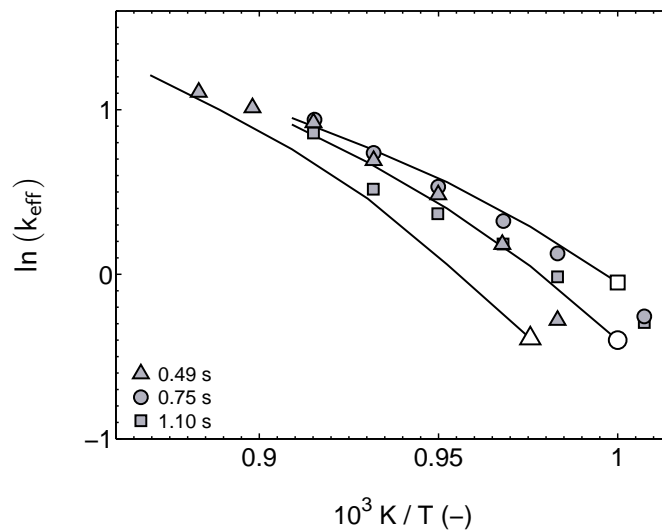


Figure 5.5: Arrhenius plot of the oxidation rate of TiCl_4 at three different residence times. Black lines with open symbols: MoMIC; Closed symbols: experimental data [Pratsinis et al. \(1990, fig. 4\)](#).

5.3.3 Scalar mixing simulations

This section checks the PF implementation in a (non-reacting) scalar mixing case. The boundary conditions in table 5.1 are used to introduce a monodisperse particle distribution at the TiCl_4 inlet to ensure non-zero valued moments. The PF model is assessed against a reference solution provided using the method of moments (MoM). This approach has previously been used in chapter 3 to validate the numerical treatment of the mass fractions.

The flow field was solved using the method of moments. We describe it as a ‘cold’ flow field because it pertains to the non-reacting case. **Figure 5.6** shows the major features of the velocity field near the TiCl_4 inlet. There is a recirculation zone near the wall immediately downstream of the inlet and a large increase in the centreline velocity due to the change in density as cold material from the TiCl_4 inlet mixes with hot material in the reactor.

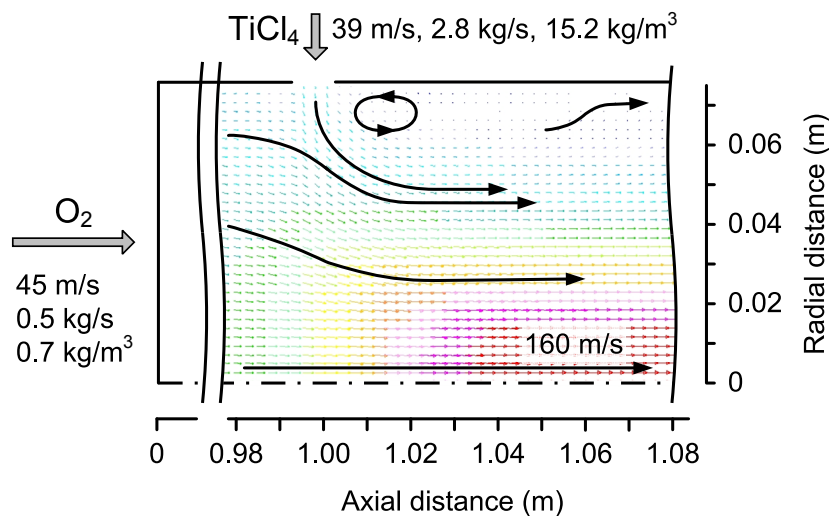


Figure 5.6: *Titania reactor ‘cold’ velocity field.*

The remaining simulations in this section (5.3.3) are performed without re-solving the flow field. This ensures that any differences between the method of moments and the PF method are due to the numerical implementation of the micromixing and diffusion terms described in section 5.1.3, as opposed to the subsequent coupling of such differences to the flow field.

5 APPLICATION TO NANOPARTICLE MODELLING

Table 5.2 shows convergence data to validate the PF implementation against the method of moments reference solution. The convergence was assessed for the mean and standard deviation of the composition using the metrics

$$\varepsilon_{\text{mean}} = \varepsilon \left(\langle \phi_\alpha \rangle_N, \langle \phi_\alpha \rangle_{\text{MoM}} \right), \quad (5.68)$$

$$\varepsilon_{\text{sd}} = \varepsilon \left(\sqrt{\langle \phi_\alpha'^2 \rangle_N}, \sqrt{\langle \phi_\alpha'^2 \rangle_{\text{MoM}}} \right), \quad (5.69)$$

where

$$\varepsilon(x, y) = \frac{\|x - y\|}{\|x + y\|}, \quad (5.70)$$

and $\|\cdot\|$ denotes an L^2 -norm over space. The variances are defined

$$\langle \phi_\alpha'^2 \rangle_N = \langle \phi_\alpha^2 \rangle_N - \langle \phi_\alpha \rangle_N^2, \quad (5.71)$$

and likewise for the method of moments

$$\langle \phi_\alpha'^2 \rangle_{\text{MoM}} = \langle \phi_\alpha^2 \rangle_{\text{MoM}} - \langle \phi_\alpha \rangle_{\text{MoM}}^2. \quad (5.72)$$

The means are in excellent agreement. The standard deviations are in good agreement and show the same value of ε_{sd} for all scalars on a given grid. The data show some minor grid dependence, but are sufficient to demonstrate equivalent numerical treatment of the enthalpy and number moments per unit mass versus that validated for the mass fractions in chapter 3. Note that the magnitude of ε_{sd} differs from previously (*cf.* table 3.2) because the metric in equation (5.70) is normalised to allow direct comparison between all scalars.

5.3 Titania production in a ‘slot’ reactor

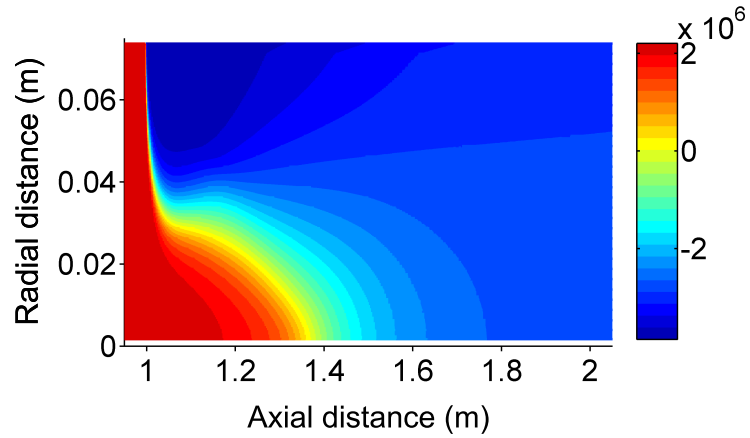
Table 5.2: Convergence of the PF empirical mean and standard deviation versus the method of moments for the inert titania reactor case.

Grid	$\mathcal{E}_{\text{mean}}$	\mathcal{E}_{sd}
	$\phi_{\alpha}^{\top} = \left[Y_1 \cdots Y_s \frac{M_0}{\langle \rho \rangle} \cdots \frac{M_2}{\langle \rho \rangle} h \right]$	$\phi_{\alpha}^{\top} = \left[Y_1 \cdots Y_s \frac{M_0}{\langle \rho \rangle} \cdots \frac{M_2}{\langle \rho \rangle} h \right]$
Base	$< 10^{-8}$	1.2×10^{-2}
Refined	$< 10^{-8}$	7.8×10^{-3}

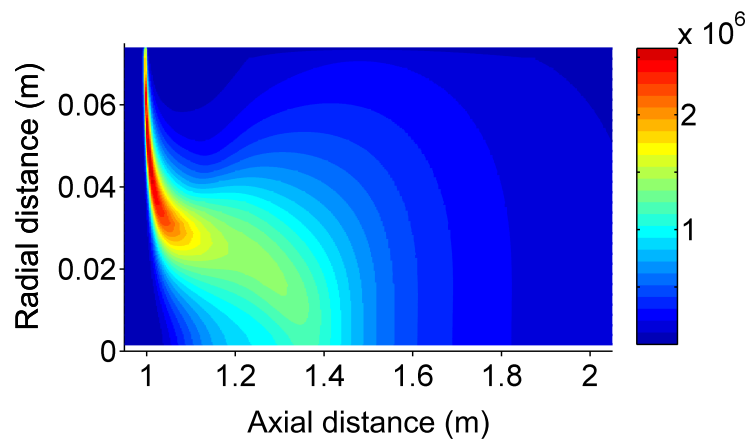
Figure 5.7 presents empirical moments of the enthalpy fields from the PF model on the refined grid for 1 m of reactor downstream of the TiCl_4 inlet. **Figure 5.7(a)** shows the mean enthalpy. The mean mass fraction and number moment per unit mass fields share the same topology, with values scaled by the corresponding inlet boundary conditions. **Figure 5.7(b)** shows the standard deviation of the enthalpy. Again, the standard deviation of the mass fractions and number moments per unit mass share the same topology, but scaled by the difference between the corresponding inlet boundary values. The ‘plume’ from the TiCl_4 inlet marks the mixing zone in the reactor.

Figure 5.8 presents temperature data corresponding to figure 5.7. **Figure 5.8(a)** shows the mean temperature field and an outlet temperature of 1082 K consistent with figure 5.4(a). The temperature is a non-linear function of the mass fractions and enthalpy, so looks slightly different from figure 5.7(a). The calculation of the mean temperature is closed by the PF method, but unclosed in the method of moments. The method of moments case estimates an approximate temperature from the *mean* mass fractions and enthalpy. The effect of this approximation is shown in figure 5.8(b) and correlates with the location of the standard deviation in figure 5.7(b). The method of moments case overestimates the temperature in the mixing zone by up to 200 K.

5 APPLICATION TO NANOPARTICLE MODELLING



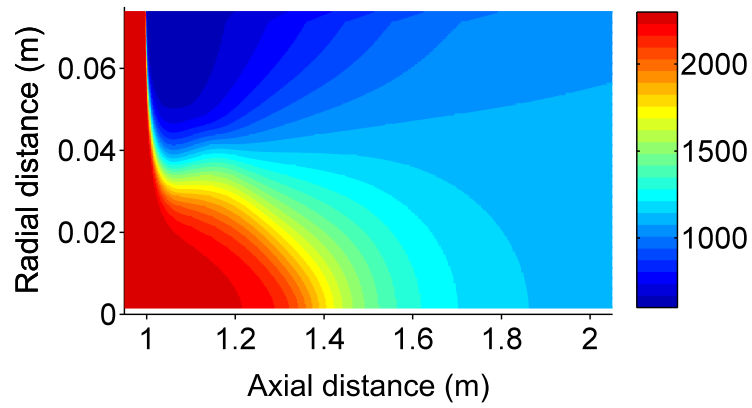
(a) Mean enthalpy $\langle h \rangle_{N=2}$ (J/kg).



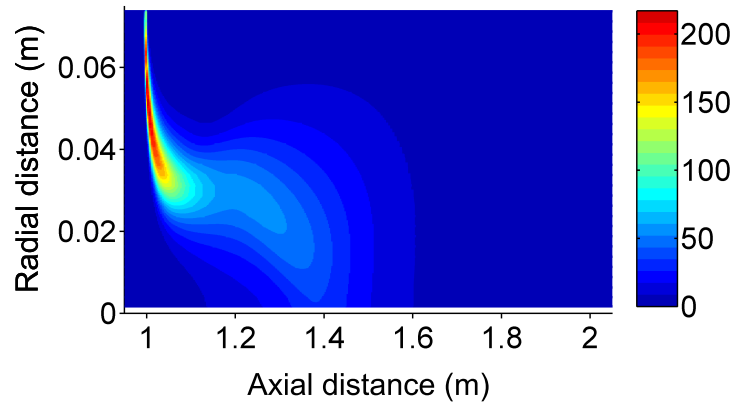
(b) Enthalpy standard deviation $\sqrt{\langle h^2 \rangle}_{N=2}$ (J/kg).

Figure 5.7: Titania reactor empirical moments of enthalpy for the inert case.

5.3 Titania production in a 'slot' reactor



(a) Mean temperature $\langle T \rangle_{N=2}$ (K).



(b) Temperature difference $\langle T \rangle_{MoM} - \langle T \rangle_{N=2}$ (K).

Figure 5.8: Titania reactor empirical moments of temperature for the inert case.

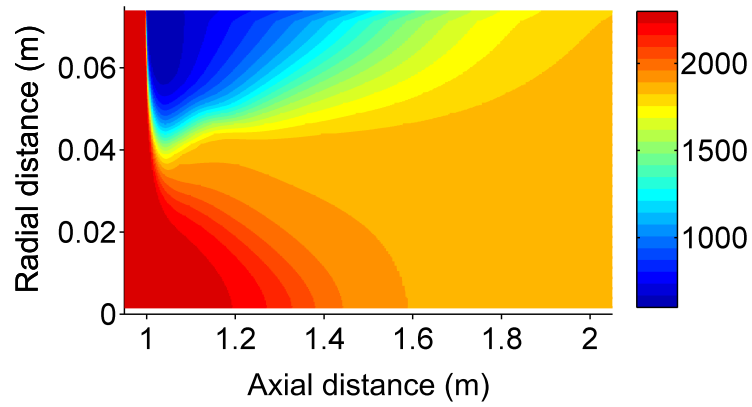
5.3.4 Titania reactor simulations

This section describes the application of the PF method to simulations of the titania reactor discussed in section 5.3.1. All simulations were performed on both grids with $U = 3$ moments and include fully coupled solution of the flow, detailed gas-phase chemistry and titania nanoparticles undergoing simultaneous inception, coagulation and surface growth. The figures present data for the refined grid.

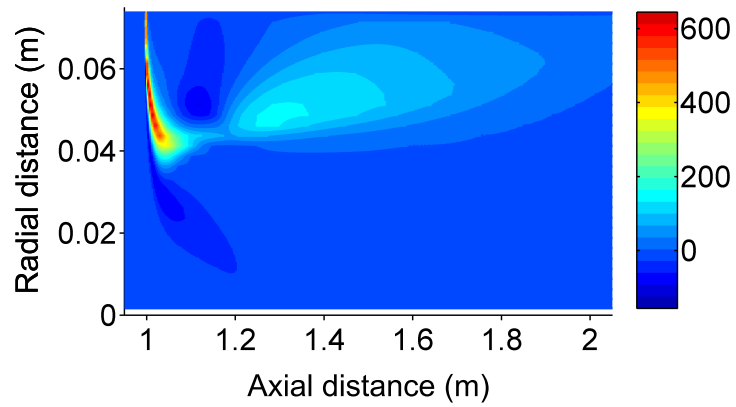
Figure 5.9 shows the mean temperature in the reactor. Comparison of figures 5.8(a) and 5.9(a) shows a significant exotherm due to the reaction. The temperature rise starts in the mixing zone between the inlet streams and extends the length of the reactor downstream, with radial gradients broadening due to mixing. The outlet temperature is 1860 K and is consistent with figure 5.4(a). Figure 5.9(b) shows the difference in mean temperature from a perfect mixing case that solves the PF equations for the $N = 1$ case. This is equivalent to assuming infinitely fast mixing and is a common engineering approximation. The perfect mixing case overestimates the temperature in the mixing zone by up to 600 K.

Figure 5.10 shows the zeroth and first moments of the particle number density. The zeroth moment corresponds to the total number of particles per unit volume, the first moment is proportional to the total mass of particles per unit volume. Figure 5.10(a) shows an area of high number density caused by inception at the leading edge of the mixing zone. The inception zone persists downstream in the area corresponding to a mean temperature $1450 \leq \langle T \rangle_{N=2} \leq 1850$ K. Elsewhere the number density decreases due to coagulation and mixing. Figure 5.10(c) shows that most mass is added to the population due to surface growth starting just downstream of the inception zone. The region of largest mass is concentrated in the area of higher number density downstream of the TiCl_4 inlet. Figures 5.10(b) and (d) compare the results to the perfect mixing case. The differences are most pronounced in the mixing zone near the TiCl_4 inlet and are of the same order of magnitude as the data in figures 5.10(a) and (c). The differences decrease downstream due to mixing. All the moments ($M_r^{(n)}$, $r = 0, 1, 2$) were assessed against the criteria specified by Wright Jr (2006) and correspond to valid moment sets. This is attributed to the use of upwind differencing.

5.3 Titania production in a 'slot' reactor



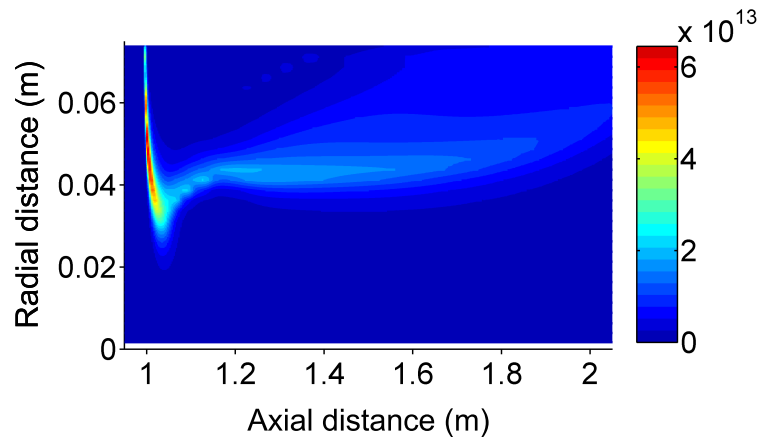
(a) Mean temperature $\langle T \rangle_{N=2}$ (K).



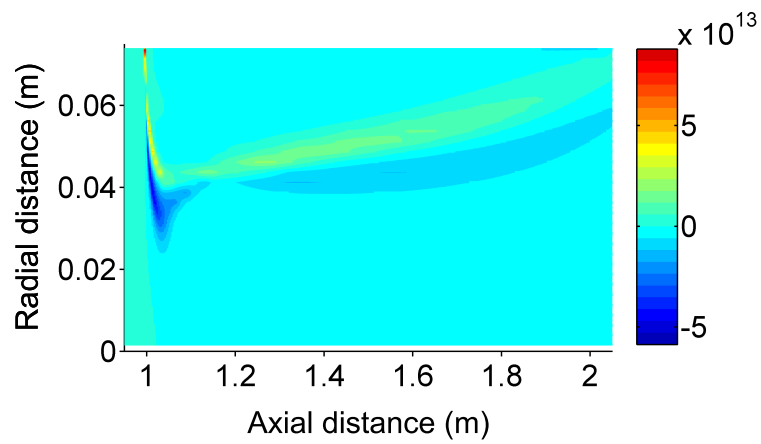
(b) Difference $\langle T \rangle_{perfect\ mixing} - \langle T \rangle_{N=2}$ (K).

Figure 5.9: Titania reactor empirical mean temperature for the reacting case.

5 APPLICATION TO NANOPARTICLE MODELLING



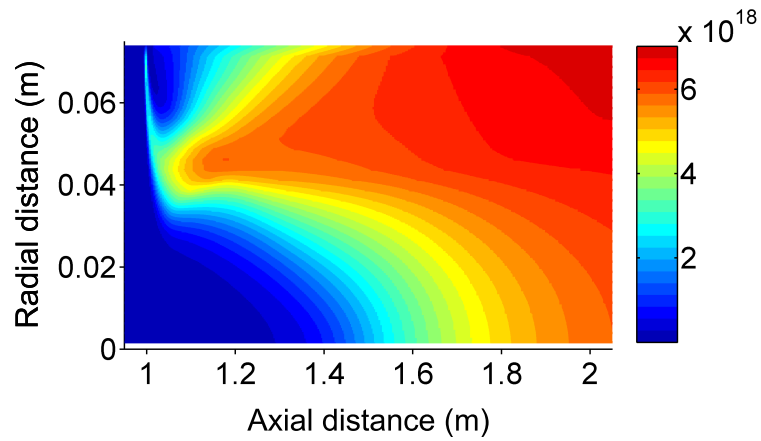
(a) Mean zero moment $\langle M_0 \rangle_{N=2}$ (#/cm³).



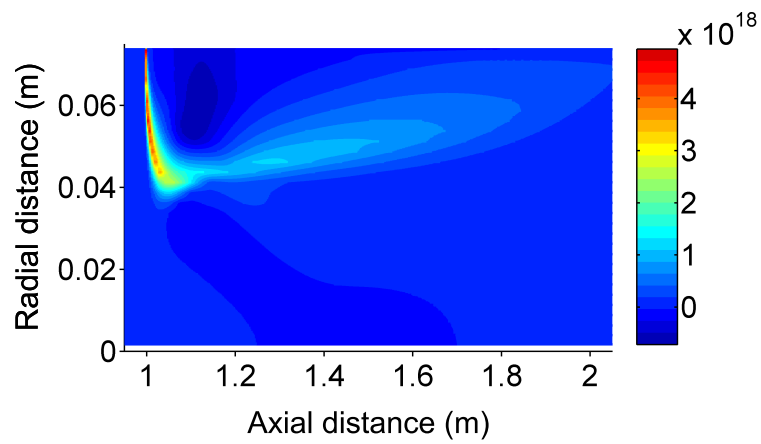
(b) Difference $\langle M_0 \rangle_{perfect\ mixing} - \langle M_0 \rangle_{N=2}$ (#/cm³).

Figure 5.10: Titania reactor empirical mean particle number moments for the reacting case (part 1).

5.3 Titania production in a 'slot' reactor



(c) Mean first moment $\langle M_1 \rangle_{N=2}$ ($\#/cm^3$).



(d) Difference $\langle M_1 \rangle_{perfect\ mixing} - \langle M_1 \rangle_{N=2}$ ($\#/cm^3$).

Figure 5.10: Titania reactor empirical mean particle number moments for the reacting case (part 2).

5 APPLICATION TO NANOPARTICLE MODELLING

Figure 5.11 shows the mean molar concentrations of TiCl_4 and $\text{Ti}_x\text{O}_y\text{Cl}_z$. **Figure 5.11(a)** shows that TiCl_4 exists in the low-temperature region downstream of the inlet. It decomposes via TiCl_z , $z < 4$ and oxidises to form $\text{Ti}_x\text{O}_y\text{Cl}_z$ species as the temperature increases due to mixing with material from the O_2 inlet. **Figure 5.11(b)** shows the total concentration of all $\text{Ti}_x\text{O}_y\text{Cl}_z$ species. The inception model in equation (5.1) specifies $\text{Ti}_x\text{O}_y\text{Cl}_z$ as the incepting species and strong correlation is observed between the concentration in **figure 5.11(b)** and the particle number density in **figure 5.10(a)**.

Figure 5.12 presents the number moments in terms of the particle diameter

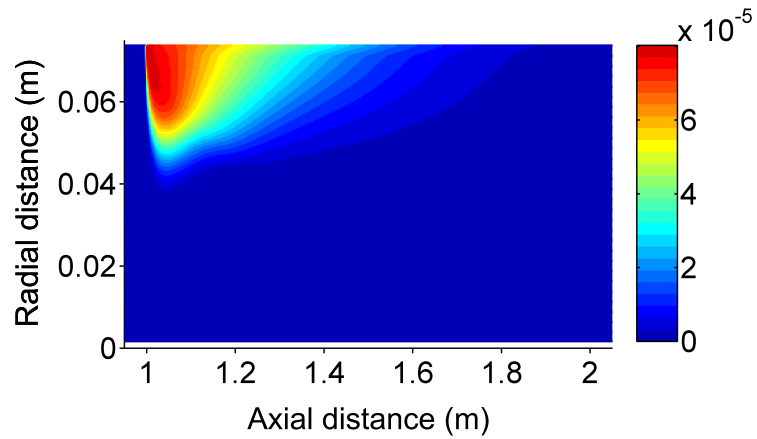
$$d = d_1 \mu_{\frac{1}{3}}, \quad (5.73)$$

$$\sigma = d_1 \sqrt{\mu_{\frac{2}{3}} - \mu_{\frac{1}{3}}^2}. \quad (5.74)$$

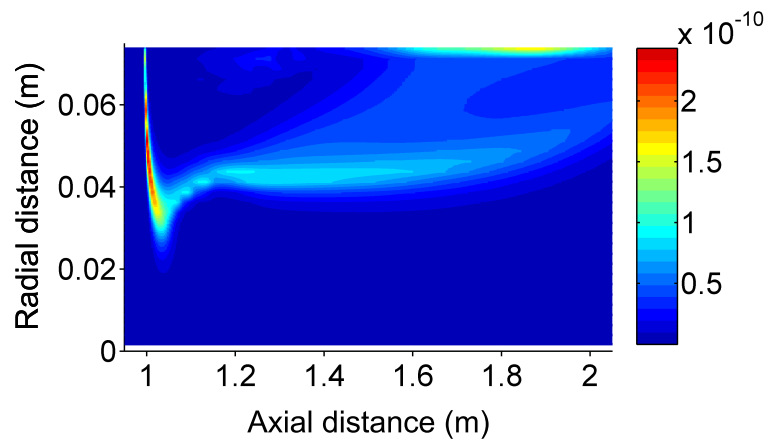
where d is the mean and σ is the standard deviation of the diameter. Note that these plots show the *full length of the reactor* downstream of the TiCl_4 inlet. The data show lower diameter and standard deviation corresponding to the inception zone in **figure 5.10(a)**. Elsewhere the diameter increases due to surface growth and coagulation. The standard deviation shows a narrower distribution in the region where **figure 5.10(c)** shows most surface growth. This is consistent with previous studies where surface growth is shown to decrease the width of the distribution ([Pratsinis and Spicer, 1998](#); [Tsantilis and Pratsinis, 2004](#)). These effects diminish downstream due to mixing. In this example, there are effectively no remaining radial gradients at the outlet.

The model estimates a maximum titania volume fraction of approximately 0.02%. This is significantly lower than the 0.1% upper limit placed on the validity of the Smoluchowski equation by [Heine and Pratsinis \(2007b\)](#). Further assessment of the applicability of the Smoluchowski equation requires a more detailed particle model and is not attempted here. The most that we can say for now is that we expect a particle model that describes the aggregate structure of the particles to predict a maximum effective volume fraction greater than 0.02%.

5.3 Titania production in a 'slot' reactor



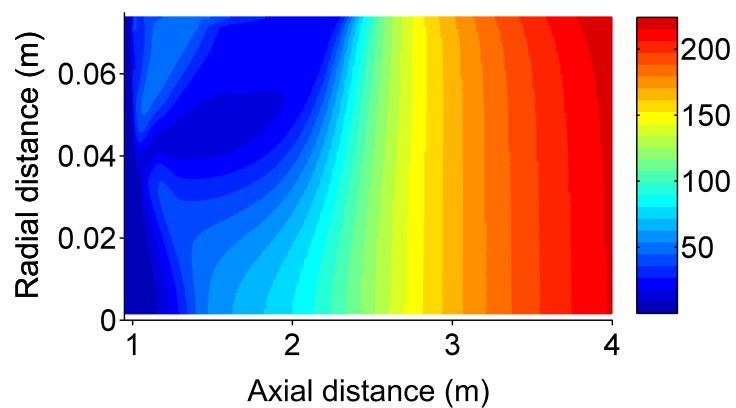
(a) Mean concentration $\langle C_{\text{TiCl}_4} \rangle_{N=2}$ (mol/cm^3).



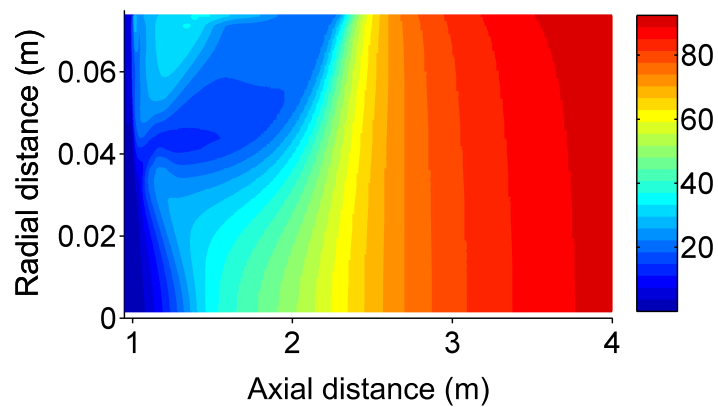
(b) Mean concentration $\langle C_{\text{Ti}_x\text{O}_y\text{Cl}_z} \rangle_{N=2}$ (mol/cm^3).

Figure 5.11: Titania reactor empirical mean concentrations for the reacting case.

5 APPLICATION TO NANOPARTICLE MODELLING



(a) Mean particle diameter $\langle d \rangle_{N=2}$ (nm).



(b) Standard deviation $\langle \sigma \rangle_{N=2}$ (nm).

Figure 5.12: Titania reactor empirical moments of the particle size for the reacting case.

5.4 Chapter summary

This chapter has investigated the first part of a two-stage methodology for the detailed modelling of nanoparticle formation in turbulent reacting flows, including detailed chemistry and full coupling between the flow, material and energy balance equations. The chapter considers the example of the chloride process for the industrial synthesis of titania nanoparticles in a representative ‘slot’ reactor.

The objective of the first stage of the methodology is to achieve a reasonable description of the flow and joint composition PDF for minimum computational effort. The second stage is to apply a detailed population balance model to investigate the evolution of the nanoparticles without the need to re-solve the chemistry or flow. The objective of the second stage is to allow free choice of the population balance so that it can be chosen based on the objectives of the study, rather than considerations of how to couple it to the simulation of the chemistry and flow.

A projected fields (PF) method has been extended to combine the method of moments with interpolative closure (MoMIC) population balance model and detailed titania chemistry. The implementation of MoMIC and the chemistry is validated against ideal reactor simulations using an established population balance model and against experimental data. The numerical treatment of the PF method within the Star-CD CFD code is validated against a reference solution provided using the method of moments for a non-reacting test case. The data show a substantial mixing zone near the reactor inlets, indicated by a region of high standard deviation in mixture enthalpy, particle number moments and mass fractions.

The feasibility of the first stage is demonstrated for fully coupled simulations of titania formation in a ‘slot’ reactor, including particles undergoing simultaneous inception, coagulation and surface growth. The data show radial inhomogeneities near the slot. The inhomogeneities diminish downstream due to mixing. However, designs with multiple inlets would introduce such inhomogeneities throughout the reactor. The temperature and particle properties are compared with a perfect mixing case and show significant differences near the slot. The second stage will need to consider the full composition PDF, not just the mean composition. The details of how to implement the second stage remain an open question.

Chapter 6

Conclusions

6.1 Conclusions of the thesis

This thesis investigated the application of DQMoM-IEM and SF as mean reaction rate closures for simulations of nanoparticle formation in turbulent reacting flow. The literature shows that such simulations entail compromise between the level of detail and accuracy of the simulation, the chemistry for which the model is valid, the computational cost of the calculation and the compatibility of the method with existing software. The thesis focussed on methods that are capable of varying the level of approximation and computational effort, that make no assumptions about the chemistry and that can be implemented in existing CFD software.

The numerical behaviour and implementation of DQMoM-IEM have been investigated in detail. The method uses a *weighted field* approximation to discretise a joint composition PDF transport equation. A projection method is used to derive transport equations that force the statistics of the fields to obey specified moments of the discretised PDF transport equation. We distinguish between the *model* and the *numerical method*. We consider the PDF transport equation to be the model and the weighted field approximation and projection to be the numerical method. We describe DQMoM-IEM as a *projected fields (PF)* method. This highlights the projection that distinguishes it from a wider class of mathematically related field methods and is consistent with existing terminology.

6 CONCLUSIONS

A new analytic expression is introduced for the DQMoM-IEM source terms. It prescribes the choice of the moment set in the derivation of the model equations and is general in the sense that it is valid for any number of fields and scalars. Explicit terms can be identified relating to *reaction*, *micromixing* and turbulent *diffusion* processes. The diffusion term is responsible for a number of numerical difficulties reported in previous studies of DQMoM-IEM. It can cause loss of boundedness and is discontinuous and singular if two or more fields take equal values for a given scalar at any point in physical space.

The analytic form of the diffusion term negates the need to use numerical methods to evaluate the DQMoM-IEM source terms, reducing the numerical complexity of the method. Two new solvers are introduced to take advantage of this development. The first (general) solver can be applied to cases with any number of fields and scalars. The diffusion term is calculated by *functional evaluation* and a filter function is introduced to eliminate discontinuities and enforce boundedness. The source terms are then integrated numerically. The second (analytic) solver is specific to $N=2$ fields. It uses *analytic solutions* for the integrals of the diffusion and micromixing source terms and can be applied to any number of scalars.

The new DQMoM-IEM solvers are coupled to the Star-CD CFD code using an operator splitting technique and validated against the method of moments and a constant density turbulent reaction test problem. The choice of boundary conditions to represent a given physical condition is not arbitrary. The correct scalar mixing was only reproduced when the boundary conditions were specified to be consistent with each field being assigned to a specific inlet.

On paper, DQMoM-IEM offers an attractive method because it is deterministic and the number of fields can be selected based on the level of approximation appropriate to the problem. The weighted fields mean that only a few fields are typically required; $N=2,3$ was shown to be sufficient for the constant density test problem in chapter 3. These features suggest a computationally efficient method. In practice, the key challenge remains the efficient treatment of the diffusion term. The analytic solver provides an elegant approach to the $N=2$ case, but in general, a constraint on the number of fields is likely to be imposed by the difficulty of numerically integrating the diffusion term.

The performance of DQMoM-IEM is compared to the SF method. The methods share many similarities. The SF method uses an *equi-weighted field* approximation to discretise a joint composition PDF transport equation. Explicit terms relating to *reaction*, *micromixing* and turbulent *diffusion* processes can again be identified. The diffusion term is modelled as a stochastic process and the numerical implementation is simpler than DQMoM-IEM. The fields evolve such that they remain statistically equivalent to the joint composition PDF. A greater number of fields can be used than for DQMoM-IEM, but are also required to overcome the restriction to equi-weighted fields and to control statistical error. The use of antithetic sampling is introduced as a variance reduction technique to improve the statistical efficiency of the method.

The SF method was applied to the same test problems as DQMoM-IEM. The expected convergence was demonstrated, however the data retained significant variance and a minor grid-dependence not seen with DQMoM-IEM. Antithetic sampling was shown to enable better convergence to be achieved with fewer fields in axisymmetric cases, although achieving this benefit required careful consideration of the symmetry in the test case. Overall, DQMoM-IEM was more easily able to achieve a grid-independent solution and gave deterministic and accurate results more quickly for the test case considered.

A PF method based on the analytic DQMoM-IEM solver is introduced to combine detailed chemistry and the MoMIC population balance model in Star-CD. The PF method includes full coupling between the flow, chemistry and particles undergoing simultaneous inception, coagulation and surface growth, and is applied to the example of the chloride process for the industrial synthesis of titania nanoparticles in a ‘slot’ reactor. The implementation is systematically validated against ideal reactor simulations using an established population balance model, against experimental data and against the method of moments. The data show substantial radial inhomogeneities in a mixing zone near the slot. The temperature and particle properties are compared with a perfect mixing case and show significant differences in the mixing zone. In the example considered, the inhomogeneities diminish downstream due to mixing. However, reactor designs with multiple slots would introduce inhomogeneities at each inlet down the length of the reactor.

6.2 Suggestions for future work

Suggestions for future work fall into three broad categories: further development of the method, optimisation of the code and application of the new model.

6.2.1 Further development of the method

The PF-MoMIC method is the first part of a proposed two-stage methodology. The objective of the first stage is to achieve a reasonable description of the flow and composition for minimum computational effort. The second stage is to apply a more detailed population balance model to investigate the evolution of the nanoparticles without the need to re-solve the chemistry or flow. The objective is to allow free choice of the population balance method so that it can be chosen to suit the study, rather than based on considerations of how to couple it to the chemistry and flow. The final part of this thesis shows that the second stage will need to consider the full composition PDF, not just the mean composition. How to implement the second stage remains an open question and is work in progress.

The investigations in this thesis represent a first look at methods for the detailed modelling of nanoparticle formation in turbulent reacting flows. The methods have been developed systematically, with features added as required. However, they are by no means feature-complete. Many gaps need to be addressed in future work. For example, a heat transfer model to describe cooling at the walls and radiative heat transfer within the reactor could be included in the titania simulations. Likewise, the spherical particle assumption could be relaxed. One approach may be to consider non-spherical particles of fixed shape.

The numerical methods developed in this thesis present several opportunities for further improvement. The diffusion term in the general DQMoM-IEM solver remains problematic as the number of fields is increased, both in terms of computational time and numerical difficulty. Future work may wish to revisit this. For example, could an alternative ODE solver improve the performance of the general solver? Other progress may come from sharing ideas between methods. For example, could the SF method benefit from weighted fields?

6.2.2 Optimisation of the code

The code developed for this thesis was not optimised for speed and an obvious task is to improve the efficiency of the code. Aside from the diffusion term in the general DQMoM-IEM solver, most of the computational cost is due to the reaction term. This is common to all methods in this thesis and reducing this cost will be critical to making them more practical for applications involving complex chemistry. Much research has already sought to increase the speed of reaction methods and one option may be to implement a tabulation scheme such as ISAT.

6.2.3 Application of the new model

Many important open questions remain. The wider objective of this thesis was to develop methods that could be applied to a range of industrial processes. The methods were stipulated to require sufficient accuracy for engineering purposes and this is necessarily application specific. For example, to what extent do the advantages demonstrated by DQMoM-IEM over SF for the constant density test case translate to the titania model and what is the optimal number of fields? How are the titania properties affected by the process conditions and reactor?

Answering these questions will need many of the developments considered above. For example, a faster code with a heat transfer model. It will also require more detailed process data. This is awkward for titania, where even sampling the gas-phase along the reactor can be prohibitively difficult. An alternative may be to study related systems. Sooting flames have been widely investigated and could perhaps be used to assess how the model responds to the number of fields.

Appendix A

Derivations

This appendix presents further information on the MoM, DQMoM and SF methods investigated in this thesis. It begins with a brief discussion of the joint composition PDF transport equation, from which it derives the equations given in the main text. The objective is to present the derivations in a consistent notation and to make explicit the assumptions within the governing equations.

A.1 Joint composition PDF transport equation

The material in section A.1.1 borrows from Pope (1985) and Peters (2000). Readers who would like more detail are kindly referred to these texts. Note that the x - t dependencies of terms in this appendix are suppressed for clarity of presentation.

A.1.1 Governing equations

Mass fraction and enthalpy equations

Pope (1985) shows that the mass fraction (A.1) and enthalpy (A.2) equations

$$\rho \frac{\partial Y_\alpha}{\partial t} + \rho U_i \frac{\partial Y_\alpha}{\partial x_i} = - \frac{\partial J_i^\alpha}{\partial x_i} + \rho S_\alpha, \quad (\text{A.1})$$

$$\rho \frac{\partial h}{\partial t} + \rho U_i \frac{\partial h}{\partial x_i} = - \frac{\partial J_i^h}{\partial x_i} + \rho S_h, \quad (\text{A.2})$$

can be written in a common form

$$\rho \frac{\partial \phi_\alpha}{\partial t} + \rho U_i \frac{\partial \phi_\alpha}{\partial x_i} = - \frac{\partial J_i^\alpha}{\partial x_i} + \rho S_\alpha, \quad \alpha = 1, \dots, K, \quad (\text{A.3})$$

where ϕ is a set of $K = s + 1$ scalars $\phi(x, t)$ defined by

$$\phi_\alpha = \begin{cases} Y_\alpha, & \alpha = 1, \dots, s \\ h, & \alpha = K. \end{cases} \quad (\text{A.4})$$

J_i^α is the diffusive mass flux vector of species α , J_i^h is the specific energy flux vector, S_α is the mass rate of addition (per unit mass) of species α , S_h is the source of specific enthalpy due to compressibility, viscous dissipation and radiation.

Equation (A.3) makes no assumptions regarding the source terms S_α or molecular transport terms J_i^α . For a given reference pressure p_0 (assumed constant), the chemical sources and density depend only on the set of scalars ϕ

$$S_\alpha = S_\alpha(\phi), \quad \rho = \rho(\phi). \quad (\text{A.5})$$

A.1 Joint composition PDF transport equation

Diffusive fluxes

The molecular processes that cause the diffusive fluxes are quite complicated. In turbulent reaction, molecular diffusion is frequently less important than turbulent transport and simplified versions of the molecular fluxes are often considered. The simplest approximation is the binary flux approximation.

Peters (2000) describes the treatment of the diffusive fluxes using the binary flux approximation. The mass flux is written using Fick's law

$$J_i^\alpha = -\rho\Gamma_\alpha \frac{\partial Y_\alpha}{\partial x_i}, \quad \alpha = 1, \dots, s, \quad (\text{A.6})$$

where Γ_α is a binary diffusion coefficient with respect to an abundant species. Note that the sum of all fluxes must vanish and equation (A.6) may violate mass balance in multicomponent systems unless equal diffusivities $\Gamma_\alpha = \Gamma$ are assumed.

The specific energy flux includes the effect of the thermal conductivity of the mixture λ and enthalpy transport by the mass fluxes J_i^α

$$J_i^h = -\lambda \frac{\partial T}{\partial x_i} + \sum_{\alpha=1}^s h_\alpha J_i^\alpha. \quad (\text{A.7})$$

where T is the temperature and h_α is the specific enthalpy of species α . Equation (A.7) can be rewritten in terms of the mixture enthalpy h and species mass fractions Y_α . The mixture heat capacity c_p and enthalpy h are defined

$$c_p = \sum_{\alpha=1}^s c_{p\alpha} Y_\alpha, \quad (\text{A.8})$$

$$h = \sum_{\alpha=1}^s h_\alpha Y_\alpha, \quad (\text{A.9})$$

and for an ideal gas, h_α is a function of temperature only

$$h_\alpha = h_{\alpha,\text{ref}} + \int_{T_{\text{ref}}}^T c_{p\alpha}(T) dT, \quad \alpha = 1, \dots, s, \quad (\text{A.10})$$

A DERIVATIONS

where $c_{p\alpha}$ is the specific heat capacity of species α . Equation (A.9) can be written in differential form, using equation (A.10) to substitute $dh_\alpha = c_{p\alpha} dT$

$$\begin{aligned}
 dh &= \sum_{\alpha=1}^s dh_\alpha Y_\alpha + \sum_{\alpha=1}^s h_\alpha dY_\alpha \\
 &= \sum_{\alpha=1}^s c_{p\alpha} Y_\alpha dT + \sum_{\alpha=1}^s h_\alpha dY_\alpha \\
 &= c_p dT + \sum_{\alpha=1}^s h_\alpha dY_\alpha.
 \end{aligned} \tag{A.11}$$

Equation (A.7) is now rewritten using equations (A.6) and (A.11) to substitute J_i^α and $\partial T / \partial x_i$

$$\begin{aligned}
 J_i^h &= -\frac{\lambda}{c_p} \left(\frac{\partial h}{\partial x_i} - \sum_{\alpha=1}^s h_\alpha \frac{\partial Y_\alpha}{\partial x_i} \right) - \sum_{\alpha=1}^s h_\alpha \rho \Gamma_\alpha \frac{\partial Y_\alpha}{\partial x_i} \\
 &= -\frac{\lambda}{c_p} \frac{\partial h}{\partial x_i} + \sum_{\alpha=1}^s h_\alpha \left(\left[\frac{\lambda}{c_p} - \rho \Gamma_\alpha \right] \frac{\partial Y_\alpha}{\partial x_i} \right).
 \end{aligned} \tag{A.12}$$

The final term in equation (A.12) is null in the event that all Lewis numbers $Le_\alpha = \lambda / \rho c_p \Gamma_\alpha$ are unity

$$J_i^h = -\frac{\lambda}{c_p} \frac{\partial h}{\partial x_i}, \tag{A.13}$$

and assuming equal diffusivities for each species $\Gamma_\alpha = \Gamma$ such that $Le = \lambda / \rho c_p \Gamma$

$$J_i^h = -\rho \Gamma \frac{\partial h}{\partial x_i}. \tag{A.14}$$

A.1 Joint composition PDF transport equation

Species source term

The general species source term is given (Fox, 2003)

$$S_\alpha(C) = \sum_{i=1}^I (v_{\alpha i}^r - v_{\alpha i}^f) R_i(C), \quad (\text{A.15})$$

for a set of I elementary reactions of species A_α

$$\sum_{\alpha=1}^s v_{\alpha i}^f A_\alpha \xrightleftharpoons[k_i^r]{k_i^f} \sum_{\alpha=1}^s v_{\alpha i}^r A_\alpha \quad \text{for } i \in 1, \dots, I, \quad (\text{A.16})$$

with stoichiometric coefficients $v_{\alpha i}^f$, $v_{\alpha i}^r$, rate constants k_i^f , k_i^r , and reaction rate

$$R_i(C) = k_i^f \prod_{\alpha=1}^s C_\alpha^{v_{\alpha i}^f} - k_i^r \prod_{\alpha=1}^s C_\alpha^{v_{\alpha i}^r} \quad \text{for } i \in 1, \dots, I, \quad (\text{A.17})$$

where C is the set of molar concentrations $C_\alpha = \rho Y_\alpha / W_\alpha$, $\alpha = 1, \dots, s$.

Enthalpy source term

The enthalpy source term is given (Pope, 1985)

$$\rho S_h = \tau_{ij} \frac{\partial U_i}{\partial x_j} + \frac{\partial p}{\partial t} + U_i \frac{\partial p}{\partial x_i} + (A - \varepsilon), \quad (\text{A.18})$$

where τ_{ij} is the the sum of the viscous and viscous-diffusive stress tensors, and A and ε are the rates of absorption and emission of radiative energy (per unit mass). The term in τ_{ij} describes frictional heating due to viscous dissipation and is negligible at low Mach numbers. The local and convective change of pressure is important for acoustic interactions and pressure waves. The transient term $\partial p / \partial t$ is important for reciprocating engines, but can be neglected in open flames. The convective term $\partial p / \partial x_i$ may be neglected at low Mach numbers.

A DERIVATIONS

Temperature transport equation

Peters (2000) shows that a temperature transport equation can be derived from the enthalpy equation (A.2)

$$\begin{aligned} \rho c_p \frac{\partial T}{\partial t} + \rho c_p U_i \frac{\partial T}{\partial x_i} = \\ \frac{\partial}{\partial x_i} \left(\lambda \frac{\partial T}{\partial x_i} \right) + \rho \frac{\partial T}{\partial x_i} \sum_{\alpha=1}^s c_{p\alpha} \Gamma_\alpha \frac{\partial Y_\alpha}{\partial x_i} - \rho \sum_{\alpha=1}^s h_\alpha S_\alpha + \rho S_h, \end{aligned} \quad (\text{A.19})$$

using equations for the species transport (A.1), the diffusive fluxes (A.6) and (A.7) and the differential relationship between enthalpy and temperature (A.11).

Equation (A.19) is often less convenient than the enthalpy equation (A.2). The source terms are more complicated, it requires physical properties to be available in order to evaluate $c_{p\alpha}(T)$ and it is not so easily written in a common form with the mass fraction equation (A.1).

A.1.2 Favre-averaged PDF transport equation

Pope (1985) derives a transport equation for the Favre-averaged joint composition PDF \tilde{f}_ϕ , where the composition space ϕ obeys equations (A.3) and (A.4)

$$\begin{aligned} \frac{\partial}{\partial t} \left(\langle \rho \rangle \tilde{f}_\phi \right) + \frac{\partial}{\partial x_i} \left(\tilde{U}_i \langle \rho \rangle \tilde{f}_\phi \right) + \frac{\partial}{\partial \psi_\alpha} \left(S_\alpha(\psi) \langle \rho \rangle \tilde{f}_\phi \right) = \\ \frac{\partial}{\partial \psi_\alpha} \left(\left\langle \frac{1}{\rho} \frac{\partial J_i^\alpha}{\partial x_i} \middle| \psi \right\rangle \langle \rho \rangle \tilde{f}_\phi \right) - \frac{\partial}{\partial x_i} \left(\langle u_i'' | \psi \rangle \langle \rho \rangle \tilde{f}_\phi \right). \end{aligned} \quad (\text{A.20})$$

The terms on the left hand side of equation (A.20) are closed. The terms on the right hand side describe the diffusive and turbulent convective fluxes. They are unclosed and need to be modelled.

The turbulent convective flux is closed by a gradient diffusion model (Pope, 1985)

$$\langle u_i'' | \psi \rangle \langle \rho \rangle \tilde{f}_\phi = -\Gamma_T \frac{\partial \tilde{f}_\phi}{\partial x_i}, \quad (\text{A.21})$$

A.1 Joint composition PDF transport equation

where Γ_T is a turbulent diffusivity

$$\Gamma_T = \nu_T / \sigma_T, \quad (\text{A.22})$$

ν_T is a turbulent viscosity prescribed by the turbulence model and σ_T is a turbulent Schmidt / Prandtl number (depending on context) and is typically close to unity.

The diffusive mass flux is assumed to obey a binary flux approximation with equal molecular diffusivities and unity Lewis numbers for all species. Using equations (A.6) and (A.14) and assuming equal diffusivities for all species, the diffusive fluxes can be written

$$\left\langle \frac{1}{\rho} \frac{\partial J_i^\alpha}{\partial x_i} \middle| \psi \right\rangle = - \langle \Gamma \nabla^2 \phi_\alpha | \psi \rangle, \quad (\text{A.23})$$

and are closed with the IEM micromixing model (Villermaux and Devillon, 1972)

$$\langle \Gamma \nabla^2 \phi_\alpha | \psi \rangle = \frac{C_\phi}{2\tau_\phi} (\langle \phi_\alpha \rangle - \psi_\alpha), \quad (\text{A.24})$$

where C_ϕ is an empirical constant and τ_ϕ is the scalar mixing time.

Under the assumptions of a constant pressure system at low Mach number and in the absence of radiative heat transfer, the source terms can be written

$$S_\alpha(\psi) = \begin{cases} S_\alpha, & \alpha = 1, \dots, s \\ S_h, & \alpha = K, \end{cases} \quad (\text{A.25})$$

$$S_h = 0. \quad (\text{A.26})$$

The unsteady and convective flux terms can be rewritten in unconservative form and the closed form of equation (A.20) is given

$$\begin{aligned} \langle \rho \rangle \frac{\partial \tilde{f}_\phi}{\partial t} + \langle \rho \rangle \tilde{U}_i \frac{\partial \tilde{f}_\phi}{\partial x_i} - \frac{\partial}{\partial x_i} \left(\Gamma_T \frac{\partial \tilde{f}_\phi}{\partial x_i} \right) = \\ - \frac{\partial}{\partial \psi_\alpha} \left(\left[\frac{C_\phi}{2\tau_\phi} (\langle \phi_\alpha \rangle - \psi_\alpha) + S_\alpha(\psi) \right] \langle \rho \rangle \tilde{f}_\phi \right). \end{aligned} \quad (\text{A.27})$$

A DERIVATIONS

A.1.3 Constant density PDF transport equation

Many of the SF and DQMoM references, including Valiño (1998) and Fox (2003), consider a constant density transport equation for the joint composition PDF f_ϕ . The equation is written in closed form

$$\begin{aligned} \frac{\partial f_\phi}{\partial t} + \langle U_i \rangle \frac{\partial f_\phi}{\partial x_i} - \frac{\partial}{\partial x_i} \left(\Gamma_T \frac{\partial f_\phi}{\partial x_i} \right) = \\ - \frac{\partial}{\partial \psi_\alpha} \left(\left[\frac{C_\phi}{2\tau_\phi} (\langle \phi_\alpha \rangle - \psi_\alpha) + S_\alpha(\psi) \right] f_\phi \right), \end{aligned} \quad (\text{A.28})$$

using the IEM micromixing model to close the diffusive flux and a gradient diffusion model to close the turbulent convective flux

$$\langle u'_i | \psi \rangle f_\phi = -\Gamma_T \frac{\partial f_\phi}{\partial x_i}, \quad \Gamma_T = \nu_T / \rho \sigma_T. \quad (\text{A.29})$$

A.1.4 Dimensional consistency

Table A.1 summarises the units and dimensions of key equations and quantities as presented in this section and in much of the literature. The dimensions of the turbulent diffusivity Γ_T differ between the Favre-averaged and constant density cases. Further, the dimensions of equation (A.3) depend on the dimensions of the composition vector, given in this case by equation (A.4).

There is potential for confusion. Where the main text refers to Favre-averaged systems derived from equation (A.27), Γ_T should be interpreted as having dimensions M/LT. Where it refers to constant density systems derived from equation (A.28), Γ_T should be interpreted as having dimensions L²/T. In order to retain generality, the remaining derivations are given in terms of a Favre-averaged system and Γ_T should be interpreted as having dimensions M/LT. The constant density equations can be recovered by substituting

$$\langle \rho \rangle \tilde{f}_\phi(\psi(x, t)) = \rho f_\phi(\psi(x, t)), \quad (\text{A.30})$$

and cancelling the constant density ρ from each term. The resulting constant density form of Γ_T should be interpreted as having dimensions L²/T.

A.1 Joint composition PDF transport equation

Table A.1: Units and dimensions of key equations and quantities.

	SI units	Dimensions in M, L, T, N, Θ	
Equation (A.1)	kg/m ³ s	[M/L ³ T]	
Equation (A.2)	J/m ³ s	[M/LT ³]	
Equation (A.3)	kg/m ³ s	[M/L ³ T]	for $\alpha = 1, \dots, s$
	J/m ³ s	[M/LT ³]	for $\alpha = K$
Y, Y_α	—	[—]	
h, h_α	J/kg	[L ² /T ²]	
C, C_α	mol/m ³	[N/L ³]	
W_α	kg/mol	[M/N]	
J_i^α	kg/m ² s	[M/L ² T]	
J_i^h	J/m ² s	[M/T ³]	
S_α	1/s	[1/T]	
S_h	J/kg s	[L ² /T ³]	
$c_p, c_{p\alpha}$	J/kg K	[L ² /T ² Θ]	
Γ, Γ_α	m ² /s	[L ² /T]	
λ	J/m K s	[ML/T ³ Θ]	
ρ	kg/m ³	[M/L ³]	
C_ϕ	—	[—]	
τ_ϕ	s	[T]	
v_T	kg/m s	[M/LT]	
σ_T	—	[—]	
Γ_T	kg/m s	[M/LT]	in equations (A.21, A.22, A.27)
	m ² /s	[L ² /T]	in equations (A.28, A.29)
t	s	[T]	
T	K	[Θ]	
U_i	m/s	[L/T]	
x_i	m	[L]	
Dimensions			
M	Mass	N	Amount
L	Length	Θ	Temperature
T	Time		

A.2 The direct quadrature method of moments

This section summarises the formal derivation of the DQMoM and DQMoM-IEM equations for turbulent reacting flows described by a closed joint composition PDF transport equation that includes the IEM mixing model. The equations are well documented in the literature and their derivation is summarised by Fox (2003, appendix B). We start with a general Favre-averaged system, then consider DQMoM-IEM and a constant density system as special cases.

A.2.1 Favre-averaged case

The derivation starts with the one-point one-time closed Favre-averaged joint composition PDF transport equation (A.27)

$$\begin{aligned} \langle \rho \rangle \frac{\partial \tilde{f}_\phi}{\partial t} + \langle \rho \rangle \tilde{U}_i \frac{\partial \tilde{f}_\phi}{\partial x_i} - \frac{\partial}{\partial x_i} \left(\Gamma_T \frac{\partial \tilde{f}_\phi}{\partial x_i} \right) = \\ - \frac{\partial}{\partial \psi_\alpha} \left(\left[\frac{C_\phi}{2\tau_\phi} (\langle \phi_\alpha \rangle - \psi_\alpha) + S_\alpha(\psi) \right] \langle \rho \rangle \tilde{f}_\phi \right). \end{aligned}$$

The PDF \tilde{f}_ϕ is discretised using a weighted field approximation

$$\begin{aligned} \tilde{f}_\phi(\psi(x, t)) \, d\psi &= \tilde{f}_\phi(\psi_1, \dots, \psi_K(x, t)) \, d\psi_1 \cdots d\psi_K \\ &\approx \sum_{n=1}^N w^{(n)}(x, t) \prod_{\alpha=1}^K \delta_{\psi_\alpha^{(n)}(x, t)}(d\psi_\alpha), \end{aligned} \quad (\text{A.31})$$

where

$$\delta_{\psi_\alpha^{(n)}(x, t)}(d\psi_\alpha) \equiv \delta(\psi_\alpha - \psi_\alpha^{(n)}(x, t)) \, d\psi_\alpha, \quad (\text{A.32})$$

and the substitutions defined in equations (A.41), (A.42) and (A.43) are used to derive a non-constant coefficient linear equation (A.33) in the source terms of the transport equations for the weights (A.34) and weighted compositions (A.35).

A.2 The direct quadrature method of moments

The **non-constant coefficient linear equation** can be written

$$\begin{aligned}
& \sum_{n=1}^N \left[\prod_{\alpha=1}^K \delta_{\psi_{\alpha}^{(n)}} + \sum_{\alpha=1}^K \psi_{\alpha}^{(n)} \frac{\partial}{\partial \psi_{\alpha}} \prod_{\alpha=1}^K \delta_{\psi_{\alpha}^{(n)}} \right] a^{(n)} \\
& - \sum_{n=1}^N \sum_{\alpha=1}^K \left[\frac{\partial}{\partial \psi_{\alpha}} \prod_{\alpha=1}^K \delta_{\psi_{\alpha}^{(n)}} \right] b_{\alpha}^{(n)} \\
& = \sum_{n=1}^N \sum_{\alpha=1}^K \sum_{\beta=1}^K \left[w^{(n)} c_{\alpha\beta}^{(n)} \frac{\partial^2}{\partial \psi_{\alpha} \partial \psi_{\beta}} \prod_{\alpha=1}^K \delta_{\psi_{\alpha}^{(n)}} \right] \\
& \quad - \frac{\partial}{\partial \psi_{\alpha}} \left(r_{\alpha}^{(n)} \tilde{f}_{\phi} \right),
\end{aligned} \tag{A.33}$$

where

$$\frac{\partial w^{(n)}}{\partial t} + \tilde{U}_i \frac{\partial w^{(n)}}{\partial x_i} - \frac{1}{\langle \rho \rangle} \frac{\partial}{\partial x_i} \left(\Gamma_{\text{T}} \frac{\partial w^{(n)}}{\partial x_i} \right) = a^{(n)}, \tag{A.34}$$

$$\frac{\partial s_{\alpha}^{(n)}}{\partial t} + \tilde{U}_i \frac{\partial s_{\alpha}^{(n)}}{\partial x_i} - \frac{1}{\langle \rho \rangle} \frac{\partial}{\partial x_i} \left(\Gamma_{\text{T}} \frac{\partial s_{\alpha}^{(n)}}{\partial x_i} \right) = b_{\alpha}^{(n)}, \tag{A.35}$$

and

$$s_{\alpha}^{(n)} \equiv w^{(n)} \psi_{\alpha}^{(n)}, \tag{A.36}$$

$$c_{\alpha\beta}^{(n)} \equiv \frac{\Gamma_{\text{T}}}{\langle \rho \rangle} \frac{\partial \psi_{\alpha}^{(n)}}{\partial x_i} \frac{\partial \psi_{\beta}^{(n)}}{\partial x_i}, \tag{A.37}$$

$$r_{\alpha}^{(n)} \equiv \frac{C_{\phi}}{2\tau_{\phi}} \left(\langle \phi_{\alpha} \rangle_N - \psi_{\alpha}^{(n)} \right) + S_{\alpha} \left(\psi^{(n)} \right), \tag{A.38}$$

and where the dependencies on x and t have been suppressed for clarity. The derivation up to this point is exact in that, apart from the approximation in equation (A.31), no arbitrary choices have been made.

A DERIVATIONS

The **substitutions** are formally derived

$$\frac{\partial}{\partial x_i} \prod_{\alpha=1}^K \delta_{\psi_\alpha^{(n)}} = - \sum_{\alpha=1}^K \frac{\partial \psi_\alpha^{(n)}}{\partial x_i} \frac{\partial}{\partial \psi_\alpha} \prod_{\alpha=1}^K \delta_{\psi_\alpha^{(n)}} \quad (\text{A.39})$$

$$= - \frac{1}{w^{(n)}} \sum_{\alpha=1}^K \left[\left(\frac{\partial s_\alpha^{(n)}}{\partial x_i} - \psi_\alpha^{(n)} \frac{\partial w^{(n)}}{\partial x_i} \right) \frac{\partial}{\partial \psi_\alpha} \prod_{\alpha=1}^K \delta_{\psi_\alpha^{(n)}} \right], \quad (\text{A.40})$$

where $\partial \psi_\alpha^{(n)} / \partial x_i$ has been substituted using the definition of $s_\alpha^{(n)}$ in equation (A.36). Using the product rule and equations (A.31) and (A.40)

$$\begin{aligned} \frac{\partial \tilde{f}_\phi}{\partial x_i} &= \frac{\partial}{\partial x_i} \left(\sum_{n=1}^N w^{(n)} \prod_{\alpha=1}^K \delta_{\psi_\alpha^{(n)}} \right) \\ &= \sum_{n=1}^N \left[\frac{\partial w^{(n)}}{\partial x_i} \prod_{\alpha=1}^K \delta_{\psi_\alpha^{(n)}} - \sum_{\alpha=1}^K w^{(n)} \frac{\partial \psi_\alpha^{(n)}}{\partial x_i} \frac{\partial}{\partial \psi_\alpha} \prod_{\alpha=1}^K \delta_{\psi_\alpha^{(n)}} \right] \\ &= \sum_{n=1}^N \frac{\partial w^{(n)}}{\partial x_i} \left(\prod_{\alpha=1}^K \delta_{\psi_\alpha^{(n)}} + \sum_{\alpha=1}^K \psi_\alpha^{(n)} \frac{\partial}{\partial \psi_\alpha} \prod_{\alpha=1}^K \delta_{\psi_\alpha^{(n)}} \right) \\ &\quad - \sum_{n=1}^N \sum_{\alpha=1}^K \frac{\partial s_\alpha^{(n)}}{\partial x_i} \left(\frac{\partial}{\partial \psi_\alpha} \prod_{\alpha=1}^K \delta_{\psi_\alpha^{(n)}} \right). \end{aligned} \quad (\text{A.41})$$

Applying the product rule to equation (A.41)

$$\begin{aligned} \frac{\partial}{\partial x_i} \left(\Gamma_T \frac{\partial \tilde{f}_\phi}{\partial x_i} \right) &= \sum_{n=1}^N \frac{\partial}{\partial x_i} \left(\Gamma_T \frac{\partial w^{(n)}}{\partial x_i} \right) \left(\prod_{\alpha=1}^K \delta_{\psi_\alpha^{(n)}} + \sum_{\alpha=1}^K \psi_\alpha^{(n)} \frac{\partial}{\partial \psi_\alpha} \prod_{\alpha=1}^K \delta_{\psi_\alpha^{(n)}} \right) \\ &\quad + \sum_{n=1}^N \Gamma_T \frac{\partial w^{(n)}}{\partial x_i} \frac{\partial}{\partial x_i} \left(\prod_{\alpha=1}^K \delta_{\psi_\alpha^{(n)}} + \sum_{\alpha=1}^K \psi_\alpha^{(n)} \frac{\partial}{\partial \psi_\alpha} \prod_{\alpha=1}^K \delta_{\psi_\alpha^{(n)}} \right) \\ &\quad - \sum_{n=1}^N \sum_{\alpha=1}^K \frac{\partial}{\partial x_i} \left(\Gamma_T \frac{\partial s_\alpha^{(n)}}{\partial x_i} \right) \left(\frac{\partial}{\partial \psi_\alpha} \prod_{\alpha=1}^K \delta_{\psi_\alpha^{(n)}} \right) \\ &\quad - \sum_{n=1}^N \sum_{\alpha=1}^K \Gamma_T \frac{\partial s_\alpha^{(n)}}{\partial x_i} \frac{\partial}{\partial x_i} \left(\frac{\partial}{\partial \psi_\alpha} \prod_{\alpha=1}^K \delta_{\psi_\alpha^{(n)}} \right) \end{aligned}$$

A.2 The direct quadrature method of moments

$$\begin{aligned}
&= \sum_{n=1}^N \frac{\partial}{\partial x_i} \left(\Gamma_T \frac{\partial w^{(n)}}{\partial x_i} \right) \left(\prod_{\alpha=1}^K \delta_{\psi_\alpha^{(n)}} + \sum_{\alpha=1}^K \psi_\alpha^{(n)} \frac{\partial}{\partial \psi_\alpha} \prod_{\alpha=1}^K \delta_{\psi_\alpha^{(n)}} \right) \\
&\quad - \sum_{n=1}^N \sum_{\alpha=1}^K \frac{\partial}{\partial x_i} \left(\Gamma_T \frac{\partial s_\alpha^{(n)}}{\partial x_i} \right) \left(\frac{\partial}{\partial \psi_\alpha} \prod_{\alpha=1}^K \delta_{\psi_\alpha^{(n)}} \right) \\
&\quad + \sum_{n=1}^N \sum_{\alpha=1}^K \sum_{\beta=1}^K w^{(n)} \Gamma_T \frac{\partial \psi_\alpha^{(n)}}{\partial x_i} \frac{\partial \psi_\beta^{(n)}}{\partial x_i} \frac{\partial^2}{\partial \psi_\alpha \partial \psi_\beta} \prod_{\alpha=1}^K \delta_{\psi_\alpha^{(n)}},
\end{aligned} \tag{A.42}$$

where the underlined terms are simplified using the product rule

$$\begin{aligned}
&\underline{\Gamma_T \frac{\partial w^{(n)}}{\partial x_i} \frac{\partial}{\partial x_i} \left(\prod_{\alpha=1}^K \delta_{\psi_\alpha^{(n)}} + \sum_{\alpha=1}^K \psi_\alpha^{(n)} \frac{\partial}{\partial \psi_\alpha} \prod_{\alpha=1}^K \delta_{\psi_\alpha^{(n)}} \right)} \\
&\quad - \underline{\sum_{\alpha=1}^K \Gamma_T \frac{\partial s_\alpha^{(n)}}{\partial x_i} \frac{\partial}{\partial x_i} \left(\frac{\partial}{\partial \psi_\alpha} \prod_{\alpha=1}^K \delta_{\psi_\alpha^{(n)}} \right)} \\
&= \sum_{\alpha=1}^K \Gamma_T \left(\psi_\alpha^{(n)} \frac{\partial w^{(n)}}{\partial x_i} - \frac{\partial s_\alpha^{(n)}}{\partial x_i} \right) \frac{\partial}{\partial x_i} \left(\frac{\partial}{\partial \psi_\alpha} \prod_{\alpha=1}^K \delta_{\psi_\alpha^{(n)}} \right) \\
&\quad + \Gamma_T \frac{\partial w^{(n)}}{\partial x_i} \underbrace{\left(\frac{\partial}{\partial x_i} \prod_{\alpha=1}^K \delta_{\psi_\alpha^{(n)}} + \sum_{\alpha=1}^K \frac{\partial \psi_\alpha^{(n)}}{\partial x_i} \frac{\partial}{\partial \psi_\alpha} \prod_{\alpha=1}^K \delta_{\psi_\alpha^{(n)}} \right)}_{0 \text{ by equation (A.39)}} \\
&= \sum_{\alpha=1}^K \Gamma_T \left(-w^{(n)} \frac{\partial \psi_\alpha^{(n)}}{\partial x_i} \right) \left(- \sum_{\beta=1}^K \frac{\partial \psi_\beta^{(n)}}{\partial x_i} \frac{\partial^2}{\partial \psi_\alpha \partial \psi_\beta} \prod_{\alpha=1}^K \delta_{\psi_\alpha^{(n)}} \right) \\
&= \sum_{\alpha=1}^K \sum_{\beta=1}^K w^{(n)} \Gamma_T \frac{\partial \psi_\alpha^{(n)}}{\partial x_i} \frac{\partial \psi_\beta^{(n)}}{\partial x_i} \frac{\partial^2}{\partial \psi_\alpha \partial \psi_\beta} \prod_{\alpha=1}^K \delta_{\psi_\alpha^{(n)}}.
\end{aligned}$$

By analogy with equation (A.41)

$$\begin{aligned}
\frac{\partial \tilde{f}_\phi}{\partial t} &= \sum_{n=1}^N \frac{\partial w^{(n)}}{\partial t} \left(\prod_{\alpha=1}^K \delta_{\psi_\alpha^{(n)}} + \sum_{\alpha=1}^K \psi_\alpha^{(n)} \frac{\partial}{\partial \psi_\alpha} \prod_{\alpha=1}^K \delta_{\psi_\alpha^{(n)}} \right) \\
&\quad - \sum_{n=1}^N \sum_{\alpha=1}^K \frac{\partial s_\alpha^{(n)}}{\partial t} \left(\frac{\partial}{\partial \psi_\alpha} \prod_{\alpha=1}^K \delta_{\psi_\alpha^{(n)}} \right).
\end{aligned} \tag{A.43}$$

A DERIVATIONS

The next step is to use equation (A.33) to derive a linear system that matches the number of equations to the $N(K + 1)$ unknown source terms $a^{(n)}$ and $b_\alpha^{(n)}$. The aim is to solve equations (A.34) and (A.35) to transport the weights and weighted compositions, using the linear system to determine the source terms $a^{(n)}$ and $b_\alpha^{(n)}$.

The linear system is derived by taking $M = N(K + 1)$ moments of the discretised PDF transport equation (A.33) by termwise application of

$$\int \cdots \int \prod_{\alpha=1}^K \psi_\alpha^{m_{\lambda\alpha}}(\cdot) d\psi_1 \cdots d\psi_K, \quad (\text{A.44})$$

where, for example, the empirical moments of \tilde{f}_ϕ are defined

$$\begin{aligned} \langle \phi_1^{m_{\lambda 1}} \cdots \phi_K^{m_{\lambda K}} \rangle_N &= \int \cdots \int \prod_{\alpha=1}^K \psi_\alpha^{m_{\lambda\alpha}} \tilde{f}_\phi d\psi_1 \cdots d\psi_K \\ &= \sum_{n=1}^N w^{(n)} \prod_{\alpha=1}^K \psi_\alpha^{(n)m_{\lambda\alpha}} \quad \text{for } \lambda = 1, \dots, M. \end{aligned} \quad (\text{A.45})$$

The use of the linear system to evaluate the source terms of equations (A.34) and (A.35) imposes a projection. It constrains the statistics of the fields to obey the discretised PDF transport equation (A.33) for each of the empirical moments specified by equation (A.45). The indices $m_{\lambda\alpha}$ are typically low order non-negative integers. The zeroth and first-order moments are required to ensure that the weights sum to unity and that the empirical means (of non-reacting scalars) are conserved. The choice of moments is otherwise arbitrary.

Taking moments of (A.33) by termwise application of equation (A.44) yields

$$\begin{aligned} \sum_{n=1}^N A_{1,\lambda n} a^{(n)} + \sum_{n=1}^N \sum_{\alpha=1}^K A_{2,\alpha,\lambda n} b_\alpha^{(n)} \\ = \sum_{n=1}^N \sum_{\alpha=1}^K \sum_{\beta=1}^K A_{3,\alpha\beta,\lambda n} w^{(n)} c_{\alpha\beta}^{(n)} + \sum_{n=1}^N \sum_{\alpha=1}^K A_{2,\alpha,\lambda n} w^{(n)} r_\alpha^{(n)}, \end{aligned} \quad (\text{A.46})$$

A.2 The direct quadrature method of moments

for each moment λ , where $A_{1,\lambda n}$, $A_{2,\alpha,\lambda n}$ and $A_{3_{\alpha\beta},\lambda n}$ are defined

$$A_{1,\lambda n} = \left(1 - \sum_{\alpha=1}^K m_{\lambda\alpha}\right) \prod_{\alpha=1}^K \psi_{\alpha}^{(n)m_{\lambda\alpha}}, \quad (\text{A.47})$$

$$A_{2,\alpha,\lambda n} = m_{\lambda\alpha} \psi_{\alpha}^{(n)m_{\lambda\alpha}-1} \prod_{\substack{\beta=1 \\ \beta \neq \alpha}}^K \psi_{\beta}^{(n)m_{\lambda\beta}}, \quad (\text{A.48})$$

$$A_{3_{\alpha\beta},\lambda n} = \begin{cases} m_{\lambda\alpha} \psi_{\alpha}^{(n)m_{\lambda\alpha}-1} m_{\lambda\beta} \psi_{\beta}^{(n)m_{\lambda\beta}-1} \prod_{\substack{\gamma=1 \\ \gamma \neq \beta}}^K \psi_{\gamma}^{(n)m_{\lambda\gamma}} & \text{if } \alpha \neq \beta \\ m_{\lambda\alpha} (m_{\lambda\alpha} - 1) \psi_{\alpha}^{(n)m_{\lambda\alpha}-2} \prod_{\substack{\beta=1 \\ \beta \neq \alpha}}^K \psi_{\beta}^{(n)m_{\lambda\beta}} & \text{otherwise.} \end{cases} \quad (\text{A.49})$$

Note that the derivatives of the delta function are defined such that (Pope, 2000)

$$\int_{-\infty}^{+\infty} g(\psi_{\alpha}) \delta_{\psi_{\alpha}^{(n)}}^{(m)} d\psi_{\alpha} = (-1)^m g^{(m)}(\psi_{\alpha}^{(n)}), \quad (\text{A.50})$$

where $g^{(m)}(\psi_{\alpha})$ is the m^{th} derivative of $g(\psi_{\alpha})$. The coefficient of the equation (A.46) term in $r_{\alpha}^{(n)}$ is found using integration by parts

$$\begin{aligned} & \int_{-\infty}^{+\infty} \dots \int_{-\infty}^{+\infty} \prod_{\alpha=1}^K \psi_{\alpha}^{m_{\lambda\alpha}} \frac{\partial}{\partial \psi_{\alpha}} \left(r_{\alpha}^{(n)} \tilde{f}_{\phi} \right) d\psi_1 \dots d\psi_K \\ &= \underbrace{\left[\prod_{\alpha=1}^K \psi_{\alpha}^{m_{\lambda\alpha}} r_{\alpha}^{(n)} \tilde{f}_{\phi} \right]_{-\infty}^{+\infty}}_0 - \int_{-\infty}^{+\infty} r_{\alpha}^{(n)} \tilde{f}_{\phi} \frac{\partial}{\partial \psi_{\alpha}} \prod_{\alpha=1}^K \psi_{\alpha}^{m_{\lambda\alpha}} d\psi_1 \dots d\psi_K \\ &= - \sum_{n=1}^N \sum_{\alpha=1}^K m_{\lambda\alpha} \psi_{\alpha}^{(n)m_{\lambda\alpha}-1} \prod_{\substack{\beta=1 \\ \beta \neq \alpha}}^K \psi_{\beta}^{(n)m_{\lambda\beta}} \cdot w^{(n)} r_{\alpha}^{(n)}. \end{aligned} \quad (\text{A.51})$$

A DERIVATIONS

The linear system given by the set of moments $\lambda = 1, \dots, M$ can be written

$$A \alpha = \beta, \quad (\text{A.52})$$

$$\alpha^\top = [a \ b_1 \ \dots \ b_K], \quad (\text{A.53})$$

$$\beta = A_3 W_3 c + A_2 W_2 r. \quad (\text{A.54})$$

A is a square $M \times N(K+1)$ matrix and a and b_α are vectors of length N

$$A = [A_1 \ A_2], \quad (\text{A.55})$$

$$a^\top = [a^{(1)} \ \dots \ a^{(N)}], \quad (\text{A.56})$$

$$b_\alpha^\top = [b_\alpha^{(1)} \ \dots \ b_\alpha^{(N)}], \quad (\text{A.57})$$

A_2 and A_3 are $M \times NK$ and $M \times NK^2$ matrices

$$A_2 = [A_{2_1} \ \dots \ A_{2_K}], \quad (\text{A.58})$$

$$A_3 = [A_{3_{11}} \ \dots \ A_{3_{1K}} \ \dots \ A_{3_{K1}} \ \dots \ A_{3_{KK}}], \quad (\text{A.59})$$

A_1 , A_{2_α} and $A_{3_{\alpha\beta}}$ are $M \times N$ matrices with components as per equations (A.47), (A.48) and (A.49). W_2 and W_3 are $NK \times NK$ and $NK^2 \times NK^2$ matrices, c and r are vectors of length NK^2 and NK

$$W_2 = \text{diag} [w_1 \ \dots \ w_K], \quad (\text{A.60})$$

$$W_3 = \text{diag} [w_{11} \ \dots \ w_{1K} \ \dots \ w_{K1} \ \dots \ w_{KK}], \quad (\text{A.61})$$

$$c^\top = [c_{11} \ \dots \ c_{1K} \ \dots \ c_{K1} \ \dots \ c_{KK}], \quad (\text{A.62})$$

$$r^\top = [r_1 \ \dots \ r_K], \quad (\text{A.63})$$

where w_α , $w_{\alpha\beta}$, $c_{\alpha\beta}$ are r_α are vectors of length N with components

$$w_\alpha^\top = w_{\alpha\beta}^\top = [w_\alpha^{(1)} \ \dots \ w_\alpha^{(N)}], \quad (\text{A.64})$$

$$c_{\alpha\beta}^\top = [c_{\alpha\beta}^{(1)} \ \dots \ c_{\alpha\beta}^{(N)}], \quad (\text{A.65})$$

$$r_\alpha^\top = [r_\alpha^{(1)} \ \dots \ r_\alpha^{(N)}]. \quad (\text{A.66})$$

A.2 The direct quadrature method of moments

DQMoM-IEM

DQMoM-IEM is a special case of DQMoM where the projection is constrained to consider only *conserved weights* and *unmixed moments*.

The DQMoM derivation can be modified to implement DQMoM-IEM by setting

$$a^{(n)} = 0, \quad (\text{A.67})$$

and taking a set of $M = NK$ unmixed empirical moments of equation (A.33)

$$\langle \phi_\alpha^{m_{\lambda\alpha}} \rangle_N = \sum_{n=1}^N w^{(n)} \psi_\alpha^{(n)m_{\lambda\alpha}} \quad \text{for } \lambda = 1, \dots, M, \quad (\text{A.68})$$

to derive a linear system of NK equations of the form

$$\sum_{n=1}^N \psi_\alpha^{(n)m_{\lambda\alpha}-1} (b_\alpha^{(n)} - w^{(n)} r_\alpha^{(n)}) = \sum_{n=1}^N (m_{\lambda\alpha} - 1) \psi_\alpha^{(n)m_{\lambda\alpha}-2} w^{(n)} c_{\alpha\alpha}^{(n)} \quad (\text{A.69})$$

where $r_\alpha^{(n)}$ and $c_{\alpha\alpha}^{(n)}$ are defined as per equations (A.37) and (A.38). The zeroth moment is no longer required because the source term for the weights is null. Chapter 3 shows for the first time that equation (A.69) can be solved analytically for the source terms $b_\alpha^{(n)}$

$$b_\alpha^{(n)} = w^{(n)} r_\alpha^{(n)} + w^{(n)} c_{\alpha\alpha}^{(n)} \sum_{\substack{i=1 \\ i \neq n}}^N \frac{1}{\psi_\alpha^{(n)} - \psi_\alpha^{(i)}} + \prod_{\substack{i=1 \\ i \neq n}}^N \frac{1}{\psi_\alpha^{(n)} - \psi_\alpha^{(i)}} \sum_{\substack{j=1 \\ j \neq n}}^N w^{(j)} c_{\alpha\alpha}^{(j)} \prod_{\substack{k=1 \\ k \neq j, n}}^N (\psi_\alpha^{(j)} - \psi_\alpha^{(k)}), \quad (\text{A.70})$$

under the constraint

$$m_{\lambda\alpha} = \begin{cases} n & \text{where } n = \lambda - (\alpha - 1)N \quad \text{if } n \geq 1 \text{ and } n \leq N \\ 0 & \text{otherwise} \end{cases} \quad (\text{A.71})$$

$$\text{for } \lambda = 1, \dots, M \quad \text{and} \quad \alpha = 1, \dots, K.$$

A DERIVATIONS

A.2.2 Constant density case

In the constant density case, the DQMoM transport equations can be written

$$\frac{\partial w^{(n)}}{\partial t} + \langle U_i \rangle \frac{\partial w^{(n)}}{\partial x_i} - \frac{\partial}{\partial x_i} \left(\Gamma_T \frac{\partial w^{(n)}}{\partial x_i} \right) = a^{(n)}, \quad (\text{A.72})$$

$$\frac{\partial s_\alpha^{(n)}}{\partial t} + \langle U_i \rangle \frac{\partial s_\alpha^{(n)}}{\partial x_i} - \frac{\partial}{\partial x_i} \left(\Gamma_T \frac{\partial s_\alpha^{(n)}}{\partial x_i} \right) = b_\alpha^{(n)}, \quad (\text{A.73})$$

where

$$s_\alpha^{(n)} \equiv w^{(n)} \psi_\alpha^{(n)}, \quad (\text{A.74})$$

$$c_{\alpha\beta}^{(n)} \equiv \Gamma_T \frac{\partial \psi_\alpha^{(n)}}{\partial x_i} \frac{\partial \psi_\beta^{(n)}}{\partial x_i}, \quad (\text{A.75})$$

$$r_\alpha^{(n)} \equiv \frac{C_\phi}{2\tau_\phi} \left(\langle \phi_\alpha \rangle_N - \psi_\alpha^{(n)} \right) + S_\alpha \left(\psi^{(n)} \right). \quad (\text{A.76})$$

Γ_T should be interpreted as having dimensions L^2/T as per section A.1.4. The definition of the components of matrices A_1 , A_{2_α} and $A_{3_{\alpha\beta}}$ in equations (A.47–A.49) and the linear system in equations (A.52–A.66) and remain unchanged.

The constant density DQMoM-IEM transport equations are written

$$\frac{\partial w^{(n)}}{\partial t} + \langle U_i \rangle \frac{\partial w^{(n)}}{\partial x_i} - \frac{\partial}{\partial x_i} \left(\Gamma_T \frac{\partial w^{(n)}}{\partial x_i} \right) = 0, \quad (\text{A.77})$$

$$\frac{\partial s_\alpha^{(n)}}{\partial t} + \langle U_i \rangle \frac{\partial s_\alpha^{(n)}}{\partial x_i} - \frac{\partial}{\partial x_i} \left(\Gamma_T \frac{\partial s_\alpha^{(n)}}{\partial x_i} \right) = b_\alpha^{(n)}, \quad (\text{A.78})$$

and the definitions of the linear system and the analytic solution in equations (A.69–A.70) remain unchanged, subject to the definition of $c_{\alpha\alpha}^{(n)}$ and $r_\alpha^{(n)}$ as per equations (A.75) and (A.76) and Γ_T interpreted with dimensions L^2/T .

A.3 The stochastic fields method

This section summarises the formal derivation of the Itô SPDE given by equation (4.2). The method follows the approach outlined by Valiño (1998) and requires that the fields are twice differentiable in space. We start with a general Favre-averaged system, then consider a constant density system as a special case.

A.3.1 Favre-averaged case

The derivation starts with the one-point one-time closed Favre-averaged joint composition PDF transport equation (A.27)

$$\begin{aligned} \langle \rho \rangle \frac{\partial \tilde{f}_\phi}{\partial t} + \langle \rho \rangle \tilde{U}_i \frac{\partial \tilde{f}_\phi}{\partial x_i} - \frac{\partial}{\partial x_i} \left(\Gamma_\Gamma \frac{\partial \tilde{f}_\phi}{\partial x_i} \right) = \\ - \frac{\partial}{\partial \psi_\alpha} \left(\left[\frac{C_\phi}{2\tau_\phi} (\langle \phi_\alpha \rangle - \psi_\alpha) + S_\alpha(\psi) \right] \langle \rho \rangle \tilde{f}_\phi \right). \end{aligned}$$

We define a weighted field approximation

$$\begin{aligned} \tilde{f}_\phi(\psi(x,t)) \, d\psi &= \tilde{f}_\phi(\psi_1, \dots, \psi_K(x,t)) \, d\psi_1 \cdots d\psi_K \\ &\approx \frac{1}{N} \sum_{n=1}^N \prod_{\alpha=1}^K \delta_{\psi_\alpha^{(n)}(x,t)}(d\psi_\alpha), \end{aligned} \quad (\text{A.79})$$

where

$$\delta_{\psi_\alpha^{(n)}(x,t)}(d\psi_\alpha) \equiv \delta(\psi_\alpha - \psi_\alpha^{(n)}(x,t)) \, d\psi_\alpha, \quad (\text{A.80})$$

and consider the contributions due to convection and diffusion, and micromixing and reaction separately. The PDF \tilde{f}_ϕ evolves by **convection and diffusion**

$$\langle \rho \rangle \frac{\partial \tilde{f}_\phi}{\partial t} = - \langle \rho \rangle \tilde{U}_i \frac{\partial \tilde{f}_\phi}{\partial x_i} + \frac{\partial}{\partial x_i} \left(\Gamma_\Gamma \frac{\partial \tilde{f}_\phi}{\partial x_i} \right). \quad (\text{A.81})$$

We formally substitute the PDF \tilde{f}_ϕ in equation (A.81) to give

$$\langle \rho \rangle \frac{\partial \tilde{f}_\phi}{\partial t} = \frac{1}{N} \sum_{n=1}^N \left[- \langle \rho \rangle \tilde{U}_i \frac{\partial}{\partial x_i} \prod_{\alpha=1}^K \delta_{\psi_\alpha^{(n)}(x,t)} + \frac{\partial}{\partial x_i} \left(\Gamma_\Gamma \frac{\partial}{\partial x_i} \prod_{\alpha=1}^K \delta_{\psi_\alpha^{(n)}(x,t)} \right) \right],$$

A DERIVATIONS

such that (suppressing the dependence of the delta functions on x and t)

$$\begin{aligned} \frac{\partial \tilde{f}_\phi}{\partial t} = & \frac{1}{N} \sum_{n=1}^N \left[\sum_{\alpha=1}^K \frac{\partial}{\partial \psi_\alpha} \left(\tilde{U}_i \frac{\partial \psi_\alpha^{(n)}}{\partial x_i} \prod_{\beta=1}^K \delta_{\psi_\beta^{(n)}} \right) \right. \\ & - \sum_{\alpha=1}^K \frac{\partial}{\partial \psi_\alpha} \left(\frac{1}{\langle \rho \rangle} \frac{\partial}{\partial x_i} \left(\Gamma_T \frac{\partial \psi_\alpha^{(n)}}{\partial x_i} \right) \prod_{\beta=1}^K \delta_{\psi_\beta^{(n)}} \right) \\ & \left. + \frac{1}{2} \sum_{\alpha=1}^K \sum_{\beta=1}^K \frac{\partial^2}{\partial \psi_\alpha \partial \psi_\beta} \left(\frac{2\Gamma_T}{\langle \rho \rangle} \frac{\partial \psi_\alpha^{(n)}}{\partial x_i} \frac{\partial \psi_\beta^{(n)}}{\partial x_i} \prod_{\gamma=1}^K \delta_{\psi_\gamma^{(n)}} \right) \right], \end{aligned} \quad (\text{A.82})$$

where we have substituted

$$\begin{aligned} \frac{\partial}{\partial x_i} \prod_{\alpha=1}^K \delta_{\psi_\alpha^{(n)}} &= - \sum_{\alpha=1}^K \frac{\partial \psi_\alpha^{(n)}}{\partial x_i} \delta'_{\psi_\alpha^{(n)}} \prod_{\substack{\beta=1 \\ \beta \neq \alpha}}^K \delta_{\psi_\beta^{(n)}} \\ &= - \sum_{\alpha=1}^K \frac{\partial}{\partial \psi_\alpha} \left(\frac{\partial \psi_\alpha^{(n)}}{\partial x_i} \prod_{\beta=1}^K \delta_{\psi_\beta^{(n)}} \right), \end{aligned} \quad (\text{A.83})$$

and using equation (A.83)

$$\begin{aligned} \frac{\partial}{\partial x_i} \left(\Gamma_T \frac{\partial}{\partial x_i} \prod_{\alpha=1}^K \delta_{\psi_\alpha^{(n)}} \right) &= - \sum_{\alpha=1}^K \frac{\partial}{\partial \psi_\alpha} \frac{\partial}{\partial x_i} \left(\Gamma_T \frac{\partial \psi_\alpha^{(n)}}{\partial x_i} \prod_{\beta=1}^K \delta_{\psi_\beta^{(n)}} \right) \\ &= - \sum_{\alpha=1}^K \frac{\partial}{\partial \psi_\alpha} \left(\frac{\partial}{\partial x_i} \left(\Gamma_T \frac{\partial \psi_\alpha^{(n)}}{\partial x_i} \right) \prod_{\beta=1}^K \delta_{\psi_\beta^{(n)}} \right) \\ &\quad + \sum_{\alpha=1}^K \sum_{\beta=1}^K \frac{\partial^2}{\partial \psi_\alpha \partial \psi_\beta} \left(\Gamma_T \frac{\partial \psi_\alpha^{(n)}}{\partial x_i} \frac{\partial \psi_\beta^{(n)}}{\partial x_i} \prod_{\gamma=1}^K \delta_{\psi_\gamma^{(n)}} \right). \end{aligned} \quad (\text{A.84})$$

Equation (A.82) is a Forward Kolmogorov equation in time-composition and has an equivalent SPDE (Gardiner, 2004) describing the contribution to each field

$$d\psi_\alpha^{(n)} = -\tilde{U}_i \frac{\partial \psi_\alpha^{(n)}}{\partial x_i} dt + \frac{1}{\langle \rho \rangle} \frac{\partial}{\partial x_i} \left(\Gamma_T \frac{\partial \psi_\alpha^{(n)}}{\partial x_i} \right) dt + \left(\frac{2\Gamma_T}{\langle \rho \rangle} \right)^{1/2} \frac{\partial \psi_\alpha^{(n)}}{\partial x_i} dW_i^{(n)}. \quad (\text{A.85})$$

Likewise, the contributions to equation (A.27) from **micromixing and reaction**

$$\langle \rho \rangle \frac{\partial \tilde{f}_\phi}{\partial t} = - \frac{\partial}{\partial \psi_\alpha} \left(\left[\frac{C_\phi}{2\tau_\phi} (\langle \phi_\alpha \rangle - \psi_\alpha) + S_\alpha(\psi) \right] \langle \rho \rangle \tilde{f}_\phi \right), \quad (\text{A.86})$$

imply the following contributions to each field

$$d\psi_\alpha^{(n)} = \frac{C_\phi}{2\tau_\phi} (\langle \phi_\alpha \rangle_N - \psi_\alpha^{(n)}) dt + S_\alpha(\psi^{(n)}) dt. \quad (\text{A.87})$$

The SPDE describing the **total contribution** to each field is given by the sum of equations (A.85) and (A.87)

$$\begin{aligned} d\psi_\alpha^{(n)} = & -\tilde{U}_i \frac{\partial \psi_\alpha^{(n)}}{\partial x_i} dt + \frac{1}{\langle \rho \rangle} \frac{\partial}{\partial x_i} \left(\Gamma_T \frac{\partial \psi_\alpha^{(n)}}{\partial x_i} \right) dt \\ & + \left(\frac{2\Gamma_T}{\langle \rho \rangle} \right)^{1/2} \frac{\partial \psi_\alpha^{(n)}}{\partial x_i} dW_i^{(n)} \\ & + \frac{C_\phi}{2\tau_\phi} (\langle \phi_\alpha \rangle_N - \psi_\alpha^{(n)}) dt + S_\alpha(\psi^{(n)}) dt. \end{aligned} \quad (\text{A.88})$$

A.3.2 Constant density case

In the constant density case, equation (A.88) can be rewritten

$$\begin{aligned} d\psi_\alpha^{(n)} = & -\langle U_i \rangle \frac{\partial \psi_\alpha^{(n)}}{\partial x_i} dt + \frac{\partial}{\partial x_i} \left(\Gamma_T \frac{\partial \psi_\alpha^{(n)}}{\partial x_i} \right) dt \\ & + \left(2\Gamma_T \right)^{1/2} \frac{\partial \psi_\alpha^{(n)}}{\partial x_i} dW_i^{(n)} \\ & + \frac{C_\phi}{2\tau_\phi} (\langle \phi_\alpha \rangle_N - \psi_\alpha^{(n)}) dt + S_\alpha(\psi^{(n)}) dt, \end{aligned} \quad (\text{A.89})$$

where Γ_T should be interpreted as having dimensions M/LT in equation (A.88), but dimensions L^2/T in equation (A.89) as per the discussion in section A.1.4.

A.4 The method of moments

This section outlines the formal derivation of the MoM equations that are solved to provide the reference data in chapters 3, 4 and 5. We start with a general Favre-averaged system, then consider a constant density system as a special case.

A.4.1 Favre-averaged case

The derivation starts with the one-point one-time closed Favre-averaged joint composition PDF transport equation (A.27)

$$\begin{aligned} \langle \rho \rangle \frac{\partial \tilde{f}_\phi}{\partial t} + \langle \rho \rangle \tilde{U}_i \frac{\partial \tilde{f}_\phi}{\partial x_i} - \frac{\partial}{\partial x_i} \left(\Gamma_\Gamma \frac{\partial \tilde{f}_\phi}{\partial x_i} \right) = \\ - \frac{\partial}{\partial \psi_\alpha} \left(\left[\frac{C_\phi}{2\tau_\phi} (\langle \phi_\alpha \rangle - \psi_\alpha) + S_\alpha(\psi) \right] \langle \rho \rangle \tilde{f}_\phi \right). \end{aligned}$$

Taking moments of equation (A.27) yields a transport equation for the moments λ of the PDF \tilde{f}_ϕ

$$\frac{\partial \lambda}{\partial t} + \tilde{U}_i \frac{\partial \lambda}{\partial x_i} - \frac{1}{\langle \rho \rangle} \frac{\partial}{\partial x_i} \left(\Gamma_\Gamma \frac{\partial \lambda}{\partial x_i} \right) = R_\lambda, \quad (\text{A.90})$$

where the source term is given

$$R_\lambda = \int_{-\infty}^{+\infty} \cdots \int \prod_{\alpha=1}^K \psi_\alpha^{m_\alpha} R(\psi) \, d\psi_1 \cdots d\psi_K, \quad (\text{A.91})$$

with

$$R(\psi) = - \frac{\partial}{\partial \psi_\alpha} \left(\left[\frac{C_\phi}{2\tau_\phi} (\langle \phi_\alpha \rangle - \psi_\alpha) + S_\alpha(\psi) \right] \tilde{f}_\phi \right). \quad (\text{A.92})$$

Expressions for the source terms R_λ can be found by integrating equation (A.91) by parts. The micromixing and reaction terms can be considered separately.

A.4 The method of moments

The reaction source term R_λ^{rx} is derived in a general form in equation (A.93). It forms an *unclosed* set of coupled ODEs for non-linear reactions. This follows from the fact that knowledge of all moments is required to fully define the PDF.

$$\begin{aligned}
 R_\lambda^{\text{rx}} &= \int \cdots \int \prod_{\alpha=1}^K \psi_\alpha^{m_\alpha} \left(-\frac{\partial}{\partial \psi_\alpha} \left(S_\alpha(\psi) \tilde{f}_\phi \right) \right) d\psi_1 \cdots d\psi_K \\
 &= \sum_{\alpha=1}^K \int \cdots \int m_\alpha \psi_\alpha^{-1} \prod_{\beta=1}^K \psi_\beta^{m_\beta} S_\alpha(\psi) \tilde{f}_\phi d\psi_\alpha \prod_{\substack{\beta=1 \\ \beta \neq \alpha}}^K d\psi_\beta \\
 &\quad - \sum_{\alpha=1}^K \int \cdots \int \underbrace{\left[\prod_{\beta=1}^K \psi_\beta^{m_\beta} S_\alpha(\psi) \tilde{f}_\phi \right]}_{=0} \Big|_{\psi_\alpha=-\infty}^{\psi_\alpha=\infty} \prod_{\substack{\beta=1 \\ \beta \neq \alpha}}^K d\psi_\beta,
 \end{aligned}$$

and using equation (A.15) for the general form of the species source term and the source terms in equation (A.25)

$$\begin{aligned}
 R_\lambda^{\text{rx}} &= \sum_{i=1}^I \left[\right. & (A.93) \\
 &\quad m_1 \left(v_{1i}^r - v_{1i}^f \right) \left(k_{1i}^f \lambda_{m_{1i}^f-1, m_{2i}^f, \dots, m_{si}^f, m_K} - k_{1i}^r \lambda_{m_{1i}^r-1, m_{2i}^r, \dots, m_{si}^r, m_K} \right) \\
 &\quad + m_2 \left(v_{2i}^r - v_{2i}^f \right) \left(k_{2i}^f \lambda_{m_{1i}^f, m_{2i}^f-1, \dots, m_{si}^f, m_K} - k_{2i}^r \lambda_{m_{1i}^r, m_{2i}^r-1, \dots, m_{si}^r, m_K} \right) \\
 &\quad \vdots \\
 &\quad \left. + m_s \left(v_{si}^r - v_{si}^f \right) \left(k_{si}^f \lambda_{m_{1i}^f, m_{2i}^f, \dots, m_{si}^f-1, m_K} - k_{si}^r \lambda_{m_{1i}^r, m_{2i}^r, \dots, m_{si}^r-1, m_K} \right) \right],
 \end{aligned}$$

where

$$m_{\alpha i}^f = m_\alpha + v_{\alpha i}^f, \quad m_{\alpha i}^r = m_\alpha + v_{\alpha i}^r, \quad (A.94)$$

$$k_{\alpha i}^f = k_i^f \cdot \frac{W_\alpha}{\langle \rho \rangle} \prod_{\beta=1}^s \left(\frac{\langle \rho \rangle}{W_\beta} \right)^{v_{\beta i}^f}, \quad k_{\alpha i}^r = k_i^r \cdot \frac{W_\alpha}{\langle \rho \rangle} \prod_{\beta=1}^s \left(\frac{\langle \rho \rangle}{W_\beta} \right)^{v_{\beta i}^r}. \quad (A.95)$$

The molecular mass and density terms appear because of the relations

$$S_\alpha(Y) = \frac{W_\alpha}{\rho} \cdot S_\alpha(C), \quad C_\alpha = \frac{\rho Y_\alpha}{W_\alpha} \quad \text{for } \alpha = 1, \dots, s, \quad (A.96)$$

where the moments λ are defined in terms of the mass fractions and specific enthalpy as per the composition space of equation (A.27) given in equation (A.4).

A DERIVATIONS

The source term for the IEM micromixing model R_λ^{mx} is derived in equation (A.97) and forms a *closed* set of coupled ODEs. This is expected. The purpose of the IEM model is to close the molecular mixing term in the PDF transport equation from which equation (A.27) is derived.

$$\begin{aligned}
R_\lambda^{\text{mx}} &= \int_{-\infty}^{+\infty} \cdots \int_{-\infty}^{+\infty} \prod_{\alpha=1}^K \psi_\alpha^{m_\alpha} \left(-\frac{\partial}{\partial \psi_\alpha} \left(\frac{C_\phi}{2\tau_\phi} (\langle \phi_\alpha \rangle - \psi_\alpha) \tilde{f}_\phi \right) \right) d\psi_1 \cdots d\psi_K \\
&= \frac{C_\phi}{2\tau_\phi} \sum_{\alpha=1}^K \int_{-\infty}^{+\infty} \cdots \int_{-\infty}^{+\infty} m_\alpha \psi_\alpha^{-1} \prod_{\substack{\beta=1 \\ \beta \neq \alpha}}^K \psi_\beta^{m_\beta} (\langle \phi_\alpha \rangle - \psi_\alpha) \tilde{f}_\phi d\psi_\alpha \prod_{\substack{\beta=1 \\ \beta \neq \alpha}}^K d\psi_\beta \\
&\quad - \frac{C_\phi}{2\tau_\phi} \sum_{\alpha=1}^K \int_{-\infty}^{+\infty} \cdots \int_{-\infty}^{+\infty} \underbrace{\left[\prod_{\beta=1}^K \psi_\beta^{m_\beta} (\langle \phi_\alpha \rangle - \psi_\alpha) \tilde{f}_\phi \right]}_{=0} \Big|_{\psi_\alpha=-\infty}^{\psi_\alpha=\infty} \prod_{\substack{\beta=1 \\ \beta \neq \alpha}}^K d\psi_\beta \\
&= \frac{C_\phi}{2\tau_\phi} \left[m_1 \left(\lambda_{1,0,\dots,0} \lambda_{m_1-1,m_2,\dots,m_K} - \lambda_{m_1,m_2,\dots,m_K} \right) \right. \\
&\quad + m_2 \left(\lambda_{0,1,\dots,0} \lambda_{m_1,m_2-1,\dots,m_K} - \lambda_{m_1,m_2,\dots,m_K} \right) \\
&\quad \vdots \\
&\quad \left. + m_K \left(\lambda_{0,0,\dots,1} \lambda_{m_1,m_2,\dots,m_K-1} - \lambda_{m_1,m_2,\dots,m_K} \right) \right]. \tag{A.97}
\end{aligned}$$

A.4.2 Constant density case

In the constant density case, equation (A.90) can be rewritten

$$\frac{\partial \lambda}{\partial t} + \langle U_i \rangle \frac{\partial \lambda}{\partial x_i} - \frac{\partial}{\partial x_i} \left(\Gamma_T \frac{\partial \lambda}{\partial x_i} \right) = R_\lambda, \tag{A.98}$$

where Γ_T should be interpreted as per the discussion in section A.1.4. Aside from replacing $\langle \rho \rangle$ with ρ in equation (A.95), the expressions for the source terms in equations (A.93–A.97) remain unchanged.

Appendix B

Numerical treatment

This appendix presents further information on the MoM coupling to Star-CD and summarises the combinations of operator splittings and numerical methods applied to the DQMoM-IEM / PF and SF methods in this thesis. It provides further information about the choice of filter functions considered during the development of the DQMoM-IEM algorithm in chapter 3, and the method used to estimate the particle size distributions in chapter 5.

B.1 More on filter functions

Table B.1 summarises the filters that were considered during the development of the general DQMoM-IEM solver described in chapter 3. The choice of filter is not arbitrary and affects the performance of the function defined by equation (3.27)

$$f_p(\Delta\psi) = \begin{cases} \frac{1}{\Delta\psi} f\left(\frac{\Delta\psi}{\varepsilon_p}\right) & \text{if } \Delta\psi \neq 0 \\ 0 & \text{otherwise.} \end{cases}$$

Table B.1: Filter functions considered for the general DQMoM-IEM solver.

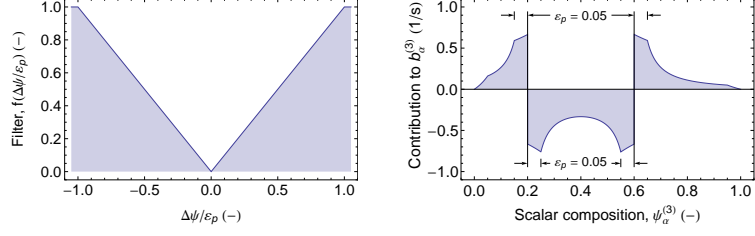
Filter	Filter function $f\left(\frac{\Delta\psi}{\varepsilon_p}\right)$
1, figure B.1(a)	$\min\left(1, \left \frac{\Delta\psi}{\varepsilon_p}\right \right)$
2, figure B.1(b)	$\min\left(1, \left(\frac{\Delta\psi}{\varepsilon_p}\right)^2\right)$
3, figure B.1(c)	$0.5\left(1 - \cos\left[\pi \min\left(1, \left \frac{\Delta\psi}{\varepsilon_p}\right \right)\right]\right)$
4, figure B.1(d)	$0.5\left[1 - \cos\left(\pi \min\left[1, \max\left(0, \frac{3}{2}\left \frac{\Delta\psi}{\varepsilon_p}\right - \frac{1}{2}\right)\right]\right)\right]$
5, figure B.1(e)	$\left[\sin\left(\frac{\pi}{2} \min\left[1, \max\left(0, \frac{3}{2}\left \frac{\Delta\psi}{\varepsilon_p}\right - \frac{1}{2}\right)\right]\right)\right]^4$

Figure B.1 shows the filters and their effect on the diffusion source terms given by figure 3.2(b). An exaggerated value of ε_p is used for clarity.

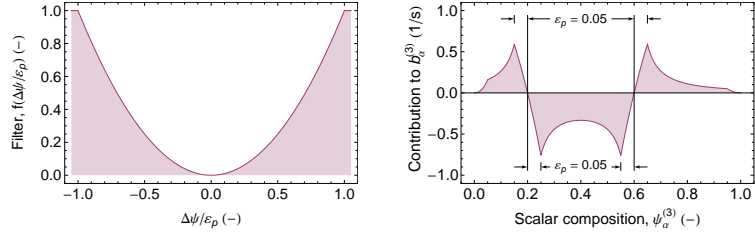
Filter 1 is equivalent to imposing a minimum separation ε_p . It controls the singularities, but the filtered source term in figure B.1(a) is still discontinuous.

Filter 2 imposes a linear source term in the range $-1 < \Delta\psi/\varepsilon_p < 1$. However, numerical integration of the filtered source term in figure B.1(b) remains challenging because the derivatives of the source term are still discontinuous.

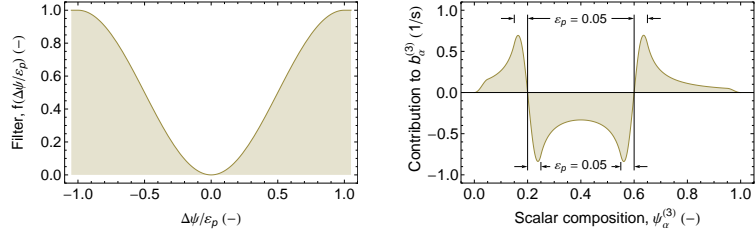
B.1 More on filter functions



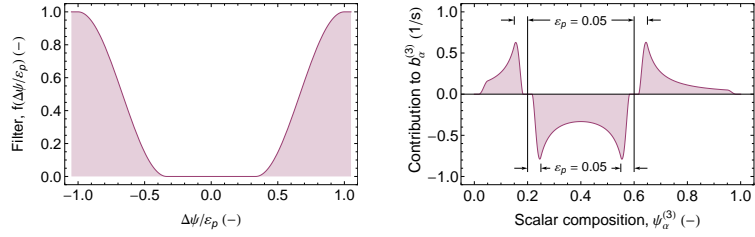
(a) Filter function 1, filtered source term from figure 3.2(b).



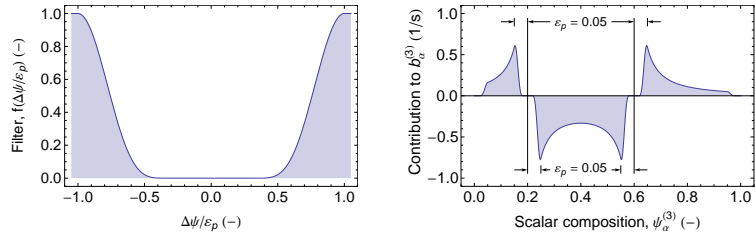
(b) Filter function 2, filtered source term from figure 3.2(b).



(c) Filter function 3, filtered source term from figure 3.2(b).



(d) Filter function 4, filtered source term from figure 3.2(b).



(e) Filter function 5, filtered source term from figure 3.2(b).

Figure B.1: Filtered diffusion source terms for $N=3$ fields.

B NUMERICAL TREATMENT

Filter 3 imposes a smooth filter. Both the filtered source term in figure B.1(c) and its derivatives are continuous. However, numerical integration remains challenging where the source term changes sign either side of a stable discontinuity (see figure 3.2), that is to say where the source term has negative gradient in regions $\Delta\psi/\varepsilon_p \rightarrow 0$. The solution was observed to oscillate about such points, resulting in increased computational times for no significant benefit.

Filters 4 and 5 impose smooth flat-bottomed filters designed to prevent oscillation of the solution about stable discontinuities. Both return a value $f(\Delta\psi/\varepsilon_p) = 0$ in the region $-1/3 < \Delta\psi/\varepsilon_p < 1/3$. In practice, filter 5 was observed to give better results for the test case in chapter 3 and is the filter depicted in figure 3.3. Filter 5 was used for all the general DQMoM-IEM solver cases reported in this thesis.

B.2 Estimation of the particle number distribution

This section outlines details of the method⁴ used to calculate the particle number distributions given in figure 5.3. The data are calculated from a stochastic population balance model that represents the population as a set of N equi-weighted stochastic particles in a sample volume V . Each stochastic particle has an associated collision diameter $D^{(n)}$. In the case of a spherical particle model such as in chapter 5, the collision diameter and actual particle diameter are equivalent.

The probability density function of the collision diameter $f(D)$ is estimated as a sum of log-normal distributions

$$f(D) = \frac{1}{N} \sum_{n=1}^N \frac{1}{D\sigma\sqrt{2\pi}} \exp\left(-\frac{(\ln D - \mu)^2}{2\sigma^2}\right), \quad (\text{B.1})$$

where the mean and standard deviation are given

$$\mu = \ln D^{(n)}, \quad (\text{B.2})$$

$$\sigma = 0.07. \quad (\text{B.3})$$

⁴ Sebastian Mosbach.

B.3 Method of moments coupling to Star-CD

The number density function $g(D) = dn/dD$ and $dn/d\ln D$ are calculated

$$g(D) = \frac{N}{V} f(D), \quad (\text{B.4})$$

$$\begin{aligned} \frac{dn}{d\ln D} &= D \frac{dn}{dD} \\ &= D g(D). \end{aligned} \quad (\text{B.5})$$

It is conventional to present the distribution in the form $dn/d\ln D$ because it is independent of the units of the collision diameter D as per the first line of equation (B.5). The standard deviation σ acts as a smoothing filter. It is assumed to be the same for each distribution in equation (B.1) and is treated as a parameter of the method. The value of the standard deviation in equation (B.2) is chosen to give reasonable smoothing without obscuring the features of the distribution. The choice of whether to plot the distribution against D on a linear or logarithmic scale is arbitrary. In the case of a linear scale, equation (B.1) should be replaced with a sum of normal distributions centred on each collision diameter $D^{(n)}$. Likewise, the mean and standard deviation in equation (B.2) should be adjusted accordingly.

B.3 Method of moments coupling to Star-CD

This section summarises the numerical treatment of the MoM scalar mixing cases used to validate the DQMoM-IEM, SF and PF methods in chapters 3, 4 and 5. The MoM transport equations (A.90) and (A.98) defined in appendix A are solved for the first four unmixed moments of each scalar λ_{m_α} , where $m_\alpha \in \{1, \dots, 4\}$ and $m_{\beta \neq \alpha} = 0$. The standard deviation $\sqrt{(\lambda_2 - \lambda_1)^2}$ is calculated in post processing. The micromixing source term $R_{\lambda_{m_\alpha}}^{\text{mx}}$ is defined by equation (A.97) and the chemical source term is zero, $S_\alpha = 0$ such that $R_{\lambda_{m_\alpha}}^{\text{rx}} = 0$. We start with the Favre-averaged case, then consider the constant density system as a special case. Note that the x - t dependencies of terms in this section are suppressed for clarity of presentation.

B NUMERICAL TREATMENT

B.3.1 Favre-averaged case

The Favre-averaged MoM transport equation (A.90) is solved as a transient problem using a [Strang \(1968\)](#) splitting analogous to that described in section 5.2.1

$$\frac{\partial \lambda_{m_\alpha}}{\partial t} = -\tilde{U}_i \frac{\partial \lambda_{m_\alpha}}{\partial x_i} + \frac{1}{\langle \rho \rangle} \frac{\partial}{\partial x_i} \left(\Gamma_T \frac{\partial \lambda_{m_\alpha}}{\partial x_i} \right), \quad (\text{B.6})$$

$$\frac{\partial \lambda_{m_\alpha}}{\partial t} = R_{\lambda_{m_\alpha}}^{\text{mx}}. \quad (\text{B.7})$$

Equation (B.6) is solved using Star-CD with upwind differencing to transport the moments λ_{m_α} as passive scalars with time step Δt , and equation (B.7) is solved with time step $\frac{1}{2}\Delta t$ before the first and after the last iteration, and time step Δt otherwise. Note that the splitting is not strictly necessary because $R_{\lambda_{m_\alpha}}^{\text{mx}}$ is in a form that can be supplied directly to Star-CD. However, the splitting is retained to ensure an equivalent implementation to that in chapters 3, 4 and 5.

The Star-CD version, turbulence model and model constants are the same as those described in each of chapters 3, 4 and 5. The initial and inlet boundary conditions are calculated as empirical moments of the conditions defined in each chapter

$$\lambda_{m_\alpha} \leftarrow \langle \phi_\alpha^{m_\alpha} \rangle_N, \quad \langle \phi_\alpha^{m_\alpha} \rangle_N = \sum_{n=1}^N w^{(n)} \psi_\alpha^{(n)m_\alpha}, \quad (\text{B.8})$$

where the weights are given $w^{(n)} = 1/N$ in the case of the SF method. Changes in the composition and temperature are optionally coupled to the flow field using the *weak pressure coupling* described in section 5.2.3, where the empirical means appearing in section 5.2.3 are replaced by their MoM equivalents and the mean temperature is estimated using the mean mass fraction and enthalpy.

The source terms for the unmixed moments $R_{\lambda_{m_\alpha}}^{\text{mx}}$ are defined as a special case of equation (A.97)

$$R_{\lambda_{m_\alpha}}^{\text{mx}} = \frac{C_\phi}{2\tau_\phi} m_\alpha \left(\lambda_1 \lambda_{m_\alpha-1} - \lambda_{m_\alpha} \right), \quad m_\alpha \in \mathbb{N}, m_{\beta \neq \alpha} = 0, \quad (\text{B.9})$$

B.3 Method of moments coupling to Star-CD

and equation (B.15) can be integrated numerically, for example using RADAU5, or solved analytically to give

$$\lambda_1(t + \Delta t) = \lambda_1, \quad (\text{B.10})$$

$$\lambda_2(t + \Delta t) = \lambda_1^2 + \exp\left(-\frac{2C_\phi}{2\tau_\phi} \Delta t\right) \left[\lambda_2 - \lambda_1^2\right], \quad (\text{B.11})$$

$$\begin{aligned} \lambda_3(t + \Delta t) = \lambda_1^3 + \exp\left(-\frac{2C_\phi}{2\tau_\phi} \Delta t\right) \left[3\lambda_2\lambda_1 - 3\lambda_1^3\right] \\ + \exp\left(-\frac{3C_\phi}{2\tau_\phi} \Delta t\right) \left[\lambda_3 - 3\lambda_2\lambda_1 + 2\lambda_1^3\right], \end{aligned} \quad (\text{B.12})$$

$$\begin{aligned} \lambda_4(t + \Delta t) = \lambda_1^4 + \exp\left(-\frac{2C_\phi}{2\tau_\phi} \Delta t\right) \left[6\lambda_2\lambda_1^2 - 6\lambda_1^4\right] \\ + \exp\left(-\frac{3C_\phi}{2\tau_\phi} \Delta t\right) \left[4\lambda_3\lambda_1 - 12\lambda_2\lambda_1^2 + 8\lambda_1^4\right] \\ + \exp\left(-\frac{4C_\phi}{2\tau_\phi} \Delta t\right) \left[\lambda_4 - 4\lambda_3\lambda_1 + 6\lambda_2\lambda_1^2 - 3\lambda_1^4\right]. \end{aligned} \quad (\text{B.13})$$

All the MoM data in this thesis were produced using the analytic implementation.

B.3.2 Constant density case

In the constant density case, the operator splitting is rewritten in terms of the constant density MoM transport equation (A.98)

$$\frac{\partial \lambda_{m_\alpha}}{\partial t} = -\langle U_i \rangle \frac{\partial \lambda_{m_\alpha}}{\partial x_i} + \frac{\partial}{\partial x_i} \left(\Gamma_T \frac{\partial \lambda_{m_\alpha}}{\partial x_i} \right), \quad (\text{B.14})$$

$$\frac{\partial \lambda_{m_\alpha}}{\partial t} = R_{\lambda_{m_\alpha}}^{\text{mx}}. \quad (\text{B.15})$$

Note that change in the interpretation of Γ_T as per section A.1.4. The treatment of equations (B.14) and (B.15) remains otherwise as per equations (B.6) and (B.7).

B.4 Summary of numerical methods

Figure B.2 shows the operator splittings used within the DQMoM-IEM / PF and SF implementations described in this thesis. **Table B.2** summarises the solution variables and the numerical methods used within each step.

The DQMoM-IEM, SF and PF methods are discussed in chapters 3, 4 and 5. The micromixing and diffusion steps are solved in terms of the compositions $\psi_\alpha^{(n)}$ to maximise the code that is shared between methods, and there is a change of variable between $s_\alpha^{(n)}$ and $\psi_\alpha^{(n)}$ before and after each DQMoM-IEM / PF step. The reaction steps are solved separately in terms of the molar concentrations $C_\alpha^{(n)}$, the number moments per unit volume $M_r^{(n)}$ and the temperature $T^{(n)}$ and there is a corresponding change of variables at the beginning and end of each reaction step. This avoids the need to calculate the temperature from the enthalpy at each evaluation of the reaction rates and is a particularly convenient choice for the non-constant density case, where it is straightforward to account for expansion of the gas-phase due to changes in temperature and composition (see section 5.2.2). The separate reaction step also leaves scope to refine the treatment of the method by applying alternative ODE solvers or tabulation algorithms, for example ISAT (Pope, 1997). The analytic DQMoM-IEM / PF and SF methods share the code used to solve the IEM micromixing step. All methods share the code used to solve the reaction step. This significantly helped debugging and validation.

B.4 Summary of numerical methods

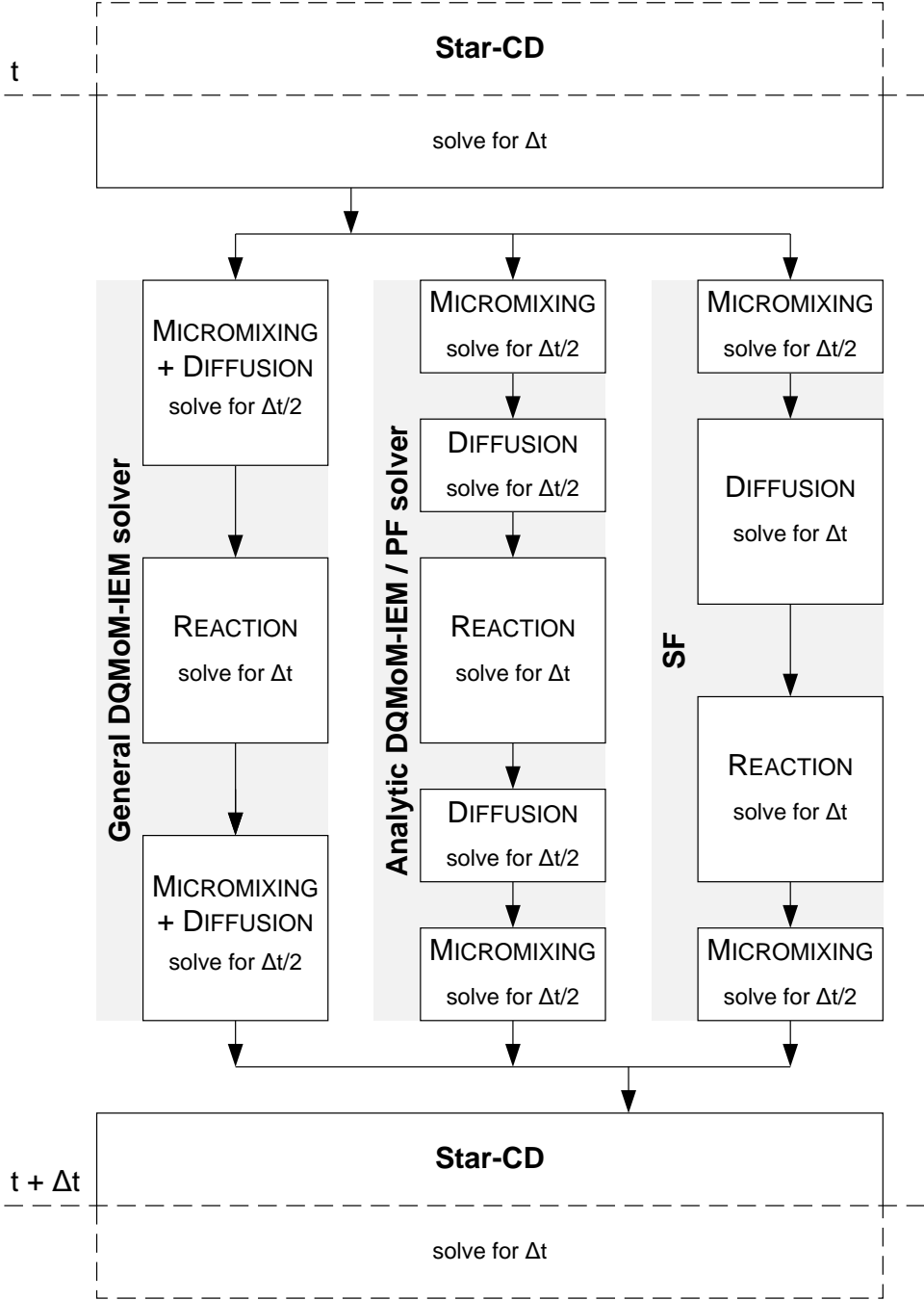


Figure B.2: Operator splittings used to implement DQMoM-IEM / PF and SF.

Table B.2: Summary of numerical methods.

Operator	Method	Solution variables	
Transport	Star-CD	U, p, k, ε SF: $\psi_\alpha^{(n)}$, DQMoM-IEM / PF: $w^{(n)}, s_\alpha^{(n)}$	
Analytic DQMoM-IEM			
Micromixing ^a Diffusion	Solved analytically	$\psi_\alpha^{(n)} = Y_\alpha^{(n)}, \alpha = 1, \dots, S$ $\langle \rho \rangle, \langle \mu \rangle, \psi_\alpha^{(n)} = \begin{cases} Y_\alpha^{(n)}, & \alpha = 1, \dots, S \\ M_r^{(n)} / \langle \rho \rangle, & \alpha = 1+s+r, r = 0, \dots, U-1 \\ h^{(n)}, & \alpha = 1+s+U \end{cases}$	Chapter 3, 4 Chapter 5
General DQMoM-IEM			
Micromixing Diffusion	RADAU5	$\psi_\alpha^{(n)} = Y_\alpha^{(n)}, \alpha = 1, \dots, S$	Chapter 3, 4
SF			
Micromixing ^a Diffusion	Solved analytically	$\psi_\alpha^{(n)} = Y_\alpha^{(n)}, \alpha = 1, \dots, S$	Chapter 3, 4
Reaction ^b	RADAU5	$C_\alpha^{(n)}$ $\langle \rho \rangle, \langle \mu \rangle, C_\alpha^{(n)}, M_r^{(n)}, T^{(n)}$	Chapter 3, 4 Chapter 5

^a The code used to solve the IEM micromixing operator is shared by the analytic DQMoM-IEM / PF and SF methods.

^b The code used to solve the reaction operator is shared by all methods.

Nomenclature

Upper-case Roman

A	Rate of radiative energy absorption
A	Surface area of the population per unit volume
A_i	Surface area of particle of size i
A_α	Chemical species α
C_i	Cunningham slip correction factor for particles of size i
C_α	Molar concentration of species α
C_ϕ	IEM micromixing model constant
D	Collision diameter
D_H	Hydraulic diameter
I	Number of elementary reactions
J^h	Specific energy flux
J^α	Diffusive flux of scalar α
K	Number of scalars
K_c, K_c'	Size-independent parts of $\beta_{i,j}^c$
K_f	Size-independent part of $\beta_{i,j}^f$
Kn	Knudsen number
L	Length scale
Le	Lewis number
M	Number of empirical moments
M_r	Moment of the number density distribution of order r

NOMENCLATURE

N	Number of fields
N	Number of stochastic particles
\mathbb{N}	Natural numbers (positive integers)
\mathbb{N}_0	Natural numbers (positive integers and zero)
N_A	Avagadro constant
N_{cells}	Number of cells in the CFD domain
$\mathcal{N}(\mu, \sigma)$	Normal distribution with mean μ and variance σ^2
R	Universal gas constant
\mathbb{R}	Real numbers
R_i	Rate of reaction i
R_λ	Source term of moment λ
Re	Reynolds number
S_h	Specific enthalpy source term
S_α	Source term of scalar α
$S_{\Delta t}$	Solution operator for an evolution equation
T	Temperature
U	Number of MoMIC number density moments
U	Eulerian velocity
\tilde{U}	Favre-averaged Eulerian velocity
V	Volume
W	Wiener process, see Gardiner (2004)
W_α	Relative molecular mass of species α
Y	Yield
Y_α	Mass fraction of species α
\mathbb{Z}	Integer numbers (positive, negative and zero)

Lower-case Roman

$a^{(n)}$	Source term for the weights $w^{(n)}$
$b_\alpha^{(n)}$	Source term for the weighted compositions $s_\alpha^{(n)}$

NOMENCLATURE

c_p	Specific heat capacity at constant pressure
$c_{\alpha\beta}^{(n)}$	Turbulent diffusion-spatial gradient term for scalars α and β
d	Mean particle diameter
d_i	Diameter of particle of size i
$f(\Delta\psi/\varepsilon_p)$	Filter function
$f_b(\psi, b_{dx})$	Bounding function
$f_p(\Delta\psi)$	Particle function
f_v	Particle volume fraction
${}^m f_{x,y}$	Grid function
f_ϕ	Joint composition PDF of ϕ
\tilde{f}_ϕ	Favre-averaged joint composition PDF of ϕ
g	Body force per unit mass
g	Number density function
h	Specific enthalpy
k	Turbulent kinetic energy
k_B	Boltzmann constant
k_i	Rate constant of reaction i
k_s	Rate constant for surface growth reaction
l	Mixing length
m_i	Mass of particle of size i
m_α	Moment order of scalar α
$m_{\lambda\alpha}$	Moment order of the λ^{th} empirical moment of scalar α
n	Number of moles
n	Total number density
n_i	Number density of particles of size i
p	Pressure
r	Moment order of the number density moment M_r
r_i	Radius of particle of size i
$r_\alpha^{(n)}$	Micromixing and chemical source term
s	Number of species

NOMENCLATURE

$s_\alpha^{(n)}$	Weighted composition of scalar α
t	Time
u'	Fluctuating velocity field $u' = U - \langle U \rangle$
u''	Fluctuating velocity field $u'' = U - \tilde{U}$
$w^{(n)}$	Weight
x	Position

Upper-case Greek

Γ	Thermal diffusivity
Γ_T	Turbulent diffusivity

Lower-case Greek

$\beta_{i,j}$	Frequency factor for collisions between particles of size i and j
γ	Rate of gas-phase expansion
δ	Dirac delta function
δ_{ij}	Kronecker delta
ε	Rate of radiative energy emission
ε_{m_α}	Convergence metric for the empirical moment $\langle \phi_\alpha^{m_\alpha} \rangle_N$
$\varepsilon_{\text{mean}}$	Convergence metric for the empirical mean
ε_{sd}	Convergence metric for the empirical standard deviation
ε	Turbulent dissipation rate
ε_b	Bounding function clipping distance
ε_p	Particle function filter half-width
ε_{ij}	Enhancement factor for collisions between particles of size i and j
λ	Mean free path
λ	Thermal conductivity
λ	Moment of the joint composition PDF f_ϕ
μ	Absolute viscosity

$\mu_{i,j}$	Reduced mass of particles of size i and j
μ_r	Reduced moment of the population number density, $\mu_r = M_r/M_0$
ν	Kinematic viscosity
ν_T	Turbulent viscosity
ν_α	Stoichiometric coefficient of species α
$\xi_i^{(n)}$	Variate relating to direction i and field n
ρ	Density
σ	Standard deviation of the particle diameter
σ_T	Turbulent Schmidt / Prandtl number
τ_{ij}	Stress tensor
τ_ϕ	IEM micromixing model mixing time
ϕ	Eulerian scalar composition
$\tilde{\phi}$	Favre-averaged Eulerian scalar composition
ϕ'	Fluctuating scalar field $\phi' = \phi - \langle \phi \rangle$
ϕ''	Fluctuating scalar field $\phi'' = \phi - \tilde{\phi}$
ψ	Sample space variable corresponding to ϕ

Superscripts

f	Denotes the forward reaction
n	Denotes the n^{th} field
r	Denotes the reverse reaction

Subscripts

c	Denotes the continuum regime
cg	Denotes coagulation
dx	Denotes the diffusion term
f	Denotes the free molecular regime
g	Denotes the gas-phase

NOMENCLATURE

glb	Denotes a global lower bound
gub	Denotes a global upper bound
in	Denotes inception
lb	Denotes a lower bound
mx	Denotes the micromixing term
nb	Denotes a neighbour cell
rx	Denotes the reaction term
s	Denotes the solid-phase
sg	Denotes surface growth
ub	Denotes a upper bound

Symbols

\top	Transpose operator
∇	Gradient operator
∇^2	Laplacian operator
$ \cdot $	Absolute value
$\ \cdot\ $	L^2 -norm
$[\cdot]$	Molar concentration
$\lfloor x \rfloor$	Floor, $\lfloor x \rfloor = \max\{m \in \mathbb{Z} \mid m \leq x\}$
$\lceil x \rceil$	Ceiling, $\lceil x \rceil = \min\{n \in \mathbb{Z} \mid n \geq x\}$
$[a, b]$	Interval, $[a, b] = \{x \in \mathbb{R} \mid a \leq x \leq b\}$
$\mathbb{P}(\cdot)$	Probability
$\langle \cdot \rangle$	Expectation
$\langle \cdot^2 \rangle$	Expected second moment
$\langle \cdot'^2 \rangle$	Expected variance
$\langle \cdot \psi \rangle$	Expectation conditioned on $\phi = \psi$
$\langle \cdot \rangle_{\text{MoM}}$	Expectation calculated using the method of moments
$\langle \cdot \rangle_N$	Empirical expectation calculated over N fields

Abbreviations

CPU	Central processing unit
CFD	Computational fluid dynamics
DNS	Direct numerical simulation
DQMoM	Direct quadrature method of moments
GDP	Gross domestic product
IEM	Interaction by exchange with the mean
ISAT	<i>In situ</i> adaptive tabulation
LES	Large-eddy simulation
LMSE	Linear mean-square estimation
MEPDF	Multi-environment probability density function
MoM	Method of moments
MoMIC	Method of moments with interpolative closure
ODE	Ordinary differential equation
PBE	Population balance equation
PDE	Partial differential equation
PDF	Probability density function
PF	Projected fields method
QMoM	Quadrature method of moments
RANS	Reynolds-averaged Navier-Stokes
SF	Stochastic fields method
SPDE	Stochastic partial differential equation
TI	Turbulence intensity

Bibliography

- Acheson, D. J. (1990). *Elementary Fluid Dynamics*. Oxford University Press, Oxford.
- Ahrens, J. H., Dieter, U. (1973). Extensions of Forsythe's method for random sampling from the normal distribution. *Mathematics of Computation* **27** (124), 927–937. URL <http://www.jstor.org/stable/2005527>.
- Akroyd, J., Smith, A., McGlashan, L. R., Kraft, M. (2010). Numerical investigation of DQMoM-IEM as a turbulent reaction closure. *Chemical Engineering Science* **65** (6), 1915–1924. doi:[10.1016/j.ces.2009.11.010](https://doi.org/10.1016/j.ces.2009.11.010).
- Ali, S., Vikhansky, A., Løvås, T. (2011). Direct quadrature conditional moment closure for modelling of turbulent combustion. *Flow, Turbulence and Combustion*, in press. doi:[10.1007/s10494-010-9318-8](https://doi.org/10.1007/s10494-010-9318-8).
- Allen, A., Gergely, J. S. (1998). Process for the addition of boron in a TiO₂ manufacturing process. U.S. Patent 5,728,205. URL <http://www.google.com/patents/?id=3iAaAAAAEBAJ>.
- Appel, J., Bockhorn, H., Frenklach, M. (2000). Kinetic modeling of soot formation with detailed chemistry and physics: Laminar premixed flames of C₂ hydrocarbons. *Combustion and Flame* **121** (1–2), 122–136. doi:[10.1016/S0010-2180\(99\)00135-2](https://doi.org/10.1016/S0010-2180(99)00135-2).
- Balthasar, M. (2000). Detailed soot modelling in laminar and turbulent reacting flows. Ph.D. thesis, Lund Institute of Technology.
- Balthasar, M., Frenklach, M. (2005). Detailed kinetic modeling of soot aggregate formation in laminar premixed flames. *Combustion and Flame* **140** (1–2), 130–145. doi:[10.1016/j.combustflame.2004.11.004](https://doi.org/10.1016/j.combustflame.2004.11.004).

BIBLIOGRAPHY

- Balthasar, M., Kraft, M. (2003). A stochastic approach to calculate the particle size distribution function of soot particles in laminar premixed flames. *Combustion and Flame* **133** (3), 289–298. doi:[10.1016/S0010-2180\(03\)00003-8](https://doi.org/10.1016/S0010-2180(03)00003-8).
- Balthasar, M., Mauss, F., Knobel, A., Kraft, M. (2002). Detailed modeling of soot formation in a partially stirred plug flow reactor. *Combustion and Flame* **128** (4), 395–409. doi:[10.1016/S0010-2180\(01\)00344-3](https://doi.org/10.1016/S0010-2180(01)00344-3).
- Boulos, M. I., Jurewicz, J. W., Nessim, C. A. A. M. (2002). Plasma synthesis of metal oxide nanopowder and apparatus therefor. U.S. Patent 6,994,837. URL <http://www.google.com/patents?id=VWx3AAAAEBAJ>.
- Bourne, J. R., Rys, P. (1981). Mixing and fast chemical reaction—I: Test reactions to determine segregation. *Chemical Engineering Science* **36** (10), 1643–1648. doi:[10.1016/0009-2509\(81\)80008-5](https://doi.org/10.1016/0009-2509(81)80008-5).
- Boyle, P., Brodie, M., Glasserman, P. (1997). Monte Carlo methods for security pricing. *Journal of Economic Dynamics and Control* **21** (8–9), 1267–1321. doi:[10.1016/S0165-1889\(97\)00028-6](https://doi.org/10.1016/S0165-1889(97)00028-6).
- Büchel, K. H., Moretto, H.-H., Woditsch, P. (2000). *Industrial Inorganic Chemistry* (translated by D. R. Terrell), 2nd edition, ch. 5, pp. 553–558. Wiley-VCH, Weinheim.
- Buckingham, D. A., Gambogi, J. (2006). Titanium dioxide end-use statistics. *Survey data*, U.S. Geological Survey, downloadable from <http://minerals.usgs.gov/ds/2005/140/> in either pdf or xls format.
- Buesser, B., Heine, M. C., Pratsinis, S. E. (2009). Coagulation of highly concentrated aerosols. *Journal of Aerosol Science* **40** (2), 89–100. doi:[10.1016/j.jaerosci.2008.09.005](https://doi.org/10.1016/j.jaerosci.2008.09.005).
- Cant, S. R., Mastorakos, E. (2008). *An Introduction to Turbulent Reacting Flows*. Imperial College Press, London.
- CD-adapco (2008). Star-CD v4.08.006. URL <http://www.cd-adapco.com/>.
- CD-adapco (2009). Star-CD v4.12.003. URL <http://www.cd-adapco.com/>.
- Celnik, M. S., Patterson, R. I. A., Kraft, M., Wagner, W. (2007). Coupling a stochastic soot population balance to gas-phase chemistry using operator splitting. *Combustion and Flame* **148** (3), 158–176. doi:[10.1016/j.combustflame.2006.10.007](https://doi.org/10.1016/j.combustflame.2006.10.007).

BIBLIOGRAPHY

- Celnik, M. S., Patterson, R. I. A., Kraft, M., Wagner, W. (2009). A predictor-corrector algorithm for the coupling of stiff ODEs to a particle population balance. *Journal of Computational Physics* **228** (8), 2758–2769. doi:[10.1016/j.jcp.2008.12.030](https://doi.org/10.1016/j.jcp.2008.12.030).
- Cheng, R. C. H. (1982). The use of antithetic variates in computer simulations. *Journal of the Operational Research Society* **33** (3), 229–237. URL <http://www.jstor.org/stable/2581487>.
- Chittipotula, T., Janiga, G., Thévenin, D. (2011). Improved soot prediction models for turbulent non-premixed ethylene/air flames. In *Proceedings of the Combustion Institute*, vol. 33, pp. 559–567. The Combustion Institute. doi:[10.1016/j.proci.2010.06.102](https://doi.org/10.1016/j.proci.2010.06.102).
- Curl, R. L. (1963). Dispersed phase mixing: I. theory and effects in simple reactors. *AIChE Journal* **9** (2), 175–181. doi:[10.1002/aic.690090207](https://doi.org/10.1002/aic.690090207).
- Deberry, J. C., Robinson, M., Pomponi, M. D., Beach, A. J., Xiong, Y., Akhtar, K. (2002). Controlled vapor phase oxidation of titanium tetrachloride to manufacture titanium dioxide. U.S. Patent 6,387,347 B1. URL <http://www.google.com/patents/?id=r3gKAAAEBAJ>.
- Denison, M., Borodai, S., Fox, R., Bockelie, M. (2010). Multi-environment probability density function method for modeling turbulent combustion in industrial equipment. In *IMECE2009: Proceedings of the ASME 2009 International Mechanical Engineering Congress & Exposition*, vol. 3, pp. 143–149. doi:[10.1115/IMECE2009-12061](https://doi.org/10.1115/IMECE2009-12061).
- Desjardins, O., Fox, R. O., Villedieu, P. (2008). A quadrature-based moment method for dilute fluid-particle flows. *Journal of Computational Physics* **227** (4), 2514–2539. doi:[10.1016/j.jcp.2007.10.026](https://doi.org/10.1016/j.jcp.2007.10.026).
- Dopazo, C. (1994). Recent developments in PDF methods. In [Libby and Williams \(1994\)](#), ch. 7, pp. 375–474.
- Dopazo, C., O'Brien, E. E. (1974). An approach to the autoignition of a turbulent mixture. *Acta Astronautica* **1** (9–10), 1239–1266. doi:[10.1016/0094-5765\(74\)90050-2](https://doi.org/10.1016/0094-5765(74)90050-2).

BIBLIOGRAPHY

- DuPont Titanium Technologies (2002). Mechanisms for light scattering. URL http://www2.dupont.com/Titanium_Technologies/en_US/tech_info/literature/Paper/PA_B_Mechanism_for_Light_Scattering.pdf.
- DuPont Titanium Technologies (2007). DuPont™ Ti-Pure® titanium dioxide—Polymers, light and the science of TiO₂ (H-88382-6). URL http://www2.dupont.com/Titanium_Technologies/en_US/tech_info/literature/Plastics/PL_B_Polymers_Light_Science.pdf.
- Eibeck, A., Wagner, W. (2000). An efficient stochastic algorithm for studying coagulation dynamics and gelation phenomena. *SIAM Journal of Scientific Computing* **22** (3), 802–821. doi:[10.1137/S1064827599353488](https://doi.org/10.1137/S1064827599353488).
- Eibeck, A., Wagner, W. (2001). Stochastic particle approximations for Smoluchoski's coagulation equation. *Annals of Applied Probability* **11** (4), 1137–1165. doi:[10.1214/aoap/1015345398](https://doi.org/10.1214/aoap/1015345398).
- Eibeck, A., Wagner, W. (2003). Stochastic interacting particle systems and nonlinear kinetic equations. *Annals of Applied Probability* **13** (3), 845–889. doi:[10.1214/aoap/1060202829](https://doi.org/10.1214/aoap/1060202829).
- Fan, R., Fox, R. O. (2008). Segregation in polydisperse fluidized beds: Validation of a multi-fluid model. *Chemical Engineering Science* **63** (1), 272–285. doi:[10.1016/j.ces.2007.09.038](https://doi.org/10.1016/j.ces.2007.09.038).
- Fan, R., Marchisio, D. L., Fox, R. O. (2004). Application of the direct quadrature method of moments to polydisperse gas-solid fluidized beds. *Powder Technology* **139** (1), 7–20. doi:[10.1016/j.powtec.2003.10.005](https://doi.org/10.1016/j.powtec.2003.10.005).
- Fishman, G. S. (1996). *Monte Carlo: Concepts, Algorithms and Applications*. Springer-Verlag, New York.
- Fishman, G. S., Huang, B. D. (1983). Antithetic variates revisited. *Communications of the ACM* **26** (11), 964–971. doi:[10.1145/182.358462](https://doi.org/10.1145/182.358462).
- Fissore, D., Marchisio, D. L., Barresi, A. A. (2002). On the comparison between probability density function models for CFD applications. *The Canadian Journal of Chemical Engineering* **80** (4), 1–11. doi:[10.1002/cjce.5450800412](https://doi.org/10.1002/cjce.5450800412).
- Fox, R. O. (2003). *Computational Models for Turbulent Reacting Flows*. Cambridge University Press, Cambridge.

- Fox, R. O. (2006a). Bivariate direct quadrature method of moments for coagulation and sintering of particle populations. *Journal of Aerosol Science* **37** (11), 1562–1580. doi:[10.1016/j.jaerosci.2006.03.005](https://doi.org/10.1016/j.jaerosci.2006.03.005).
- Fox, R. O. (2006b). CFD models for analysis and design of chemical reactors. In Marin, G. B. (Ed.), *Advances in Chemical Engineering*, vol. 31, ch. 4, pp. 231–305. Academic Press, London. doi:[10.1016/S0065-2377\(06\)31004-6](https://doi.org/10.1016/S0065-2377(06)31004-6).
- Fox, R. O. (2008). A quadrature-based third-order moment method for dilute gas-particle flows. *Journal of Computational Physics* **227** (12), 6313–6350. doi:[10.1016/j.jcp.2008.03.014](https://doi.org/10.1016/j.jcp.2008.03.014).
- Fox, R. O., Laurent, F., Massot, M. (2008). Numerical simulation of spray coalescence in an Eulerian framework: Direct quadrature method of moments and multi-fluid method. *Journal of Computational Physics* **227** (6), 3058–3088. doi:[10.1016/j.jcp.2007.10.028](https://doi.org/10.1016/j.jcp.2007.10.028).
- Fox, R. O., Raman, V. (2004). A multienvironment conditional probability density function model for turbulent reacting flows. *Physics of Fluids* **16** (2), 4551–4565. doi:[10.1063/1.1807771](https://doi.org/10.1063/1.1807771).
- Frenklach, M. (2002). Method of moments with interpolative closure. *Chemical Engineering Science* **57** (12), 2229–2239. doi:[10.1016/S0009-2509\(02\)00113-6](https://doi.org/10.1016/S0009-2509(02)00113-6).
- Frenklach, M., Harris, S. J. (1987). Aerosol dynamics modeling using the method of moments. *Journal of Colloid and Interface Science* **118** (1), 252–261. doi:[10.1016/0021-9797\(87\)90454-1](https://doi.org/10.1016/0021-9797(87)90454-1).
- Fujishima, A., Hashimoto, K., Watanabe, T. (1999). *TiO₂ Photocatalysis: Fundamentals and Applications*. BKC Inc., Tokyo.
- Gardiner, C. W. (2004). *Handbook of Stochastic Methods*, 3rd edition. Springer, Berlin.
- Garmory, A. (2007). Micromixing effects in atmospheric reacting flows. Ph.D. thesis, University of Cambridge.
- Garmory, A., Britter, R. E., Mastorakos, E. (2008). Simulation of the evolution of aircraft exhaust plumes including detailed chemistry and segregation. *Journal of Geophysical Research* **113**, D08308. doi:[10.1029/2007JD009104](https://doi.org/10.1029/2007JD009104).

BIBLIOGRAPHY

- Garmory, A., Kim, I. S., Britter, R. E., Mastorakos, E. (2009). Simulations of the dispersion of reactive pollutants in a street canyon, considering different chemical mechanisms and micromixing. *Atmospheric Environment* **43** (31), 4670–4680. doi:[10.1016/j.atmosenv.2008.07.033](https://doi.org/10.1016/j.atmosenv.2008.07.033).
- Garmory, A., Mastorakos, E. (2008). Aerosol nucleation and growth in a turbulent jet using the Stochastic Fields method. *Chemical Engineering Science* **63** (26), 4078–4089. doi:[10.1016/j.ces.2008.05.012](https://doi.org/10.1016/j.ces.2008.05.012).
- Garmory, A., Richardson, E. S., Mastorakos, E. (2006). Micromixing effects in a reacting plume by the Stochastic Fields method. *Atmospheric Environment* **40** (6), 1078–1091. doi:[10.1016/j.atmosenv.2005.11.002](https://doi.org/10.1016/j.atmosenv.2005.11.002).
- Gavi, E., Marchisio, D. L., Baressi, A. A. (2007a). CFD modelling and scale-up of confined impinging jet reactors. *Chemical Engineering Science* **62** (8), 2228–2241. doi:[10.1016/j.ces.2006.12.077](https://doi.org/10.1016/j.ces.2006.12.077).
- Gavi, E., Rivautella, L., Marchisio, D. L., Vanni, M., Baressi, A. A., Baldi, G. (2007b). CFD modelling of nano-particle precipitation in confined impinging jet reactors. *Chemical Engineering Research and Design* **85** (A5 Special Issue: 12th European Conference on Mixing), 1–10. doi:[10.1205/cherd06176](https://doi.org/10.1205/cherd06176).
- Geweke, J. (1988). Antithetic acceleration of Monte Carlo integration in Bayesian inference. *Journal of Econometrics* **38** (1–2), 73–89. doi:[10.1016/0304-4076\(88\)90027-9](https://doi.org/10.1016/0304-4076(88)90027-9).
- Ghoshtagore, R. N. (1970). Mechanism of heterogeneous deposition of thin film rutile. *Journal of the Electrochemical Society* **117** (4), 529–534. doi:[10.1149/1.2407561](https://doi.org/10.1149/1.2407561).
- Goodson, M., Kraft, M. (2002). An efficient stochastic algorithm for simulating nano-particle dynamics. *Journal of Computational Physics* **183** (1), 210–232. doi:[10.1006/jcph.2002.7192](https://doi.org/10.1006/jcph.2002.7192).
- Grant, S., Freer, A. A., Winfield, J. M., Gray, C., Overton, T. L., Lennon, D. (2004). An undergraduate teaching exercise that explores contemporary issues in the manufacture of titanium dioxide on the industrial scale. *Green Chemistry* **6**, 25–32. doi:[10.1039/b309878h](https://doi.org/10.1039/b309878h).
- Grosch, R., Briesen, H., Marquardt, W., Wulkow, M. (2007). Generalization and numerical investigation of QMOM. *AIChE Journal* **53** (1), 207–227. doi:[10.1002/aic.11041](https://doi.org/10.1002/aic.11041).

BIBLIOGRAPHY

- Grosschmidt, D., Bockhorn, H., Goodson, M., Kraft, M. (2002). Two approaches to the simulation of silica particle synthesis. In *Proceedings of the Combustion Institute*, vol. 29, pp. 1039–1046. The Combustion Institute. doi:[10.1016/S1540-7489\(02\)80131-6](https://doi.org/10.1016/S1540-7489(02)80131-6).
- Haddow, A. J. (1997). Oxidation of titanium tetrachloride to form titanium dioxide. U.S. Patent 5,599,519. URL <http://www.google.com/patents/?id=8WMdAAAAEBAJ>.
- Hairer, E., Wanner, G. (1996). *Solving Ordinary Differential Equations II. Stiff and Differential-Algebraic Problems*, 2nd revised edition, vol. 14 of Springer Series in Computational Mathematics. Springer Verlag, Berlin.
- Hammersley, J. M., Handscomb, D. C. (1958). Proof of the antithetic variates theorem for $n > 2$. *Mathematical Proceedings of the Cambridge Philosophical Society* **54** (2), 300–301. doi:[10.1017/S0305004100033454](https://doi.org/10.1017/S0305004100033454).
- Hammersley, J. M., Mauldon, J. G. (1956). General principles of antithetic variates. *Mathematical Proceedings of the Cambridge Philosophical Society* **52** (3), 476–481. doi:[10.1017/S0305004100031467](https://doi.org/10.1017/S0305004100031467).
- Hammersley, J. M., Morton, K. W. (1956). A new Monte Carlo technique: antithetic variates. *Mathematical Proceedings of the Cambridge Philosophical Society* **52** (3), 449–475. doi:[10.1017/S0305004100031455](https://doi.org/10.1017/S0305004100031455).
- Hartmann, A. (1996). Process for the use of rutile promoter and control additives in the manufacture of titanium dioxide by the chloride process. U.S. Patent 5,536,487. URL http://www.google.com/patents?id=S_sZAAAAEBAJ.
- Hauke, G., Valiño, L. (2004). Computing reactive flows with a field Monte Carlo formulation and multi-scale methods. *Computer methods in applied mechanics and engineering* **193** (15–16), 1455–1470. doi:[10.1016/j.cma.2003.12.033](https://doi.org/10.1016/j.cma.2003.12.033).
- Haworth, D. C. (2010). Progress in probability density function methods for turbulent reacting flows. *Progress in Energy and Combustion Science* **36** (2), 168–259. doi:[10.1016/j.peccs.2009.09.003](https://doi.org/10.1016/j.peccs.2009.09.003).
- Heine, M. C., Pratsinis, S. E. (2007a). Polydispersity of primary particles in agglomerates made by coagulation and sintering. *Journal of Aerosol Science* **38** (1), 17–38. doi:[10.1016/j.jaerosci.2006.09.005](https://doi.org/10.1016/j.jaerosci.2006.09.005).

BIBLIOGRAPHY

- Heine, M. C., Pratsinis, S. E. (2007b). Agglomerate TiO₂ aerosol dynamics at high concentrations. *Particle & Particle Systems Characterization* **24** (1), 56–65. doi:[10.1002/ppsc.200601076](https://doi.org/10.1002/ppsc.200601076).
- Heine, M. C., Pratsinis, S. E. (2007c). Brownian coagulation at high concentration. *Langmuir* **23** (19), 9882–9890. doi:[10.1021/la7012599](https://doi.org/10.1021/la7012599).
- Hill, S. (2009). The future of titanium dioxide, market forecasts to 2016. *Market report*, Pira International. URL <http://www.intertechpira.com/Core/DownloadDoc.aspx?documentID=2875>.
- Hulbert, H. M., Katz, S. (1964). Some problems in particle technology: A statistical mechanical formulation. *Chemical Engineering Science* **19** (8), 555–574. doi:[10.1016/0009-2509\(64\)85047-8](https://doi.org/10.1016/0009-2509(64)85047-8).
- ICIS (2011). Titanium Dioxide (TiO₂) Production and Manufacturing Process. URL <http://www.icis.com/v2/chemicals/9076547/titanium-dioxide/process.html>.
- Johannessen, T., Pratsinis, S. E., Livbjerg, H. (2001). Computational analysis of coagulation and coalescence in the flame synthesis of titania particles. *Powder Technology* **118** (3), 242–250. doi:[10.1016/S0032-5910\(00\)00401-0](https://doi.org/10.1016/S0032-5910(00)00401-0).
- Jones, W. P. (1994). Turbulence modelling and numerical solution methods. In [Libby and Williams \(1994\)](#), ch. 6, pp. 309–374.
- Jones, W. P., Navarro-Martinez, S. (2007). Large eddy simulation of autoignition with a subgrid probability density function method. *Combustion and Flame* **150** (3), 170–187. doi:[10.1016/j.combustflame.2007.04.003](https://doi.org/10.1016/j.combustflame.2007.04.003).
- Jones, W. P., Navarro-Martinez, S. (2009). Numerical study of n-heptane auto-ignition using LES-PDF methods. *Flow, Turbulence and Combustion* **83** (3), 407–423. doi:[10.1007/s10494-009-9228-9](https://doi.org/10.1007/s10494-009-9228-9).
- Jones, W. P., Navarro-Martinez, S., Röhl, O. (2007). Large eddy simulation of hydrogen auto-ignition with a probability density function method. In *Proceedings of the Combustion Institute*, vol. 31, pp. 1765–1771. The Combustion Institute. doi:[10.1016/j.proci.2006.07.041](https://doi.org/10.1016/j.proci.2006.07.041).
- Jones, W. P., Prasad, V. N. (2010). Large Eddy Simulation of the Sandia Flame Series (D–F) using the Eulerian stochastic field method. *Combustion and Flame* **157** (9), 1621–1636. doi:[10.1016/j.combustflame.2010.05.010](https://doi.org/10.1016/j.combustflame.2010.05.010).

BIBLIOGRAPHY

- Jones, W. P., Prasad, V. N. (2011). LES-pdf simulation of a spark ignited turbulent methane jet. In *Proceedings of the Combustion Institute*, vol. 33, pp. 1355–1363. The Combustion Institute. doi:[10.1016/j.proci.2010.06.076](https://doi.org/10.1016/j.proci.2010.06.076).
- Jones, W. P., Tyliczszak, A. (2010). Large eddy simulation of spark ignition in a gas turbine combustor. *Flow, Turbulence and Combustion* **85** (3–4), 711–734. doi:[10.1007/s10494-010-9289-9](https://doi.org/10.1007/s10494-010-9289-9).
- Kee, J., Grcar, K., Smooke, M. D., Miller, J. A. (1985). A Fortran program for modelling steady laminar one-dimensional premixed flames. *Sandia report SAND85-8240*, Sandia National Laboratories.
- Klimenko, A. Y., Bilger, R. W. (1999). Conditional moment closure for turbulent combustion. *Progress in Energy and Combustion Science* **25** (6), 595–687. doi:[10.1016/S0360-1285\(99\)00006-4](https://doi.org/10.1016/S0360-1285(99)00006-4).
- Kloeden, P. E., Platen, E. (1995). *Numerical Solution of Stochastic Differential Equations*, 2nd corrected printing edition. Springer, Berlin.
- Kollmann, W. (1990). The PDF approach to turbulent flow. *Theoretical and Computational Fluid Dynamics* **1** (5), 249–285. doi:[10.1007/BF00271582](https://doi.org/10.1007/BF00271582).
- Krchma, I. J., Schaumann, H. H. (1951). Production of titanium dioxide. U.S. Patent 2,559,638. URL <http://www.google.com/patents/about?id=au5IAAAAEBAJ&dq=2559638>.
- Levenspiel, O. (1999). *Chemical Reaction Engineering*, 3rd edition. John Wiley & Sons, New York.
- Li, K. T., Toor, H. L. (1986). Turbulent reactive mixing with a series-parallel reaction: Effect of mixing on yield. *AIChE Journal* **32** (8), 1312–1320. doi:[10.1002/aic.690320809](https://doi.org/10.1002/aic.690320809).
- Libby, P. A., Williams, F. A. (1980). *Turbulent Reacting Flows*. Springer-Verlag, Berlin.
- Libby, P. A., Williams, F. A. (1994). *Turbulent Reacting Flows*. Academic Press Limited, London.
- Lindstedt, R. P., Louloudi, S. A. (2005). Joint-scalar transported PDF modeling of soot formation and oxidation. In *Proceedings of the Combustion Institute*, vol. 30, pp. 775–783. The Combustion Institute. doi:[10.1016/j.proci.2004.08.080](https://doi.org/10.1016/j.proci.2004.08.080).

BIBLIOGRAPHY

- Liu, B. J. D., Pope, S. B. (2005). The performance of *in situ* adaptive tabulation in computations of turbulent flames. *Combustion Theory and Modelling* **9** (4), 549–568. doi:[10.1080/13647830500307436](https://doi.org/10.1080/13647830500307436).
- Lu, L., Pope, S. B. (2009). An improved algorithm for *in situ* adaptive tabulation. *Journal of Computational Physics* **228** (2), 361–386. doi:[10.1016/j.jcp.2008.09.015](https://doi.org/10.1016/j.jcp.2008.09.015).
- Lui, Y., Fox, R. O. (2006). CFD predictions for chemical processing in a confined impinging-jets reactor. *AIChE Journal* **52** (2), 731–744. doi:[10.1002/aic.10633](https://doi.org/10.1002/aic.10633).
- Magnussen, B. F., Hjertager, B. H. (1977). On mathematical modeling of turbulent combustion with special emphasis on soot formation and combustion. In *Proceedings of the Combustion Institute*, vol. 16, pp. 719–729. The Combustion Institute. doi:[10.1016/S0082-0784\(77\)80366-4](https://doi.org/10.1016/S0082-0784(77)80366-4).
- Marchisio, D. L. (2009). Large eddy simulation of mixing and reaction in a confined impinging jets reactor. *Computers and Chemical Engineering* **33** (2), 408–420. doi:[10.1016/j.compchemeng.2008.11.009](https://doi.org/10.1016/j.compchemeng.2008.11.009).
- Marchisio, D. L., Fox, R. O. (2005). Solution of population balance equations using the direct quadrature method of moments. *Journal of Aerosol Science* **36** (1), 43–73. doi:[10.1016/j.jaerosci.2004.07.009](https://doi.org/10.1016/j.jaerosci.2004.07.009).
- Marchisio, D. L., Soos, M., Sefcik, J., Morbidelli, M. (2006). Role of turbulent shear rate distribution in aggregation and breakage processes. *AIChE Journal* **52** (1), 158–173. doi:[10.1002/aic.10614](https://doi.org/10.1002/aic.10614).
- Matsumoto, M., Nishimura, T. (1998). Mersenne Twister: A 623-dimensionally equidistributed uniform pseudo-random number generator. *ACM Transactions on Modeling and Computer Simulation* **8** (1), 3–30. doi:[10.1145/272991.272995](https://doi.org/10.1145/272991.272995).
- McGraw, R. (1997). Description of aerosol dynamics by the quadrature method of moments. *Aerosol Science and Technology* **27** (2), 255–349. doi:[10.1080/02786829708965471](https://doi.org/10.1080/02786829708965471).
- Mehta, M., Sung, Y., Raman, V., Fox, R. O. (2010). Multiscale modeling of TiO₂ nanoparticle production in flame reactors: Effect of chemical mechanism. *Industrial & Engineering Chemistry Research* **49** (21), 10663–10673. doi:[10.1021/ie100560h](https://doi.org/10.1021/ie100560h).

- Moody, E. G., Collins, L. R. (2003). Effect of mixing on the nucleation and growth of titania particles. *Aerosol Science and Technology* **37** (5), 403–424. doi:[10.1080/02786820300979](https://doi.org/10.1080/02786820300979).
- Morgan, E. R. (2008). Solar water purification with PET bottles coated with titanium dioxide using improved binding agents. Ph.D. thesis, University of Massachusetts Lowell.
- Morgan, N., Kraft, M., Balthasar, M., Wong, D., Frenklach, M., Mitchell, P. (2007). Numerical simulations of soot aggregation in premixed laminar flames. In *Proceedings of the Combustion Institute*, vol. 31, pp. 693–700. The Combustion Institute. doi:[10.1016/j.proci.2006.08.021](https://doi.org/10.1016/j.proci.2006.08.021).
- Morgan, N., Wells, C., Kraft, M., Wagner, W. (2005). Modelling nanoparticle dynamics: coagulation, sintering, particle inception and surface growth. *Combustion Theory and Modelling* **9** (3), 449–461. doi:[10.1080/13647830500277183](https://doi.org/10.1080/13647830500277183).
- Morgan, N., Wells, C. G., Goodson, M. J., Kraft, M., Wagner, W. (2006). A new numerical approach for the simulation of the growth of inorganic nanoparticles. *Journal of Computational Physics* **211** (23), 638–658. doi:[10.1016/j.jcp.2005.04.027](https://doi.org/10.1016/j.jcp.2005.04.027).
- Morris, A. J., Coe, M. D. (1989). System for increasing the capacity of a titanium dioxide producing process. U.S. Patent 4,803,056. URL <http://www.google.com/patents/?id=R805AAAAEBAJ>.
- Mueller, M. E., Blanquart, G., Pitsch, H. (2009). A joint volume-surface model of soot aggregation with the method of moments. In *Proceedings of the Combustion Institute*, vol. 32, pp. 785–792. The Combustion Institute. doi:[10.1016/j.proci.2008.06.207](https://doi.org/10.1016/j.proci.2008.06.207).
- Mustata, R., Valiño, L., Jiménez, C., Jones, W. P., Bondi, S. (2006). A probability density function Eulerian Monte Carlo field method for large eddy simulations: Application to a turbulent piloted methane/air diffusion flame (Sandia D). *Combustion and Flame* **145** (1–2), 88–104. doi:[10.1016/j.combustflame.2005.12.002](https://doi.org/10.1016/j.combustflame.2005.12.002).
- Niedenzu, P. M., Herkimer, S. M., Chaney, R. L. (1996). Process for preparing salinized TiO₂ pigments using a media mill. U.S. Patent 5,501,732. URL <http://www.google.com/patents?id=5Y8cAAAAEBAJ>.

BIBLIOGRAPHY

- Paskov, S., Traub, J. (1995). Faster valuation of financial derivatives. *The Journal of Portfolio Management* **22** (1), 113–123. doi:[10.3905/jpm.1995.409541](https://doi.org/10.3905/jpm.1995.409541).
- Patterson, R. I. A., Singh, J., Balthasar, M., Kraft, M., Norris, J. (2006a). The linear process deferment algorithm: A new technique for solving population balance equations. *SIAM Journal on Scientific Computing* **28** (1), 303–320. doi:[10.1137/040618953](https://doi.org/10.1137/040618953).
- Patterson, R. I. A., Singh, J., Balthasar, M., Kraft, M., Wagner, W. (2006b). Extending stochastic soot simulation to higher pressures. *Combustion and Flame* **145** (3), 638–642. doi:[10.1016/j.combustflame.2006.02.005](https://doi.org/10.1016/j.combustflame.2006.02.005).
- Peters, N. (2000). *Turbulent Combustion*. Cambridge University Press, Cambridge.
- Pope, S. B. (1982). An improved turbulent mixing model. *Combustion Science and Technology* **28** (3-4), 131–135. doi:[10.1080/00102208208952549](https://doi.org/10.1080/00102208208952549).
- Pope, S. B. (1985). PDF methods for turbulent reacting flows. *Progress in Energy and Combustion Science* **11** (2), 119–192. doi:[10.1016/0360-1285\(85\)90002-4](https://doi.org/10.1016/0360-1285(85)90002-4).
- Pope, S. B. (1991). Computations of turbulent combustion: Progress and challenges. In *Proceedings of the Combustion Institute*, vol. 23, pp. 591–612. The Combustion Institute. doi:[10.1016/S0082-0784\(06\)80307-3](https://doi.org/10.1016/S0082-0784(06)80307-3).
- Pope, S. B. (1997). Computationally efficient implementation of combustion chemistry using *in situ* adaptive tabulation. *Combustion Theory and Modelling* **1** (1), 41–63. doi:[10.1080/713665229](https://doi.org/10.1080/713665229).
- Pope, S. B. (2000). *Turbulent Flows*. Cambridge University Press, Cambridge.
- Pratsinis, S. E. (1988). Simultaneous nucleation, condensation, and coagulation in aerosol reactors. *Journal of Colloid and Interface Science* **124** (2), 416–427. doi:[10.1016/0021-9797\(88\)90180-4](https://doi.org/10.1016/0021-9797(88)90180-4).
- Pratsinis, S. E. (1998). Flame aerosol synthesis of ceramic powders. *Progress in Energy and Combustion Science* **24** (3), 197–219. doi:[10.1016/S0360-1285\(97\)00028-2](https://doi.org/10.1016/S0360-1285(97)00028-2).
- Pratsinis, S. E., Bai, H., Biswas, P., Frenklach, M., Mastrangelo, S. V. R. (1990). Kinetics of titanium (IV) chloride oxidation. *Journal of the American Ceramic Society* **73** (7), 2158–2162. doi:[10.1111/j.1151-2916.1990.tb05295.x](https://doi.org/10.1111/j.1151-2916.1990.tb05295.x).

- Pratsinis, S. E., Spicer, P. T. (1998). Competition between gas phase and surface oxidation of TiCl_4 during synthesis of TiO_2 particles. *Chemical Engineering Science* **53** (10), 1861–1868. doi:[10.1016/S0009-2509\(98\)00026-8](https://doi.org/10.1016/S0009-2509(98)00026-8).
- Pratsinis, S. E., Vemury, S., Fotou, G. P., Gutsch, A. (1997). Process for producing ceramic powders, especially titanium dioxide useful as a photocatalyst. U.S. Patent 5,698,177. URL <http://www.google.com/patents/?id=OgwFAAAAEBAJ>.
- Raman, V., Pitsch, H., Fox, R. O. (2006). Eulerian transported probability density function sub-filter model for large-eddy simulations of turbulent combustion. *Combustion Theory and Modelling* **10** (3), 439–548. doi:[10.1080/13647830500460474](https://doi.org/10.1080/13647830500460474).
- Ramkrishna, D. (2000). *Population Balances — Theory and Applications to Particulate Systems in Engineering*. Academic Press, San Diego.
- Revzan, K. L., Brown, N. J., Frenklach, M. (1999). Soot formation codes. URL <http://www.me.berkeley.edu/soot>.
- Rigopoulos, S. (2007). PDF method for population balance in turbulent reactive flow. *Chemical Engineering Science* **62** (23), 6865–6878. doi:[10.1016/j.ces.2007.05.039](https://doi.org/10.1016/j.ces.2007.05.039).
- Rigopoulos, S. (2010). Population balance modelling of polydispersed particles in reactive flows. *Progress in Energy and Combustion Science* **36** (4), 412–443. doi:[10.1016/j.pecs.2009.12.001](https://doi.org/10.1016/j.pecs.2009.12.001).
- Rosner, D. E. (2005). Flame synthesis of valuable nanoparticles: Recent progress/current needs in areas of rate laws, population dynamics, and characterization. *Industrial & Engineering Chemistry Research* **44** (16), 6045–6055. doi:[10.1021/ie0492092](https://doi.org/10.1021/ie0492092).
- Rosner, D. E. (2009). Spray combustor design/performance: Chemical engineering contributions and the emergence of an “interacting population-balance” perspective. *Industrial & Engineering Chemistry Research* **48** (14), 6453–6464. doi:[10.1021/ie900167h](https://doi.org/10.1021/ie900167h).
- Roth, P. (2007). Particle synthesis in flames. In *Proceedings of the Combustion Institute*, vol. 31, pp. 1773–1788. The Combustion Institute. doi:[10.1016/j.proci.2006.08.118](https://doi.org/10.1016/j.proci.2006.08.118).

BIBLIOGRAPHY

- Sabel'nikov, V., Souldard, O. (2005a). Rapidly decorrelating velocity-field model as a tool for solving one-point Fokker-Planck equations for probability density functions of turbulent reactive scalars. *Physical Review E* **72** (1), 16301. doi:[10.1103/PhysRevE.72.016301](https://doi.org/10.1103/PhysRevE.72.016301).
- Sabel'nikov, V., Souldard, O. (2005b). Simulation of a turbulent premixed methane flame with an Eulerian Monte Carlo solver. In Dias, V., Vandooren, J. (Eds.), *Proceedings of the European Combustion Institute*, p. E100. Belgian Section of the Combustion Institute, Louvain.
- Sabel'nikov, V., Souldard, O. (2006). White in time scalar advection model as a tool for solving joint composition PDF equations. *Flow, Turbulence and Combustion* **77** (1–4), 333–357. doi:[10.1007/s10494-006-9049-z](https://doi.org/10.1007/s10494-006-9049-z).
- Saffman, P. G., Turner, J. S. (1956). On the collision of drops in turbulent clouds. *Journal of Fluid Mechanics* **1** (1), 16–30. doi:[10.1017/S0022112056000020](https://doi.org/10.1017/S0022112056000020).
- Sander, M., Patterson, R. I. A., Braumann, A., Raj, A., Kraft, M. (2011). Developing the PAH-PP soot particle model using process informatics and uncertainty propagation. In *Proceedings of the Combustion Institute*, vol. 33, pp. 675–683. The Combustion Institute. doi:[10.1016/j.proci.2010.06.156](https://doi.org/10.1016/j.proci.2010.06.156).
- Sander, M., West, R. H., Celnik, M. S., Kraft, M. (2009). A detailed model for the sintering of polydispersed nanoparticle agglomerates. *Aerosol Science and Technology* **43** (10), 978–989. doi:[10.1080/02786820903092416](https://doi.org/10.1080/02786820903092416).
- Santos, P. C. (1970). Production of titanium dioxide pigments. U.S. Patent 3,505,091. URL <http://www.google.com/patents?id=FiVjAAAAEBAJ>.
- Schaumann, H. H. (1949). Production of titanium oxide pigments. U.S. Patent 2,488,439. URL <http://www.freepatentsonline.com/2488439.html>.
- Seto, T., Hirota, A., Fujimoto, T., Shimada, M., Okuyama, K. (1997). Sintering of polydisperse nanometer-sized agglomerates. *Aerosol Science and Technology* **27** (3), 422–438. doi:[10.1080/02786829708965482](https://doi.org/10.1080/02786829708965482).
- Shekar, S., Sander, M., Riehl, R. C., Smith, A. J., Braumann, A., Kraft, M. (2011). Flame synthesis of silica nanoparticles from tetraethoxysilane. *Chemical Engineering Science*, in press. doi:[10.1016/j.ces.2011.06.010](https://doi.org/10.1016/j.ces.2011.06.010).

BIBLIOGRAPHY

- Shirley, R., Akroyd, J., Miller, L. A., Inderwildi, O., Riedel, U., Kraft, M. (2011). Theoretical insights into the surface growth of rutile TiO₂. *Combustion and Flame*, in press. doi:[10.1016/j.combustflame.2011.06.007](https://doi.org/10.1016/j.combustflame.2011.06.007).
- Shirley, R., Liu, Y., Totton, T. S., West, R. H., Kraft, M. (2009). First-principles thermochemistry for the combustion of a TiCl₄ and AlCl₃ mixture. *Journal of Physical Chemistry A* **113** (49), 13790–13796. doi:[10.1021/jp905244w](https://doi.org/10.1021/jp905244w).
- Singer, M. A., Pope, S. B., Najm, H. N. (2006a). Modeling unsteady reacting flow with operator splitting and ISAT. *Combustion and Flame* **147** (1–2), 150–162. doi:[10.1016/j.combustflame.2006.06.007](https://doi.org/10.1016/j.combustflame.2006.06.007).
- Singer, M. A., Pope, S. B., Najm, H. N. (2006b). Operator-splitting with ISAT to model reacting flow with detailed chemistry. *Combustion Theory and Modelling* **10** (2), 199–217. doi:[10.1080/13647830500307501](https://doi.org/10.1080/13647830500307501).
- Singh, J., Balthasar, M., Kraft, M., Wagner, W. (2005). Stochastic modeling of soot particle size and age distributions in laminar premixed flames. In *Proceedings of the Combustion Institute*, vol. 30, pp. 1457–1465. The Combustion Institute. doi:[10.1016/j.proci.2004.08.120](https://doi.org/10.1016/j.proci.2004.08.120).
- Slepetyts, R. A. (1970). Fluid energy milling TiO₂ pigment. U.S. Patent 3,549,091. URL <http://www.google.com/patents?id=hARgAAAAEBAJ>.
- Smith, S. T., Fox, R. O. (2007). A term-by-term direct numerical simulation validation study of the multi-environment conditional probability-density-function model for turbulent reacting flows. *Physics of Fluids* **19** (8), 085102–1–19. doi:[10.1063/1.2757699](https://doi.org/10.1063/1.2757699).
- Smoluchowski, M. v. (1917). Versuch einer mathematischen Theorie der Koagulationskinetik kolloidaler Lösungen. *Zeitschrift für Physikalische Chemie* **92**, 129–168.
- Soulard, O., Sabel'nikov, V. (2006). Eulerian Monte Carlo method for the joint velocity and mass-fraction probability density function in turbulent reactive gas flows. *Combustion, Explosion and Shock Waves* **42** (6), 753–762. doi:[10.1007/s10573-006-0111-x](https://doi.org/10.1007/s10573-006-0111-x).
- Souza, L. G. M. d., Janiga, G., John, V., Thévenin, D. (2010). Reconstruction of a distribution from a finite number of moments with an adaptive spline-based algorithm. *Chemical Engineering Science* **65** (9), 2741–2750. doi:[10.1016/j.ces.2010.01.007](https://doi.org/10.1016/j.ces.2010.01.007).

BIBLIOGRAPHY

- Spalding, D. B. (1971). Mixing and chemical reaction in steady confined turbulent flames. In *Proceedings of the Combustion Institute*, vol. 13, pp. 649–657. The Combustion Institute. doi:[10.1016/S0082-0784\(71\)80067-X](https://doi.org/10.1016/S0082-0784(71)80067-X).
- Spicer, P. T., Chaoul, O., Tsantilis, S., Pratsinis, S. E. (2002). Titania formation by TiCl_4 gas phase oxidation, surface growth and coagulation. *Journal of Aerosol Science* **33** (1), 17–34. doi:[10.1016/S0021-8502\(01\)00069-6](https://doi.org/10.1016/S0021-8502(01)00069-6).
- Strang, G. (1968). On the construction and comparison of difference schemes. *SIAM Journal on Numerical Analysis* **5** (3), 506–517. doi:[10.1137/0705041](https://doi.org/10.1137/0705041).
- Tang, Q., Zhao, W., Bockelie, M., Fox, R. O. (2007). Multi-environment probability density function method for modelling turbulent combustion using realistic chemical kinetics. *Combustion Theory and Modelling* **11** (6), 889–907. doi:[10.1080/13647830701268890](https://doi.org/10.1080/13647830701268890).
- Tennekes, H., Lumley, J. L. (1972). *A First Course in Turbulence*. MIT Press, Cambridge, Massachusetts.
- Terry, D. A., McGraw, R., Rangel, R. H. (2001). Method of moments solutions for a laminar flow aerosol reactor model. *Aerosol Science and Technology* **34** (4), 353–362. doi:[10.1080/02786820118736](https://doi.org/10.1080/02786820118736).
- Tsai, K., Fox, R. O. (1994). PDF simulation of a turbulent series-parallel reaction in an axisymmetric reactor. *Chemical Engineering Science* **49** (24B), 5154–5158. doi:[10.1016/0009-2509\(94\)00270-3](https://doi.org/10.1016/0009-2509(94)00270-3).
- Tsai, K., Gillis, P. A., Sen, S., Fox, R. O. (2002). A finite-mode PDF model for turbulent reacting flows. *Journal of Fluids Engineering* **124** (1), 102–107. doi:[10.1115/1.1431546](https://doi.org/10.1115/1.1431546).
- Tsantilis, S., Pratsinis, S. E. (2004). Narrowing the size distribution of aerosol-made titania by surface growth and coagulation. *Journal of Aerosol Science* **35** (3), 405–420. doi:[10.1016/j.jaerosci.2003.09.006](https://doi.org/10.1016/j.jaerosci.2003.09.006).
- Upadhyay, R. R., Ezekoye, O. A. (2006). Treatment of size-dependent aerosol transport processes using quadrature based moment methods. *Journal of Aerosol Science* **37** (7), 799–819. doi:[10.1016/j.jaerosci.2005.06.002](https://doi.org/10.1016/j.jaerosci.2005.06.002).
- Valiño, L. (1998). A field Monte Carlo formulation for calculating the probability density function of a single scalar in a turbulent flow. *Flow, Turbulence and Combustion* **60** (2), 157–172. doi:[10.1023/A:1009968902446](https://doi.org/10.1023/A:1009968902446).

BIBLIOGRAPHY

- Veroli, G. d., Rigopoulos, S. (2010). Modeling of turbulent precipitation: A transported population balance-PDF method. *AIChE Journal* **56** (4), 878–892. doi:[10.1002/aic.12064](https://doi.org/10.1002/aic.12064).
- Veynante, D., Vervisch, L. (2002). Turbulent combustion modelling. *Progress in Energy and Combustion Science* **28** (3), 193–266. doi:[10.1016/S0360-1285\(01\)00017-X](https://doi.org/10.1016/S0360-1285(01)00017-X).
- Villermaux, J., Devillon, J. C. (1972). Représentation de la coalescence et de la redispersion des domaines de ségrégation dans un fluide par un modèle d'interaction phénoménologique. In *Proceedings of the 2nd International Symposium on Chemical Reaction Engineering*, pp. 1–13. International Symposium on Chemical Reaction Engineering, Elsevier, New York.
- Wang, G., Garrick, S. C. (2005). Modeling and simulation of titania synthesis in two-dimensional methane-air flames. *Journal of Nanoparticle Research* **7** (6), 621–632. doi:[10.1007/s11051-005-4966-7](https://doi.org/10.1007/s11051-005-4966-7).
- Wang, L., Fox, R. O. (2004). Comparison of micromixing models for CFD simulation of nanoparticle formation. *AIChE Journal* **50** (9), 2217–2232. doi:[10.1002/aic.10173](https://doi.org/10.1002/aic.10173).
- Wegner, K., Pratsinis, S. E. (2003). Scale-up of nanoparticle synthesis in diffusion flame reactors. *Chemical Engineering science* **58** (20), 4581–4589. doi:[10.1016/j.ces.2003.07.010](https://doi.org/10.1016/j.ces.2003.07.010).
- Wells, C. G. (2006). A stochastic approximation scheme and convergence theorem for particle interactions with perfectly reflecting boundary conditions. *Monte Carlo Methods and Applications* **12** (3), 291–342. doi:[10.1163/156939606778705182](https://doi.org/10.1163/156939606778705182).
- Wells, C. G., Kraft, M. (2005). Direct simulation and mass flow stochastic algorithms to solve a sintering-coagulation equation. *Monte Carlo Methods and Applications* **11** (2), 175–197. doi:[10.1515/156939605777585980](https://doi.org/10.1515/156939605777585980).
- Wells, C. G., Morgan, N., Kraft, M., Wagner, W. (2006). A new method for calculating the diameters of partially-sintered nanoparticles and its effect on simulated particle properties. *Chemical Engineering Science* **61** (1), 158–166. doi:[10.1016/j.ces.2005.01.048](https://doi.org/10.1016/j.ces.2005.01.048).

BIBLIOGRAPHY

- West, R. H., Beran, G. J. O., Green, W. H., Kraft, M. (2007a). First-principles thermochemistry for the production of TiO_2 from TiCl_4 . *Journal of Physical Chemistry A* **111** (18), 3560–3565. doi:[10.1021/jp0661950](https://doi.org/10.1021/jp0661950).
- West, R. H., Celnik, M. S., Inderwildi, O. R., Kraft, M., Beran, G. J. O., Green, W. H. (2007b). Toward a comprehensive model of the synthesis of TiO_2 particles from TiCl_4 . *Industrial & Engineering Chemistry Research* **46** (19), 6147–6156. doi:[10.1021/ie0706414](https://doi.org/10.1021/ie0706414).
- West, R. H., Shirley, R., Kraft, M., Goldsmith, C. F., Green, W. H. (2009). A detailed kinetic model for combustion synthesis of titania from TiCl_4 . *Combustion and Flame* **156** (9), 1764–1770. doi:[10.1016/j.combustflame.2009.04.011](https://doi.org/10.1016/j.combustflame.2009.04.011).
- Williams, R., Duffy, J. (2009). Solar water purification: Storage test for the determination of bacteria regrowth and taste test in TiO_2 coated PET bottles. URL <http://energy.caeds.eng.uml.edu/peru-07/ASES09StorageTestforTiO2CoatedPETBottles-jjd.pdf>.
- Wilson, J. R. (1979). Proof of the antithetic-variates theorem for unbounded functions. *Mathematical Proceedings of the Cambridge Philosophical Society* **86** (03), 477–479. doi:[10.1017/S0305004100056334](https://doi.org/10.1017/S0305004100056334).
- Wilson, J. R. (1983). Antithetic sampling with multivariate inputs. *American Journal of Mathematical and Management Sciences* **3**, 121–144.
- World Bank (2011). GDP annual growth data. URL <http://data.worldbank.org/indicator/NY.GDP.MKTP.KD.ZG/countries/1W?display=graph>.
- Wright Jr, D. L. (2006). Numerical advection of moments of the particle size distribution in Eulerian models. *Journal of Aerosol Science* **38** (3), 352–369. doi:[10.1016/j.jaerosci.2006.11.011](https://doi.org/10.1016/j.jaerosci.2006.11.011).
- Wright Jr, D. L., McGraw, R., Rosner, D. E. (2001). Bivariate extension of the quadrature method of moments for modeling simultaneous coagulation and sintering of particle populations. *Journal of Colloid and Interface Science* **236** (2), 242–251. doi:[10.1006/jcis.2000.7409](https://doi.org/10.1006/jcis.2000.7409).
- Xiong, Y., Pratsinis, S. E. (1993). Formation of agglomerate particles by coagulation and sintering—Part I. A two-dimensional solution of the population balance equation. *Journal of Aerosol Science* **24** (3), 283–300. doi:[10.1016/0021-8502\(93\)90003-R](https://doi.org/10.1016/0021-8502(93)90003-R).

BIBLIOGRAPHY

- Zhao, B., Yang, Z., Johnston, M. V., Wang, H., Wexler, A. S., Balthasar, M., Kraft, M. (2003). Measurement and numerical simulation of soot particle size distribution functions in a laminar premixed ethylene-oxygen-argon flame. *Combustion and Flame* **133** (1–2), 173–188. doi:[10.1016/S0010-2180\(02\)00574-6](https://doi.org/10.1016/S0010-2180(02)00574-6).
- Zhao, W., Zhang, C., Chen, C. (2011). Large eddy simulation of bluff-body stabilized flames using a multi-environment filtered density function model. In *Proceedings of the Combustion Institute*, vol. 33, pp. 1347–1353. The Combustion Institute. doi:[10.1016/j.proci.2010.07.005](https://doi.org/10.1016/j.proci.2010.07.005).
- Zucca, A., Marchisio, D. L., Baressi, A. A., Fox, R. O. (2006). Implementation of the population balance equation in CFD codes for modelling soot formation in turbulent flames. *Chemical Engineering Science* **61** (1), 87–95. doi:[10.1016/j.ces.2004.11.061](https://doi.org/10.1016/j.ces.2004.11.061).
- Zucca, A., Marchisio, D. L., Vanni, M., Barresi, A. A. (2007). Validation of bivariate DQMOM for nanoparticle simulation. *AIChE Journal* **53** (4), 918–931. doi:[10.1002/aic.11125](https://doi.org/10.1002/aic.11125).

Citation index

- Acheson (1990), [15](#)
Ahrens and Dieter (1973), [66](#)
Akroyd et al. (2010), [31](#), [43](#), [44](#), [50](#),
[56–58](#)
Ali et al. (2011), [26](#)
Allen and Gergely (1998), [6](#), [9](#)
Appel et al. (2000), [13](#)
Büchel et al. (2000), [8–10](#)
Balthasar and Frenklach (2005), [13](#)
Balthasar and Kraft (2003), [13](#), [30](#),
[88](#)
Balthasar et al. (2002), [88](#)
Balthasar (2000), [90](#)
Boulos et al. (2002), [6](#), [7](#)
Bourne and Rys (1981), [17](#)
Boyle et al. (1997), [67](#)
Buckingham and Gambogi (2006), [7](#)
Buesser et al. (2009), [15](#)
CD-adapco (2008), [37](#), [47](#), [64](#), [68](#)
CD-adapco (2009), [96](#), [101](#)
Cant and Mastorakos (2008), [20](#), [23](#)
Celnik et al. (2007), [15](#)
Celnik et al. (2009), [15](#), [102](#)
Cheng (1982), [67](#)
Chittipotula et al. (2011), [28](#)
Curl (1963), [22](#)
Deberry et al. (2002), [9](#)
Denison et al. (2010), [26](#), [31](#)
Desjardins et al. (2008), [14](#)
Dopazo and O'Brien (1974), [22](#)
Dopazo (1994), [22](#), [23](#)
DuPont Titanium Technologies
(2002), [6](#)
DuPont Titanium Technologies
(2007), [7](#), [9](#)
Eibeck and Wagner (2000), [15](#)
Eibeck and Wagner (2001), [15](#)
Eibeck and Wagner (2003), [15](#)
Fan and Fox (2008), [14](#)
Fan et al. (2004), [14](#), [26](#)
Fishman and Huang (1983), [67](#)
Fishman (1996), [67](#)
Fissore et al. (2002), [25](#)
Fox and Raman (2004), [26](#)
Fox et al. (2008), [14](#)
Fox (2003), [20](#), [21](#), [25](#), [31](#), [33](#), [34](#),
[58](#), [93](#), [131](#), [134](#), [136](#)
Fox (2006a), [14](#)
Fox (2006b), [28](#)
Fox (2008), [13](#)
Frenklach and Harris (1987), [13](#), [86](#)
Frenklach (2002), [13](#), [88](#), [92](#), [93](#)
Fujishima et al. (1999), [7](#)
Gardiner (2004), [63](#), [66](#), [146](#), [162](#)
Garmory and Mastorakos (2008), [28](#)
Garmory et al. (2006), [24](#)
Garmory et al. (2008), [24](#)
Garmory et al. (2009), [24](#)

CITATION INDEX

- Garmory (2007), [24](#), [66](#), [69](#)
Gavi et al. (2007a), [26](#)
Gavi et al. (2007b), [13](#), [26](#), [28](#), [74](#)
Geweke (1988), [67](#)
Ghoshtagore (1970), [11](#)
Goodson and Kraft (2002), [15](#), [102](#)
Grant et al. (2004), [1](#), [8](#)
Grosch et al. (2007), [13](#)
Grosschmidt et al. (2002), [13](#), [30](#), [88](#)
Haddow (1997), [9](#)
Hairer and Wanner (1996), [39](#), [44](#)
Hammersley and Handscomb (1958), [66](#)
Hammersley and Mauldon (1956), [66](#)
Hammersley and Morton (1956), [66](#)
Hartmann (1996), [9](#)
Hauke and Valiño (2004), [24](#), [63](#)
Haworth (2010), [20](#), [22](#), [23](#)
Heine and Pratsinis (2007a), [11](#), [14](#), [15](#)
Heine and Pratsinis (2007b), [15](#), [116](#)
Heine and Pratsinis (2007c), [15](#)
Hill (2009), [1](#), [8](#)
Hulbert and Katz (1964), [13](#)
ICIS (2011), [9](#)
Johannessen et al. (2001), [29](#), [86](#)
Jones and Navarro-Martinez (2007), [24](#)
Jones and Navarro-Martinez (2009), [24](#)
Jones and Prasad (2010), [24](#)
Jones and Prasad (2011), [24](#)
Jones and Tyliczszak (2010), [24](#)
Jones et al. (2007), [24](#)
Jones (1994), [19](#)
Kee et al. (1985), [13](#)
Klimenko and Bilger (1999), [20](#), [21](#)
Kloeden and Platen (1995), [66](#)
Kollmann (1990), [23](#)
Krchma and Schaumann (1951), [9](#)
Levenspiel (1999), [20](#)
Li and Toor (1986), [47](#), [51](#), [56](#), [74](#)
Libby and Williams (1980), [20](#)
Libby and Williams (1994), [20](#)
Lindstedt and Louloudi (2005), [28](#)
Liu and Pope (2005), [27](#)
Lu and Pope (2009), [27](#)
Lui and Fox (2006), [26](#), [49](#)
Magnussen and Hjertager (1977), [21](#)
Marchisio and Fox (2005), [14](#), [30](#)
Marchisio et al. (2006), [13](#)
Marchisio (2009), [26](#)
Matsumoto and Nishimura (1998), [66](#)
McGraw (1997), [13](#), [30](#)
Mehta et al. (2010), [11](#), [29](#)
Moody and Collins (2003), [29](#)
Morgan et al. (2005), [11](#)
Morgan et al. (2006), [11](#)
Morgan et al. (2007), [15](#), [28](#), [86](#)
Morgan (2008), [7](#)
Morris and Coe (1989), [9](#)
Mueller et al. (2009), [13](#)
Mustata et al. (2006), [24](#)
Niedenzu et al. (1996), [9](#)
Paskov and Traub (1995), [67](#)
Patterson et al. (2006a), [15](#), [102](#)
Patterson et al. (2006b), [15](#), [102](#)
Peters (2000), [20](#), [21](#), [128](#), [129](#), [132](#)
Pope (1982), [22](#)
Pope (1985), [16](#), [22](#), [23](#), [128](#), [131](#), [132](#)
Pope (1991), [23](#)

- Pope (1997), [27](#), [158](#)
Pope (2000), [15](#), [16](#), [18](#), [19](#), [22](#), [141](#)
Pratsinis and Spicer (1998), [11](#), [116](#)
Pratsinis et al. (1990), [11](#), [106](#)
Pratsinis et al. (1997), [9](#)
Pratsinis (1988), [13](#)
Pratsinis (1998), [27](#)
Raman et al. (2006), [26](#), [43](#)
Ramkrishna (2000), [12](#)
Revzan et al. (1999), [13](#)
Rigopoulos (2007), [28](#), [29](#)
Rigopoulos (2010), [28](#)
Rosner (2005), [27](#)
Rosner (2009), [27](#), [28](#)
Roth (2007), [27](#)
Sabel'nikov and Soulard (2005a), [23](#),
[24](#), [62](#), [69](#)
Sabel'nikov and Soulard (2005b), [24](#)
Sabel'nikov and Soulard (2006), [24](#)
Saffman and Turner (1956), [88](#)
Sander et al. (2009), [12](#)
Sander et al. (2011), [12](#)
Santos (1970), [9](#)
Schaumann (1949), [9](#)
Seto et al. (1997), [14](#)
Shekar et al. (2011), [12](#)
Shirley et al. (2009), [11](#)
Shirley et al. (2011), [11](#), [87](#), [106](#)
Singer et al. (2006a), [27](#)
Singer et al. (2006b), [27](#)
Singh et al. (2005), [13](#), [15](#), [28](#), [86](#)
Slepetyts (1970), [9](#)
Smith and Fox (2007), [26](#)
Smoluchowski (1917), [12](#)
Soulard and Sabel'nikov (2006), [24](#)
Souza et al. (2010), [14](#)
Spalding (1971), [21](#)
Spicer et al. (2002), [12](#), [14](#)
Strang (1968), [37](#), [64](#), [96](#), [156](#)
Tang et al. (2007), [26](#), [27](#), [31](#), [43](#)
Tennekes and Lumley (1972), [15](#)
Terry et al. (2001), [13](#)
Tsai and Fox (1994), [47–49](#), [51](#), [56](#),
[74](#)
Tsai et al. (2002), [25](#), [47](#), [49](#)
Tsantilis and Pratsinis (2004), [11](#), [12](#),
[14](#), [116](#)
Upadhyay and Ezekoye (2006), [26](#)
Valiño (1998), [23](#), [24](#), [62](#), [134](#), [145](#)
Veroli and Rigopoulos (2010), [29](#), [30](#)
Veynante and Vervisch (2002), [20](#)
Villermaux and Devillon (1972), [22](#),
[133](#)
Wang and Fox (2004), [25](#), [31](#)
Wang and Garrick (2005), [29](#)
Wegner and Pratsinis (2003), [27](#)
Wells and Kraft (2005), [15](#), [102](#)
Wells et al. (2006), [15](#)
Wells (2006), [15](#)
West et al. (2007a), [11](#)
West et al. (2007b), [11](#)
West et al. (2009), [11](#), [87](#), [98](#), [106](#)
Williams and Duffy (2009), [7](#)
Wilson (1979), [66](#)
Wilson (1983), [66](#)
World Bank (2011), [8](#)
Wright Jr et al. (2001), [13](#)
Wright Jr (2006), [14](#), [112](#)
Xiong and Pratsinis (1993), [12](#)
Zhao et al. (2003), [13](#), [15](#), [28](#), [86](#)
Zhao et al. (2011), [26](#)
Zucca et al. (2006), [14](#), [28](#)
Zucca et al. (2007), [14](#), [26](#), [28](#)